THESIS

GEOCHEMICAL STUDY OF THE LOUIS LAKE BATHOLITH AND ITS POTENTIAL AS A FLUID SOURCE FOR GOLD DEPOSITS IN THE ATLANTIC CITY DISTRICT, WY

Submitted by

Elizabeth Vaughn

Department of Geosciences

In partial fulfillment of the requirements

For the Degree of Master of Science

Colorado State University

Fort Collins, Colorado

Fall 2010

Master's Committee:

Department Head: Sally Sutton

Advisor: John Ridley

Judy Hannah
Branka Ladanyi

ABSTRACT OF THESIS

GEOCHEMICAL STUDY OF THE LOUIS LAKE BATHOLITH AND ITS POTENTIAL AS A FLUID SOURCE FOR GOLD DEPOSITS IN THE ATLANTIC CITY DISTRICT, WY

The Louis Lake Batholith is positioned in the southern tip of the Wind River Range, an upthrust exposure of the Wyoming Craton. The Archean batholith varies from granite to granodiorite and is dated at 2630 ± 2 Ma (Frost et al., 1998). The Louis Lake Batholith consists of several phases of granite, aplitic dikes, pegmatite dikes, quartz veins and segregations, and localized mafic enclaves. Pressures of crystallization were determined by hornblende geobarometry to be between 2 and 6 kbar at the southern end of the batholith.

Because the Louis Lake Batholith is adjacent to a known gold mineralized area, it was investigated as a potential fluid source for these deposits. The area has experienced very little deformation since the Archean, making it plausible to study any possible links between the granite and the deposits. The South Pass Greenstone Belt contains lode gold deposits and minor copper vein stockwork systems, similar in age to the crystallization age of the batholith. U-Pb titanite ages for shear zones associated with the Atlantic City District gold deposits range from 2635 to 2616 ± 2 Ma (Frost et al., 2006). Gold

mineralization is shear-hosted, and minor copper mineralization is found as lodes and stockworks that cut the gold mineralization (Hausel, 1991).

The Louis Lake Batholith samples range from biotite granite to granodiorite, with localized hornblende. The samples were analyzed using a variety of techniques, including whole rock geochemistry, petrography, mineral chemistry, and studies of fluid inclusions. Whole rock data demonstrate that the batholith was formed in a volcanic arc setting. REE spider diagrams reveal that all phases are genetically related and show a slight negative Eu anomaly, except for a mafic enclave, which has a slight positive Eu anomaly, and thus likely a different source. Aplites show flat REE profiles because they are more highly fractionated. Magnetite is widespread, typically as aggregates or as clusters with titanite, biotite, and hornblende (if present). Euhedral titanites are widespread and can contain inclusions of magnetite. The presence of magnetite and titanite implies a relatively oxidizing environment at the time of crystallization. Apatite grains are widespread and occur as inclusions in mafic minerals and as isolated zoned crystals. Minor amounts of allanite are present, generating radioactive halos in adjacent minerals, such as apatite and titanite. The sulfide content of the melt is marked by trace amounts of chalcopyrite that can be seen as small inclusions in magnetite, and more rarely in quartz grains.

Trace element contents of igneous and hydrothermal minerals were determined by an electron microprobe. Several samples were found to have anomalous concentrations of Cu, Au, and Ag, both in whole rock data and in magnetites and hematites analyzed by microprobe. Oxides contain the highest concentrations of Cu, Au, and Ag.

Fluid inclusions were analyzed from a variety of late-magmatic phases: quartz veins and irregular segregations in unaltered host granite, pegmatite dikes, and aplite dikes. Four types of inclusions were found in the Louis Lake samples. Type 1 inclusions contain high salinity, aqueous fluids with varying amounts of daughter minerals and sometimes a few mol % CO_2. Type II inclusions are a low to moderate salinity, aqueous-carbonic fluid that sometimes contains small daughter minerals. Type III inclusions are moderate salinity, aqueous-carbonic inclusions with daughter minerals, and are thought to be an intermediate between Types I and II. Type IV inclusions are CO_2-rich, 60-70 mol % CO_2, and low salinity. Type I and II fluid inclusions from one sample were analyzed using LA-ICP-MS for a suite of elements.

Upon investigation of the Louis Lake Batholith, several parallels with felsic to intermediate intrusions associated with ore deposits become apparent. Gold-related plutons are comparable to the batholith in this study in that that have a similar oxidation state, lack extreme fractionation, and show evidence for a release of an early-crystallized sulfide phase. The trend of SO_3 concentration in apatites implies fluids exsolved relatively early during fractionation of the granite. Geochemical analysis of the mafic enclave indicates that gold and other metals were introduced to the granite by mixing with mafic magmas. The elevated Au and Cu content of enclaves is congruent with that recorded in intrusions associated with some ore deposit types. Types I and II fluid inclusions are Na-dominated, with similarities to hydrothermal fluids in ore deposits. High salinity fluids contain similar metal contents as intrusion-related ore systems, while low salinity fluids share affinities with both intrusion-related ore systems and orogenic gold systems. The model of Core et al (2006) in which magma mixing is an important step in the creation of high copper content of enclaves is therefore also proposed for large porphyry deposits (Core et al, 2006). A genetic model was constructed for the Louis Lake

Batholith. First, metals, namely Cu and Au, were concentrated within Fe-oxide globules. These metals were later scavenged by a S-rich fluid that carried the metals away and deposited them within shears in the South Pass Greenstone Belt.

ACKNOWLEDGEMENTS

I would like to thank the Society for Economic Geologists, Wyoming Geological Survey, the CSU Geosciences Department and Newmont Mining Corporation for funding this project. I would also like to thank Peter Schmitz, Susan Swapp, and Quinton Hennigh for their help during this project. Lastly, I would like to thank the Fremont County Sheriff's Office, the U.S. Forest Service, and the staff at the Louis Lake Lodge. I would especially like to thank my friends and family for support during this endeavor.

TABLE OF CONTENTS

TABLE OF FIGURES

TABLE OF TABLES

TABLE OF PLATES

1. INTRODUCTION

The Wind River Mountains, a portion of the Wyoming Craton, consist of Archean granites, granitic gneisses, and metamorphosed and deformed supracrustal rocks that were uplifted along the basement-involved Wind River Thrust (Bayley 1973). During the Laramide Orogeny (Cretaceous- Eocene), this block of Archean basement was thrust over Paleozoic and Mesozoic sediments (Hausel 1991). The rocks of the Wind River block can be split into two different packages: the metamorphosed supracrustal rocks of the South Pass Greenstone Belt (SPGB) and the granites and granitic gneisses that formed basement to the supracrustal rocks and intrude them. The granites and gneisses make up the high peaks of the Wind River Range, while the SPGB is exposed in a rolling landscape along the southern edge of the uplift.

Significant gold and iron mineralization is found within the SPGB, with non-economic deposits of copper, silver, tungsten and uranium, but mineralization is minor within the granitic intrusives (Hausel 1991). The largest deposits within the SPGB are epigenetic hydrothermal lode gold deposits and stratiform iron stone deposits. Gold was discovered in the district in 1863 in paleoplacer deposits within Tertiary sedimentary cover, and was followed by mining of gold-rich quartz veins until the beginning of World War II, though this was never large-scale (Hausel 1991). The estimated gold production from the SPGB is estimated by Hausel (1991) to be 348,600 oz, but actual tonnage is unknown because of lack of adequate historical records. Additional exploration reveal as yet unknown ore shoots. The source of the auriferous fluids that formed the deposits is important to understanding lode deposit genesis in the area.

The deposits within the SPGB have been classified as typical orogenic gold, based on their setting, mineralogy and structural control (McGowan 1990). Orogenic gold deposits are common in Archean cratons, although the deposits in the SPGB are found dominantly within turbidite sequences rather than in the globally more usual volcanic sequence hosts (McGowan 1990). A widely cited model detailed by Groves (2003) suggests that orogenic gold deposits form at convergent margins during the later part of the deformational history with a strong structural control of ore deposition. Conditions of formation vary between deposits with ranges in metamorphic facies, host rock type, and mineralization style. Typical mineral associations are Au-Ag±As±B±Bi±Sb±Te±W, and typical ore forming fluids are low salinity, near neutral pH, aqueous fluids with CO_2, CH_4 and N_2.

The origin for hydrothermal and auriferous fluids in these types of systems has long been in debate. Three broad classes of models have been proposed to explain the origin of such ore-bearing fluids: fluids exsolved from a crystallizing magma (Burrows et al. 1986; Ramsay et al. 1998), metamorphic devolatilization (Kerrich and Fyfe 1981; Goldfarb et al. 1998), and deep circulating meteoric waters (Nesbitt 1988; Nesbitt and Muehlenbach 1991). In order to determine the validity of the model that proposes fluid exsolution from granitic bodies, this study focuses on the adjacent Louis Lake Batholith (LLB) and within this batholith on its late phases (i.e. aplites, pegmatites, and quartz veins).

As described in more detail in the following chapter, the Louis Lake Batholith is a 2629.2 ± 2.8 Ma granitic to granodioritic polyphase intrusion that makes up the southernmost end of the Wind River Range (Frost et al 1998). The LLB intrudes the SPGB along the northern margin of the greenstone belt and is also in fault contact along the Anderson Ridge Fault. In order for this study of a link between orogenic gold mineralization and the LLB to be a valid test of the crystallizing magma model of gold deposits, we need to ensure overlap in age. The youngest formation found in the SPGB yields a depositional age of 2669 ± 4 Ma based on U-Pb dating of zircon, and a metamorphism age from titanite of 2635 ± 2 Ma (Frost et al. 2006). Titanites dated from the alteration zone of one of the gold-bearing veins yielded an age of mineralization between 2635 ± 2 and 2616 ± 2 Ma (Frost et al. 2006). The age of the LLB and the abundance of crosscutting late phases of the granite and similarity in age to the mineralization provide evidence to allow a relationship between granite intrusion and mineralization.

This study utilizes a multidisciplinary approach of field observations, petrographic observations, fluid inclusion studies, and mineral chemistry to characterize the granite. Field work involved mapping contacts and noting large-scale textures and crosscutting relationships. Samples of granite, late-phase intrusions, altered granite, mafic enclaves, and granitic gneiss were collected and analyzed. Detailed petrographic descriptions were made for the samples. Whole rock, trace element and rare earth chemistry were completed on samples of the main granite and late phase dikes. Analysis of hornblendes and oxides were completed in order to determine the conditions within the batholith at the time of crystallization. Fluid inclusions from quartz within pegmatites, quartz veins, and quartz segregations were analyzed to determine fluid chemistry at the time of late phase movement in the batholith. Fluid inclusions were analyzed petrographically, microthermometrically, and using laser ablation inductively coupled plasma mass spectrometry (LA-ICP-MS).

Using the geochemical information from the LLB, it is possible to create a history of the crystallization of the batholith and to characterize the granite. It is also possible to compare the main and late phase fluid chemistries of the LLB with characteristics of orogenic gold deposits worldwide and with fluids of other common ore deposit types. By comparing these fluids, it is possible to note any similarities between fluids, and the potential of a LLB fluid source for the lode deposits of the SPGB.

2. REGIONAL GEOLOGY

2.1 GEOLOGY OF THE WYOMING PROVINCE

The Wyoming Craton is a piece of Archean age crust that composes ten percent of the outcrop within the Wyoming Province (Frost 2006). It is the most southwestern of the North American Archean provinces, was cratonized by 3.0 Ga (Frost et al 1998), and likely correlates with the pre-granite rocks of the Superior Province (Bayley 1973). The province is bounded by the Great Falls tectonic zone, the Trans-Hudson orogen, and the Cheyenne Belt, making it approximately 500,000 km^2 (Mueller and Frost 2006). Precambrian crust is only exposed within Laramide Orogeny uplifts (Frost et al 2006). McGowan (1991) noted that the Wyoming Craton is composed of three exposed Archean rock types: early quartzofeldspathic gneisses, metamorphosed supracrustal rocks, and late Archean granites. The Wyoming Province most likely grew by incorporation of mantle-derived melts into large granitic bodies, as there is only minor evidence of laterally accreted juvenile crust, and abundant evidence for copious amounts of Archean magmatism (Frost 1998).

The field area is located in the Wind River Range, a part of the Wyoming Craton, which is composed of Archean granites and minor supracrustal rocks that were uplifted during the Laramide Orogeny at approximately 60 Ma (Frost et al 1998). Major movement in the range was along the Wind River Thrust on the western side of the range. The Wind River Thrust is a northwest trending, northeast dipping structure that brought up 10,000 km^2 of Precambrian crust (Frost 1998). Bayley (1973) notes that the maximum displacement along the Wind River Thrust is 10.7 km, making it the largest offsetting Laramide structure in Wyoming (Wilks and Harper 1997).

The range was first explored by groups focusing on mineralization in the area (i.e. Hayden in 1871; Raymond in 1879 and 1873; Aughley in 1886; and others). The first geologic map was created in 1901, but it also focused mainly on mineralized areas (Ulmo 1979). The first detailed maps of the South Pass area were created much later by Bayley (1965). Figure 1.1 shows a map of the Wind River Range, including the field area and the outline of the Louis Lake Batholith.

2.2 THE SOUTH PASS SEQUENCE

The South Pass Greenstone Belt, or SPGB, is a series of steeply dipping Archean supracrustal metasediments and metavolcanics that lie about 30 miles south of Lander, Wyoming. These metamorphic rocks are mostly amphibolite facies, but with some greenschist facies rocks. The approximately 26.5 km wide SPGB is bounded on the north and east by Archean granites. Frost et al (2006) have defined the metavolcanics of the sequence to be komatiitic to tholeiitic and containing calc-alkalic basalt to andesite, dacite and rhyolite. Previous geochemistry by McGowan (1991) tells us that amphibolites of the SPGB are LREE enriched compared to other Archean terranes, indicating an evolved magma source. Condie (1972) proposed that the SPGB is the result of 2 colliding volcanic arcs. The potential presence of a dismembered ophiolite in the SPGB has been used to infer a volcanic arc setting (Harper 1985), but the presence of an ophiolite is dismissed by others (i.e. Schmitz 2005). Geochemical analysis of the mafic rocks is consistent with a Mid-Ocean Ridge Basalt to Island Arc Tholeiite composition (Harper 1985). Overall REE patterns suggest a thick lithosphere during the Archean (McGowan 1991). Gravity data by Balsam (1986) suggests that the SPGB is currently up to 5 km thick.

The South Pass Sequence has been divided into four main formations, interpreted to represent a volcanic arc. These formations are the Diamond Springs Formation, Goldman Meadows Formation, the Roundtop Mountain Greenstone Formation and the Miners Delight Formation.

The oldest formation, the Diamond Springs Formation, was first mapped by Hausel (1991), and is not part of the original stratigraphy of Bayley et al (1973). The formation is dominated by serpentinite, tremolite-talc-chlorite schist and amphibolite (Hausel 1991). Hausel (1991) believed that these rocks represent high Mg flows and sills. Harper (1985) believed that these rocks represented an ophiolite, giving evidence of cumulate textures, igneous layering, relict diabasic textures, and chilled margins. Hausel (1991) interpreted these same rocks as simply komatiitic and mafic flows.

The Goldman Meadows Formation, which overlies the Diamond Springs Formation, is composed of quartzite, banded iron formation, pelitic schist and amphibolite (Hausel 1991). These units represent a shallow shelf environment that was interrupted by volcanism (Hausel 1991). Ironstone within this formation has been folded and thickened at Iron Mountain to create an iron deposit that has been historically mined. Iron content of the quartz-magnetite formations at the Atlantic City Iron Mine is 33.5% according to Hausel (1991).

Above the Goldman Meadows Formation lies the Roundtop Mountain Greenstone. This greenstone consists mostly of chlorite, actinolite, epidote, and minor apatite (Hausel 1991). The Roundtop Mountain Greenstone Formation has been defined by Balsam (1986) as a metabasalt with pillow structures. Hausel (1991) believed that these are oceanic basalts with interlayered tuffs, which implies intermittent volcanic activity.

The Miners Delight Formation makes up most of the SPGB. The contact with the Roundtop Mountain Greenstone is the Roundtop Mountain Fault, which defines the Roundtop Mountain Deformation Zone (RMDZ). This formation has been down-dropped along the RMDZ relative to the other formations (McGowan 1991). It is primarily a series of poorly-sorted greywackes that are noted by Balsam (1986) to be turbidites based on the presence of graded bedding. The feldspathic to biotitic greywackes are interbedded with mica schist (Hausel 1991), and likely accumulated in a deep oceanic basin from sediments shed off an island arc (Hausel 1991). This formation also hosts most of the lode gold deposits in the SPGB. Metamorphism of this formation was dated at 2635 ± 2 Ma by Frost et al. (2006).

The formations of the SPGB have been cut by seven episodes of igneous activity according to Bayley (1973). The oldest igneous intrusion is a serpentinite, which has been found only in the Goldman Meadows Formation (Bayley 1973). This was followed intrusion of metagabbro dikes and sills, common in the northeast SPGB and in the frontal gneisses of the LLB (Bayley 1973). Next, metadiorite dikes or sills were emplaced at Peabody Ridge (Bayley 1973). Metaleucodacite and metatonalite dikes and small sills were the emplaced after the metadiorite (Bayley 1973), and exist as two dikes and a few small stocks. More metagabbro dikes were then injected into the SPGB (Bayley 1973). Felsic magmatism caused the formation of the LLB and segregations and other small satellite plutons (Bayley 1973). Lastly, diabase dikes cut both the SPGB and the LLB around 2170 ± 8 Ma (Harlan et al. 2003).

Several studies have been completed on these rocks to determine structural history on this complex set of rocks. Frost et al (2000) described five deformations and four metamorphism events for the Wind River Range. These events include the emplacement of the Bridger and Louis Lake Batholith and deformation of the SPGB and granites and granitic gneisses of the range. Bayley (1973) noted that the SPGB is inferred to be part of a synclinorium that was formed before the intrusion of the LLB. Schmidtz (2005) recorded three episodes of deformation within this package, which are related to the intrusion of the LLB and consequent solid-state deformation. One of the major structures in the area is the Roundtop Mountain Deformation Zone (RMDZ). It separates the Roundtop Mountain and Miner's Delight Formations. After the magmatism and accretion of the SPGB, there was very little deformation or tectonism until the Laramide Orogeny (Cretaceous to Eocene). Tilting during Laramide deformation resulted in an increase in paleodepth from east to west (McGowan 1991) and created a number of brittle faults.

2.3 MINERALIZATION WITHIN THE SPGB

The SPGB contains deposits of several significant mineral resources. Gold ore is found in lodes and as placer deposits in Tertiary cover. Copper ore is found as minor lodes and stockworks (Hausel 1991). Iron ore is found within structurally thickened sections of banded iron formation (Hausel 1991). Other mineralization includes silver, tungsten as scheelite veins and placers, uranium, asbestos, and pegmatite minerals such as tourmaline, beryl, and aquamarine (Hausel 1991).

Placer deposits played a major role in the discovery of gold in the district. The original gold discovery occurred in 1863 in the Dickie Springs-Oregon Gulch area within Tertiary conglomerates (Hausel 1991). By 1867, the Carissa Lode was discovered, launching a minor gold rush (Bayley 1973). During the boom from 1867 to 1875, small mines produced an estimated 348,600 oz of ore from shears and veins hosted in a range of rock types of the SPGB and from placer deposits (Hausel 1991; Bayley 1973). The shear zones are narrow (around five feet thick), have a tendency to pinch and swell, and contain veins that are mostly quartz + carbonate (Hausel 1991). The veins and shears are steeply dipping and older than the major faults of the area (Bayley 1973). Gold mineralization is mostly restricted to units within the Miner's Delight Formation, usually near sill-like metagabbro and other weak contacts, which would have acted as conduits for gold-bearing fluids (Bayley 1973). Gold associated with the quartz veins is found within the shears and adjacent wallrock (Hausel 1991). The most productive veins are typically two to seven feet thick, and thicker veins have lower concentrations of gold. Wallrock alteration is minor, and contains the assemblage sericite + quartz with accessory calcite, chlorite and tourmaline (Hausel 1991). Pyrrhotite, pyrite, and arsenopyrite are present with the gold (Hausel 1991). Deposition of the gold is thought to have been the result of increases in fluid pH and decreases in oxygen fugacity as the fluid advected along shear zones (Hausel 1991). Frost et al (2006) date mineralization at the Carissa lode to be between 2635 and 2616 Ma.

Gold is found within the paleoplacers in the Dickie Springs-Oregon Buttes area and in the McGraw Flats area. Tertiary erosion of the rocks uplifted during the Laramide Orogeny produced fanglomerates and fluvial conglomerates which contain gold (Hausel 1991). These paleoplacer deposits have also been eroded to form concentrated gold placer deposits. The Dickie-Spring-Oregon Buttes area lies in the southern part of the SPGB. The highest Au concentrations in this area are found north of the Continental Fault, a boundary fault at the south end of the Wind River Range, which has been down-dropped since the initial uplift during the Laramide Orogeny (Hausel 1991). The placer deposits in this area are found within the conglomeratic units of the Eocene Wasatch Formation, and Tertiary rocks eroded from it (Hausel 1991). Gold content of the placer deposits may be as much as 28.5 million oz (Love et al. 1978). The Twin Creek paleoplacers are found within the White River Formation to the northeast of the SPGB (Hausel 1991). According to Antweiler et al (1980), the probability is high that these paleoplacers represent a rich, undiscovered source area.

Gold ore in the placer deposits in the Dickie Springs area was studied by Love et al. (1978), who found two different chemical signatures among the gold grains. This points to two different sources of gold ore. Love et al. (1978) note the abundance of large granite boulders, indicating that one source may be from a granitic source proximal to the conglomerate. Also, geochemical studies of the gold grains suggest that it is derived from a source other than the South Pass-Atlantic City District (Hausel 1991). Some grains are interpreted to have been eroded from the lode gold deposits of the SPGB because of geochemical similarities (Love et al. 1978).

Minor cupriferous lodes and stockworks have been noted by Hausel (1991). These veins are narrow, discordant quartz veins that pinch and swell, and occur as stockworks in felsic gneiss and along the LLB border (Hausel 1991). Copper mineralization is found as chalcopyrite-bearing quartz veins containing silver and gold, and in places displacing auriferous shears, meaning that copper mineralization post-dates the Au-bearing shears (Hausel 1991). Hausel (1991) believes that these cupriferous veins are related to the LLB, noting high concentrations of Cu-bearing veins near the edge of the batholith, a Cu-bearing shear in LLB at Burnt Meadow prospect, and a Cu stockwork located along margin of LLB near northwestern edge of SPGB.

Banded Iron Formation (BIF) was mined in the Atlantic City mine by U.S. Steel Corporation from 1962-1983, producing 90 million tons of ore (Hausel 1991). The iron formation has been structurally thickened by folding on the northern border of the SPGB at Iron Mountain (Hausel 1991). This iron-bearing unit of the Goldman Meadows Formation, or taconite, is composed mostly of thin layers of fine-grained, interbedded magnetite and quartz (Hausel 1991). Minor amounts of amphibole, chlorite and garnet are also found within this BIF (Bayley 1973).

The Archean rocks of the Wyoming Province usually are cited as sources for sedimentary uranium deposits, i.e. Granite Mountains. The Wind River Range, although of a similar age, does not have uranium deposits associated with it (Stuckless 1989).

2.4 ARCHEAN GRANITES AND GRANITIC GNEISSES OF THE WIND RIVER MOUNTAINS

The high peaks of the Wind River Range are composed of granites and granitic gneisses. These granites are in tectonic contact and intrusive contact with the South Pass

Greenstone Belt to the south, are unconformably overlain by Paleozoic and Mesozoic sedimentary rocks to the east, and nearly flat-lying Tertiary sediments to the west (Bayley 1973). Some of the youngest granites, the Sweetwater granite, South Pass pluton, and Bears Ears pluton, intrude into the SPGB as small, satellite plutons. The rocks of the range represent at least four periods of potassic calc-alkaline magmatism dated at approximately 2.8, 2.67, 2.63 and 2.55 Ga (Frost et al 1998). Each of these granites is believed to be derived by re-melting of pre-existing continental crust (Frost et al 1998).

The northeast part of the range is composed of the foliated quartzofeldspathic gneisses of the Washakie Block (> 2.8 Ga) (Frost et al 1998). The Washakie Block is bounded on the southwest by the Mount Helen Structural Belt, intruded on the northwest by migmatitic gneisses such as the Native Lake Gneiss, and on the southeast by the Bears Ears Pluton (Frost et al 1998). The Native Lake Gneiss is a migmatitic unit that cuts the fabric of the banded grey gneisses, and was dated at 2.8 Ga (Frost et al. 1998). At 2.67 Ga, the Bridger Batholith was emplaced as a dominantly granodioritic body with a faint foliation parallel to the Mount Helen Structural Belt (Frost et al 1998). The Louis Lake Batholith was subsequently emplaced at 2.63 Ga, with sharp contacts with the older rocks (Frost et al 1998). Late Archean batholiths were emplaced at 2.55 Ga, and include the Bears Ears Pluton in the center of the range, the Middle Mountain Batholith in the northern part of the range and the South Pass pluton and Sweetwater granite in the south (Frost et al 1998). In Figure 1.1, the South Pass pluton and Sweetwater granite are combined with the LLB and SPGB. The Sweetwater granite and South Pass pluton intrude into the northern part of SPGB (Frost et al 1998). The granites are geochemically similar to each other in that they all are LREE-enriched and most have a small to moderate negative Eu anomaly (Frost et al 1998). Each of the granites can be distinguished from each other by the concentration of SiO_2 and the level of alumina saturation (Frost et al 1998).

The deformed intrusive contact zone (Figure 1.1) between the SPGB and the Louis Lake Batholith to the north is composed of felsic gneiss with enclaves of amphibolite, tonalite, and ultramafics (Hausel 1991). This zone is composed of leucogranite gneiss and banded migmatitic gneiss, which is mylonitic with porphyroblasts of feldspar (Schmitz 2006). This felsic gneiss is enriched in Si and Al and depleted in Na compared to with the LLB and according to Hausel (1991) is therefore not related to the LLB. Isotopic signatures of the felsic gneiss infer an older origin, unrelated to the LLB (Hausel 1991). The gneiss is up to 1.7 km thick, and it only found along the contact with the SPGB (Plate A). The amphibolite enclaves of the gneisses are enriched in TiO_2 relative to MORB (Hausel 1991). McGowan (1991) dated these quartzofeldspathic gneisses at 2.8 to 3.0 Ga and believed these represent a protocontinental slice and basement to the SPGB.

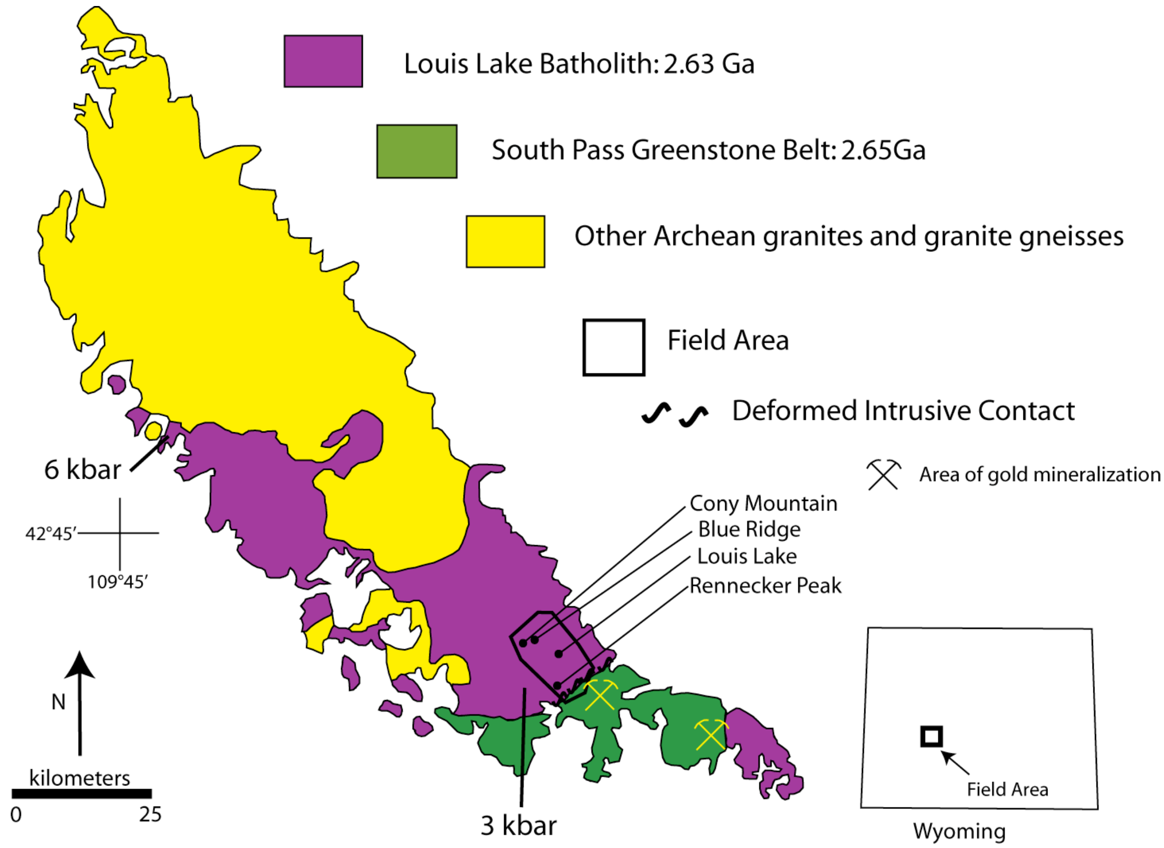

Figure 1.1: Map showing the rock types of the Wind River Range, gold mineralization, and field area, after Frost et al (2000).

3. LOUIS LAKE BATHOLITH

Original geological studies in the Wind River area were completed to better define the mineralized area to the south. It was not until later that work focused on the LLB. The LLB has been studied by several authors, but the first most complete descriptions are by Bayley (1965) and Bayley et al. (1973). They described the LLB as a uniform granodiorite with a minor foliation (Bayley et al. 1973). Bayley et al. (1973) also completed a geochemical study of the LLB and its differentiates to characterize the intrusions. Other works focused on better characterizing the LLB (Lo 1970; Stuckless 1985; Cheang et al. 1986; Hull 1988; Frost et al. 1998; Frost et al. 2000). Naylor et al (1970) were the first to name and date the LLB yielding an age of 2642 ± 13 Ma using U-Pb analyses of zircon, and subsequently the LLB has been consistently dated to 2629.2 ± 2.8 Ma, 2629.5 ± 1.5 Ma, and 2618.9 ± 1.5 Ma using U-Pb analyses of zircon (Frost et al 1998). Stuckless (1989) found that LLB did not evolve in distinct stages, but rather as chemically similar inputs of magma. Recent isotopic studies by Frost et al (2006) found that the LLB is a continental arc batholith composed of magmas that assimilated crust of the Wyoming Province.

This study focuses on the southern portion on the LLB. The southern end of the batholith is of special interest because this portion of the batholith represents a structurally higher level than that of the northern end. Tilting likely occurred during the Laramide Orogeny, but may have occurred earlier (Frost et al. 2000). Frost et al (1998) found that the pyroxene-bearing portions in the northwestern portions of the batholith were deepest structurally by using hornblende geobarometry. Frost et al (2000) determined the conditions of contact metamorphism from the Louis Lake Batholith to be about 3 kb and temperatures greater than 700°C in the south and 6 kb and 800°C in the north (Figure 2.1). This means that the southern end of the batholith is likely at a level at which late, hydrous, silicate fluids accumulated and were released.

Samples throughout the LLB were collected from all phases (all textural and compositional components in the batholith) of the LLB, a sample of mafic enclave, amphibolite, and granitic gneiss. Analysis of the samples included petrographic and geochemical techniques. This study included geochemical analysis of the LLB rocks, mineral chemistry, and fluid inclusion analysis of hydrous silicate late phases, which had not been previously completed by others. The descriptions below are based on observations from field work and chemical analyses completed for this study.

3.1 FIELD RELATIONS

3.1.1 Granodiorite

The LLB crops out in an area over 2000 km^2, making it the largest granitic body in the Wind River Range (Frost et al 2000b). It intruded contemporaneously with batholiths found across the southern portion of the Wyoming province, including granites within the Granite and Laramie Mountains (Frost 1998). The batholith intruded into the SPGB, the Bridger Batholith and the magmatic gneisses of the Washakie block at 2.63 Ga (Frost et al. 1998). The later Archean Bears Ears Batholith and other plutons intruded the LLB at around 2.55 Ga (Frost et al. 2000). Intrusion of the LLB resulted in amphibolite-grade metamorphism at the contact with the SPGB and granulite-facies metamorphism with the gneisses to the north (Frost et al. 2000). Frost et al (2000b) described charnockites from the northern part of the LLB, but this is outside the field area. Frost et al (2000b) found that the LLB is gradational from granite to granodiorite, which is why their map of the batholith differs from Worl et al (1986), who mapped the batholith as two separate phases.

Field work confirmed that the main phase of the LLB is mostly granodioritic, but varies in composition from granodiorite to granite .The granodiorite is predominately medium grained and equigranular, but is porphyritic in several locations. Biotite and hornblende grains create a faint foliation that is strongest near and subparallel to the contact with the SPGB. Further from the contact, the foliation becomes less obvious and more randomly oriented, but still creates a sheeting effect when the granodiorite is weathered along foliation. There were multiple phases present within the magma chamber. Mafic enclaves are present as evidence for multiple phases (Figure 3.1). Mafic enclaves are elongate and flattened and are found throughout the batholith. Concentrations of magnetite along the rim of the enclaves are interpreted as evidence of possible assimilation of a mafic magma. Schlieren represent smeared concentrations of mafics that may be the remnants of enclaves. Xenoliths of the schists of the SPGB are found within the granodiorite (Figure 3.1). Numerous felsic dikes, ranging from granitic dikes to aplites and pegmatites, cut the main phase of the batholith. The area is also cut by a younger, northeast to east striking Proterozoic diabase dike swarm with an age of 2170 ± 8 Ma (Hausel 1991). These phases will be described in more detail in the following sections.

The majority of the batholith has experienced little internal deformation since crystallization. Based on the lack of major post-Archean deformation, Schmitz (2005) concluded that most of the deformation experienced by the batholith is syn-intrusion and not related to later regional tectonic events. Thin epidote veins are found scattered throughout the batholith, but with no clear areas of concentration. Epidote veins are attributed to retrograde metamorphism and late brittle faulting. These veins are typically less than 3 cm wide and exhibit only minor alteration of the wallrock.

There is rare evidence of mineralization within the batholith. Hematite mineralization is present as hematite-quartz veins and within a shear zone 1.1km southeast of Louis Lake (Plate A). These hematite-quartz veins are found scattered in the batholith and have been noted by previous mappers west of the field area in the Popo Agie Wilderness Area. While completing field work, small hand dug pits where found, exposing the quartz-hematite veins near Louis Lake, indicating that they have been prospected in the past. Similar prospect pits were noted south of Christina Lake by Pearson et al (1973). Quartz-hematite veins were also noted 0.4 km west of Upper Silas Lake and 0.4km east of Atlantic Peak (Pearson et al. 1971). Pearson et al. (1973) noted minor amounts of copper mineralization 7.5 km southwest of Louis Lake on Rennecker Peak. Placer gold in recent deposits in the northern part of the range is inferred to be reworked from an Eocene paleoplacer, possibly derived from ore zones in the batholith (Pearson et al. 1971). These placers are approximately 50 miles north of the field area. These placers are small and have only been prospected.

3.1.2 Enclaves

Enclaves are found scattered throughout the batholith. They are rounded and are typically a few centimeters in diameter. The most common type of enclave contains hornblende, biotite, magnetite, and plagioclase with accessory apatite. The outer edges of the enclaves have concentrated amounts of magnetite. These rims are less than one centimeter thick and also contain concentrations of titanite. Trace amounts of chalcopyrite can be found within magnetite grains. The enclaves are equigranular, and have been identified as gabbro based on mineralogy and geochemistry.

3.1.3 Later-dikes

The main phase of the granite has been cut by numerous dikes of varying compositions. These include intermediate dikes with sharp contacts with the granodiorite. The lack of chilled margins of the dikes indicates that these dikes were emplaced before significant cooling of the granodiorite magma. The intermediate dikes are finer-grained with a greater abundance of mafic minerals than the host granodiorite. Chemical analysis of these samples gives a dioritic composition. The dikes vary in width from a few centimeters to a meter. These dikes are similar in mineralogy to the granodiorite and contain with biotite, quartz, microcline, plagioclase, titanite and trace amounts of allanite, apatite, chalcopyrite. The dikes are shallow to moderately dipping, and randomly striking.

Fine-grained granitic dikes also cut the granodiorite. They contain quartz, plagioclase, K-feldspar, biotite, magnetite, and titanite with trace apatite and chalcopyrite. They are typically a few centimeters thick, but can be as wide as a meter. The granitic dikes are steeply dipping and randomly striking, like the intermediate dikes.

3.1.4 Aplites

The Louis Lake Batholith contains abundant crosscutting aplite dikes. These vary in width from a few centimeters to a few meters and are found throughout the field area. Some areas, such as Cony Mountain (Fig. 2.1), contain up to 30% aplitic dikes in granodiorite. In the Cony Mountain area, the dikes are typically sheeted. Other areas within the center of the batholith contain rare aplite dikes. Aplites outside the Cony Mountain area are randomly striking and shallow to moderately dipping. The aplites are fine-grained and typically have sharp contacts with the granodiorite and are typically spatially related to pegmatites, but can be isolated (Figure 3.2). In composite dikes, the aplites are found on the outer margins of the dike with a gradation to the coarse pegmatites in the center. They range in color from white to pink, and lack significant mafic minerals, but can contain a few percent of magnetite. They contain quartz, plagioclase, and microcline with trace amounts of biotite, magnetite, and titanite.

3.1.5 Pegmatites

Multiple generations of pegmatites are present, and are in places spatially related to aplites. Some predate the aplites, and others post-date the aplites, implying that there were multiple generations of one or both of the dike types. Pegmatites typically contain coarse-grained quartz and alkali feldspar with trace amounts of magnetite. Quartz is typically clear, but some purple, euhedral quartz has been noted. Pegmatites range in width from a few inches to several feet in thickness. They can be found as composite dikes in some areas, such as Cony Mountain.

3.1.6 Quartz veins and Segregations

Quartz veins cross-cut all the other phases. Clear quartz is the dominant and no milky quartz was found. Quartz veins are typically a few inches in width and undeformed. Although pegmatites and aplites are not as common in some areas of the batholith, quartz segregations can be found throughout the southern area of the batholith. Quartz segregations are irregular shaped pods of vein quartz that form discontinuous lenses. Segregations are rounded, typically a few centimeters in diameter, and composed of only quartz. Lack of alteration or recrystallization surrounding the veins and segregations infers that these features were formed from fluids that were in equilibrium with the granodiorite. These two types of quartz segregations are believed to have formed at the end of crystallization, and samples were taken for fluid inclusion analysis.

3.2 GEOCHEMISTRY OF LLB ROCKS

3.2.1 Previous Geochemical Studies

Previous geochemical studies of the LLB have provided both multi-element and isotope data and have revealed much about the character of the batholith. Stuckless (1989) found the LLB to have lead and strontium compositions that point to a trondhjemitic to tonalitic protolith of Early Archean age. This data was supported by Cheang et al (1986) who found oxygen isotope data to agree with a trondhjemitic to tonalitic protolith. Oxygen isotope data and geochemical data by Cheang et al. (1986) define the granite as being a metaluminous, I-type granite that is not U-enriched (Cheang et al. 1986). Cheang et al. (1986) found that the LLB contains about two percent magnetite pointing toward a high oxygen fugacity during crystallization. Cheang et al (1986) also noted that the LLB has uniform oxygen isotope ratios, which may be attributed to convection within large magma bodies and with the lack of post-crystallization interaction with circulating waters. Wilks (1991) noted that there is a weak linear correlation between major elements and SiO_2 content, implying that fractionation occurred after genesis of the magma. Wilks (1991) noted that this granite has a relatively high Na_2O content. Lo (1970) found Sr and Ni decrease and Ba scatters widely with SiO_2. In this study, major and trace element analyses were completed in this study to better understand the genesis and relations of the phases of the LLB.

3.3 WHOLE ROCK ANALYSES

Chemical analyses of 14 samples of the different components of the LLB (granitic gneiss, aplitic phases, a sample of amphibolite from the greenstone, and a mafic enclave) were completed. These samples were analyzed by ALS Chemex for major element, trace element, and rare earth analyses. The samples were also analyzed for metals such as gold, silver, and molybdenum using the package Complete Characterization (CCP-PKG01) and Au by fire assay and ICP-AES (Au-ICP21). Analyses were done using ICP-AES techniques. Details of the analytical techniques can be found in Appendix 1.

3.3.1 Major Elements

SiO_2 values for the LLB samples ranged from 56 to 75 wt. % SiO_2 with most samples, except for the enclave and a quartz vein, falling between 65 and 75 wt. % SiO_2. The LLB was defined to be calc-alkaline, except for the mafic enclave, which is alkaline. A TAS diagram was created using the geochemistry data (Figure 3.3). This diagram shows three basic groups of samples: main phases, diorite dikes, and the enclave, which falls into the gabbro field. Harker diagrams were created using whole-rock geochemistry and can be found in Figure 3.4. These diagrams show increasing K with differentiation, and decreasing CaO, Al_2O_3, Fe_2O_3, MgO, TiO_2, MnO, and P_2O_5. The flat trend of Na_2O shows that some Na-rich plagioclase was crystallizing, but only in combination with other minerals. BaO increases until about 65 wt % SiO_2, then decreases indicating that K-feldspar was not crystallizing until 65 wt % SiO_2. The decreasing trend of P_2O_5 shows that apatite began crystallizing early in the formation of the batholith. The decreasing trend of TiO_2 shows that a Ti-bearing mineral also began crystallizing early.

3.3.2 Trace Element Analyses

Whole rock geochemistry was also used to create spider diagrams to show trace element characteristics. Most of the samples analyzed show similar patterns (Figure 3.5). A few samples fit outside this trend (e.g. WR-25B and WR-42B). WR-25B is an aplite and WR-42B has pervasive propylitic alteration. It is interpreted that parts of the LLB that were previously mapped as different inputs of magma by others (e.g. Worl et al. 1986) are genetically similar to the main Louis Lake Batholith phase, and are therefore genetically related to each other. The later phases are likely a late differentiate of the main magma pulse, and are not actually a different magma. Aplite WR-25B is interpreted to be an extremely fractionated phase, as is consistent with its REE pattern, see REE Analysis section below.

Harker diagrams were created for some trace elements vs. SiO_2 (Figure 3.6). Rb shows a weak linear correlation with increasing SiO_2. Ce and Zr decreases with increasing SiO_2. Sr shows a scattered distribution. The lack of pattern in SiO_2 vs Cs is inferred to mean that the LLB is not strongly fractionated. There is also a lack of enrichment of Cs at high SiO_2 content.

Anomalously high metal content was noted in the analyzed samples. Elevated copper was observed in the enclave (WR-4A) and a mafic dike (WR-24B). Notable amounts of gold were found in granite (WR-18D), granite surrounding the enclave (WR-4A), aplite dike (WR-28) and a quartz-hematite shear (WR-42B). Although most metals show little or no correlation with SiO_2, Ni and Zn decrease with increasing SiO_2, while Pb increases with increasing SiO_2 (Appendix 2).

3.3.3 Tectonic Setting of Magmatism

Several tectonic discrimination diagrams were created from the analyzed samples. On Rb-Hf-Ta diagrams, most of the samples fall in the volcanic arc field while some fall into the collisional settings (Figure 3.7). The samples that fall outside the others are samples WR-44 (granitic gneiss) and WR-25B (aplite), and hence may not be representative. On a Nb-Y Plot the samples plot mostly within the volcanic arc granitoids and syn-collisional granitoids field and trend toward the Within-plate granitoid field (Figure 3.8). One sample, an aplite (WR-7C), falls in the Ocean-Ridge granitoids. When a Rb vs. Nb+Y diagram is created, the samples fall in Within-plate granitoids, volcanic-arc granitoid, and syn-collisional granitoids (Figure 3.9). One sample falls well below the other points in the Volcanic Arc granitoids. This sample is the propylitically-altered granite with quartz-hematite vein, and is not reprentative of magma composition. Using a combination of all the tectonic discriminant diagrams, the granites of the LLB formed in a volcanic arc setting.

3.3.4 Rare Earth Element Analyses

REE diagrams were also created to compare REE values for the analyzed samples (Figure 3.10). The samples are enriched in LREE and depleted in HREE. Most of the samples have similar rare earth patterns. The samples show a slight to no Eu anomaly. Stuckless (1989) also noted that none of the samples had a positive Eu anomaly. The exception are the mafic enclave (WR-4A2) and an aplite (WR-25B), which have differing REE signatures. The signature of the mafic enclave points toward a separate, more mafic input of magma into the chamber during crystallization or that it formed as an early cumulate, as it has a slight positive Eu anomaly. The aplite REE signature is consistent with extreme fractionation.

3.4 Petrography of LLB rocks

Samples from each rock type were analyzed petrographically using both transmitted and reflected light microscopy. Table 3.1 lists the samples by sample type. Below is a short description of features typical of each rock type. Full descriptions of the thin sections can be found in Appendix 3.

3.4.1 Granodiorite

The dominant major mineral assemblage is quartz-plagioclase-potassium feldspar-biotite, but in some samples hornblende is also present. Orthopyroxene and clinopyroxene have been noted in the northern part of the batholith by Frost et al. (2000b), but none was found within the field area. Minor minerals include magnetite, ilmenite, apatite, and titanite. Trace amounts of zircon are present. Metamict crystals of allanite are also present in some samples. Quartz grains are generally anhedral. In most samples they are equant, but are weakly elongate within a few km of the contact with the SPGB. Serrated grain boundaries on anhedral quartz provide evidence of dynamic recrystallization in some samples. This recrystallization is minor and has left the cores of the grains unaffected (Figure 3.11). Plagioclase grains are subhedral and found both within larger potassium feldspars and as single grains. Plagioclase phenocrysts have been altered in places to sericite. Oligoclase is the dominate plagioclase feldspar. The dominant potassium feldspar is microcline, and is subhedral to anhedral. Crystals of biotite are subhedral and poikiolitic with inclusions of euhedral to subhedral apatite (Figure 3.11). Two varieties of biotite exist in most of the samples, one brown and one green. The two varieties are not intergorwn, but are typically found in clusters together. Foliation of biotite grains is evident only in those samples nearest the contact with the SPGB. Samples further from the contact have more randomly oriented biotite grains. Anhedral hornblende phenocrysts are scattered throughout the batholith, but are typically found clustered in and around mafic enclaves and schlieren. The batholith is has a relatively high magnetic susceptibility and contains euhedral to anhedral grains of magnetite. Most of these grains exhibit exsolution lamellae of ilmenite (Figure 3.11).

Titanite grains are euhedral to anhedral, and are typically found with magnetite. Chalcopyrite was found as 25μm grains within quartz grains in sample WR-3. A 14μm grain of native gold exists in a quartz grain in sample WR-7C.

The sample of granitic gneiss was also analysed. This sample contained quartz-biotite-plagioclase-potassium feldspar-epidote-muscovite and trace titanite. Quartz grains are heavily recrystallized and create the lighter bands of foliation. Porphyroblasts of microcline have inclusions of subhedral plagioclase, which is probably recrystallized. In this sample, biotite grains are partially replaced by muscovite (Figure 3.11). The mica grains create a strong foliation that has been folded. Epidotes are subhedral and found within the mica bands. Titanites are anhedral and also found in the mica bands. The granitic gneiss is found along the contact with the SPGB and is interpreted to be an earlier intrusion.

3.4.2 Enclaves

The mafic enclaves contain hornblende, biotite, magnetite, plagioclase, apatite, and trace chalcopyrite. Subhedral to anhedral hornblende and biotite make up the bulk of the enclave. Biotite and hornblende are coarser on the edge of the enclave than the center. Plagioclase is subhedral to anhedral and has minor sericite alteration. Magnetites are subhedral with ilmenite exsolution and are concentrated along the edge of the enclave. Apatite is found as abundant acicular inclusions in hornblende, biotite, and plagioclase. Chalcopyrite is found within magnetite grains and quartz grains (Figure 3.11).

3.4.3 Later Archean Dikes

Three late-phase dikes were analyzed. Two of these represent dikes with similar assemblages to the batholith, WR-18A and WR-18C, while WR-20A is more intermediate in composition. Sample WR-18C contains the assemblage quartz-K-feldspar-plagioclase-biotite-magnetite-titanite and trace allanite and chalcopyrite. Quartz is anhedral and shows little recrystallization. Plagioclase is subhedral with minor sericite alteration and patchy myrmekitic intergrowths. Biotites are anhedral, brown to green, and altered. Magnetites are subhedral with ilmenite exsolution. Titanites are subhedral to anhedral and found with magnetite grains. Allanite is metamict. Apatites are zoned, which is expressed as differences in birefringence, when in proximity to allanite. Rare grains of chalcopyrite about 22μm in size are found within quartz crystals. WR-18A is a granodioritic dike that contains plagioclase-quartz-K-feldspar- biotite-titanite-magnetite-apatite and trace chalcopyrite. This sample is similar to WR-20A, and like WR-18C it contains chalcopyrite in quartz grains. Sample WR-20A is a tonalite dike that contains the assemblage plagioclase-quartz-biotite-hornblende-apatite. Apatite inclusions are found within subhedral plagioclase and biotite. Quartz grains are subhedral to anhedral with little recrystallization. Hornblendes are subhedral to anhedral and contain inclusions of apatite, biotite and quartz.

3.4.4 Aplites

The five samples of aplite have varying amounts of plagioclase, quartz, K-feldspar, biotite, and magnetite. Plagioclase is subhedral and exhibits minor sericite alteration and patches of myrmekitic intergrowths. Quartz is anhedral and has weak undulose extinction. K-feldspar grains contain inclusions of plagioclase. Biotite is typically green and found near magnetite grains. Magnetite exhibits ilmenite exsolution. Titanite and metamict allanite are rare accessory minerals. Sample WR-25B was petrographically similar to the other samples, though the geochemical signature was extremely fractionated.

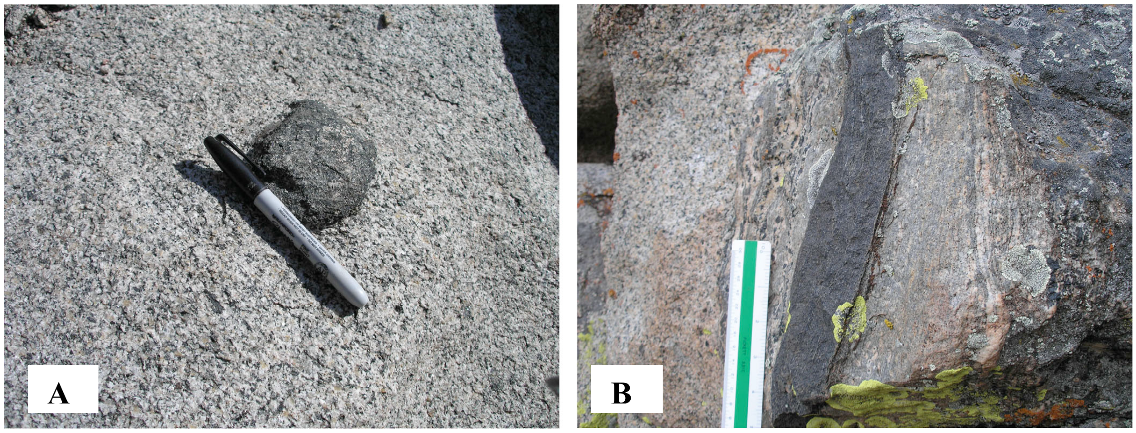

Figure 3.1: Photographs showing A) Typical mafic enclave found in the interior of the batholith along Blue Ridge; B) Xenolith of schist found southeast of Louis Lake

Figure 3.2: Layered pegmatite and aplite found along Blue Ridge

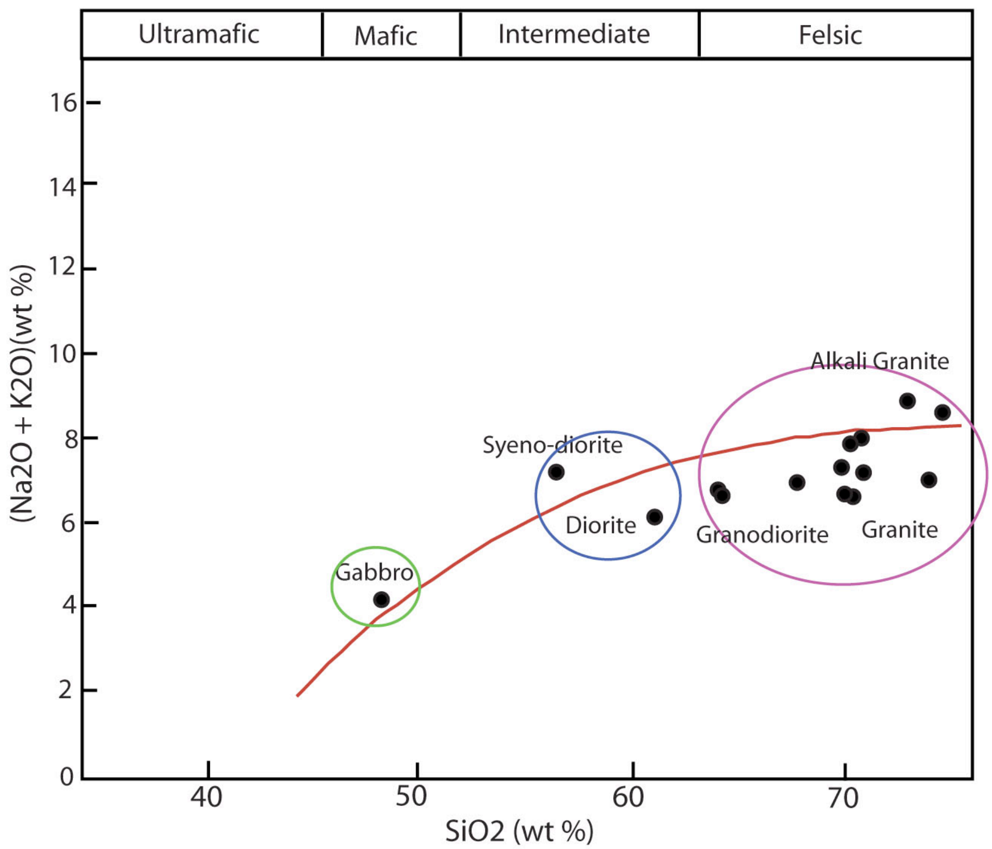

Figure 3.3: TAS Diagram showing the three main groups analyzed. Pink = main phases; Blue = later intermediate dikes; and Green = mafic enclave. The curved line separates the alkalic and subalkalic fields for plutonic rocks.

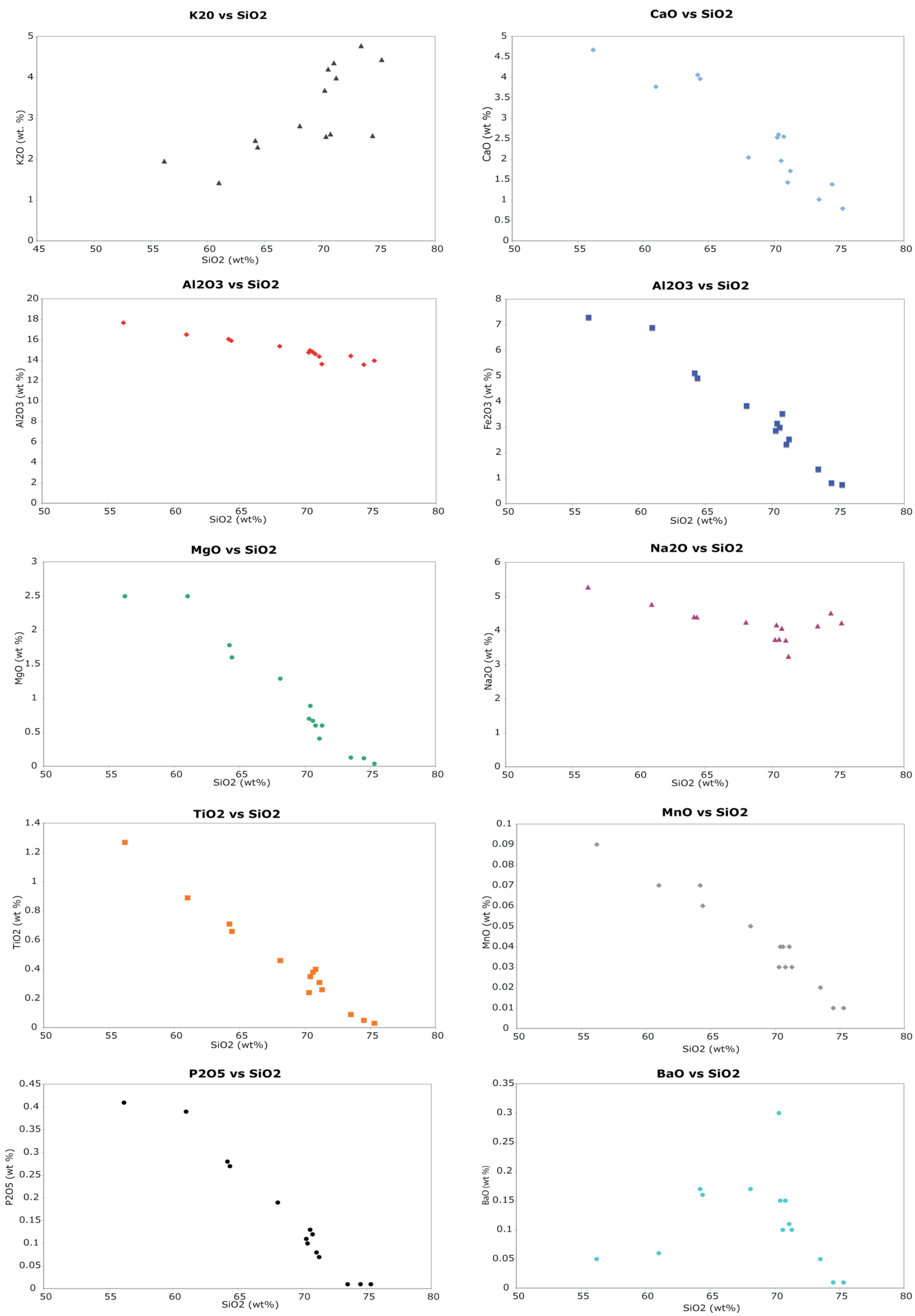

Figure 3.4: Harker diagrams of major elements for analyzed samples.

Figure 3.5: Spider Diagram of trace element vs chrondritic meteorite (Taylor and McLennan, 1985)

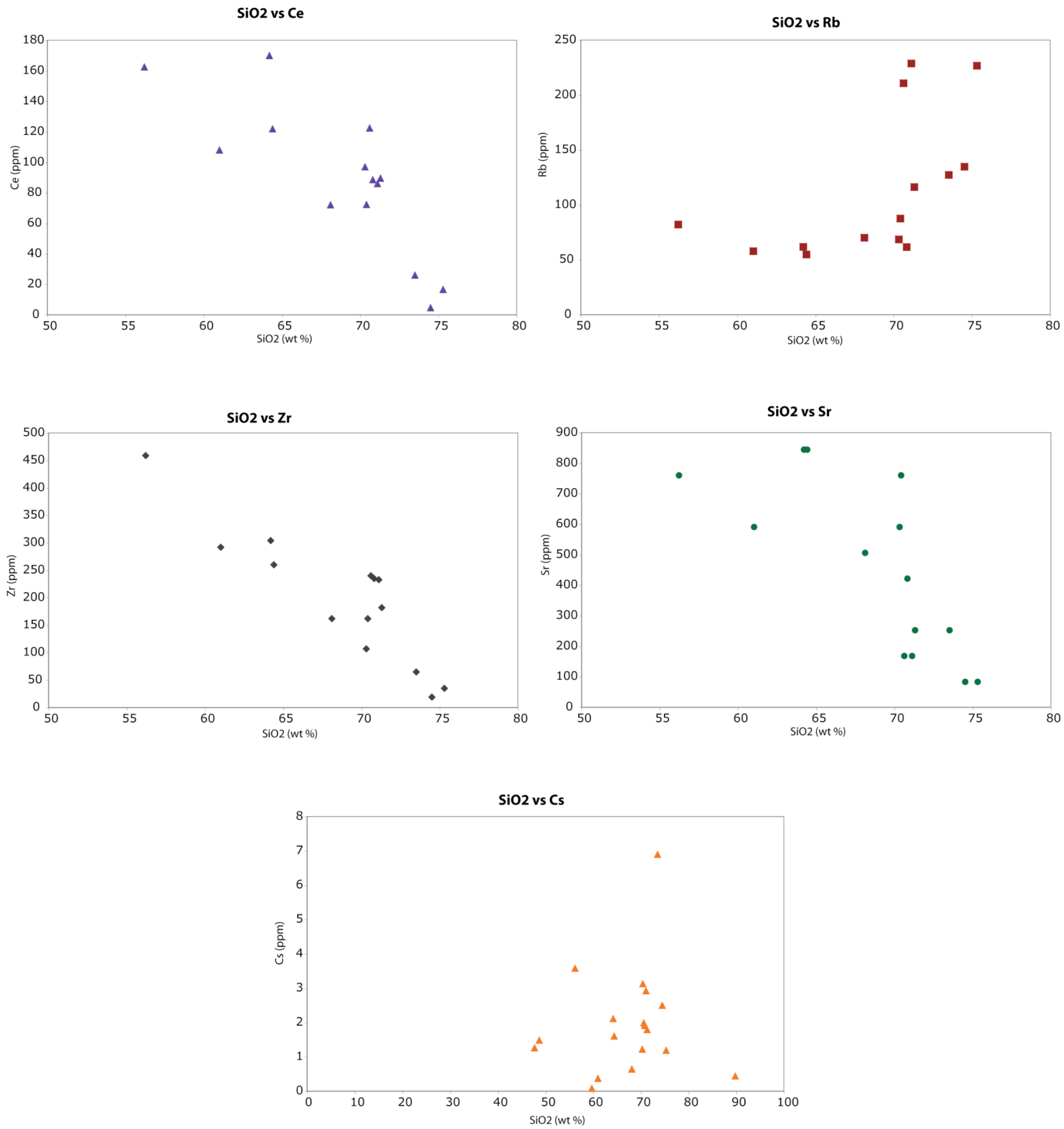

Figure 3.6: Harker Diagrams showing the trends between some trace elements and SiO_2.

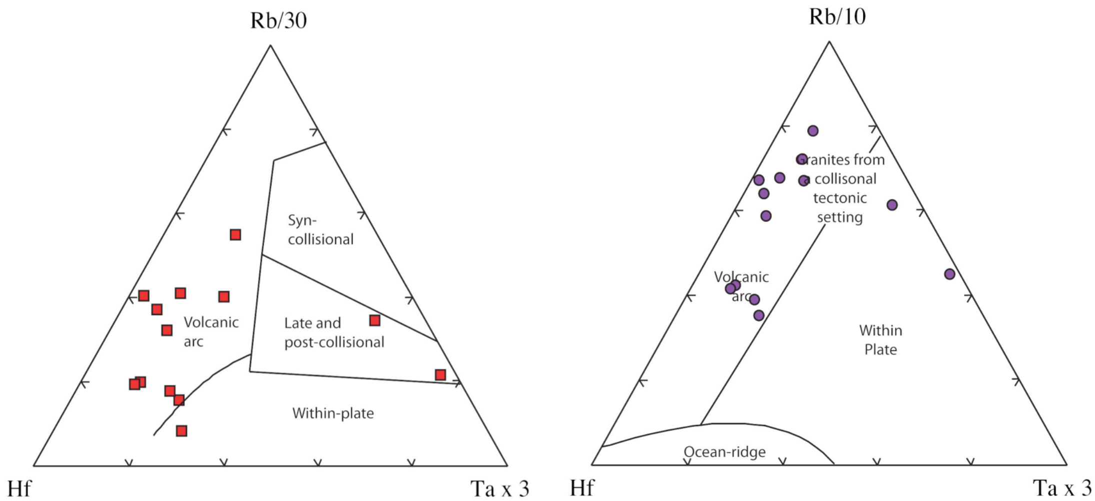

Figure 3.7: Ternary Plots of Rb/30-Hf-Ta x 3 and Rb/10-Hf-Ta x 3 giving tectonic environment (after Harris et al., 1986).

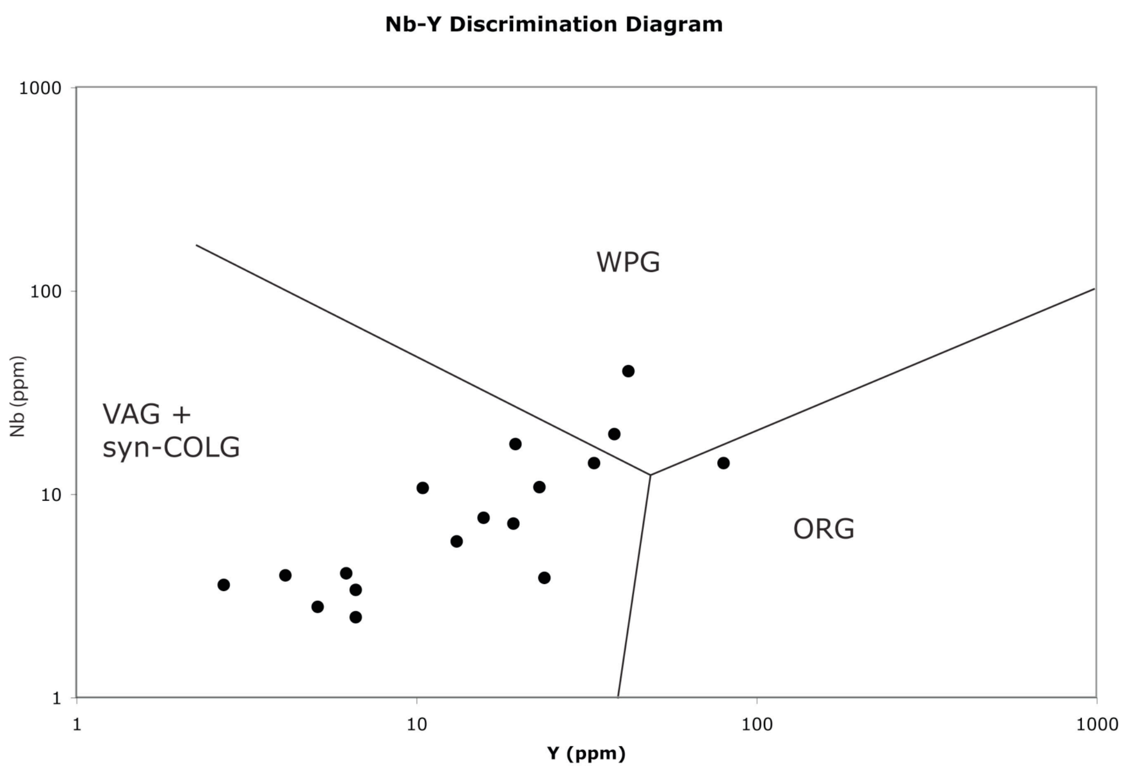

Figure 3.8: Nb-Y Discrimination Diagram for granites after Pierce et al. (1984). VAG = Volcanic Arc granitoids; WPG = Within Plate granitoids; ORG = Orogenic Granitoids; syn-COLG = Syn-collisional granitoids.

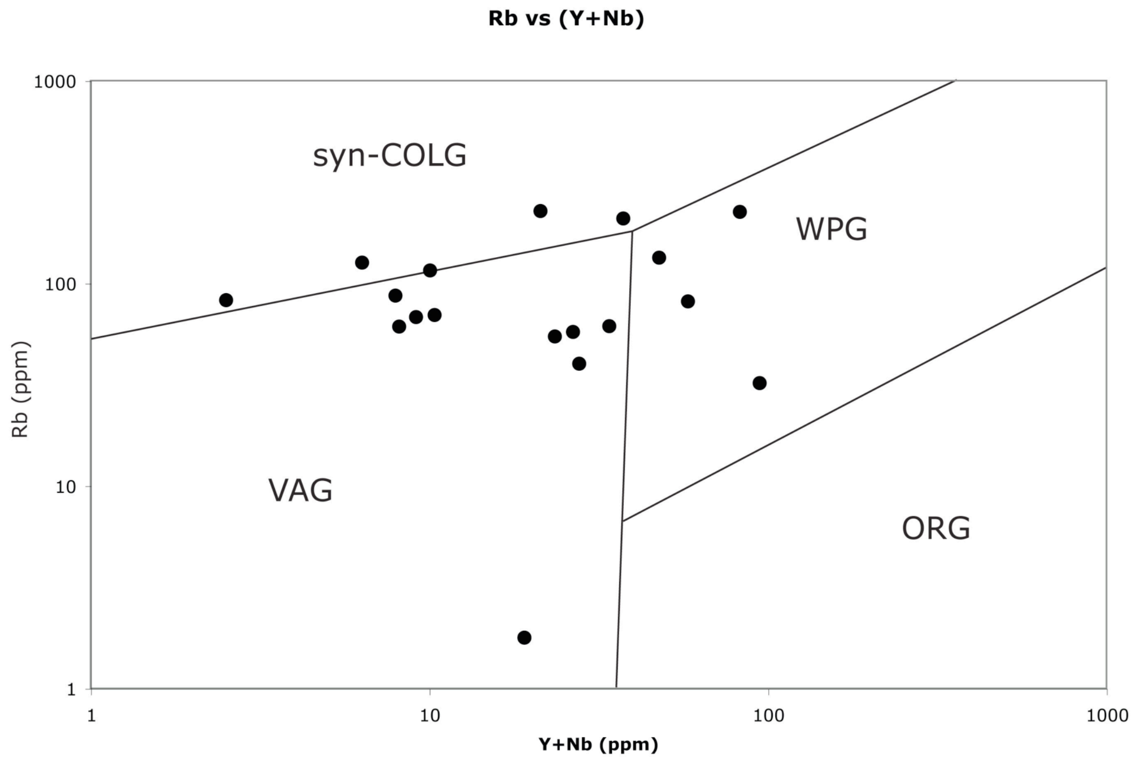

Figure 3.9: Rb vs (Y + Nb) Tectonic discrimination diagram for granites after Pierce et al. (1984). VAG = Volcanic Arc granitoid; ORG = Orogenic granitoids; WPG = Within Plate granitoids; and syn-COLG = syn-collision granitoids.

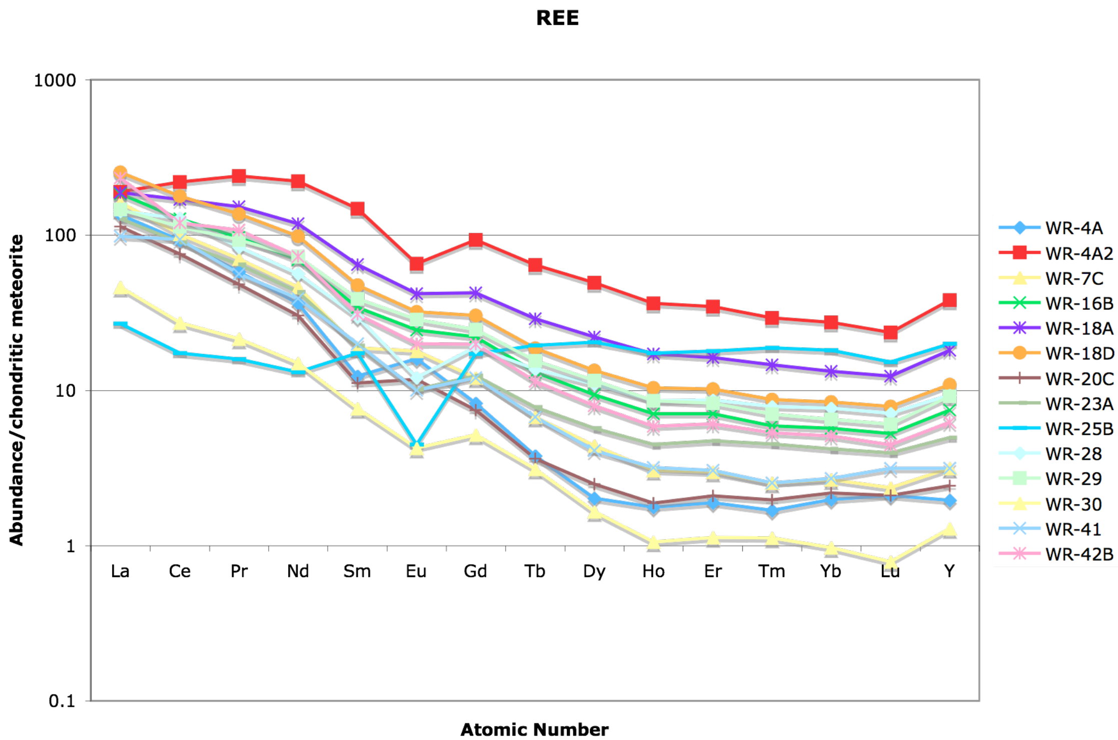

Figure 3.10: Rare Earth Diagram showing REE compared to chondrite norm of Taylor and McLennan (1985).

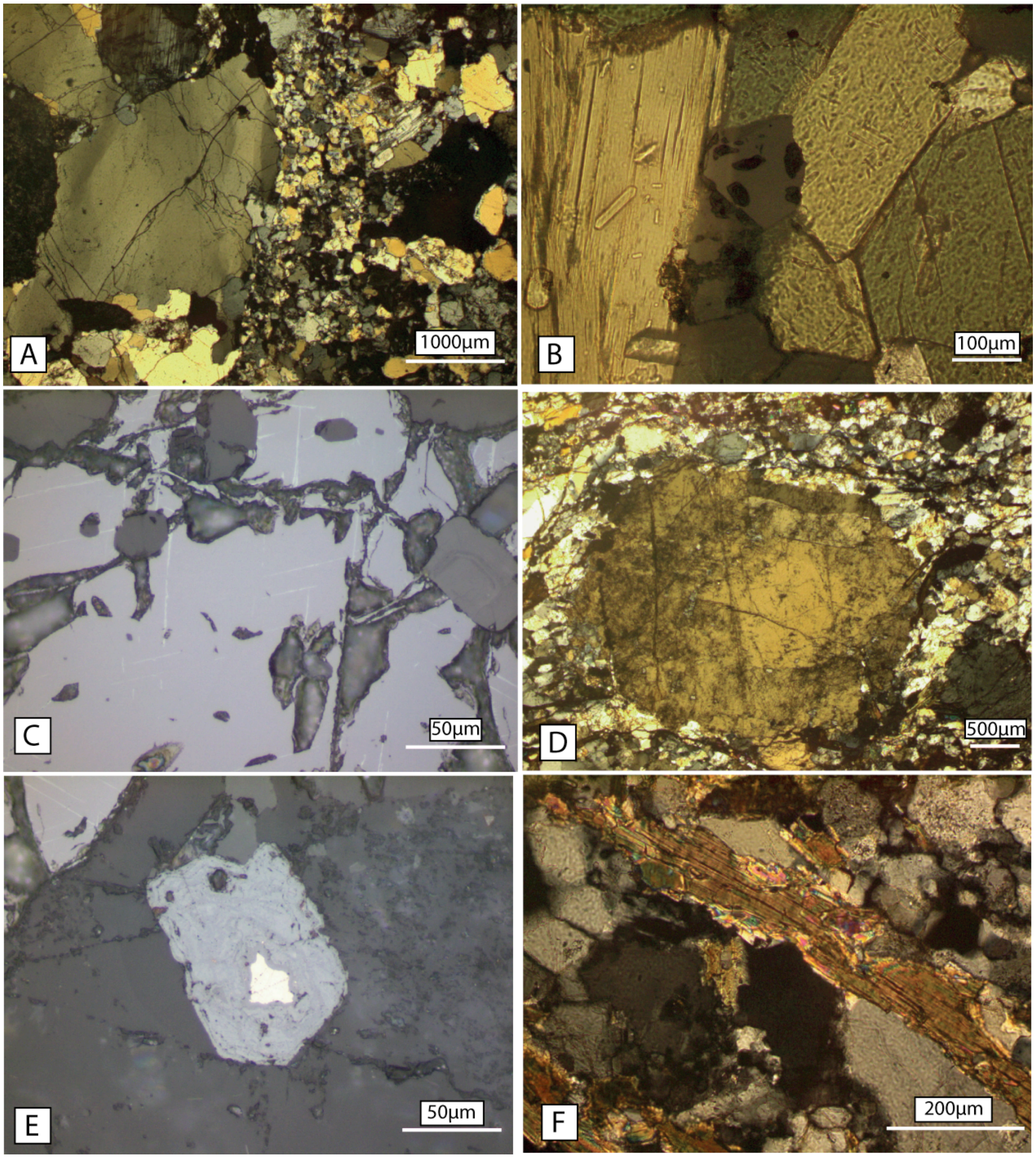

Figure 3.11: Photomicrographs showing A) Slightly recrystallized quartz in WR-3 (granodiorite). Subgrain formation is along the grain boundaries and not the cores; B) Acicular apatite inclusions in biotite in a mafic enclave, WR-4A; C) Ilmenite exsolution in magnetites in WR-3 (granodiorite); D) Recrystallized feldspars in WR-24C, a granitic gneiss. Large feldspars are K-feldspar with plagioclase cores; E) Chalcopyrite in core of 'frothy' magnetite in WR-3 (granodiorite); and F) Biotite recrystallizing to muscovite along grain boundaries in granitic gneiss- WR-24C.

Table 3.1: List of samples from LLB

Sample Number	Sample type
WR-1	Main phase of LLB
WR-3	Granodiorite/aplite contact
WR-4A *	Mafic enclave
WR-4B *	Mafic enclave
WR-5-2	Main phase of LLB
WR-6 †	Quartz vein
WR-7C *	Main phase of LLB
WR-8A †	Aplite
WR-12 †	Quartz seqgregation
WR-16B *	Main phase of the LLB
WR-18A *	Granitic dike
WR-18C	Intermediate dike
WR-18D *	Main phase
WR-20A	Intermediate dike
WR-20B *†	Quartz vein
WR-20C *	Main phase of the LLB
WR-20E †	Pegmatite dikes
WR-23A *	Leucogranite
WR-24B *	Proterozoic mafic dike
WR-24C	Deformed margin of LLB/ granitic gneiss
WR-25	Main phase
WR-25A †	Quartz vein
WR-25B *	Aplite
WR-28 *	Aplite
WR-29 *	Aplite
WR-30 *	Aplite
WR-40B	Altered granite
WR-41 *	Main phase
WR-42A	Quartz-hematite vein
WR-42B *	Quartz-hematite shear
WR-44 *	Deformed margin of LLB/ granitic gneiss
WR-45 *	Granite/pegmatite dike contact

* Denotes samples analyzed geochemically; † Denotes samples used for fluid inclusion work.

4. MINERAL CHEMISTRY

Analysis of minerals was completed by electron microprobe analysis at the Department of Geology and Geophysics, University of Wyoming. Samples were carbon-coated and analyzed for elemental compositions using a Jeol JXA-8900R WD/E combined microanalyzer. Hornblende, biotite, K feldspar, plagioclase, titanite, apatite, hematite, magnetite, and epidote were analyzed for a subset of collected samples. Three analyses were taken per grain to identify any internal zonation from core to rim. Hornblende geothermometry and geobarometry were completed using these data. Salinity was determined using the apatite results. F^- and Cl^- were analyzed in hornblendes and biotites. A detailed description of microprobe techniques can be found in Appendix 1.

4.1 HORNBLENDE

Hornblendes were analyzed from the enclave (WR-4A) and a granitic dike (WR-20A) because these samples contain a large number of unaltered hornblende phenocrysts. These amphiboles were analyzed for SiO_2, Al_2O_3, TiO_2, MgO, FeO, MnO, CaO, Na_2O, K_2O, F, and Cl. These data were used to determine amphibole type using WinAmphcal (Yavuz, 2007). Amphiboles were found to belong to the hornblende group, with compositions varying between magnesiohornblende, tschermakite, edenite, paragasite, and magesiohastingsite. Figure 3.1 plots the composition of the analyzed grains using the scheme of Leake et al. (1997). Because of variations in $(Na + K)_A$ values in the compositions, the data plot on two separate graphs. Across some grains, values are split between the two graphs. The lack of trend in Al content from core to rim indicates that there likely was not a major pressure change during crystallization (Hammarstrom and Zen, 1986).

4.2 BIOTITE

Biotites from the mafic enclave (WR-4A), two granites (WR-16B and WR-41), and two aplites (WR-28 and WR-30) were examined. Biotites were analyzed for SiO_2, Al_2O_3, TiO_2, MgO, FeO, MnO, CaO, Na_2O, K_2O, F, and Cl. Two populations of biotite are apparent in the Figure 4.2. Granites are found in both populations, and thus enclaves do not form a distinct population. The presence of two populations that vary with respect to Mg/(Mg + Fe) may be a result of sub-solidus recrystallization. This is consistent with the volatile content analysis of biotites, which also gives two populations of biotite.

4.3 FELDSPARS

Feldspars were analyzed for SiO_2, Al_2O_3, Fe_2O_3, CaO, Na_2O, and K_2O from a mafic enclave (WR-4A), two granites (WR-16B and WR-41), and two aplites (WR-28 and WR-30). Plagioclase grains were determined to be primarily oligoclase for all samples. There is minor zoning of plagioclase with rims of andesine in a fraction of grains. Alkali feldspar grains were determined to be pure K-feldspar, and may be orthoclase or microcline. Petrographic work confirms that the K-feldspar is microcline.

4.4 TITANITE

Titanites were analyzed for Si, Ti, Ca, Al, Fe, Ce, Mg, Mn, Na, Sn, and F. Titanite grains from WR-29 (aplite) and WR-16B (granite) were examined. Up to 1.2 wt % Ce_2O_3 were noted, and hence small amounts of REE are present within the grains.

4.5 APATITE

Apatites were analyzed for Ca, P, La, Ce, Nd, Sr, Na, Mg, Al, Si, Mn, Fe, F, Cl, and S. Samples of granite, aplite and a mafic enclave were examined. In thin section, some grains are zoned, and this is verified in the microprobe data with small variations in volatile content, but no consistent zonations. SiO_2 versus SO_3 concentrations are shown in Figure 4.3. The LLB values are similar to those of most magmatic rocks described in Streck and Dilles (1998), but are different from carbonatitic magmas and alkali magmas. The F-Cl-OH variability in the halogen site of apatite is given in Figure 4.4. The LLB samples are mostly fluoroapatitic in composition, with a few being hydroxylapatitic.

4.6 HEMATITE

Hematite from quartz-hematite veins was analyzed for O, Mg, Al, Ti, V, Cr, Mn, Fe, Cu, Ag, and Au. Significant values were reported for Au and Ag; however, no apparent zonation or correlation between elements were seen within the hematite grains. Up to 0.4 wt % Au and 0.1 wt% Ag were found in the grains.

4.7 MAGNETITE

Magnetite from a mafic enclave was analyzed for O, Mg, Al, Ti, V, Cr, Mn, Fe, Cu, Ag, and Au. Significant amounts of Au, Ag, Cu, and Zn were noted, but no apparent zonation or correlation between elements is apparent within the data. Values up to 0.06 wt% Cu, 0.09 wt% Zn, 0.5 wt% Au, and 0.1 wt% Ag were noted in the grains. Experimental work on crystal partitioning of Au, Ag and Cu by Simon et al (2008), determined that in the assemblage ulvospinel-magnetite solid solution-Au-Cu-rhyolite melt-vapor-brine, metal concentrations in magmatic magnetite were determined as 16 ± 9 μg/g Au and 16 ± 6 μg/g Cu. The metal content of the LLB magnetites are an order of magnitude higher than those values determined by Simon et al (2008).

4.8 HORNBLENDE THERMOBAROMETRY

Hornblende geothermometry and geobarometry were completed based on the equilibrium in the assemblage hornblende-quartz-plagioclase-K-feldspar-biotite-titanite-Fe-Ti oxides using the program WinAmphcal (Yavuz, 2007). Total aluminum content is used to estimate pressure in the Al-in-hornblende barometer after Hammarstrom and Zen (1986). Temperature and pressure were calculated using the equations from Hammarstrom and Zen (1986). Results from the thermobarometry can be found in Table 4.1. The equations give temperatures of crystallization between 716°C and 850°C, and pressures range from 1.8 kbar to 5.78 kbar.

4.9 APATITE CHEMISTRY

Apatites were used to determine salinity using the techniques of Piccoli and Candela (2002). The data were used to calculate the m^{aq}_{HCl}, C^{Ap}_{Cl}, C^{Ap}_{F} and m^{aq}_{HF} at 700°C and 800°C to represent composition of an aqueous phase in equilibrium with apatite during formation. C^{Ap}_{Cl} is the concentration of Cl^- in apatite and C^{Ap}_{F} is the concentration of F^- in apatite. The average C^{Ap}_{Cl} at 700°C is 4.6 ± 4.4 wt % Cl, and at 800°C it is 7.8 ± 7.6 wt % Cl. The average C^{Ap}_{F} is $1.8 \times 10^{-3} \pm 1.3 \times 10^{-3}$ wt % F at 700°C and $5.8 \times 10^{-3} \pm 4.2 \times 10^{-3}$ wt % F at 800°C. The average m^{aq}_{HCl} at 700°C is $4.6 \times 10^{-4} \pm 4.5 \times 10^{-4} m$ (average ± 1σ) and at 800°C is $7.8 \times 10^{-4} \pm 7.6 \times 10^{-4} m$. Average m^{aq}_{HF} at 700°C is $9.0 \times 10^{-4} \pm 6.5 \times 10^{-4} m$ and at 800°C is $2.9 \times 10^{-3} \pm 2.1 \times 10^{-3} m$. Figure 4.5 shows contours of constant Cl/OH on a plot of composition in the halogen-site of apatite at 700° and 4 kbar.

4.10 BIOTITE CHEMISTRY

Fluorine and chlorine content of biotite were used to estimate the ratio of F^- and Cl^- in the fluid of coexisting hydrothermal fluids. Figure 4.6 gives the concentration of Mg versus the F-Cl content. Contours of the logarithm of the fluorine-chlorine fugacity ratios from Munoz (1992) are plotted on the diagram. Two populations of biotites are apparent in the diagram. The trends within these populations may represent re-equilibration of the biotites with later magmatic or hydrothermal fluids, or a crystallization sequence. The population with lower XMg are from more aplitic samples and in thin section these grains appear more brown than green. Fluorine-chlorine ratios range between approximately 2 to 114 ppm. When compared to the $m^{aq}_{HF^-}/maq_{HCl^-}$ ratios from apatites, the values differ up to two orders of magnitude.

OXYGEN FUGACITY FROM TITANITES

Titanites were used to calculate the oxygen fugacity using temperatures and pressures estimated from hornblende thermobarometry and the assemblage present for the LLB samples. These results were plotted as log fO_2 versus temperature (Figure 4.7). The results show that the LLB is moderately oxidizing, and plots above the FMQ (fayalite-magnetite-quartz) buffer. These results are supported in Figure 4.8, which plots the delta log fO_2 versus temperature and also gives moderately oxidizing conditions. Delta log fO2 is the difference between the oxygen fugacity and the fayalite-magnetite-quartz buffer. Figure 4.9 is a schematic drawing of log fO_2 versus temperature. Based on this figure, the amphibole-bearing phases that are present in samples of this study should have similar minimum oxygen fugacities as the pyroxene-bearing rocks of Frost et al (2001). Using this assumption, log fO_2 values for titanites were plotted on a graph using titanite stability in anhydrous rocks based on the presence of clinopyroxene (Figure 4.10). The LLB oxygen fugacities plot below the field for crystallization conditions of typical calc-alkaline magmas.

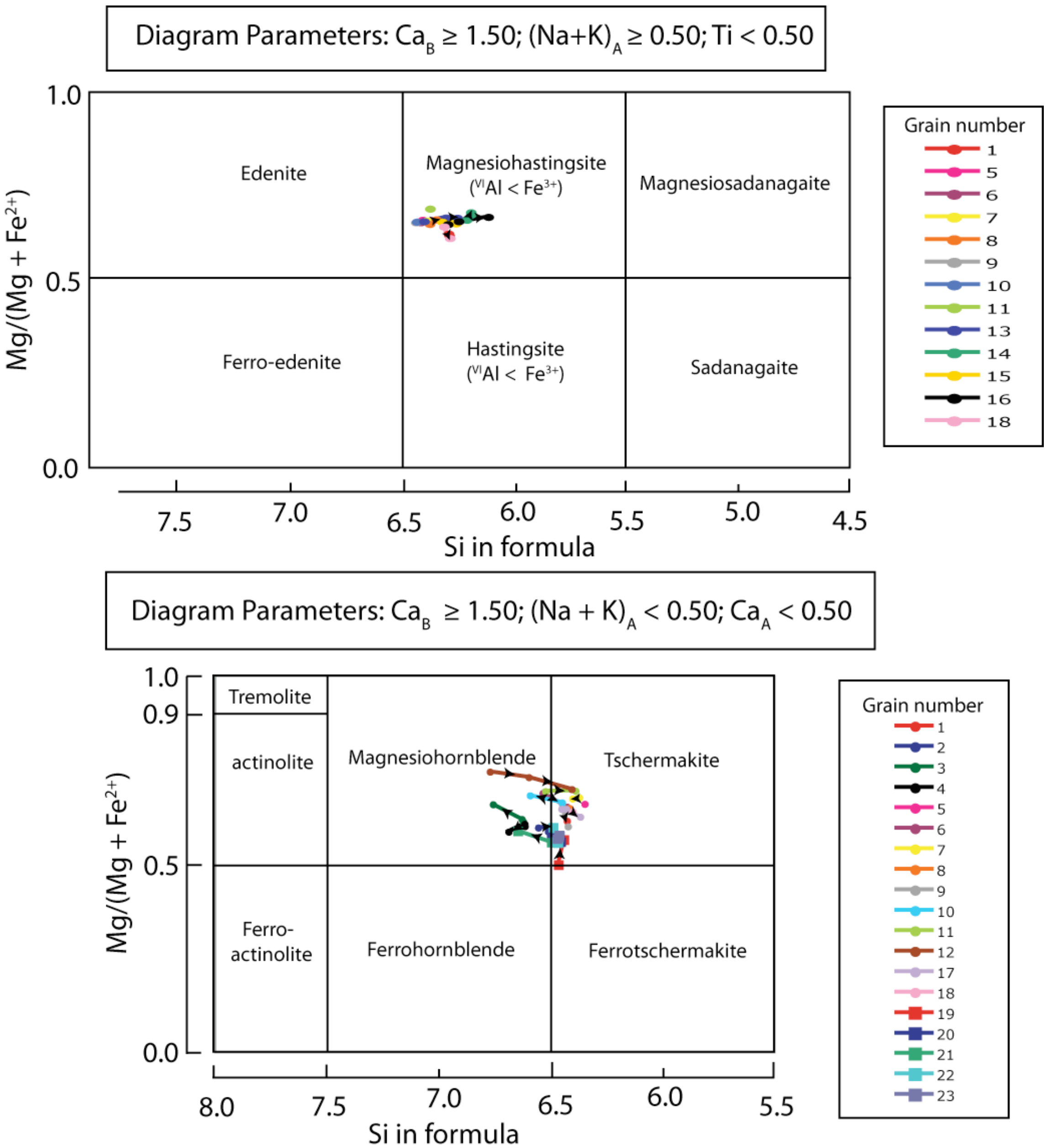

Figure 4.1: Graphs of amphibole chemistry after Leake et al (1997). Arrows indicate direction from core to rim. Grains 1-18 are from WR-4a, and grains 18-23 are from WR-20B.

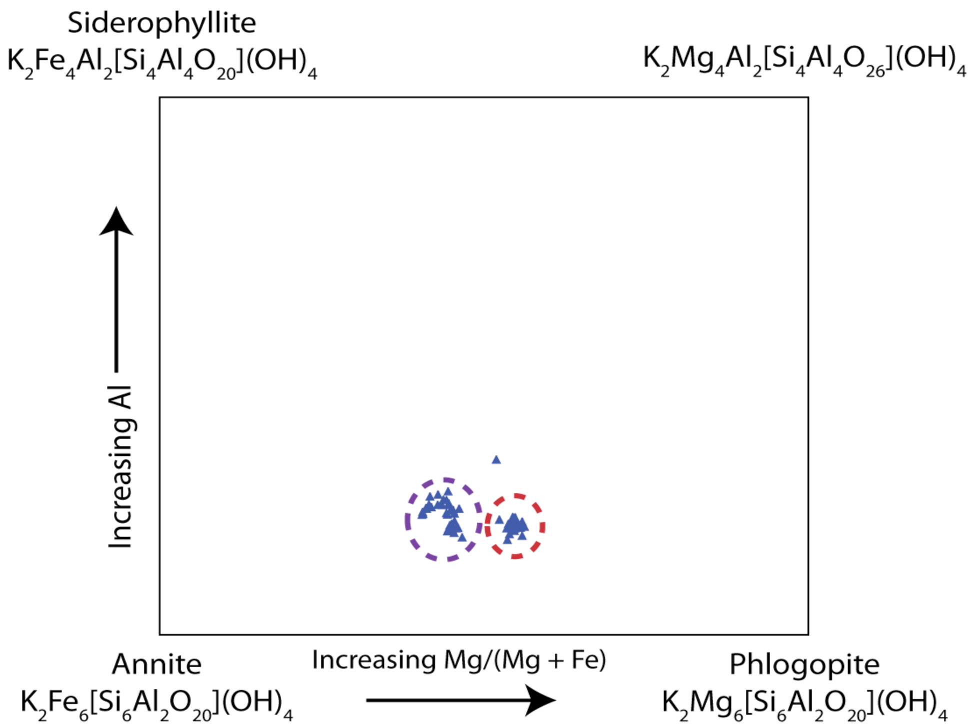

Figure 4.2: Plot of biotite composition showing two populations of biotite.

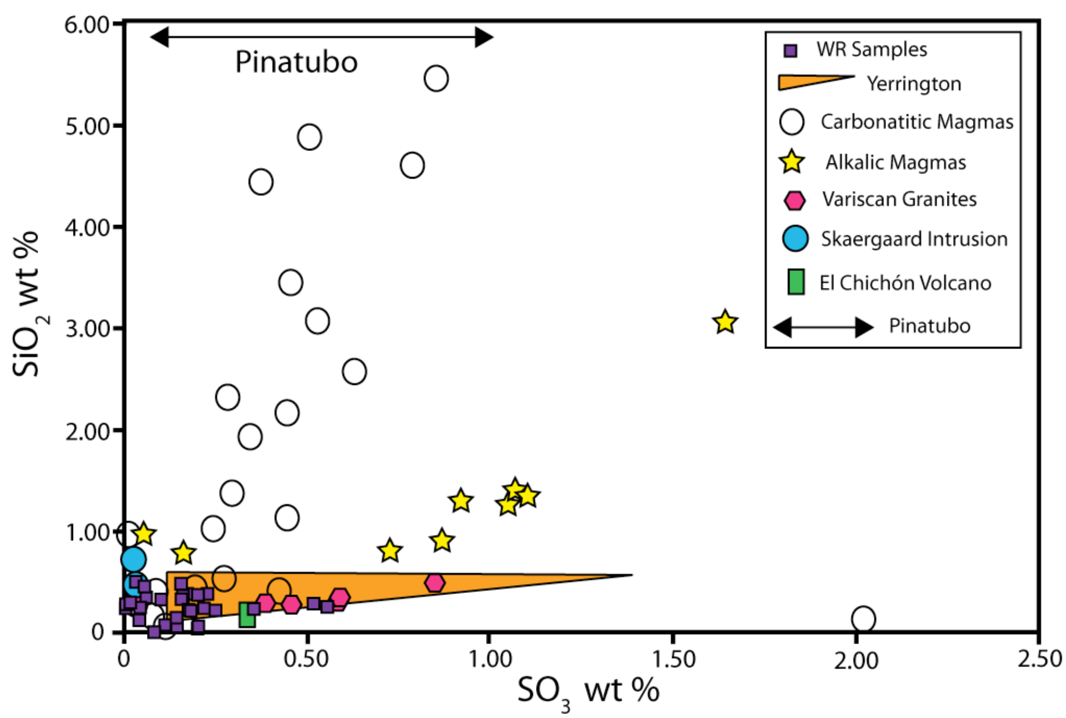

Figure 4.3: SO_3 vs SiO_2 for apatites (after Streck and Dilles, 1998) from LLB compared with values from intrusive rocks.

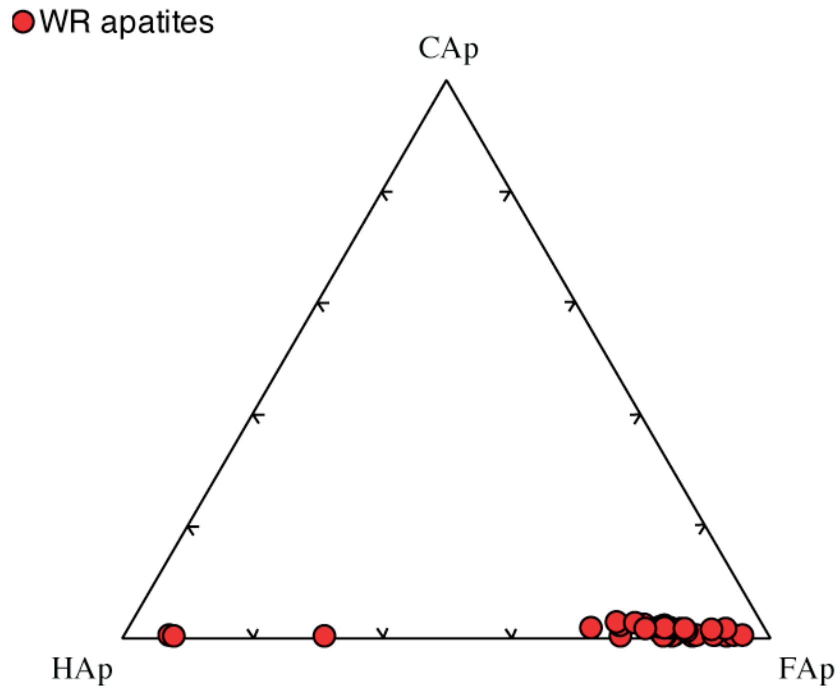

Figure 4.4: Plot of F-Cl-OH variability in the halogen site of apatites.

Table 4.1: Temperatures and Pressures from hornblende geobarometry. Results calculated using WinAmphcal (Yavuz, 2007).

Sample	P1 (kbar)	T1 (°C)	Sample	P1 (kbar)	T1 (°C)
4A-hbd1a	4.67	773.04	4ahbl23	2.66	771.33
4A-hbd1a	4.89	801.99	4ahbl24	3.91	792.58
4A-hbd1a	4.91	802.14	4ahbl25	3.51	800.21
4A-hbd2a	3.81	745.26	4ahbl26	3.96	814.07
4A-hbd2a	4.37	758.26	4ahbl28	4.69	822.66
4A-hbd2a	4.46	762.04	4ahbl29	4.72	826.53
4A-hbd3a	3.7	752.06	4ahbl30	4.77	824.68
4A-hbd3a	3.57	753.77	4ahbl31	4.51	811.07
4A-hbd3a	3.22	729.35	4ahbl32	4.21	806.19
4A-hbd4a	3.98	750.21	4ahbl33	4.6	813.59
4A-hbd4a	4.05	724.53	4ahbl34	4.69	815.07
4A-hbd4a	3.82	749.98	4ahbl35	4.41	809.15
4ahbl1	4.24	789.63	4ahbl36	4.33	850.53
4ahbl2	4.1	798.97	4ahbl37	3.96	784.56
4ahbl3	4.28	795.66	4ahbl38	3.95	780.28
4ahbl4	3.47	772.01	4ahbl39	4.53	786.5
4ahbl5	4.18	783.71	4ahbl40	4.2	785.82
4ahbl6	4.11	786.18	4ahbl41	4.52	803.4
4ahbl7	4.11	796.65	4ahbl42	4.96	796.85
4ahbl8	4.21	791.8	20ahbl43	4.81	748.13
4ahbl9	4.06	790.7	20ahbl44	4.98	743.66
4ahbl10	4.31	793.15	20ahbl45	4.89	743.94
4ahbl11	4.29	799.4	20ahbl46	5.78	636.85
4ahbl12	4.26	782.55	20ahbl47	4.82	745.13
4ahbl13	4.2	784.38	20ahbl48	4.76	735.56
4ahbl14	3.94	782.98	20ahbl55	4.71	741.78
4ahbl15	4.03	784.53	20ahbl56	4.76	735.7
4ahbl16	3.97	784.53	20ahbl57	4.41	716.64
4ahbl17	4.03	783.48	20ahbl58	4.74	744.49
4ahbl18	3.11	763.64	20ahbl59	4.78	738.12
4ahbl19	3.59	771.42	20ahbl60	4.88	737.12
4ahbl20	4.1	793.21	20ahbl61	4.7	743.69
4ahbl21	4.26	794.02	20ahbl62	4.78	745.18
4ahbl22	1.8	746.96	20ahbl63	4.68	740.58

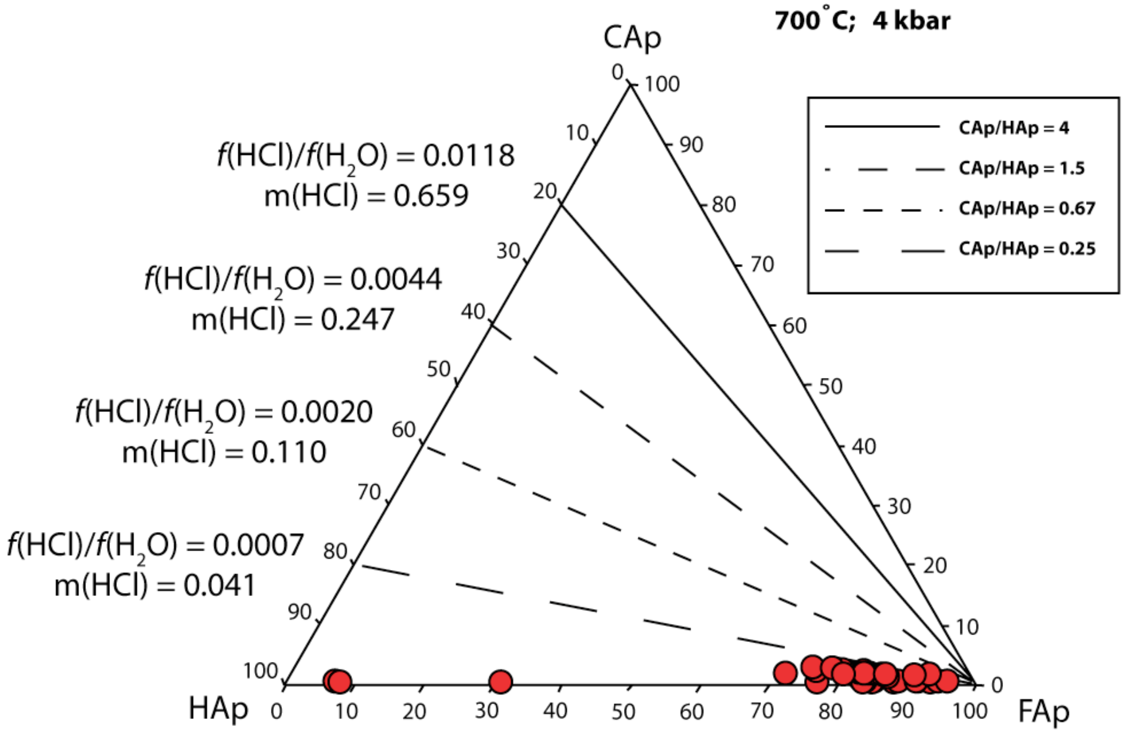

Figure 4.5: Plot of the composition in the halogen site of apatites with contours of constant Cl^-/OH^- in apatite (after Piccoli and Candela, 1992).

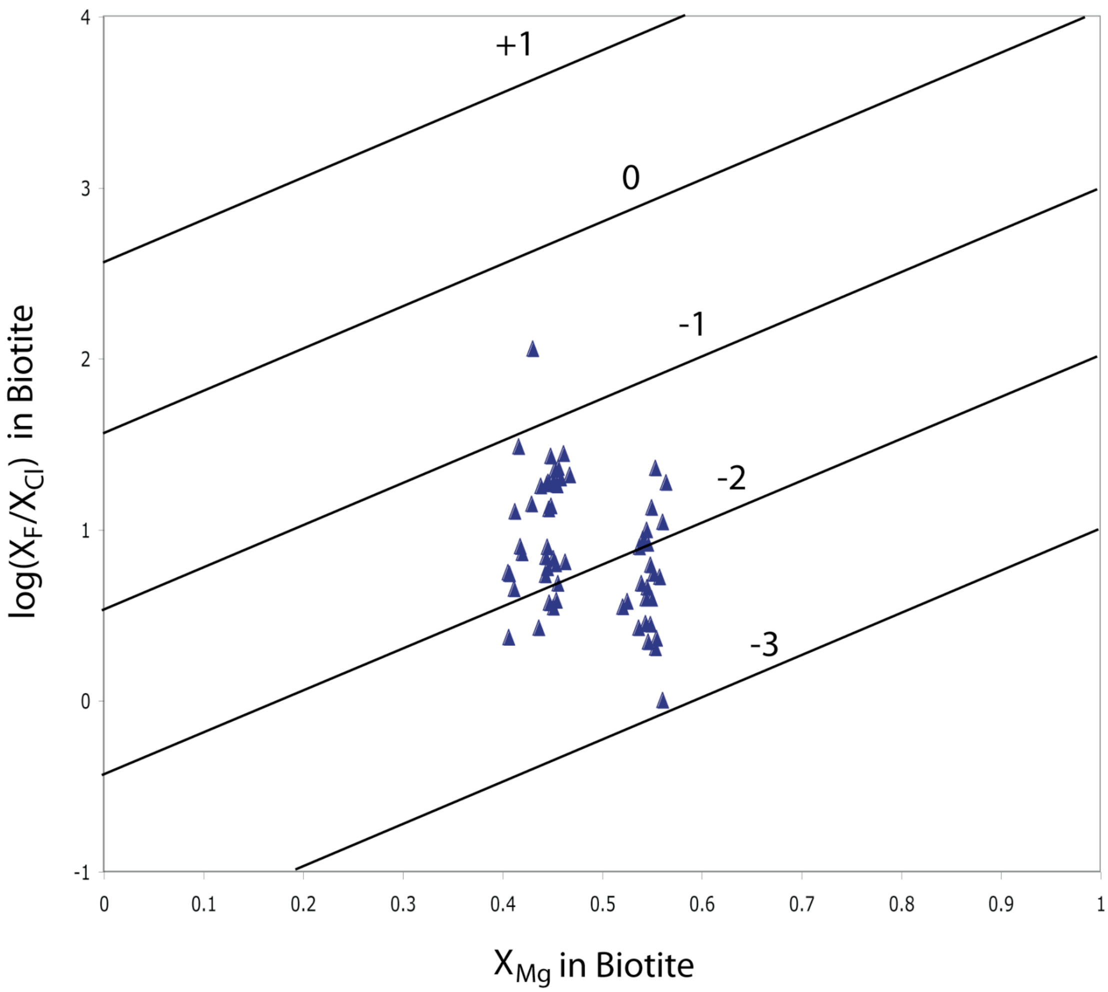

Figure 4.6: X_{Mg} vs. log (X_F/X_{Cl}) in the halogen site of biotites (after Yang and Lentz, 2005). Contours are log f_{F^-}/f_{Cl^-} in a coexisting hydrothermal fluid and are from Munoz (1992).

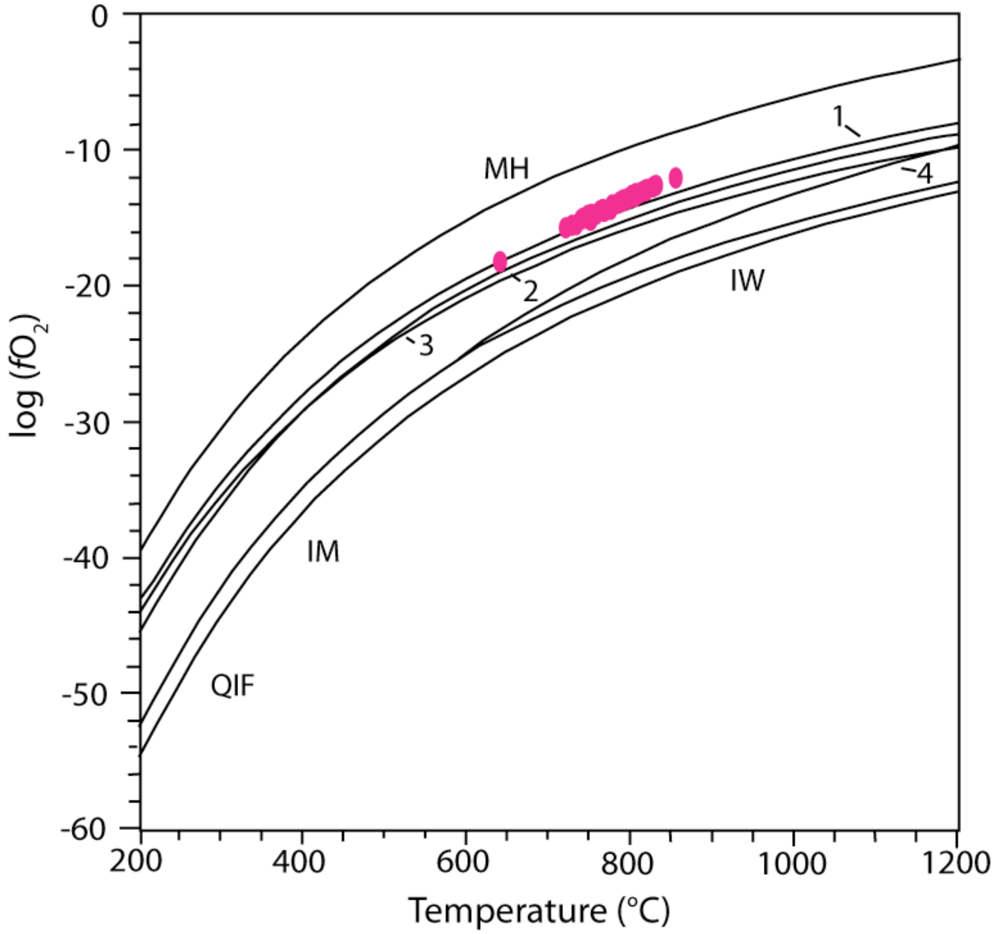

Figure 4.7: log fO2 versus temperature showing the LLB titanites in pink and common buffers used in experimental work (after Frost et al. 1991). 1= NiNiO, 2= FMQ, 3= CoCoO, 4= WM. Abbreviations are from Frost et al. (1991).

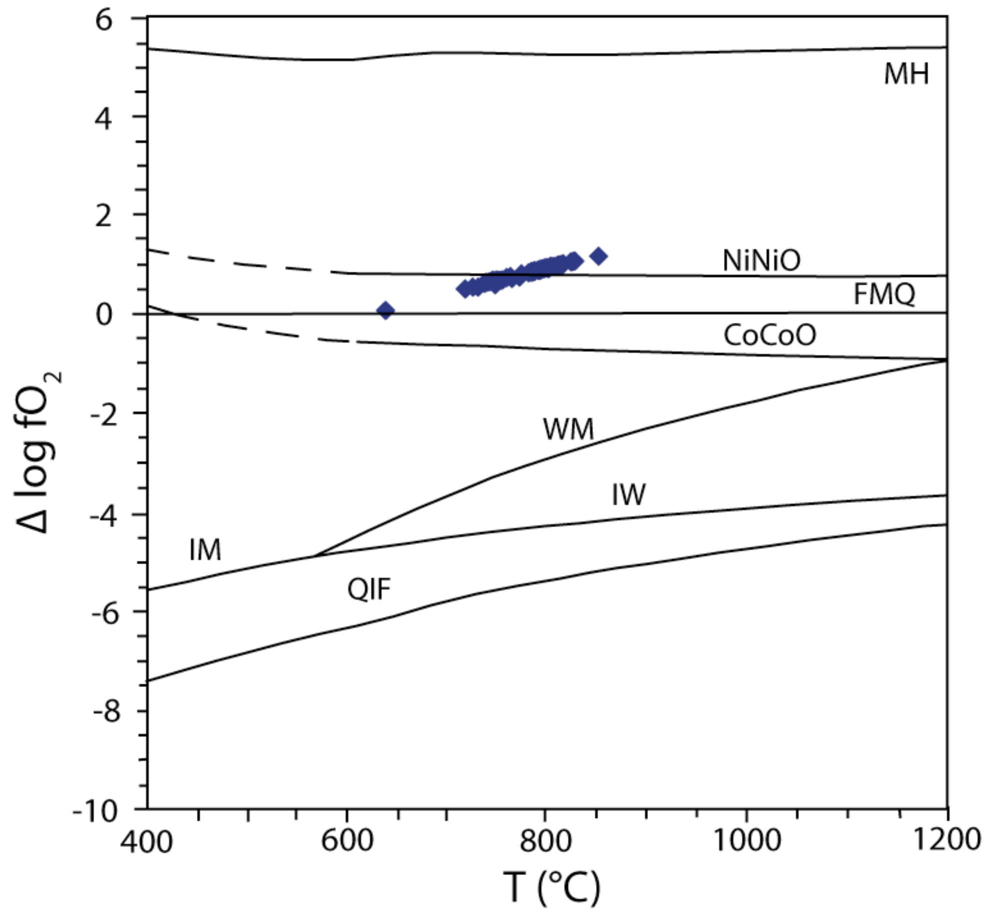

Figure 4.8: Δ log fO2- T with common experimental buffers normalized to the FMQ buffer after Frost et al. (1991). The LLB samples are represented with blue diamonds.

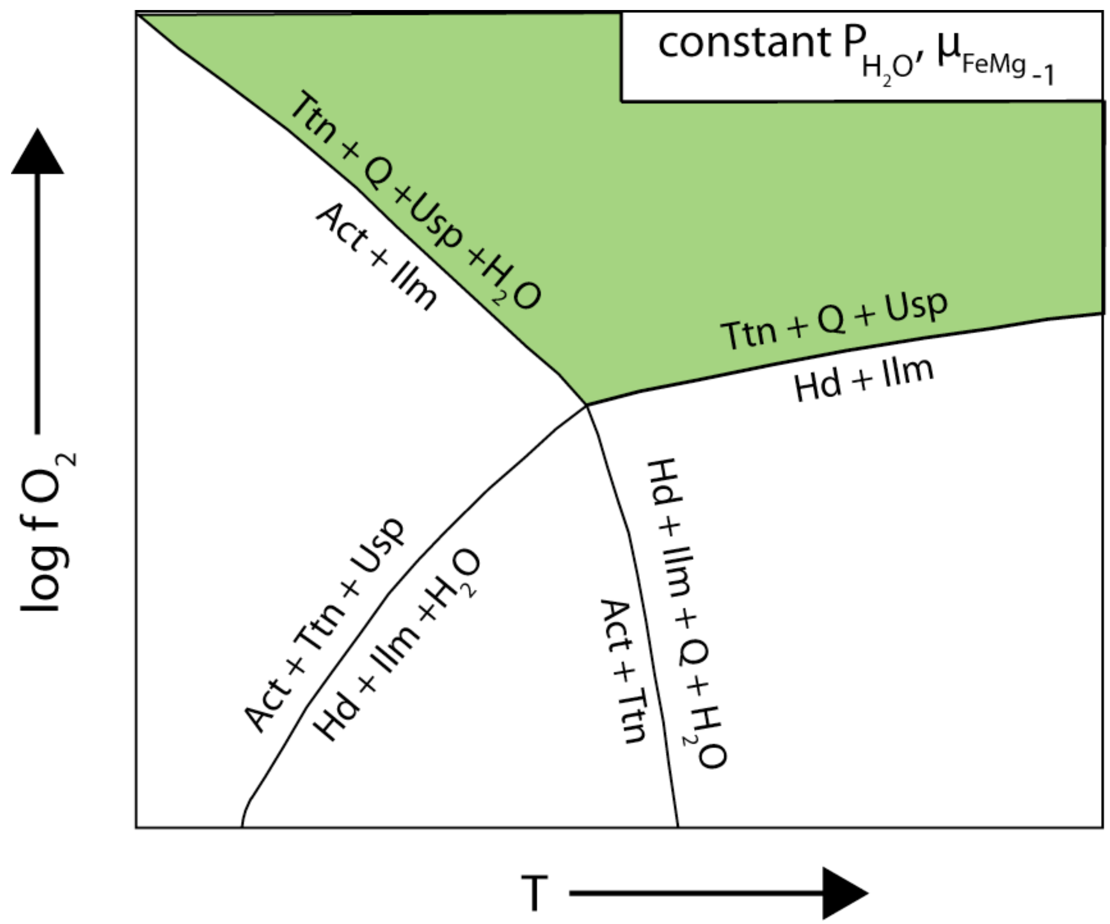

Figure 4.9: Schematic diagram of log fO_2- T after Frost et al (2001) presenting how hydration affects the stability of titanite. The field in green is the expected field for the LLB rocks.

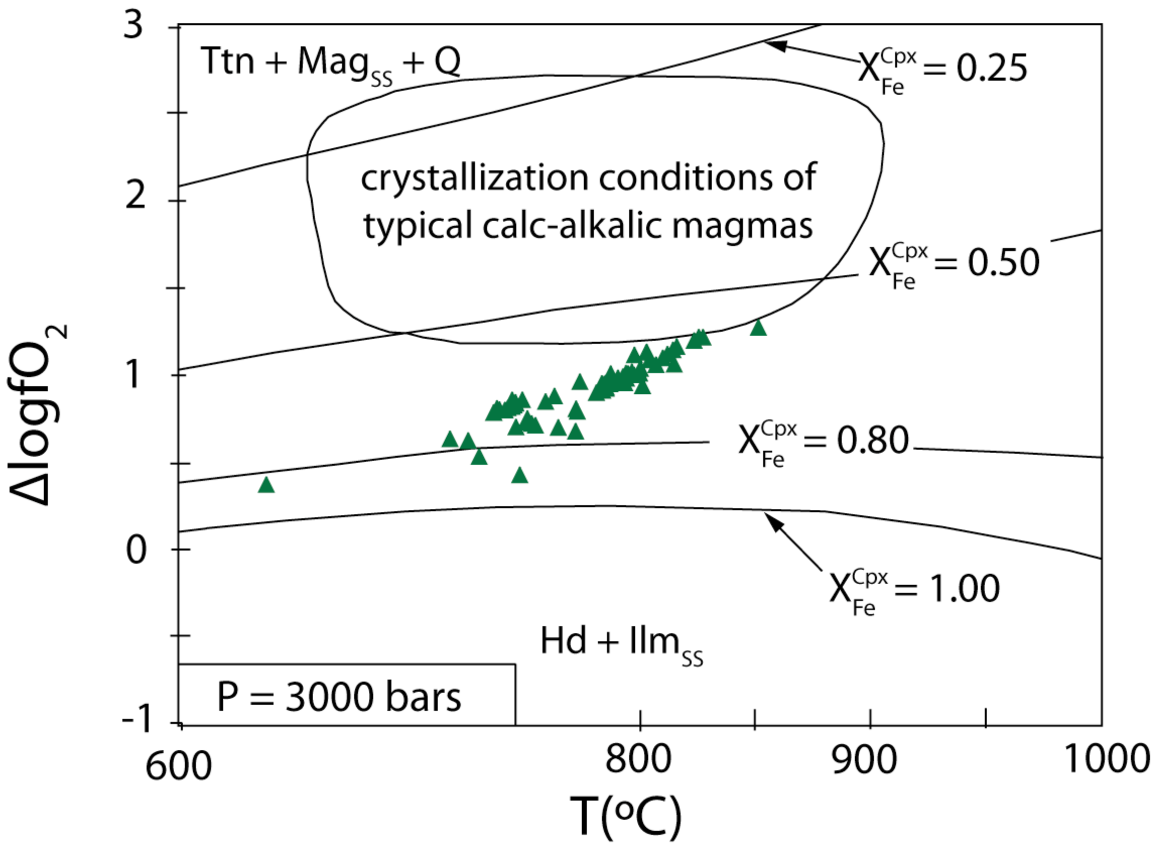

Figure 4.10: log fO_2 vs. temperature for the stability of titanite in anhydrous rocks with clinopyroxene (after Frost et al 2001). The green triangles represent the LLB titanite results.

5. FLUID INCLUSION PETROGRAPHY AND CHEMISTRY

5.1 OVERVIEW OF FLUID INCLUSIONS

Fluid inclusions were studied in quartz grains from quartz-feldspar aplite dikes, quartz grains from quartz-K-feldspar pegmatite dikes, and quartz veins and irregular segregations from unaltered granite. These phases were chosen because they likely represent late fractionates or products of magma-derived hydrothermal fluids. Four types of inclusions were discovered in the LLB samples (Figure 5.1). These types contain differing amounts of CO_2 and ranges in salinity. Fluid inclusions were examined in six samples (Table 3.1). Microthermometry was completed on all inclusion types using a Linkam THMS 600 Stage attached to an Olympus BX51 microscope. Results of CO_2 melting temperatures, clathrate melting temperatures, CO_2 homogenization temperatures, water eutectic temperatures, ice melt temperatures, and temperatures of total homogenization can be found in Appendix 4. Most inclusions decrepitated before reaching total homogenization. This is probably because the inclusions have become overpressured internally. Histograms were created from the microthermometric data (Figure 5.2). The histograms give bimodal or single peaks that are left- or right-skewed. Salinities were determined using the computer programs CLATHRATES (Bakker 1997) and FLUIDS (Bakker 2003). Isochores were also calculated using these programs. Each sample was analyzed using microthermometry. Laser ablation ICP-MS was completed on inclusions from one sample, WR-25A.

The LLB underwent a complex deformation and heating and cooling history. In order to differentiate primary or pseudosecondary (early) inclusions from secondary (late) inclusions, the petrographic relationships of the inclusions were analyzed. Inclusion trails that cross grain boundaries or are present in recrystallized rims were considered secondary, and thus late. Inclusions from the undeformed centers of quartz grains that were present as either isolated inclusions, 3-D clusters, or discontinuous linear trails were considered primary or pseudosecondary, and thus early. Microthermometry was completed predominantly on primary and pseudosecondary inclusions and trails.

5.2 PETROGRAPHY AND MICROTHERMOMETRY OF FLUID INCLUSION TYPES

5.2.1 Type I Inclusions

Type I inclusions are high salinity, aqueous fluids with varying numbers of daughter minerals, and in WR-20B and WR-25A, a few mol % CO_2. Type I inclusions are found in all analyzed samples, except WR-6. At room temperature, Type I inclusions contain aqueous liquid, aqueous vapor, and two to five solids. Petrography of daughter solids determined that they are most likely halite, pyrosmalite, nahcolite, and $CaCl_2$ based on shape, relief, and birefringence. The petrographic daughter determinations were corroborated with the results of microthermometry and elemental compositions from LA-ICP-MS. The inclusions typically have a negative crystal shape, but can be irregular. They are found as isolated inclusions, or within trails of other types of inclusions. These inclusions are inferred to be primary and pre-deformation as they are not part of trails that cut across grain boundaries. They are found within the undeformed centers of quartz grains and not in recrystallized rims, implying that they were destroyed during crystallization.

Microthermometric studies yield additional insights into this inclusion type. During freezing, additional daughter minerals may precipitate from solution. The formation of antarcticite was also inferred based on freezing temperatures and indicates the presence of $CaCl_2$. Minimum salinities are about 23 wt % NaCl and the maximum salinity is 60 wt % NaCl. Salinities were determined using halite homogenization temperatures for samples in which it was observed. For other samples, the ice melting temperatures were used to determine salinity. Temperature of total homogenization range from 106°C to above 450°C, and inclusions homogenized to the liquid. Maximum temperatures of total homogenization are based on the maximum decrepitation temperatures.

5.2.2 Type II Inclusions

Type II inclusions are low to moderate salinity (0-15 wt % NaCl), aqueous-carbonic inclusions, in some cases containing small daughter minerals. Type II inclusions are found in samples WR-6, WR-12 and WR-25A. At room temperature, aqueous liquid and carbonic liquid and vapor are present, often with small solids. The solids are tabular, and petrography determined that these are possibly nahcolite. The overall shape of the inclusions varies from negative crystal to annular. Type II inclusions form discrete, linear trails that are inferred to be pseudosecondary trails because they do not cross grain boundaries or into recrystallized areas of the quartz grains. The trails cross-cut each other, but are somewhat discontinuous, and may contain both Type I and Type II inclusions.

Microthermometric analysis of Type II inclusions determined that they contain approximately 10 mol % CO_2 and an XCH_4 between 0.01 to 0.03. The XCH_4 is the methane in the carbonic phase, calculated using Th_{CO2} and the Tm_{CO2}. Salinities were determined using the CLATHRATES (Bakker 1997) programs, based on the clathrate melting temperatures. Total homogenization temperatures range between 126°C and above 389°C (based on maximum decrepitiation temperatures) and homogenizes to the liquid.

5.2.3 Type III Inclusions

Type III inclusions are moderate salinity, aqueous-carbonic inclusions with daughter minerals similar to Type I. They are believed to be an intermediate between Types I and II. Similar to Type II inclusions, Type III inclusions are found in samples WR-6, WR-12 and WR-25A. At room temperature, an aqueous liquid and a carbonic liquid and vapor are present, along with one to three solids. The inclusions are typically negative crystal in shape, but can be irregular. Type III inclusions form discrete, linear trails, similar in morphology to Type II inclusions. They may also be part of the same trails.

Analysis of the inclusions concludes that they contain 7 to 11 mol % CO_2 and contain 0 to 0.2 XCH_4 in the carbonic phase. The inclusions have salinities between 15-23 wt % NaCl, based on clathrate melting temperatures. Temperatures of total homogenization range from 173°C to above 500°C, homogenizing to the liquid.

5.2.4 Type IV Inclusions

Type IV inclusions are CO_2-rich and low to moderate salinity. They are found in samples WR-25A, WR-20B, WR-12 and WR-6, with the largest number found in WR-25A. At room temperature, they contain mostly a carbonic vapor phase, and a minor percentage of aqueous liquid. Solids are not usually present. Larger inclusions are irregular or annular in shape, but smaller inclusions tend to be rounded or negative crystal. These inclusions form 3-D clusters that are inferred to be primary to pseudosecondary as they are found only within the undeformed center of quartz grains.

Microthermometry revealed that these vapor-rich inclusions contain between 0 and 0.02 X_{CH4} in the carbonic phase and 40-90 mol % CO_2. Salinities, which were determined using the clathrate melting temperatures, range between 3 and 30 wt % NaCl. Total homogenization temperatures range from 270°C to above 330°C, homogenizing to either the liquid or the vapor in all samples.

5.3 ISOCHORES OF FLUID INCLUSIONS

Figure 5.3 gives the calculated isochores for the analyzed samples. Molar volumes were not calculated using CLATHRATES (Bakker 1997) and FLUIDS (Bakker 2003) for some samples. This is most likely because of limitations of equations of state in the programs, and may be a result of the high salinities. The most consistent and narrowest spread in results come from samples WR-20E (pegmatite dike) and WR-25A (a quartz vein). This is inferred to be a result of less post-entrapment deformation in the samples. Isochores at lower pressures are inferred to have reequilibrated during minor deformation, which would have stretched the inclusions. Some samples also fractured during cutting, which resulted in the formation of cracks that may have allowed the inclusions to leak.

5.4 LA-ICP-MS OF FLUID INCLUSIONS

Fluid inclusions from sample WR-25A were analyzed at Virginia Tech using LA-ICP-MS for a suite of elements to characterize the fluids (Figure 5.4). The elements analyzed include Li, Na, K, Ca, Mn, Fe, Cu, Zn, As, Rb, Sr,Y, Mo, Ag, Sn, Sb, Cs, Ba, La, Ce, W, Tl, Pb and Bi. The concentrations in ppm were calculated in AMS software (Mutchler et al., 2007; Mutchler et al., 2008) using the salinities previously determined using microthermometry. Type I and Type II inclusions were analyzed, which were both determined to be Na-dominated.

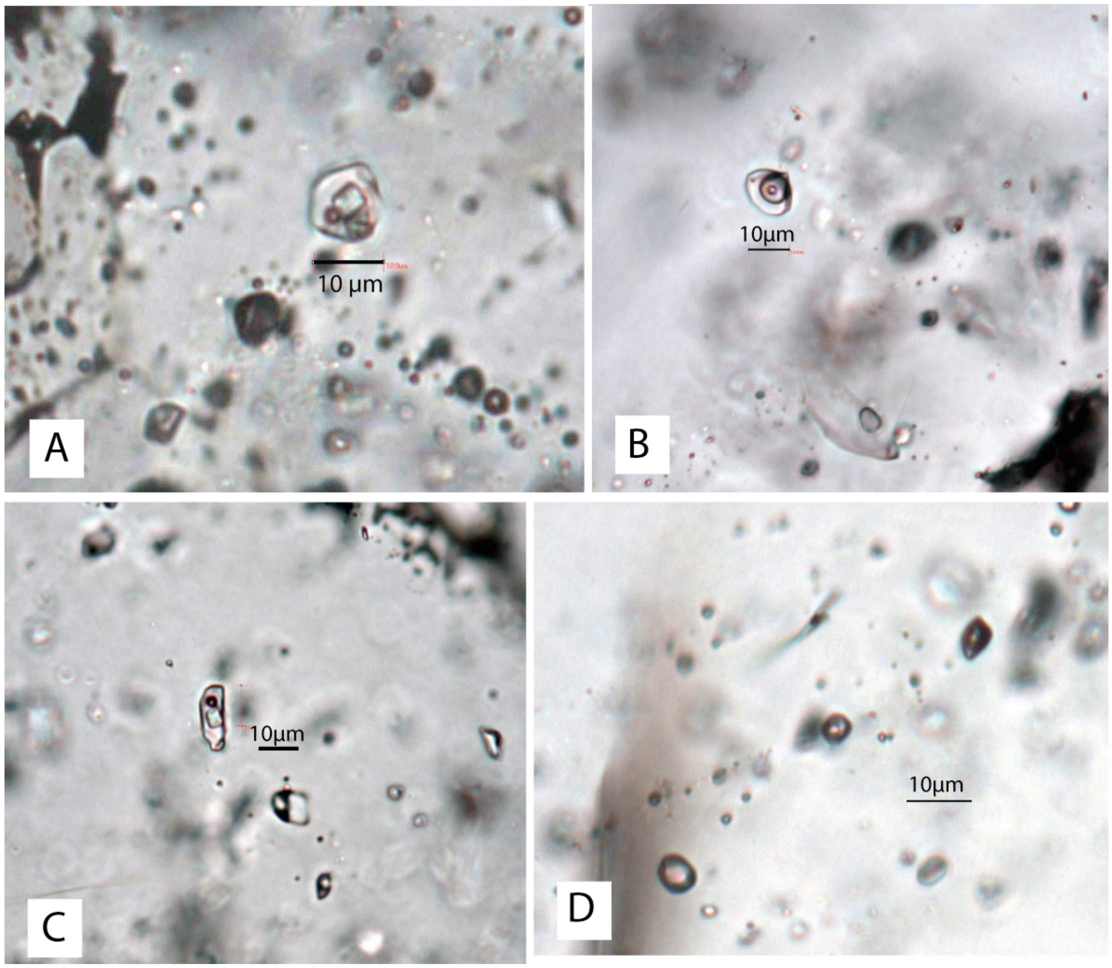

Figure 5.1: Photomicrographs at room temperature of typical A) Type I inclusions in WR-25A. H_2O, halite and one other solid (possibly $CaCl_2$) found in an isolated inclusion; B) Type II inclusions as part of a trail in WR-6, with H_2O and CO_2 with a small opaque solid; C) Type III inclusions from a trail in WR-25A with H_2O, CO_2 and halite; and D) Type IV inclusions from a 3-D cluster in WR-25A. These inclusions contain mostly CO_2 with minor amounts of H_2O.

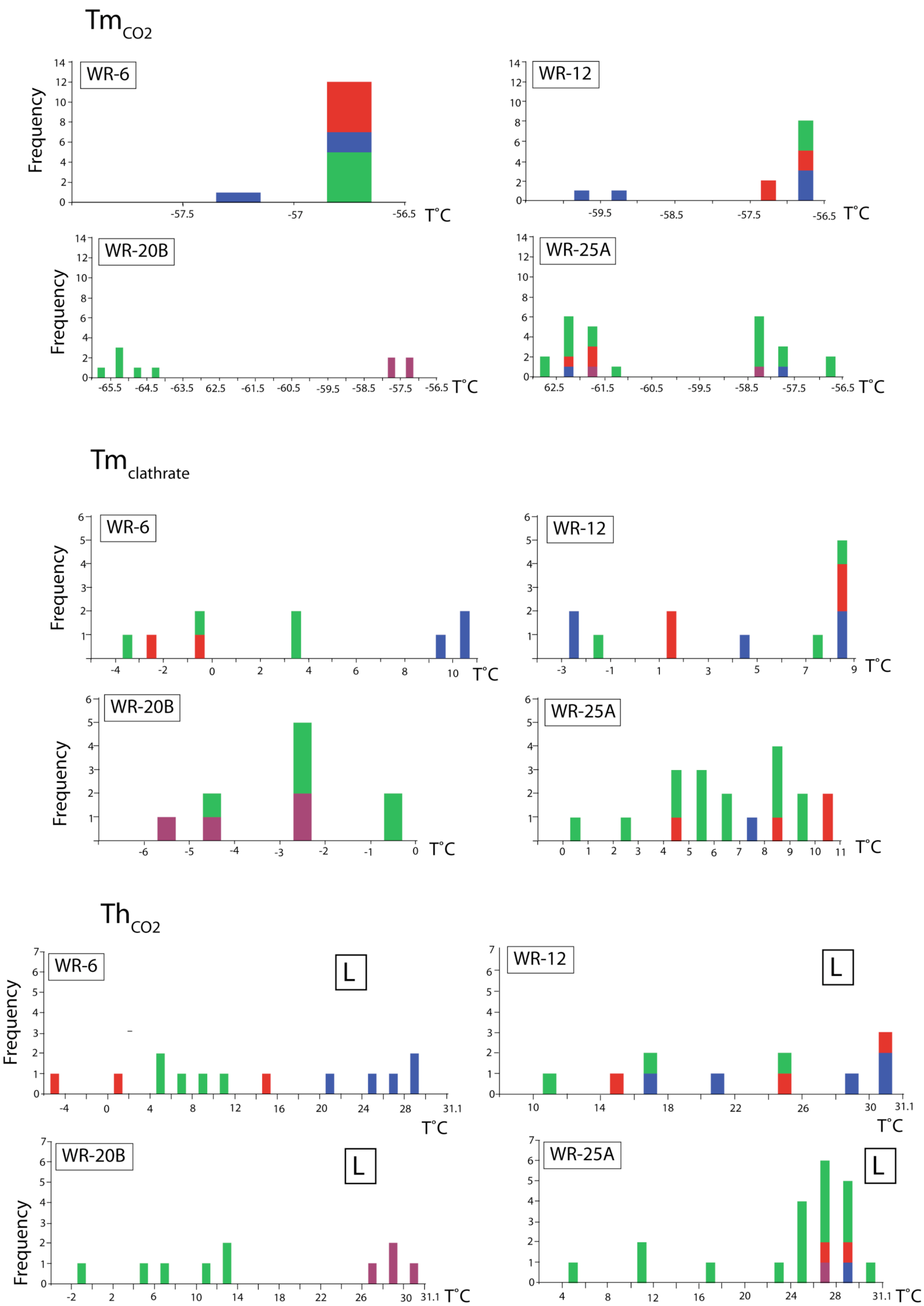

Tm CO2
WR-6
WR-12
WR-20B
WR-25A
Frequency
T°C
Tm clathrate
WR-6
WR-12
WR-20B
WR-25A
Frequency
T°C
Th CO2
WR-6
WR-12
WR-20B
WR-25A
L
Frequency
T°C

$T_{eutectic\,H_2O}$

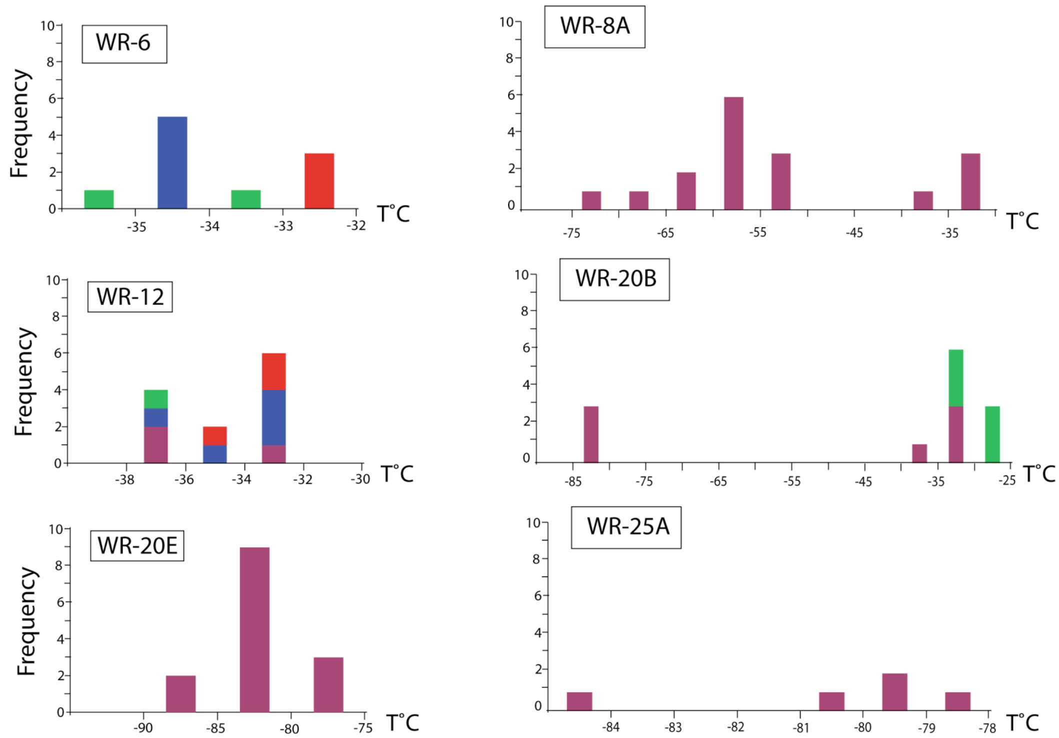

Tm_{ice}

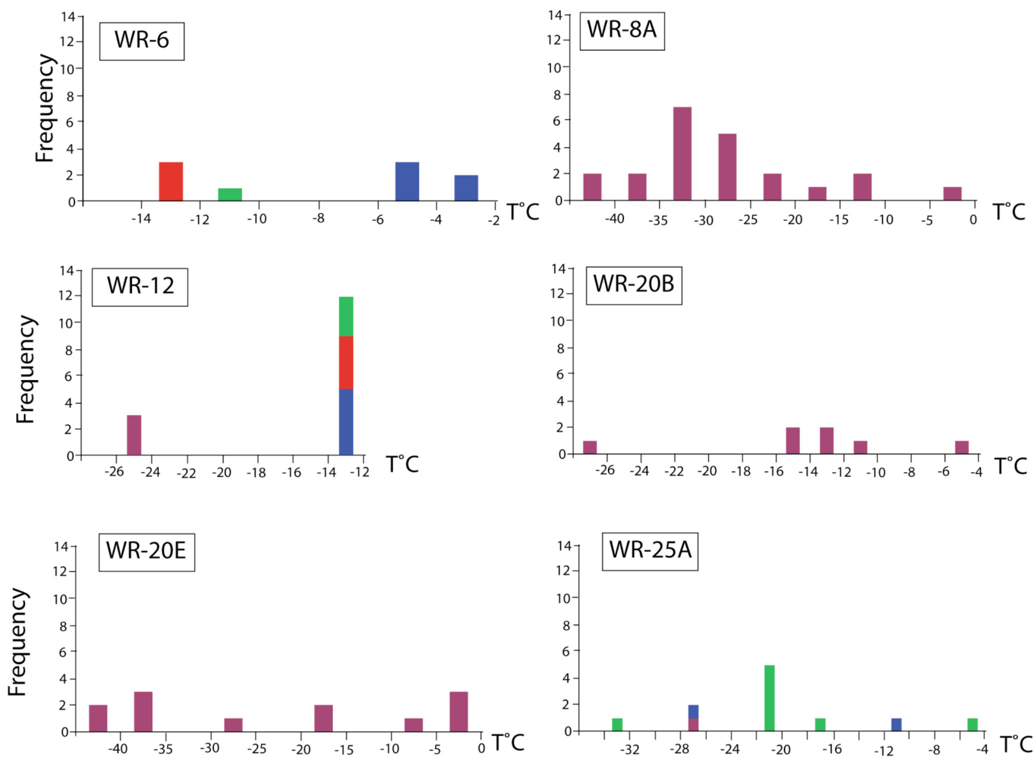

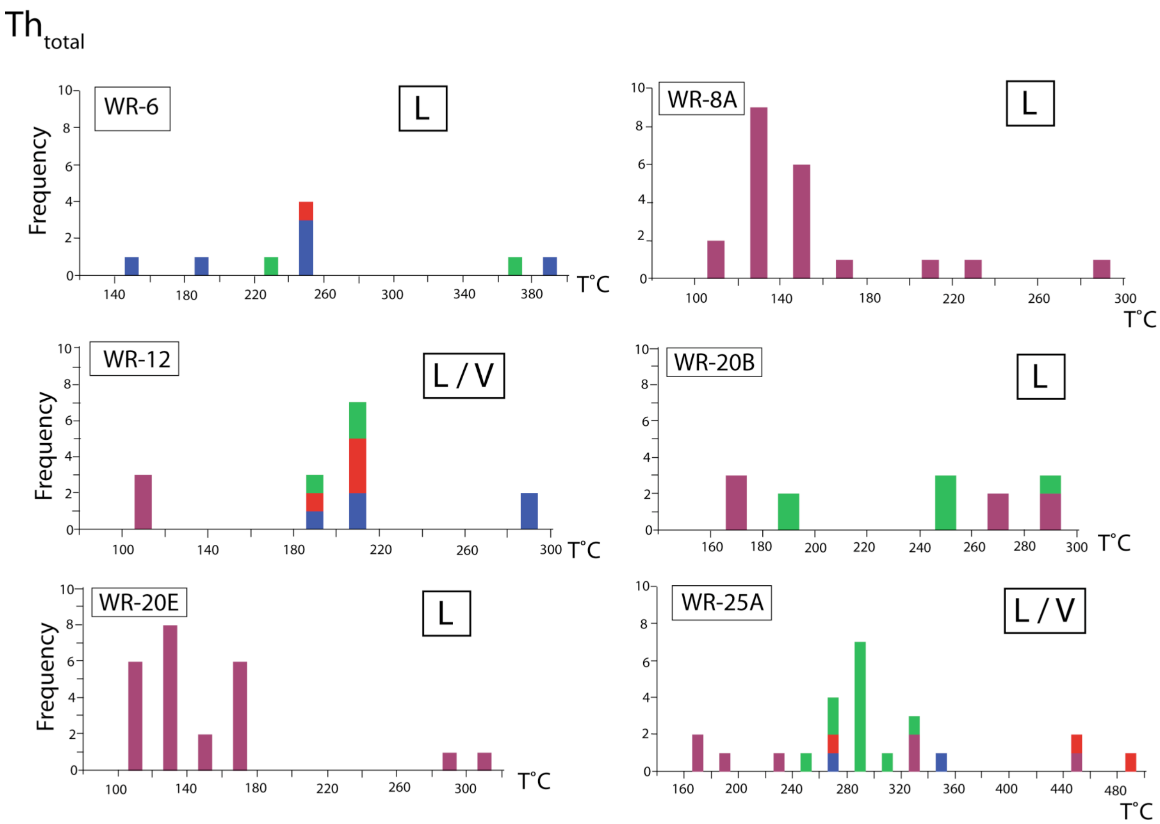

Figure 5.2: Histograms of microthermometry results for WR-6, WR-8A, WR-12, WR-20B, WR-20E and WR-25A. Type I inclusions are shown in purple, Type II are blue, Type III are red, and Type IV are green. Each sample is denoted as homogenizing to the liquid (L) or to the liquid or vapor (L/V) for Th_{CO2} and Th_{total}.

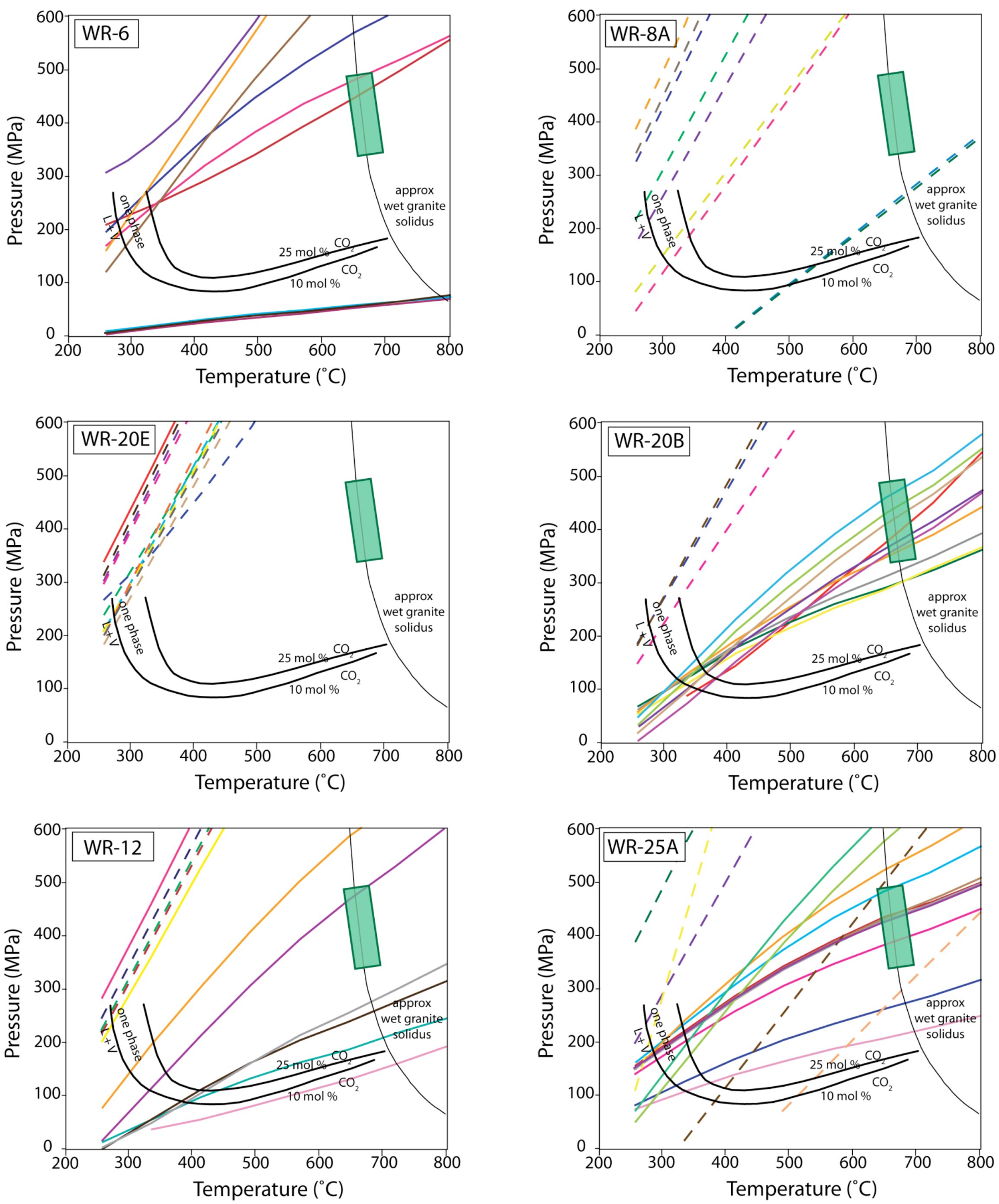

Figure 5.3: Isochores for analyzed samples. Dashed lines represent samples for which molar volumes are not calculated when analyzed using the FLUIDS and CLATHRATES packages of Bakker (2009). This is most likely due to the limitations of the programs. The green boxes represent the conditions inferred from amphibole thermobarometry.

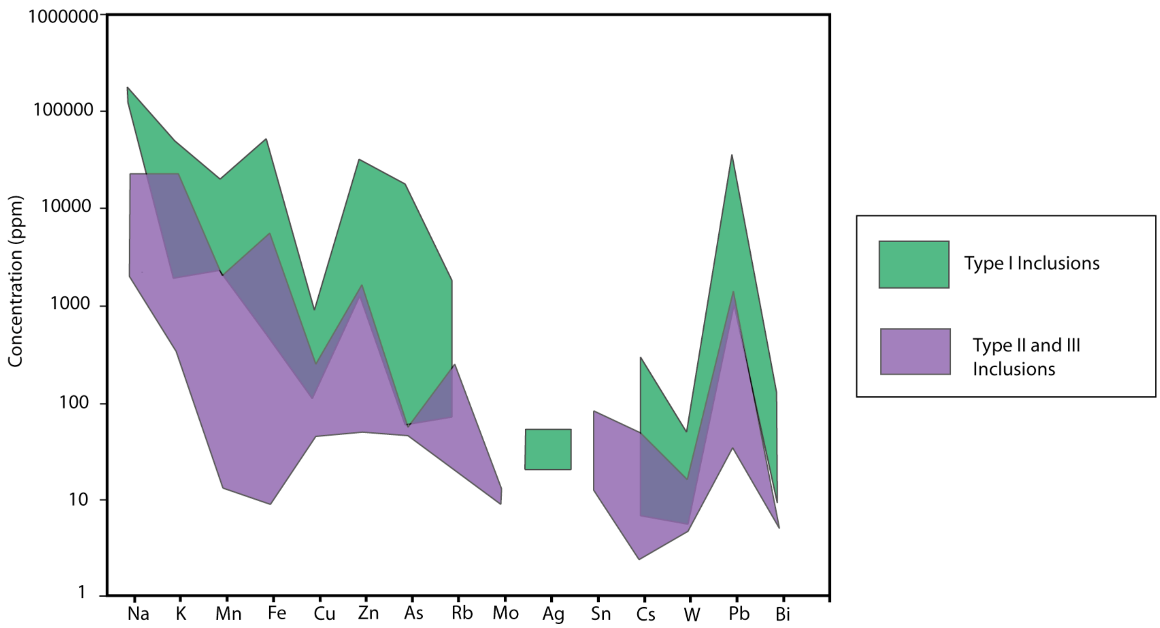

Figure 5.4: Summary of LA-ICP-MS data for a suite of elements for Type I, II, and III inclusions. Note that there is compositional overlap for some elements between the inclusion types.

6. DISCUSSION

6.1 NATURE AND EMPLACEMENT OF THE LLB

The LLB has a complex crystallization history. Several factors can be inferred from the petrography, whole rock characterization, mineral chemistry and fluid inclusion data. These factors are used to construct a likely model for the development of the batholith and hydrothermal fluid release from it. The LLB is a calc-alkaline, I-type granite with a relatively high oxygen fugacity that formed in a volcanic arc setting.

The LLB was originally intruded as a granite to granodiorite, with punctuated inputs of magma with a slightly different composition, but with a similar source. These inputs include widespread suites of magma presumed to have formed early and then entrained in the batholith during convection. These magmas assimilated with the LLB main phase granites and granite to tonalite dikes. As the magma crystallized, fractionated liquid coalesced to generate aplite and pegmatite dikes. As the amount of melt decreased and the liquid became more fractionated aplites and pegmatites became less abundant, and quartz veins began to cross-cut the batholith. Although the LLB exhibits multiple generations of magmatic phases, they lack quenching or alteration halos along contacts. This implies that the phases were in equilibrium with each other and contemporaneous. The granitic to tonalitic dikes that were emplaced during crystallization of the LLB suggests that there were multiple generations of magma within the magma chamber. Similar REE patterns suggest that these dikes originated from the same source. The presence of mafic enclaves indicates that magma mixing may have played a role in the formation of the LLB. The enclaves are presumably one or more of the following: remnants of mafic magma that was injected into the magma chamber during crystallization, early formed cumulates, or the residual material from partial melting of source rocks (restite). The REE patterns of the enclaves indicate either a different melt source than the host granodiorite or an early cumulate.

The abundance of aplites, pegmatites and quartz veins implies that near the end of crystallization copious amounts of evolved fluids were present, especially localized in areas like Cony Mountain. The evolved fluids resulted in multiple generations of cross-cutting aplite and pegmatite dikes. The quartz veins appear to be formed from the last of the fluid, as they cut all other phases. The quartz-hematite veins found near Louis Lake are likely later than the main phase because they exhibit propylitic alteration; however, this study lacks evidence for timing of alteration. The quartz-hematite veins are also present in brittle shear zones.

Geochemistry of the LLB samples gives some insight into the crystallization history of batholith. Harker Diagrams show that magnetite and apatite began crystallizing early. This is confirmed in thin section as apatite and magnetite are found as inclusions within all other minerals. This is important because these minerals would scavenge ligands, sulfur and chloride in the case of apatite, and metals in the case of magnetite, from the original melt. The dearth of a zonation trend in the type of hornblende suggests the lack of significant pressure change during crystallization. Cheang et al (1986) found uniform oxygen isotopes that related to convection in the magma chamber and little interaction with later meteoric waters. This demonstrates that the Louis Lake Batholith has experienced little interaction with externally derived later hydrothermal fluids.

6.2 INDICATION OF FLUID CHARACTERISTICS

6.2.1 Clues from Apatite

Apatites can indicate several characteristics of the aqueous fluid inside the batholith at the time of crystallization. Within the crystal lattice of apatite, F^- and Cl^- substitute for OH^- and S^{6+} substitutes for P^{5+}. Salinity can be estimated from the F^- and Cl^- content of apatites, while the S^{6+} content estimates the SO_3 content. Apatites can indicate the minimum salinity of the fluid by using the m^{aq}_{HCl}, and for the LLB, they range between $4.6 \times 10^{-4} \pm 4.5 \times 10^{-4} m$ (average ± 1σ) and $7.8 \times 10^{-4} \pm 7.6 \times 10^{-4} m$. The calculated chloride molality values (as m^{aq}_{HCl}) of the LLB are low compared with the values for ore-producing plutons (HCl molalities 0.05 or greater) of Piccoli and Candela (1992), as a result of pressure dependency in the equilibrium equation. The equation is dependent on pressures that were calculated using hornblende thermobarometry, and in this study, the median pressures were used. The actual salinity is probably higher because the fluorine-chlorine ratio is much lower than that calculated from biotite. This is likely because the equations of Piccoli and Candela (1992) calculate the concentration of HCl, while the total Cl^- was measured from biotites, and thus would include Cl^- that is bonded to other species in solution. The salinities from fluid inclusions are also much higher than the calculated molalities, adding support for a higher salinity for the batholith.

By observing the SO_3 content in apatites throughout the evolution of the batholith, a generalized graph can be created (Figure 6.1). Because we know the general evolution of the batholith, we can assume the order that the phases evolved, and thus the order that the apatites grew. The concentration of SO_3 changes during the developmental phases of the batholith. Sulfur likely increases in concentration with magmatic differentiation, but will fractionate into a hydrothermal fluid phase when it forms. The shape of the curve of SO_3 content in Figure 6.1 is likely because of an early release of a S-rich fluid. This sulfur-rich liquid would be able to scavenge metals, and possibly transport them to other parts of the batholith, or possibly away from the batholith.

6.2.2 Clues from Fluid Inclusions

Fluid inclusions give insight into the conditions during the last parts of crystallization and the only information about the compositions of the hydrothermal fluids. The variability of inclusion types within the LLB suggests intricate processes were functioning inside the batholith. The amount of CO_2 within the inclusions varies between type, from the dominant phase (Type IV) to almost non-detectable (Type I) and in-between (Type II and III). Salinities also encompass a wide range, from low (Type II) to moderate (Type III and IV) to high (Type I). Because Type III inclusions are assumed to be and intermediate of Type I and II, mixture of these types provides support for immiscibility. The occurrence of multiple daughter minerals, and the inference of the presence $CaCl_2$ implies complexity of the original hydrothermal and/or magmatic fluid and a high content of a number of cations. While a large quantity of inclusions partially or completely decrepitated before reaching total homogenization, a few small inclusions remained intact until 500°C. This provides evidence for original entrapment above 500°C. Figure 6.2 gives the likely conditions of granite crystallization compared to two-phase curves for weakly- to moderately-saline aqueous-carbonic fluids. Figure 6.2 shows that inclusions were likely trapped in the one-phase field, alluding to homogeneous rather than heterogeneous trapping. This figure however assumes that the only salt in solution is NaCl, and may not truly be representative. The presence of the four types of inclusions suggests that immiscibility can play a role in magmato-hydrothermal fluid evolution at pressures greater than 3 kbar. This may be because of the chemical complexity of the fluid, for example the high divalent cation content. This figure elucidates why the isochores do not all pass through the conditions expected for the LLB fluid. Figure 5.3 presented the isochores calculated from microthermometry results. The samples that best fit the conditions estimated for the LLB inclusions support the interpretation of entrapment during or immediately after crystallization. The other samples require an explanation for their results. Some fluid inclusions have become internally overpressured leading to greater or lower densities than those expected for the LLB fluid. Figure 6.3 shows the likely path that the LLB inclusions followed to become overpressured (in red). Evidence for internal overpressure includes the frequent decrepitation of the inclusions during microthermometry and hook-like morphology of some of the inclusions themselves (Vityk and Bodnar 1995). The inclusions underwent near-isothermal decompression, and I infer that some decompression occurred while the batholith was cooling. This may have occurred during retrograde metamorphism, but the tectonic setting and timing of this event was not explored in this study.

6.3 COMPARISON OF FLUID BEHAVIOR AND COMPOSITION IN THE LLB WITH THOSE IN ORE DEPOSITS

The LLB shares many similarities to felsic to intermediate magmas associated with ore deposits and its proximity to mineralization is extra evidence for its mineral potential. The batholith is located near a known gold-producing district, was intruded over the same time period as ore generation, and is locally mineralized with copper stockworks (Hausel 1991). Hausel (1991) noted that the low-grade chalcopyrite-bearing quartz veins containing silver, gold, and calcite gangue are concentrated in the SPGB near the contact with the LLB and also within the batholith itself. These relationships suggest that the LLB could be responsible for the copper mineralization. The LLB is similar to gold-related plutons described by Blevin and Chappell (1992) in that it shares similar oxidation state, lacks extreme fractionation, and has evidence for an early-crystallized sulfide phase.

Further evidence to support the mineral potential of the LLB comes from apatites. Figure 6.4 gives the apatite type with data on felsic-intermediate ore-related systems. The ore producing systems of Piccoli and Candela (2002) have a wider range in fluorapatite and chlorapatite composition, while the non-ore producing systems represent a smaller range in apatite composition. Upon comparison with the felsic-intermediate ore-related systems of Piccoli and Candela (1992), the LLB samples are similar. This similarity implies that the apatites formed in similar conditions as those of felsic-intermediate ore-related systems. The apatite data also presents evidence for a release of a S-rich fluid for scavenging minerals, which is essential for the formation of ore deposits. Seo et al (2009) have noted elevated sulfur levels in porphyry deposits, and noted that sulfur controls the efficiency of copper extraction from a melt into an aqueous fluid.

The trace element composition of magnetite grains add more support for a high ore potential of the LLB. The grains contain inclusions of chalcopyrite, and a high metal content (Cu and Au) as determined by microprobe work. Cu is best sequestered by sulfides, but at high fO_2, as in the LLB, most sulfides are unstable. In this case, magnetite, other oxides and silicates would sequester Cu and other metals during early crystallization (Core et al 2005). These metals may have been scavenged by sulfur-rich fluid later. Cu and Au concentrations of the LLB magnetites were higher than those from experiments of Simon et al. (2008). Geochemical analysis of the mafic enclave supports the idea that gold and other metals were introduced to the granite by mixing with mafic magmas. Enclaves with high copper content have been used to indicate that such a mixing process is responsible for the creation of large porphyry deposits, such as Bingham Porphyry Copper Deposit (Core et al, 2006). A few of the grains are similar to the Fe-oxide globules of Larocque et al. (2000) in that they have a more massive core with a frothy or spongy rim, and the presence of chalcopyrite included in the phenocrysts. Figure 6.5 gives a picture of a typical grain showing these textures. The presence of "globules' indicates that the LLB may have saturated at an early stage in the crystallization history with respect to a sulfide mineral or a sulfide melt which would have had a high metal content that was mobilized with a S-rich aqueous fluid, like that which is inferred to have exsolved from the LLB. The evidence for mixing of felsic and mafic magmas, along with the presence of the "globules" is consistent with the theory of Larocque et al. (2000) that magma mixing plays a role in the formation of magmato-hydrothermal ore deposits. Within the LLB, the sulfur-rich aqueous fluid would have caused dissolution of the sulfides and replacement by magnetite. Whole rock geochemical analysis of a mafic enclave demonstrated that Cu was found mostly within the enclave, but Au values were elevated immediately surrounding the enclave. This observation leads to the inference that Au and Cu were transported and/or deposited differently.

Comparisons of LA-ICP-MS data on the composition of LLB fluid inclusions with intrusion-centered ore systems and orogenic gold deposits reveal remarkable similarities (Figure 6.6). High salinity (Type I) fluids have elemental compositions that fall within the range for brines of other intrusion-centered ore hydrothermal systems of Audetat et al (2008). Noted differences with intrusion-centered ore hydrothermal systems are lower Mo, Sn, and W, but higher As contents. Low-salinity (Type II and III) fluids differ from fluids in ore-related intrusion-centered systems in order of magnitude lower Cu, lower Fe and Mn, and lower K/Na ratios. The low-salinity fluids are similar to the orogenic gold systems of Yardley et al. (1993), but have higher Pb and Zn. These low-salinity fluids also have relatively high concentrations of Sb, As, and B, similar to fluids in gold-forming systems.

In summary, there is abundant evidence for hydrothermal fluid exsolution, possibly of two immiscible fluids. This is substantiated by SO_3 values of apatites that imply fluids exsolved relatively early during fractionation of the granite.

6.4 MODEL FOR THE FORMATION OF AN ORE DEPOSIT FROM THE LLB

Previous investigations of the gold and copper deposits in the Atlantic City District have dismissed the LLB as a source for the fluids and metals needed to form the deposits (McGowan 1991); however, this study provides evidence for a genetic link between the batholith and the mineral deposits. I propose a model in which both fluids and metals were derived from the LLB, and were transported away and deposited in the SPGB. During the crystallization of the LLB, multiple generations of magma began mixing. Inputs of mafic magma into the chamber may have transported metals. Alternatively, the magma may have created early fractionates that preferentially contained sulfides. Convection within the magma chamber would have entrained fractionates or mafic magma and mixed them with the rest of the magma. In either case, a sulfide melt formed within the LLB, effectively scavenging Au, Cu and other metals because of their large partition coefficients (Halter et al. 2002). From this sulfide melt, ore-bearing minerals such as chalcopyrite began to crystallize, mostly within sulfide globules. As the magma crystallized, the remaining magma became enriched in Cl^- and the fO_2 increased, which caused a decrease in stability of sulfide. The instability of sulfide creates an environment conducive to the transfer of metals and sulfur into a hydrothermal ore fluid (Halter et al. 2002). Gold, copper and other metals were carried along with sulfur in the event recorded by apatites. Studies of metal content in fluid inclusions (Seo et al. 2009; Pokrovski et al. 2008) concluded that Au is preferentially transported by the vapor phase, and Cu is carried within the brine, accounting for the difference in location of Au and Cu within samples. This fluid traveled away from the batholith, and was focused into shear zones that had formed in the SPGB. Mineralization within these shear zones was aided by the composition of the host rock and changing conditions within the fluid.

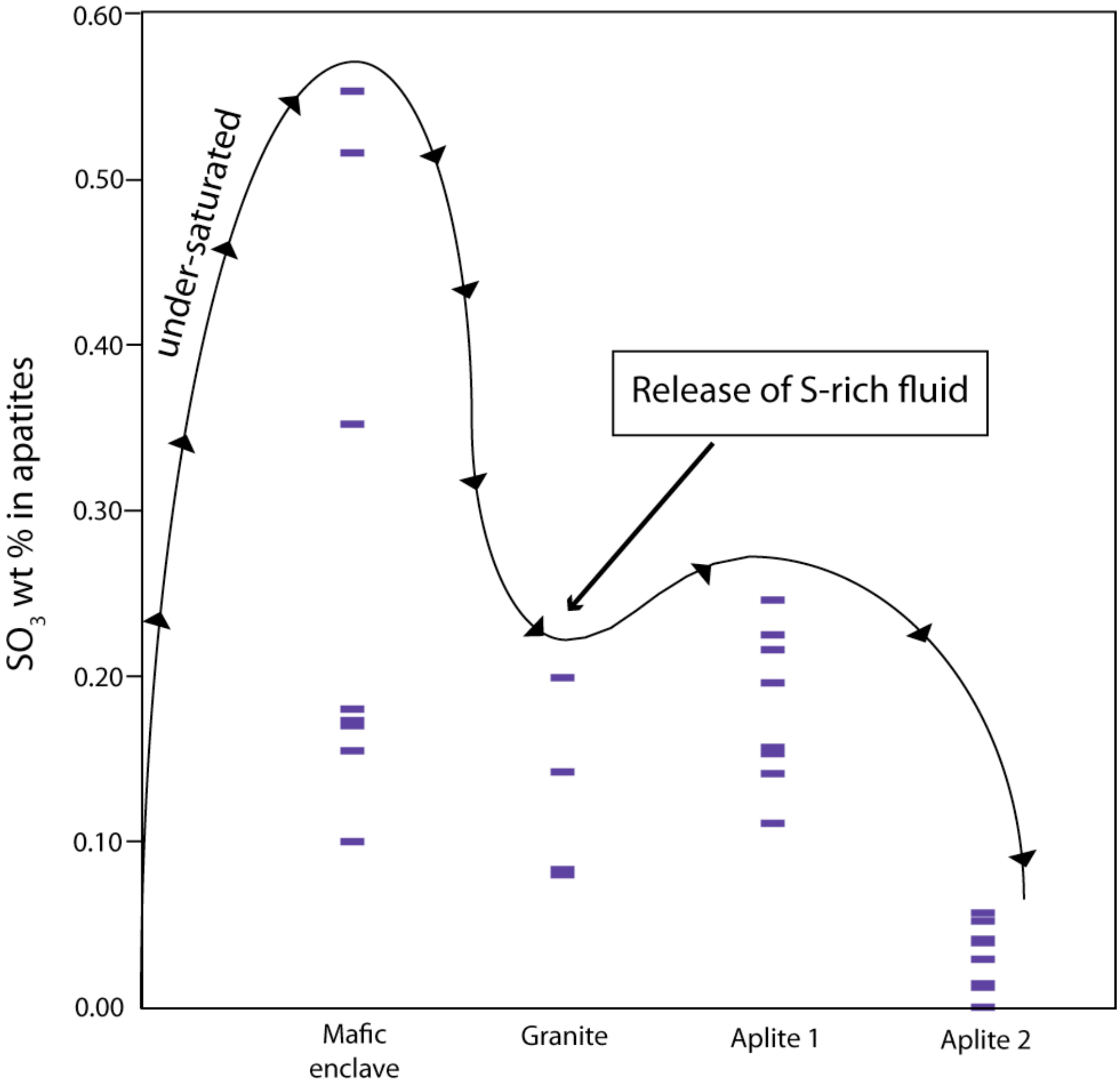

Figure 6.1: SO_3 in apatite through evolution of the batholith. Note the dip for the granite concentrations that may represent the release of a S-rich fluid.

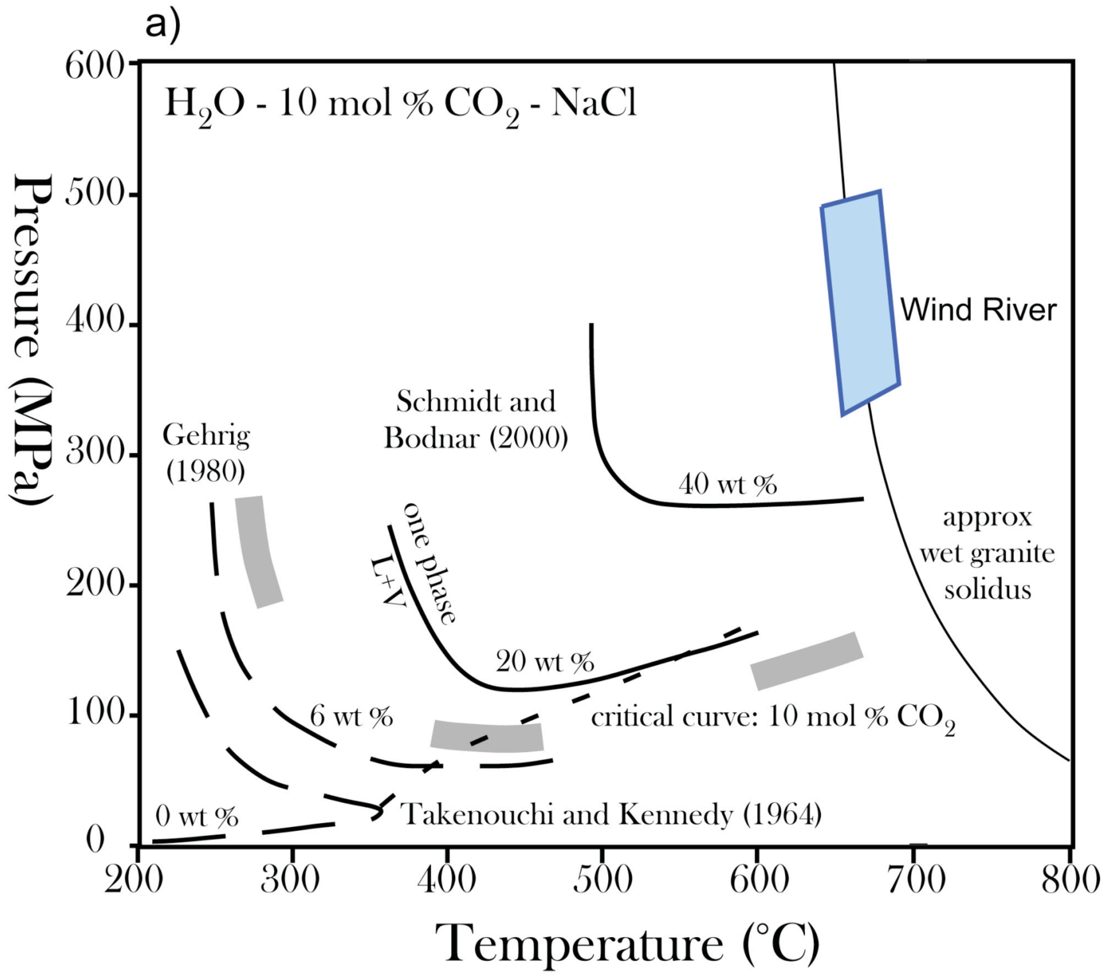

Figure 6.2: Conditions of granite crystallization estimated with hornblende barometry compared with two-phase curves for weakly- to moderately-saline aqueous carbonic fluids (after Schmidt and Bodnar, 2000). The grey dashed line shows the position the two phase curve most appropriate for the composition of the granite-hosted inclusions.

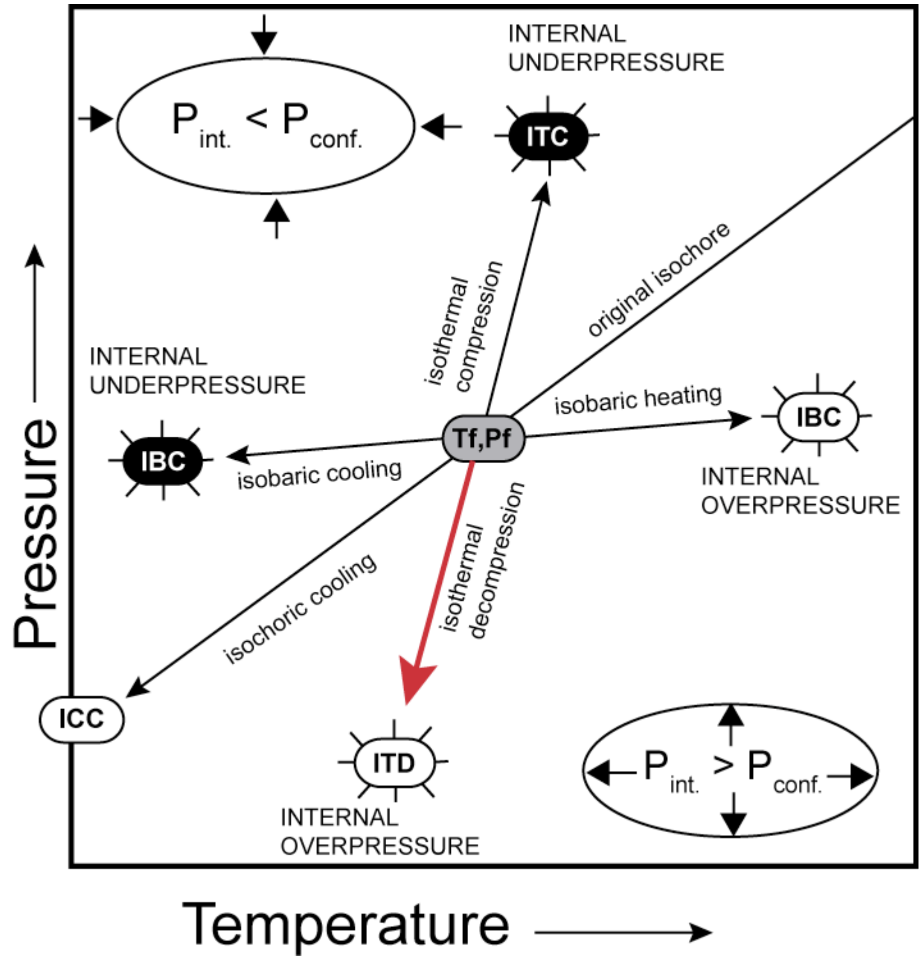

Figure 6.3: Possible P-T paths that fluid inclusions take during metamorphism after Vityk and Bodnar (1995). The red arrow shows the likely path some of the LLB inclusions experienced to reach internal overpressure, and thus shift the isochores.

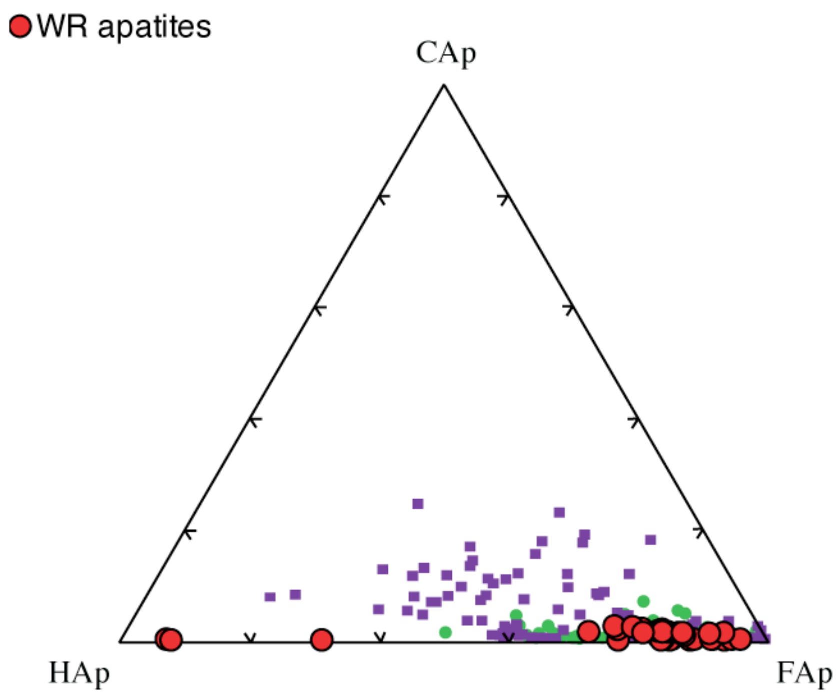

Figure 6.4: F-Cl-OH variability in LLB samples (red circles) and the data of Piccoli and Candela (2002) for Felsic-Intermediate Ore-Related Systems. Purple squares = Ore producing systems and green circles= non-ore producing systems.

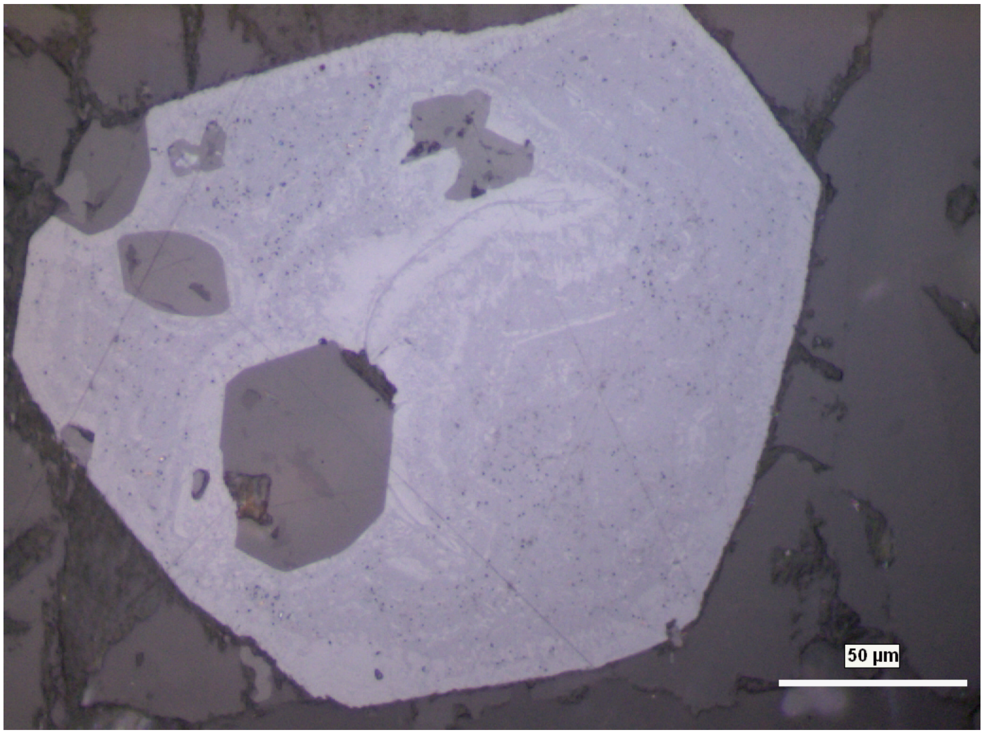

Figure 6.5: Photomicrograph of a magnetite in sample WR-4B exhibiting a distinctly different, pseudo-colloform texture which formed by replacement of earlier sulfide mineral or minerals (cf. Larocque et al., 2000).

A

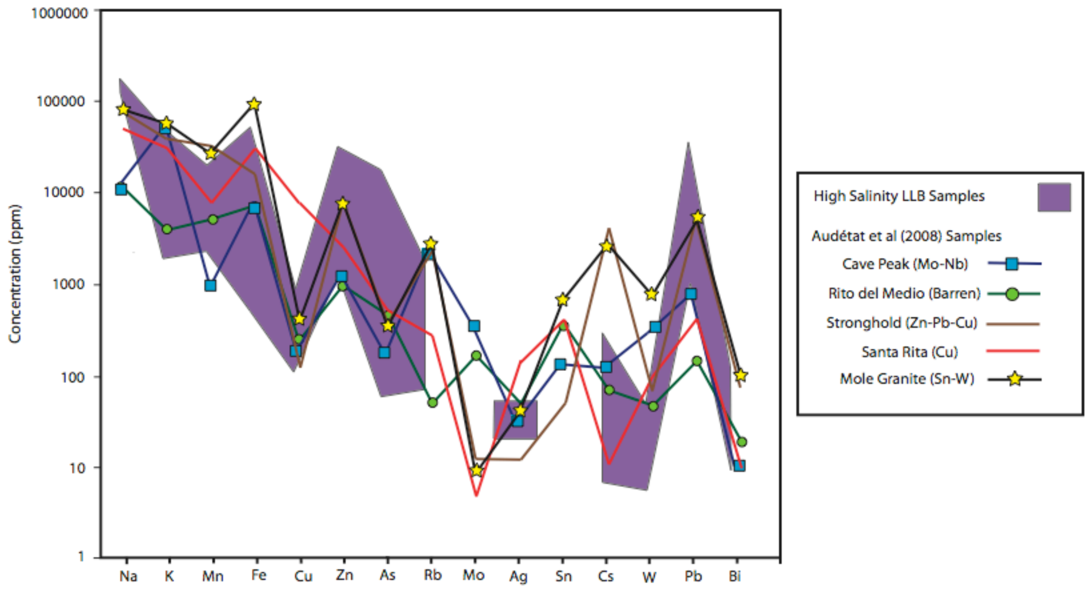

B

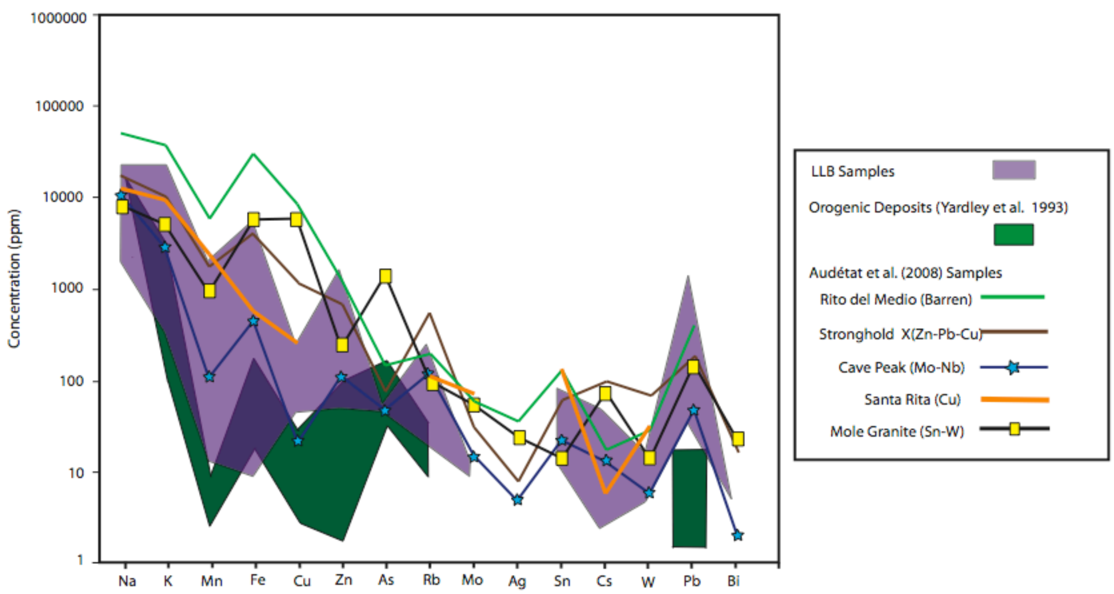

Figure 6.6: Multi-element spider diagrams comparing a suite of elements in the fluid inclusions (LA-ICP-MS data) data from known intrusion-centered ore deposits and orogenic gold deposits. Only a subset of analyzed elements are included on the graphs. A) High salinity, Type I inclusions compared with high salinity inclusions from Audétat et al. (2008); B) Low salinity, Types II and III inclusions compared to low salinity inclusions or related fluid inclusions of Audétat et al. (2008) and Yardley et al. (1993).

7. CONCLUSIONS

7.1 SUMMARY

The LLB is a 400 km^2, late-Archean batholith that formed at mid-crustal depths. Geochemical results in this study confirm the results of previous work that characterize the LLB as relatively oxidizing, metaluminous, calc-alkaline granitoid that likely formed in a volcanic arc environment. Field evidence tells us that multiple phases were present and interacting during crystallization, including a mafic component that is seen as mafic enclaves. The batholith has experienced little internal deformation since it intruded the SPGB during deformation in the Archean. The LLB also contains elevated Cu, Au, and Ag concentrations, both on the macro scale and within individual mineral grains. Studies of the silicates and oxides provide insight into the processes that were occurring during crystallization. Amphiboles provide crystallization temperatures between 637°C and 850°C and pressure between 1.8 and 5.78 kbar. Amphibole composition also indicates that there was little pressure change during crystallization. Sulfides, such as chalcopyrite, took in metals early during crystallization. These sulfides were replaced by oxides when the oxygen fugacity changed and metals may have been released into a sulfur-rich fluid. Apatite investigation tells us that a sulfur-rich fluid was likely released early in crystallization.

Primary and pseudosecondary fluid inclusions were described from a suite of samples that are believed to represent late fractionates or magma-derived fluids. Type I inclusions are high salinity aqueous inclusions with multiple daughter minerals. Type II inclusions are low to moderate salinity, aqueous-carbonic inclusions, occasionally containing daughter minerals. Type III inclusions are moderate salinity, aqueous-carbonic inclusions with varying amounts of daughter minerals, and are believed to be an intermediate between Type I and II. Type IV inclusions are CO_2-rich and low to moderate salinity. Type I and IV inclusions are believed to primary, while Types II and III are considered to be pseudosecondary. All inclusion types are inferred to have been formed at the time of crystallization, and not related to secondary fluid movement. Evidence from the petrography of fluid inclusions concludes that immiscibility played a role in magmato-hydrothermal fluid evolution; however, calculated isochores imply that they were trapped as homogeneous fluids. This discrepancy is likely because NaCl was inferred to be the only salt in the system in the calculation of isochores, and this is implausible because of the complexity of daughter minerals and the likely occurrence of $CaCl_2$. The presence of $CaCl_2$ is confirmed by the behavior of salts during microthermometry and the results of LA-ICP-MS.

Since the LLB has many similarities to felsic to intermediate plutons associated with ore deposits, it is possible that it too generated ore deposits. The oxides contain strong evidence that the LLB originally possessed a high metal content. A S-rich aqueous fluid scavenged these metals relatively early in the crystallization process and possibly transported them away from the batholith. The high Cu content of the enclaves and high Au of the surrounding granite suggests that Cu and Au were introduced by a mafic magma and released into the granitic magma as the enclaves were assimilated. The importance of mafic enclaves and a similar ore fluid model are considered for the formation of the Bingham porphyry copper deposit (Core et al 2006). These similarities introduce the possibility that the LLB may be responsible proximal for copper and gold deposits, presumably the copper lodes and stockworks and/or the lode gold deposits in the Atlantic City District.

7.2 FUTURE WORK

Further work is needed to better characterize the mineral and mineralizing potential of the LLB. A detailed geochemical study of magnetite grains and their magmatic sulfides would be useful for better defining the original metal content. Comparisons of LLB magnetites with magnetites of known deposit types may also improve the model. A detailed petrographical and geochemical study of the cupriferous lodes and stocks is also important because any relationships with the LLB would become more apparent. Geochronology of the chalcopyrite-bearing veins and the hematite veins using U-Pb or Re-Os techniques would constrain the ages of the veins and determine their relation to the batholith.

REFERENCES

Audetat, A., Pettke, T., Heinrich, C.A., and Bodnar, R.J., 2008, Special Paper: The Composition of Magmatic-Hydrothermal Fluids in Barren and Mineralized Intrusions: Economic Geology and the Bulletin of the Society of Economic Geologists, v. 103, p. 877-908.

Bakker, R.J., 1997, CLATHRATES: Computer Programs to Calculate Fluid Inclusion V-X Properties using clathrate melting temperatures: Computers & Geosciences, v. 23, p. 1-18.

Bakker, R.J., 2003, Package FLUIDS 1. Computer programs for analysis of fluid inclusion data and for modelling bulk fluid properties: Chemical Geology, v. 194, p. 3-23.

Bayley, R.W., 1965, Geologic map of the South Pass City Quadrangle, Fremont County, Wyoming: Reston, VA, United States, U.S. Geological Survey Geologic Quadrangle Map GQ-458, scale 1:24,000.

Bayley, R.W., Proctor, Paul D., and Condie, Kent C., 1973, Geology of the South Pass Area, Fremont County, Wyoming: U.S. Geological Survey Professional Paper, P 0793.

Blevin, P.L., and Chappell, B.W., 1992, The role of magma sources, oxidation states and fractionation in determining the granite metallogeny of eastern Australia: Transactions of the Royal Society of Edinburgh: Earth Sciences, v. 83, p. 305-316.

Burrows, D.R., Wood, P.C., and Spooner, E.T.C., 1986, Carbon isotope evidence for a magmatic origin for Archaean gold-quartz vein ore deposits: Nature, v. 321, p. 851-854.

Cheang, K.K., Wenner, D.B., and Stuckless, J.S., 1986, Oxygen Isotopic Constraints on the Origin of the Precambrian Granites from the Southern Wind River Range and the Granite Mountains, Central Wyoming: U.S. Geological Survey Bulletin, B 1622, p. 109-129.

Core, D.P., Kesler, S.E., and Essene, E.J., 2005, Copper and Zinc in silicate and oxide minerals in igneous rocks from the Bingham- Park City Belt, Utah: Synchrotrom X-ray fluorescence data: The Canadian Mineralogist, v. 43, p. 1781-1796.

Core, D.P., Kesler, S.E., and Essene, E.J., 2006, Unusually Cu-rich magmas associated with giant porphyry copper deposits: Evidence from Bingham, Utah: Geology, v. 34, p. 41-44.

Frost, B.R., 1991, Introduction to oxygen fugacity and its petrologic importance: Reviews in Mineralogy, v. 25, p. 1-9.

Frost, B.R., Chamberlain, K.R., and Schumacher, J.C., 2001, Sphene (titanite): phase relations and role as a geochronometer: Chemical Geology, v. 172, p. 131-148.

Frost, B.R., Chamberlain, K.R., Swapp, S.M., Frost, C.D., and Hulsebosch, T.P., 2000a, Late Archean structural and metamorphic history of the Wind River Range: Evidence for a long-lived active margin on the Archean Wyoming craton: GSA Bulletin, v. 112, p. 564-578.

Frost, B.R., Frost, C.D., Hulsebosch, T.P., and Swapp, S.M., 2000b, Origin of the Charnockites of the Louis Lake Batholith, Wind River Range, Wyoming: Journal of Petrology, v. 41, p. 1759-1776.

Frost, C.D., Frost, B.R., Chamberlain, K.R., and Hulsebosch, T.P., 1998, The Late Archean history of the Wyoming province as recorded by granitic magmatism in the Wind River Range, Wyoming: Precambrian Research, v. 89, p. 145-173.

Frost, C.D., Fruchey, B.L., Chamberlain, K.R., and Frost, B.R., 2006, Archean crustal growth by lateral accretion of juvenile supracrustal belts in the south-central Wyoming Province: Canadian Journal of Earth Sciences, v. 43, p. 1533-1555.

Goldfarb, R.J., Phillips, G.N., and Nokleberg, W.J., 1998, Tectonic Setting of synorogenic gold deposits of the Pacific Rim: Ore Geology Reviews, v. 13, p. 185-218.

Groves, D.I., Goldfarb, R.J., Robert, F., and Hart, C.J.R., 2003, Gold Deposits in Metamorphic Belts; Overview of Current Understanding, Outstanding Problems, Future Research, and Exploration Significance: Economic Geology and the Bulletin of the Society of Economic Geologists, v. 98, p. 1-29.

Halter, W.E., Pettke, T., and Heinrich, C.A., 2002, The origin of Cu/Au ratios in porphyry-type ore deposits: Science, v. 296, p. 1844-6.

Hammarstrom, J.M., and Zen, E.-a., 1986, Aluminium in hornblende: An empirical igneous geobarometer: American Mineralogist, v. 71, p. 1297-1313.

Harris, N.B.W., Pearce, J.A., and Tindle, A.G., 1986, Geochemical characteristics of collision-zone magmatism, *in* Coward, M.P., and Reis, A.C., eds., Collison Tectonics, Volume 19, Special Publication of the Geological Society, p. 67-81.

Hausel, W.D., 1991, Economic Geology of the South Pass Granite-Greenstone Belt, Southern Wind River Range, Western Wyoming: United States, Geological Survey of Wyoming : Laramie, WY, United States. 129 pp.

Hull, J.M., 1988, Structural and tectonic evolution of Archean supracrustals, southern Wind River Mountains, Wyoming, University of Rochester.

Kerrich, R., and Fyfe, W.S., 1981, The gold-carbonate association: source of CO_2 and CO_2 fixation reactions in Archean lode gold deposits: Chemical Geology, v. 33, p. 265-294.

Larocque, A.C.L., Stimac, J.A., Keith, J.D., and Huminicki, M.A.E., 2000, Evidence for open-system behavior in immiscible Fe-S-O liquids in silicate magmas: Implications for contributions of metals and sulfur to ore-forming fluids: The Canadian Mineralogist, v. 38, p. 1233-1249.

Leake, B.E., Woolley, A.R., Arps, C.E.S., Birch, W.D., Gilbert, M.C., Grice, J.D., Hawthorne, F.C., Kato, A., Kisch, H.J., Krivovichev, V., Linthout, K., Laird, J., Mandarino, J.A., Maresch, W.V., H., N.E., Schumacher, J.C., Smith, D.C., Stephenson, N.C.N., Ungaretti, L., Whittaker, E.J.W., and Youzhi, G., 1997, Nomenclature of amphiboles: Report of the subcommittee on amphiboles of the International Mineralogical Association, Commission on new minerals and mineral names: The Canadian Mineralogist, v. 35, p. 219-246.

Lo, H.H., 1970, Geochemistry of the Louis Lake pluton, Southwestern Wyoming: St. Louis, MO, Washington University.

McGowan, K.I., 1990, Thermochemical conditions for the formation of Archean lode gold mineralization at Atlantic City-South Pass, Wyoming: United States, Ph. D. thesis, Iowa State University.

Munoz, J., 1992, Calculation of HF and HCl fugacities from biotite compositions: revised equations: Geological Society of America, Abstracts with Programs, v. 24, p. 221.

Naylor, R.S., Steiger, R.H., and Wasserburg, G.J., 1970, U-Th-Pb and Rb-Sr systematics in the 2700 x 10(super 6)- year old plutons from the southern Wind River Range, Wyoming: Geochimica et Cosmochimica Acta, v. 34, p. 1133-1159.

Nesbitt, B.E., 1988, Gold deposit continuum; a genetic model for lode Au mineralization in the continental crust: Geology, v. 16, p. 1044-1048.

Nesbitt, B.E., and Muehlenbachs, K., 1991, Stable isotopic constraints on the nature of the syntectonic fluid regime of the Canadian Cordillera: Geophysical Research Letters, v. 18, p. 963-966.

Pearce, J.A., Harris, N.B.W., and A.G., T., 1984, Trace element discrimination diagrams for the tectonic interpretation of granitic rocks: Journal of Petrology, v. 25, p. 956-983.

Pearson, R.C., Kiilsgaard, T.H., and Patton, L.L., 1971, Mineral Resources of the Popo Agie Primitive Area, Fremont and Sublette Counties, U.S. Geological Survey Bulletin, 55 pp.

Pearson, R.C., Patten, L.L., and Gaskill, D.L., 1973, Mineral resources of an area near the Popo Agie Primitive Area, Fremont County, Wyoming: U.S. Geological Survey Bulletin. 18 pp.

Piccoli, P.M., and Candela, P.A., 1994, Apatite in felsic rocks- A model for the estimation of initial halogen concentrations in the Bishop Tuff (Long Valley) and Tuolumne Intrusive Suite (Sierra-Nevada Batholith) Magmas: American Journal of Science, v. 294, p. 92-135.

Piccoli, P.M., and Candela, P.A., 2002, Apatite in Igneous Systems, *in* Kohn, M.J., Rakovan, J., and Hughes, J.M., eds., Phosphates: gechemical, geobiological and materials importance, Volume 48: United States, Mineralogical Society of America and Geochemical Society : Washington, DC, United States, p. 255-292.

Pokrovski, G.S., Borisova, A.Y., and Harrichoury, J.C., 2008, The effect of sulfur on vapor– liquid fractionation of metals in hydrothermal systems: Earth and Planetary Science Letters, v. 266, p. 345–362.

Ramsay, W.R.H., Bierlein, F.P., Arne, D.C., and VandenBerg, A.H.M., 1998, Turbidite-hosted gold deposits of central Victoria, Australia; their regional setting, mineralising styles, and some genetic contraints: Ore Geology Reviews, v. 13, p. 131-151.

Schmitz, P.J., 2005, Emplacement of the late Archean Louis Lake Batholith and accretion of the Miners Delight Formation allochthon, southern Wind River Range, Wyoming: United States, Master's thesis, University of Wyoming. 129 pp.

Seo, J.H., Guilling, M., and Heinrich, C.A., 2009, The role of sulfur in the formation of magmatic-hydrothermal copper-gold deposits: Earth and Planetary Science Letters, p. 323-328.

Simon, A.C., Candela, P.A., Piccoli, P.M., Mengason, M., and Englander, L., 2008, The effect of crystal-melt partitioning on the budgets of Cu, Au, and Ag: American Mineralogist, v. 93, p. 1437-1448.

Streck, M.J., and Dilles, J.H., 1998, Sulfur evolution of oxidized arc magmas as recorded in apatite from a porphyry copper batholith: Geology, v. 26, p. 523-526.

Stuckless, J.S., 1989, Petrogenesis of Two Contrasting, Late Archean Granitoids, Wind River Range, Wyoming: U.S. Geological Survey Professional Paper. 38 pp.

Stuckless, J.S., Hedge, C.E., Worl, R.G., Simmons, K.R., Nkomo, I.T., and Wenner, D.B., 1985, Isotopic studies of the late Archean plutonic rocks of the Wind River Range, Wyoming: Geological Society of America Bulletin, v. 96, p. 850-860.

Taylor, S.R., and S.M., M., 1985, The continental crust: its composition and evolution: Oxford, Blackwell. 312 pp.

Vityk, M.O., and Bodnar, R.J., 1995, Do fluid inclusions in high-grade metamorphic terranes preserve peak metamorphic density during retrograde decompression?: American Mineralogist, v. 80, p. 641-644.

Wilks, M.E., 1991, The petrology and petrogenesis of three late Archean K-rich granites in the Archean Wyoming Province, United States: United States. Ph. D. thesis, New Mexico Institute of Mining and Technology, 262 pp.

Worl, R.G., Koesterer, M.E., and Hulsebosch, T.P., 1986, Geologic map of the Bridger Wilderness and Green-Sweetwater Roadless area, Sublette and Fremont Counties, Wyoming, U.S. Geological Survey Misc. Field Studies Map MF-1636-B.

Yang, X.-M., and Lentz, D.R., 2005, Chemical composition of rock-forming minerals in gold-related granitoid intrusion, southwestern New Brunswick, Canada: implications for crystallization conditions, volatile exsolution, and fluorine-chlorine activity: Contributions in Mineral Petrology, v. 150, p. 287-305.

Yardley, B.W.D., Banks, D.A., Bottrell, S.H., and Diamond, L.W., 1993, Post-metamorphic gold-quartz veins from N.W. Italy: the composition and origin of the ore fluid: Mineralogical Magazine, v. 57, p. 407-422.

Yavuz, F., 2007, WinAmphcal: A Windows program for the IMA-04 amphibole classification: Geochemistry Geophysics Geosystems, v. 8. 12 pp.

APPENDIX 1: ANALYTICAL TECHNIQUES

WHOLE ROCK ANALYSIS

Weathering rinds were removed from the fist-sized samples before they were sent to ALS Chemex for geochemical analysis. Samples were analyzed for a suite of elements, including Au and Cu. Samples were crushed to less than 2mm by ALS Chemex and processed using a variety of techniques as follows: Whole rock and Au concentrations were examined using ICP-AES, total carbon and sulfur were examined using LECO, a suite of elements using ICP-MS, and loss on ignition (LOI) was calculated using WST-SEQ.

Table A-1: Results of whole rock geochemical analysis

SAMPLE	Recvd Wt.	Au	SiO2	Al2O3	Fe2O3	CaO	MgO	Na2O	K2O	Cr2O3	TiO2	MnO	P2O5	SrO
DESCRIPTION	kg	ppm	%	%	%	%	%	%	%	%	%	%	%	%
WR-4A	1.11	0.005	70.8	14.6	3.53	2.55	0.6	4.06	2.61	<0.01	0.4	0.03	0.12	0.05
WR-4A2	0.17	0.052	47.7	12.75	13.9	9.76	8.42	2.65	1.58	0.05	1.02	0.3	0.66	0.06
WR-7C	0.92	0.003	70.3	14.75	2.87	2.53	0.7	3.73	3.68	<0.01	0.24	0.03	0.11	0.07
WR-16B	0.75	0.002	64.4	15.9	4.92	3.96	1.6	4.39	2.29	<0.01	0.66	0.06	0.27	0.1
WR-18A	0.55	0.002	56.2	17.65	7.3	4.67	2.5	5.27	1.95	<0.01	1.27	0.09	0.41	0.09
WR-18D	0.95	0.019	64.2	16.05	5.12	4.06	1.78	4.4	2.45	<0.01	0.71	0.07	0.28	0.1
WR-20B	0.87	0.002	89.8	4.62	0.41	0.17	0.01	0.93	2.38	<0.01	0.01	<0.01	<0.01	<0.01
WR-20C	0.63	0.005	70.4	14.95	3.15	2.6	0.89	4.16	2.55	<0.01	0.35	0.04	0.1	0.09
WR-23A	0.31	<0.001	71.1	14.35	2.33	1.43	0.41	3.71	4.35	<0.01	0.31	0.04	0.08	0.02
WR-24B	0.28	<0.001	48.7	15.05	12.95	10.5	7.34	2.08	0.86	0.04	1.18	0.19	0.11	0.01
WR-25B	0.35	0.001	75.3	13.95	0.75	0.79	0.04	4.22	4.43	<0.01	0.03	0.01	0.01	<0.01
WR-28	0.62	0.015	70.6	14.8	2.99	1.96	0.67	3.74	4.2	<0.01	0.38	0.04	0.13	0.02
WR-29	1.54	0.003	61	16.5	6.9	3.77	2.5	4.76	1.42	<0.01	0.89	0.07	0.39	0.07
WR-30	0.16	<0.001	73.5	14.4	1.36	1.01	0.13	4.13	4.77	<0.01	0.09	0.02	0.01	0.03
WR-41	0.57	0.004	71.3	13.6	2.53	1.71	0.6	3.24	3.98	<0.01	0.26	0.03	0.07	0.03
WR-42B	0.24	0.013	59.7	15.45	10.1	0.96	2.46	7.58	0.05	<0.01	0.62	0.04	0.26	0.01
WR-44	0.34	0.005	74.5	13.55	0.82	1.38	0.12	4.51	2.57	<0.01	0.05	0.01	0.01	<0.01
WR-45	0.73	<0.001	68.1	15.35	3.84	2.04	1.29	4.24	2.81	<0.01	0.46	0.05	0.19	0.06

SAMPLE	BaO	C	S	Ag	Ba	Ce	Co	Cr	Cs	Cu	Dy	Er	Eu	Ga	Gd	Hf
DESCRIPTION	%	%	%	ppm	ppm	ppm	ppm	ppm	ppm	ppm	ppm	ppm	ppm	ppm	ppm	ppm
WR-4A	0.15	0.05	0.01	<1	1235	88.6	5.1	30	1.91	50	0.77	0.47	1.39	19.3	2.53	6.6
WR-4A2	0.09	0.08	0.01	<1	733	210	36.6	370	1.26	10	18.8	8.6	5.69	26.3	28.4	6.6
WR-7C	0.3	0.08	<0.01	<1	2470	97	4.3	20	1.22	6	1.68	0.74	1.56	17.7	3.68	2.8
WR-16B	0.16	0.04	0.01	<1	1325	122	10.5	30	1.6	9	3.57	1.76	2.12	22.5	6.77	6.5
WR-18A	0.05	0.04	0.01	<1	423	162.5	17.4	30	3.58	11	8.43	4.05	3.65	27.9	12.95	11.4
WR-18D	0.17	0.04	0.01	<1	1435	170	11.2	30	2.11	9	5.12	2.53	2.78	23.4	9.29	7.6
WR-20B	0.01	0.04	<0.01	<1	82.9	2.1	<0.5	30	0.44	<5	0.35	0.2	0.09	5.3	0.25	<0.2
WR-20C	0.15	0.02	0.01	<1	1255	72.4	6.6	20	3.13	<5	0.95	0.52	1.02	19.9	2.28	4.5
WR-23A	0.11	0.06	0.01	<1	920	86	3.4	20	2.92	<5	2.17	1.18	0.88	24.6	3.79	6.5
WR-24B	0.01	0.03	0.01	<1	98.2	12.7	46.6	260	1.48	63	4.63	2.73	1.11	18	3.75	2.3
WR-25B	0.01	0.11	0.01	<1	73.5	16.6	0.7	10	1.19	20	7.77	4.46	0.39	30.6	5.25	2.5
WR-28	0.1	0.03	<0.01	<1	798	122.5	5	20	1.99	<5	4.17	2.16	1.05	25.8	5.81	7.2
WR-29	0.06	0.02	<0.01	<1	481	108	13	20	0.37	<5	4.4	2.06	2.49	24.3	7.53	7.2
WR-30	0.05	0.08	0.01	<1	439	26	1.4	10	6.9	8	0.63	0.28	0.37	21.9	1.58	2.4
WR-41	0.1	0.02	<0.01	<1	857	89.6	3.6	20	1.79	11	1.56	0.76	0.87	16.4	3.68	5.6
WR-42B	<0.01	0.02	<0.01	<1	22.3	114.5	10.4	20	0.08	<5	3.03	1.51	1.73	19.1	6.05	6.1
WR-44	0.01	0.07	0.01	<1	91.4	4.7	1	10	2.5	5	5.08	4.06	0.23	19.9	1.99	0.8
WR-45	0.17	0.04	0.01	<1	1395	72.1	6.9	20	0.64	<5	1.35	0.7	1.46	19.6	3.09	4.2

SAMPLE	BaO	C	S	Ag	Ba	Ce	Co	Cr	Cs	Cu	Dy	Er	Eu	Ga	Gd
DESCRIPTION	%	%	%	ppm	ppm	ppm	ppm	ppm	ppm	ppm	ppm	ppm	ppm	ppm	ppm
WR-4A	0.15	0.05	0.01	<1	1235	88.6	5.1	30	1.91	50	0.77	0.47	1.39	19.3	2.53
WR-4A2	0.09	0.08	0.01	<1	733	210	36.6	370	1.26	10	18.8	8.6	5.69	26.3	28.4
WR-7C	0.3	0.08	<0.01	<1	2470	97	4.3	20	1.22	6	1.68	0.74	1.56	17.7	3.68
WR-16B	0.16	0.04	0.01	<1	1325	122	10.5	30	1.6	9	3.57	1.76	2.12	22.5	6.77
WR-18A	0.05	0.04	0.01	<1	423	162.5	17.4	30	3.58	11	8.43	4.05	3.65	27.9	12.95
WR-18D	0.17	0.04	0.01	<1	1435	170	11.2	30	2.11	9	5.12	2.53	2.78	23.4	9.29
WR-20B	0.01	0.04	<0.01	<1	82.9	2.1	<0.5	30	0.44	<5	0.35	0.2	0.09	5.3	0.25
WR-20C	0.15	0.02	0.01	<1	1255	72.4	6.6	20	3.13	<5	0.95	0.52	1.02	19.9	2.28
WR-23A	0.11	0.06	0.01	<1	920	86	3.4	20	2.92	<5	2.17	1.18	0.88	24.6	3.79
WR-24B	0.01	0.03	0.01	<1	98.2	12.7	46.6	260	1.48	63	4.63	2.73	1.11	18	3.75
WR-25B	0.01	0.11	0.01	<1	73.5	16.6	0.7	10	1.19	20	7.77	4.46	0.39	30.6	5.25
WR-28	0.1	0.03	<0.01	<1	798	122.5	5	20	1.99	<5	4.17	2.16	1.05	25.8	5.81
WR-29	0.06	0.02	<0.01	<1	481	108	13	20	0.37	<5	4.4	2.06	2.49	24.3	7.53
WR-30	0.05	0.08	0.01	<1	439	26	1.4	10	6.9	8	0.63	0.28	0.37	21.9	1.58
WR-41	0.1	0.02	<0.01	<1	857	89.6	3.6	20	1.79	11	1.56	0.76	0.87	16.4	3.68
WR-42B	<0.01	0.02	<0.01	<1	22.3	114.5	10.4	20	0.08	<5	3.03	1.51	1.73	19.1	6.05
WR-44	0.01	0.07	0.01	<1	91.4	4.7	1	10	2.5	5	5.08	4.06	0.23	19.9	1.99
WR-45	0.17	0.04	0.01	<1	1395	72.1	6.9	20	0.64	<5	1.35	0.7	1.46	19.6	3.09

SAMPLE	Hf	Tl	Tm	U	V	W	Y	Yb	Zn	Zr	As	Bi	Hg	Sb	Se	Te
DESCRIPTION	ppm	ppm	ppm	ppm	ppm	ppm	ppm	ppm	ppm	ppm	ppm	ppm	ppm	ppm	ppm	ppm
WR-4A	6.6	<0.5	0.06	2.96	37	3	4.1	0.49	57	235	1.3	0.08	<0.005	0.09	0.2	0.01
WR-4A2	6.6	<0.5	1.04	1.57	173	2	79.8	6.79	268	237	1.3	0.14	<0.005	0.09	1.5	0.01
WR-7C	2.8	<0.5	0.09	1.46	36	2	6.6	0.66	50	107	0.5	0.04	0.005	0.05	0.2	<0.01
WR-16B	6.5	<0.5	0.21	2.59	71	1	15.7	1.41	100	260	1.1	0.1	<0.005	0.07	0.5	<0.01
WR-18A	11.4	<0.5	0.52	3.76	117	2	38	3.29	151	459	0.9	0.12	0.005	0.05	1	<0.01
WR-18D	7.6	<0.5	0.31	3.11	77	1	22.9	2.09	100	304	1.2	0.13	<0.005	0.07	0.7	<0.01
WR-20B	<0.2	<0.5	0.04	0.1	<5	2	2.2	0.23	14	6	0.3	0.02	<0.005	<0.05	<0.2	<0.01
WR-20C	4.5	<0.5	0.07	2.32	44	2	5.1	0.54	61	162	0.6	0.09	0.006	0.06	0.2	<0.01
WR-23A	6.5	0.8	0.16	3.01	23	2	10.4	1.04	58	233	0.5	0.04	<0.005	0.08	0.2	<0.01
WR-24B	2.3	<0.5	0.41	0.26	298	2	23.7	2.78	109	83	0.5	0.2	<0.005	0.09	0.4	0.01
WR-25B	2.5	0.6	0.67	10.35	<5	2	41.8	4.48	14	35	0.3	0.04	0.006	0.06	0.9	<0.01
WR-28	7.2	0.7	0.28	7.01	33	1	19.5	1.9	53	240	1	0.07	<0.005	0.08	0.7	<0.01
WR-29	7.2	<0.5	0.25	3.73	97	2	19.2	1.61	63	292	0.4	0.04	<0.005	<0.05	0.5	0.01
WR-30	2.4	0.6	0.04	1.33	5	3	2.7	0.24	41	65	0.6	0.6	<0.005	0.14	<0.2	<0.01
WR-41	5.6	0.5	0.09	2.94	21	2	6.6	0.67	53	182	0.4	0.03	<0.005	0.05	0.2	<0.01
WR-42B	6.1	<0.5	0.19	2.11	179	5	13.1	1.26	66	245	0.8	0.05	<0.005	0.07	0.4	<0.01
WR-44	0.8	<0.5	0.62	1.73	7	2	33.2	4.31	14	19	1.1	0.25	<0.005	0.07	0.4	<0.01
WR-45	4.2	<0.5	0.09	2.06	51	15	6.2	0.62	65	162	0.3	0.08	<0.005	<0.05	0.2	<0.01

ANALYSIS OF SILICATES AND OXIDES USING THE ELECTRON MICROPROBE

Silicates and oxides were analyzed using a JEOL JXA-8900R WD/E combined microanalyzer at the Materials Characterization Laboratory, University of Wyoming. Samples of polished thin sections were carbon-coated before analysis. The beam energy, or voltage was set to 15kV and the beam current was set at 25 nA. A counting time of 20 seconds was used (20 seconds/ 20 seconds background). Oxygen was counted for ten seconds. The standards used were both natural and synthetic. Two to three measurements were taken for each mineral. These measurements were taken from core to rim to indicate any zonation of the minerals. Minerals examined: amphibole, apatite, hematite, magnetite, plagioclase, potassium feldspar, titanite and biotite. Cation contents were assumed using a predetermined number of oxygen per formula unit using software at the University of Wyoming. The Fe^{2+} and Fe^{3+} in hornblendes were calculated using the stoichiometric calculations after Leake et al. (1997).

Table A-2: Results of Electron Microprobe Analyses

Hematite Weight Percent													
O	Mg	Al	Ti	V	Cr	Mn	Fe	Cu	Zn	Ag	Au	Total	Sample #
29.325	0.004	0.044	0.011	0.148	0.084	0.036	69.766	0	0	0	0.032	99.45	Hem42b1
29.412	0	0.225	0.026	0	0	0.028	69.375	0.005	0	0	0	99.071	Hem42b2
29.57	0.006	0.429	0	0	0.021	0	69.427	0.021	0.021	0.053	0	99.548	Hem42b3
26.462	0.001	0.12	0.1	0.397	0.045	0.005	66.591	0	0.039	0.082	0	93.842	Hem42b4
29.588	0	0.182	0.003	0	0	0.005	69.609	0	0.038	0	0.039	99.464	Hem42b5
29.895	0.002	0	0.336	0	0.013	0.048	69.942	0	0	0	0	100.236	Hem42b6
29.638	0	0.105	0	0	0.017	0.029	70.036	0.042	0	0	0	99.867	Hem42b7
28.612	0.002	0.053	0.123	0.415	0.072	0	69.984	0.028	0.025	0.013	0	99.327	Hem42b8
29.795	0	0.005	0	0.009	0.011	0	69.858	0.024	0	0	0.409	100.111	Hem42b9
29.579	0.005	0.091	0.09	0	0	0.021	70.007	0.016	0.075	0	0.15	100.034	Hem42b10
29.744	0	0.068	0.044	0	0	0.005	70.225	0.026	0	0	0.079	100.191	Hem42b11
29.449	0	0.189	0.038	0.041	0	0	69.859	0	0	0	0.157	99.733	Hem42b12
29.302	0.008	0.083	0.041	0	0.031	0.021	70.248	0.018	0	0	0	99.752	Hem42b13
29.166	0	0.108	0	0	0	0	69.021	0.014	0.031	0.108	0.157	98.605	Hem42b14
29.975	0	0.404	0.016	0	0.036	0.012	68.836	0.025	0	0.039	0	99.343	Hem42b15
29.521	0	0.141	0.037	0	0	0	69.38	0	0	0	0.173	99.252	Hem42b16
28.264	0.071	0.258	0	0.299	0.102	0.035	68.449	0	0	0	0	97.478	Hem42b17
27.01	0.004	0.024	0	0	0	0	0.908	0	0	0.055	0.379	28.38	Hem42b18
22.465	0.025	0.14	0.009	0.363	0.082	0.026	67.462	0.004	0	0	0.078	90.654	Hem42b19
28.585	0.003	0.095	0.198	0.152	0.036	0.029	69.328	0	0	0	0.228	98.654	Hem42b20
29.049	0	0.204	0.041	0	0.032	0.007	69.03	0.045	0	0	0	98.408	Hem42b21
29.264	0	0.376	0.006	0.371	0.052	0	68.816	0.037	0	0	0	98.922	Hem42b22
29.477	0.278	0.358	0.221	0.106	0	0.002	68.396	0.018	0.014	0	0.039	98.909	Hem42b23
28.693	0.005	0.317	0.024	0.235	0.034	0.004	69.594	0	0	0	0.181	99.087	Hem42b24
28.7	0	0.17	0	0.062	0.011	0.013	69.876	0	0.01	0	0	98.842	Hem42b25

Hematite Atomic ratio

O	Mg	Al	Ti	V	Cr	Mn	Fe	Cu	Zn	Ag	Au	Total	Sample #
59.3276	0.0049	0.0524	0.0075	0.094	0.0524	0.0214	40.4345	0	0	0	0.0052	100	Hem42b1
59.492	0	0.2699	0.0178	0	0	0.0164	40.2012	0.0028	0	0	0	100	Hem42b2
59.4456	0.0085	0.512	0	0	0.0129	0	39.9845	0.0105	0.0105	0.0157	0	100.0001	Hem42b3
57.7699	0.0013	0.1549	0.0729	0.2725	0.0303	0.0031	41.6476	0	0.0211	0.0265	0	100	Hem42b4
59.5902	0	0.2178	0.002	0	0	0.0028	40.1619	0	0.0188	0	0.0064	100	Hem42b5
59.7138	0.0029	0	0.2243	0	0.008	0.0282	40.0229	0	0	0	0	100	Hem42b6
59.5279	0	0.125	0	0	0.0104	0.017	40.2984	0.0214	0	0	0	100	Hem42b7
58.5079	0.0032	0.0647	0.0839	0.2663	0.0451	0	40.9977	0.0145	0.0127	0.004	0	100	Hem42b8
59.761	0	0.0062	0	0.0055	0.0068	0	40.1417	0.0121	0	0	0.0667	100	Hem42b9
59.4399	0.0068	0.1086	0.0607	0	0	0.012	40.3025	0.0082	0.0368	0	0.0244	100	Hem42b10
59.5695	0	0.0804	0.0294	0	0	0.0028	40.292	0.0131	0	0	0.0128	100	Hem42b11
59.3575	0	0.226	0.0256	0.0258	0	0	40.3393	0	0	0	0.0258	100	Hem42b12
59.1783	0.0101	0.0999	0.0278	0	0.0192	0.0121	40.6432	0.0094	0	0	0	100	Hem42b13
59.4699	0	0.1303	0	0	0	0	40.3182	0.0072	0.0155	0.0328	0.0261	100	Hem42b14
59.9893	0	0.48	0.0105	0	0.022	0.0071	39.4668	0.0126	0	0.0117	0	100	Hem42b15
59.6299	0	0.1685	0.0248	0	0	0	40.1484	0	0	0	0.0284	100	Hem42b16
58.6291	0.0966	0.3168	0	0.1951	0.065	0.0212	40.6762	0	0	0	0	100	Hem42b17
98.8433	0.0097	0.052	0	0	0	0	0.9523	0	0	0.03	0.1127	100	Hem42b18
53.4264	0.0398	0.1975	0.0075	0.271	0.0601	0.0183	45.9617	0.0026	0	0	0.0151	100	Hem42b19
58.7484	0.0045	0.1152	0.1359	0.0981	0.0226	0.0174	40.8199	0	0	0	0.0381	100	Hem42b20
59.305	0	0.2465	0.0277	0	0.0202	0.0043	40.3734	0.0229	0	0	0	100	Hem42b21
59.3043	0	0.452	0.0042	0.236	0.0323	0	39.9523	0.0189	0	0	0	100	Hem42b22
59.447	0.3687	0.4281	0.1491	0.067	0	0.0014	39.5157	0.0094	0.007	0	0.0065	100	Hem42b23
58.6414	0.0068	0.3844	0.0161	0.1511	0.0215	0.0022	40.7465	0	0	0	0.0301	100	Hem42b24
58.7533	0	0.2067	0	0.04	0.0066	0.0079	40.9805	0	0.005	0	0	100	Hem42b25

Magnetite Weight Percent

O	Mg	Al	Ti	V	Cr	Mn	Fe	Cu	Zn	Ag	Au	Total	Sample #
27.059	0.006	0.016	0.003	0.051	0.162	0.042	72.473	0	0.034	0	0	99.846	Mag4a1
27.239	0	0.007	0	0.062	0.146	0.094	72.232	0.01	0	0	0	99.79	Mag4a2
26.867	0.006	0	0.008	0.014	0.123	0.052	72.138	0	0	0.01	0	99.218	Mag4a3
27.456	0	0	0	0.017	0.592	0.072	71.872	0	0	0.108	0.383	100.5	Mag4a4
27.2	0	0.007	0.019	0	0.513	0.023	72.218	0	0	0	0	99.98	Mag4a5
27.768	0	0.002	0.041	0	0.396	0.061	71.322	0	0	0	0.251	99.841	Mag4a6
24.496	0.491	9.142	0.022	0	0.159	0.151	10.449	0.005	0	0	0.417	45.332	Mag4a7
24.096	0.435	9.327	0.063	0	0.652	0.167	10.124	0.005	0.01	0.007	0.128	45.014	Mag4a8
24.022	0.445	9.383	0.067	0	0.658	0.132	10.109	0.003	0.021	0	0	44.84	Mag4a9
10.861	0.009	0	0.032	0	0.029	0	0.185	0.009	0	0.017	0.323	11.465	Mag4a10
11.769	0.007	0.443	0.035	0	0	0	0.647	0	0	0.052	0.285	13.238	Mag4a11
27.277	0	0	0.011	0.035	0.367	0.078	71.441	0.017	0	0	0.329	99.555	Mag4a12
27.137	0.005	0	0.001	0.035	0.234	0.079	72.001	0.027	0.018	0	0	99.537	Mag4a13
27.332	0.008	0	0.01	0.066	0.284	0.055	72.456	0.038	0.074	0	0	100.323	Mag4a14
27.068	0	0	0.053	0	0.247	0.081	72.467	0.032	0.013	0.02	0	99.981	Mag4a15
27.323	0	0.007	0.011	0.018	0.216	0.077	72.37	0	0	0	0.47	100.492	Mag4a16
27.048	0	0	0.032	0.046	0.238	0.101	72.441	0	0.083	0	0.196	100.185	Mag4a17
27.074	0.001	0.022	0	0.038	0.005	0.082	72.515	0	0.028	0	0	99.765	Mag4a18
27.438	0.014	0.012	0.023	0.078	0.051	0.071	72.097	0.006	0.027	0	0	99.817	Mag4a19
27.265	0	0.001	0.022	0.051	0.118	0.058	72.026	0	0.013	0	0.306	99.86	Mag4a20
27.338	0	0.01	0.009	0.05	0.104	0.054	72.371	0	0.065	0.049	0.353	100.403	Mag4a21
27.351	0	0.018	0.022	0.118	0.084	0.044	72.502	0.011	0	0	0.459	100.609	Mag4a22
27.149	0	0.013	0	0.083	0.111	0.075	72.585	0	0	0	0.062	100.078	Mag4a23
27.145	0.008	0.002	0.006	0.031	0.111	0.091	72.167	0	0	0	0.008	99.569	Mag4a24
26.987	0	0.009	0	0.083	0.113	0.083	71.642	0	0	0	0.343	99.26	Mag4a25
26.998	0	0	0	0.043	0.015	0.025	72.656	0	0	0.007	0	99.744	Mag4a26
27.001	0.003	0.014	0.011	0.086	0.153	0.066	72.344	0	0.032	0	0	99.71	Mag4a27
27.138	0.002	0.003	0	0.062	0.164	0.077	72.476	0	0	0	0.07	99.992	Mag4a28
27.13	0	0.015	0	0.071	0.077	0.048	72.35	0	0	0	0	99.691	Mag4a29
27.251	0.013	0.007	0.019	0.078	0.106	0.095	72.031	0.048	0.021	0	0.359	100.028	Mag4a30
27.283	0	0	0	0.051	0.097	0.058	72.65	0	0	0.062	0.164	100.365	Mag4a31
27.261	0	0.014	0.004	0	0	0.073	72.131	0.021	0.017	0.02	0	99.541	Mag4132
27.093	0	0.014	0	0	0	0.065	72.54	0	0.02	0.007	0.07	99.809	Mag4133
27.434	0.003	0.012	0	0	0	0.079	71.772	0.078	0.083	0	0.156	99.617	Mag4134

27.751	0	0.013	0	0	0.024	0.092	71.807	0	0.059	0	0	99.746	Mag4135
29.516	0	0.017	0.017	0	0	0.088	69.888	0.015	0.089	0	0.243	99.873	Mag4136
27.473	0	0.002	0	0	0.003	0.082	72.623	0.083	0.056	0	0.274	100.596	Mag4137
27.224	0.003	0.002	0	0.008	0.017	0.137	71.921	0	0	0	0.094	99.406	Mag4138
28.083	0.01	0.033	0.003	0	0.007	0.078	71.497	0	0.001	0.095	0.157	99.964	Mag4139
27.187	0	0.012	0.028	0	0	0.094	72.615	0	0	0.007	0.219	100.162	Mag4140
27.443	0	0	0.003	0.017	0.001	0.094	71.753	0	0.008	0.049	0.391	99.759	Mag4141
27.354	0	0.023	0.009	0	0.031	0.08	72.333	0	0	0.079	0	99.909	Mag4142
27.14	0.001	0.015	0	0	0.086	0.068	71.876	0.029	0.014	0	0.282	99.511	Mag4143
28.027	0	0.022	0.024	0	0.005	0.018	70.974	0	0.003	0	0	99.073	Mag4144
26.984	0	0	0.004	0	0.106	0.078	72.53	0.026	0.062	0.039	0.156	99.985	Mag16b45
27.64	0	0	0	0	0	0.106	72.948	0	0.035	0	0.258	100.987	Mag16b46
27.042	0	0.005	0	0	0.094	0.07	72.581	0.006	0.003	0	0.414	100.215	Mag16b47
27.108	0	0.026	0.016	0	0.007	0.058	72.019	0.064	0	0	0	99.298	Mag16b48
10.376	0.005	0.086	0.034	0	0	0	0.448	0	0	0	0	10.949	Mag16b49
10.16	0	0	0	0	0.049	0.009	0.173	0.006	0	0	0.144	10.541	Mag16b50
27.158	0	0.01	0	0	0.023	0.094	72.648	0	0	0	0.32	100.253	Mag16b51
27.104	0.006	0.008	0.005	0	0.053	0.093	72.795	0	0.025	0	0.031	100.12	Mag16b52
27.295	0	0	0	0	0	0.065	72.18	0	0	0.131	0.515	100.186	Mag16b53
26.98	0	0	0.012	0.022	0.04	0.093	72.442	0.036	0	0	0	99.625	Mag16b54
27.247	0	0.003	0.001	0	0	0.04	72.399	0.016	0	0.036	0.039	99.781	Mag16b55
26.961	0.003	0.007	0	0	0.025	0.045	72.482	0	0.041	0	0	99.564	Mag16b56
27.491	0	0.005	0	0	0.021	0.065	72.252	0	0	0	0.078	99.912	Mag16b57
27.466	0	0.002	0	0	0.082	0.083	72.895	0	0.006	0	0	100.534	Mag16b58
27.111	0	0.01	0	0	0.084	0.068	72.356	0.002	0.015	0.033	0	99.679	Mag16b59

Magnetite Atomic ratio

O	Mg	Al	Ti	V	Cr	Mn	Fe	Cu	Zn	Ag	Au	Total	Sample #
56.4641	0.0087	0.0194	0.002	0.0334	0.1042	0.0256	43.3253	0	0.0172	0	0	99.9999	Mag4a1
56.7118	0	0.0087	0	0.0405	0.0936	0.057	43.0833	0.0051	0	0	0	100	Mag4a2
56.445	0.0079	0	0.0055	0.0093	0.0798	0.0317	43.4178	0	0	0.0031	0	100	Mag4a3
56.8429	0	0	0	0.0113	0.377	0.0435	42.6278	0	0	0.0332	0.0644	100	Mag4a4
56.5909	0	0.0083	0.0131	0	0.3284	0.0139	43.0454	0	0	0	0	100	Mag4a5
57.4002	0	0.0028	0.0284	0	0.2519	0.037	42.2376	0	0	0	0.0421	100	Mag4a6
73.4099	0.968	16.2462	0.0219	0	0.1471	0.1318	8.9703	0.0034	0	0	0.1014	100	Mag4a7
72.799	0.865	16.7115	0.0639	0	0.6062	0.1465	8.7623	0.0035	0.0077	0.0031	0.0313	100	Mag4a8
72.6968	0.8858	16.8391	0.0677	0	0.6125	0.1161	8.7639	0.0026	0.0155	0	0	100	Mag4a9
98.9994	0.0536	0	0.0977	0	0.0813	0	0.4837	0.0217	0	0.0234	0.2391	99.9999	Mag4a10
95.9604	0.036	2.1444	0.0961	0	0	0	1.5112	0	0	0.0629	0.1889	100	Mag4a11
56.9162	0	0	0.0075	0.023	0.2355	0.0475	42.7054	0.0091	0	0	0.0557	100	Mag4a12
56.6705	0.0073	0	0.0009	0.023	0.1503	0.0483	43.0761	0.0142	0.0093	0	0	100	Mag4a13
56.6474	0.0108	0	0.0068	0.0427	0.1808	0.0334	43.0207	0.0197	0.0378	0	0	100.0001	Mag4a14
56.4388	0	0	0.037	0	0.1585	0.049	43.2872	0.017	0.0065	0.0061	0	100.0001	Mag4a15
56.6912	0	0.0081	0.0075	0.0119	0.1377	0.0466	43.0179	0	0	0	0.0791	100	Mag4a16
56.3906	0	0	0.0221	0.0302	0.1529	0.0614	43.2674	0	0.0423	0	0.0332	100	Mag4a17
56.5145	0.0019	0.0266	0	0.0247	0.0035	0.0498	43.3646	0	0.0144	0	0	100	Mag4a18
56.9421	0.0198	0.015	0.0161	0.0507	0.0323	0.043	42.864	0.0034	0.0136	0	0	100	Mag4a19
56.7971	0	0.001	0.0155	0.0331	0.0758	0.0351	42.9843	0	0.0065	0	0.0517	100	Mag4a20
56.7236	0	0.0126	0.0059	0.0325	0.0661	0.0328	43.0191	0	0.0329	0.0152	0.0595	100.0001	Mag4a21
56.6807	0	0.0216	0.0149	0.0767	0.0534	0.0268	43.043	0.0056	0	0	0.0773	100	Mag4a22
56.5156	0	0.0165	0	0.0543	0.0711	0.0452	43.2868	0	0	0	0.0106	100	Mag4a23
56.6718	0.0106	0.002	0.0043	0.0202	0.0715	0.0556	43.1626	0	0	0	0.0013	99.9999	Mag4a24
56.6604	0	0.0113	0	0.0547	0.0727	0.0507	43.0916	0	0	0	0.0585	100	Mag4a25
56.4357	0	0	0	0.0283	0.0095	0.0154	43.5092	0	0	0.002	0	100	Mag4a26
56.438	0.0048	0.0175	0.0077	0.0567	0.0981	0.0403	43.3204	0	0.0165	0	0	100	Mag4a27
56.5354	0.0026	0.0032	0	0.0407	0.105	0.0467	43.2545	0	0	0	0.0119	100	Mag4a28
56.6087	0	0.0183	0	0.0464	0.0495	0.0292	43.2479	0	0	0	0	100	Mag4a29
56.7293	0.0184	0.0085	0.0132	0.0507	0.0682	0.0576	42.9578	0.0249	0.0107	0	0.0607	100	Mag4a30
56.6262	0	0	0	0.0332	0.0621	0.0349	43.1968	0	0	0.0192	0.0276	100	Mag4a31
56.831	0	0.0169	0.0027	0	0	0.0446	43.0793	0.0108	0.0086	0.0061	0	100	Mag4132
56.546	0	0.017	0	0	0	0.0395	43.3735	0	0.01	0.002	0.0119	100	Mag4133

57.0593	0.0037	0.0146	0	0	0	0.0481	42.765	0.0408	0.0422	0	0.0264	100	Mag4134
57.3616	0	0.016	0	0	0.0156	0.0551	42.5218	0	0.0299	0	0	100	Mag4135
59.478	0	0.0207	0.0117	0	0	0.0518	40.3464	0.0077	0.0438	0	0.0399	100	Mag4136
56.808	0	0.0028	0	0	0.002	0.0493	43.0202	0.0433	0.0284	0	0.0459	99.9999	Mag4137
56.8512	0.0042	0.003	0	0.0051	0.0107	0.0836	43.0263	0	0	0	0.0159	100	Mag4138
57.7312	0.0132	0.0398	0.0018	0	0.0042	0.047	42.1069	0	0.0007	0.029	0.0262	100	Mag4139
56.5775	0	0.0144	0.0198	0	0	0.057	43.2922	0	0	0.002	0.037	99.9999	Mag4140
57.0847	0	0	0.002	0.0113	0.0005	0.057	42.7589	0	0.0043	0.0152	0.0661	100	Mag4141
56.8254	0	0.0277	0.0063	0	0.0199	0.0482	43.0482	0	0	0.0243	0	100	Mag4142
56.7535	0.0009	0.019	0	0	0.0554	0.0411	43.0597	0.0154	0.0072	0	0.0478	100	Mag4143
57.9205	0	0.0271	0.0167	0	0.0035	0.0109	42.02	0	0.0014	0	0	100.0001	Mag4144
56.3813	0	0	0.003	0	0.0683	0.0476	43.4159	0.0136	0.0316	0.0122	0.0265	100	Mag16b45
56.8742	0	0	0	0	0	0.0636	43.0014	0	0.0177	0	0.0431	100	Mag16b46
56.4278	0	0.0065	0	0	0.0603	0.0424	43.388	0.0034	0.0014	0	0.0701	100	Mag16b47
56.7164	0	0.0325	0.0112	0	0.0042	0.0352	43.1669	0.0336	0	0	0	100	Mag16b48
98.1639	0.0312	0.4844	0.1068	0	0	0	1.2138	0	0	0	0	100	Mag16b49
99.2142	0	0	0	0	0.1471	0.0269	0.4827	0.0146	0	0	0.1145	100	Mag16b50
56.5355	0	0.0123	0	0	0.0147	0.0569	43.3264	0	0	0	0.0542	100	Mag16b51
56.4421	0.0077	0.0105	0.0032	0	0.0338	0.0562	43.4283	0	0.0129	0	0.0053	100	Mag16b52
56.8016	0	0	0	0	0	0.0394	43.0315	0	0	0.0405	0.087	100	Mag16b53
56.4522	0	0.0005	0.0082	0.0143	0.026	0.0565	43.4235	0.0188	0	0	0	100	Mag16b54
56.7483	0	0.0034	0.0009	0	0	0.0241	43.197	0.0085	0	0.0111	0.0066	99.9999	Mag16b55
56.448	0.0044	0.009	0	0	0.0162	0.0272	43.4743	0	0.0209	0	0	100	Mag16b56
57.006	0	0.0063	0	0	0.0136	0.0394	42.9215	0	0	0	0.0132	100	Mag16b57
56.7473	0	0.0019	0	0	0.0519	0.0501	43.146	0	0.0029	0	0	100	Mag16b58
56.5988	0	0.012	0	0	0.0537	0.0411	43.2752	0.0011	0.0079	0.0102	0	100	Mag16b59

Apatite Weight percent

CaO	P2O5	La2O3	Ce2O3	Nd2O3	SrO	Na2O	MgO	Al2O3	SiO2	MnO	FeO	F	Cl	SO3	Total	Sample #
55.89	42.41	0.00	0.00	0.01	0.11	0.00	0.00	0.00	0.01	0.01	0.09	3.21	0.01	0.08	100.48	16B
56.45	41.34	0.00	0.06	0.00	0.16	0.01	0.00	0.00	0.00	0.00	0.00	3.45	0.01	0.08	100.11	16B
56.16	41.85	0.00	0.04	0.00	0.16	0.01	0.00	0.00	0.06	0.06	0.04	3.19	0.03	0.14	100.41	16B
56.18	42.15	0.01	0.11	0.11	0.09	0.04	0.01	0.00	0.05	0.07	0.00	3.42	0.05	0.20	101.04	16B
56.33	40.93	0.00	0.03	0.04	0.11	0.03	0.01	0.00	0.07	0.08	0.09	3.13	0.03	0.20	99.74	16B
29.69	*0.03*	*0.00*	*0.00*	*0.00*	*0.29*	*0.00*	*0.00*	*1.51*	*29.68*	*0.05*	*1.41*	*0.26*	*0.01*	*0.00*	*62.82*	*16B*
29.56	*0.02*	*0.00*	*0.00*	*0.00*	*0.31*	*0.00*	*0.00*	*1.85*	*29.68*	*0.11*	*1.33*	*0.29*	*0.00*	*0.00*	*63.03*	*16B*
52.91	41.38	0.00	0.00	0.11	0.00	0.05	0.00	0.00	0.29	0.04	0.15	3.20	0.00	0.00	96.78	28-7
52.36	40.99	0.00	0.05	0.08	0.00	0.09	0.00	0.00	0.27	0.06	0.14	3.32	0.00	0.01	95.98	28-7
53.04	40.42	0.00	0.00	0.00	0.00	0.07	0.00	0.00	0.35	0.04	0.22	3.16	0.01	0.06	96.02	28-7
29.07	*0.00*	*0.00*	*0.00*	*0.00*	*0.27*	*0.02*	*0.02*	*7.86*	*30.63*	*0.10*	*1.03*	*1.17*	*0.00*	*0.00*	*69.69*	*28-7*
52.78	41.70	0.06	0.08	0.17	0.00	0.05	0.00	0.00	0.51	0.06	0.46	2.90	0.00	0.03	97.56	28-7
54.14	42.44	0.00	0.05	0.10	0.00	0.05	0.00	0.00	0.45	0.07	0.02	3.34	0.01	0.05	99.30	28-9
54.72	43.35	0.00	0.15	0.00	0.00	0.10	0.01	0.00	0.25	0.08	0.09	3.15	0.00	0.04	100.62	28-9
54.72	42.60	0.00	0.07	0.00	0.00	0.05	0.00	0.01	0.30	0.02	0.07	3.52	0.00	0.01	99.88	28-9
55.22	43.46	0.02	0.02	0.00	0.00	0.02	0.00	0.00	0.12	0.04	0.24	3.44	0.01	0.04	101.18	28-9
54.57	41.90	0.00	0.04	0.00	0.00	0.05	0.00	0.00	0.25	0.09	0.20	3.56	0.01	0.00	99.16	28-9
55.27	42.61	0.11	0.31	0.03	0.06	0.01	0.01	0.01	0.39	0.07	0.11	2.86	0.13	0.17	100.91	4A
54.66	42.43	0.00	0.00	0.00	0.15	0.07	0.02	0.00	0.29	0.04	0.25	3.16	0.10	0.52	100.33	4A
54.66	42.48	0.03	0.22	0.30	0.10	0.00	0.02	0.01	0.33	0.07	0.28	3.00	0.14	0.16	100.51	4A
54.84	41.68	0.00	0.00	0.04	0.19	0.02	0.00	0.00	0.22	0.07	0.17	3.23	0.09	0.18	99.35	4A
54.37	42.18	0.00	0.16	0.06	0.08	0.02	0.00	0.00	0.23	0.11	0.17	3.10	0.11	0.17	99.45	4A
54.73	41.74	0.07	0.21	0.05	0.13	0.02	0.01	0.00	0.24	0.09	0.08	2.83	0.17	0.35	99.46	4A
54.49	41.64	0.03	0.11	0.12	0.13	0.01	0.00	0.01	0.33	0.06	0.19	3.12	0.13	0.10	99.12	4A
55.27	42.82	0.02	0.11	0.13	0.06	0.13	0.00	0.00	0.26	0.00	0.00	2.94	0.16	0.55	101.19	4A
55.72	42.38	0.00	0.05	0.06	0.14	0.02	0.01	0.02	0.15	0.08	0.27	3.27	0.06	0.14	100.97	29
55.56	43.26	0.10	0.11	0.00	0.11	0.00	0.00	0.00	0.24	0.04	0.12	3.13	0.10	0.22	101.65	29
55.43	42.50	0.02	0.00	0.20	0.11	0.01	0.00	0.00	0.08	0.02	0.09	3.61	0.01	0.11	100.68	29
54.98	42.61	0.04	0.08	0.30	0.11	0.00	0.00	0.00	0.23	0.01	0.06	3.25	0.09	0.25	100.61	29
54.64	42.17	0.06	0.32	0.22	0.07	0.04	0.01	0.00	0.39	0.00	0.17	3.49	0.09	0.23	100.39	29
55.17	41.80	0.07	0.20	0.10	0.10	0.01	0.03	0.00	0.38	0.03	0.24	2.70	0.10	0.20	99.95	29
55.09	41.91	0.14	0.11	0.09	0.06	0.00	0.00	0.00	0.37	0.04	0.21	3.02	0.09	0.16	99.98	29
54.66	42.22	0.15	0.36	0.00	0.05	0.01	0.01	0.01	0.49	0.06	0.28	3.41	0.08	0.15	100.48	29

Apatite Cation Total

Ca	P	La	Ce	Nd	Sr	Na	Mg	Al	Si	Mn	Fe	F	Cl	S	Total	Sample #
9.980	5.984	0.0000	0.000	0.000	0.011	0.000	0.0000	0.0000	0.002	0.002	0.013	1.693	0.0034	0.0104	16.001	16B
10.196	5.900	0.0000	0.004	0.000	0.016	0.003	0.0000	0.0000	0.000	0.000	0.000	1.839	0.0023	0.0101	16.129	16B
10.069	5.928	0.0002	0.002	0.000	0.015	0.004	0.0000	0.0000	0.011	0.009	0.005	1.690	0.0091	0.0178	16.062	16B
10.016	5.938	0.0005	0.007	0.006	0.009	0.014	0.0020	0.0000	0.008	0.010	0.000	1.801	0.0127	0.0248	16.036	16B
10.206	5.860	0.0000	0.002	0.002	0.010	0.010	0.0013	0.0000	0.011	0.011	0.013	1.675	0.0089	0.0253	16.151	16B
9.766	6.035	0.0000	0.000	0.006	0.000	0.018	0.0000	0.0000	0.049	0.006	0.022	1.745	0.0000	0.0000	15.903	28-7
9.757	6.035	0.0000	0.003	0.005	0.000	0.032	0.0000	0.0000	0.047	0.008	0.021	1.825	0.0003	0.0016	15.910	28-7
9.901	5.962	0.0000	0.000	0.000	0.000	0.022	0.0000	0.0000	0.062	0.006	0.032	1.740	0.0015	0.0075	15.992	28-7
9.649	6.023	0.0037	0.005	0.010	0.000	0.015	0.0000	0.0000	0.086	0.009	0.065	1.567	0.0000	0.0037	15.870	28-7
9.730	6.026	0.0000	0.003	0.006	0.000	0.017	0.0000	0.0000	0.076	0.010	0.002	1.770	0.0020	0.0065	15.876	28-9
9.686	6.064	0.0000	0.009	0.000	0.000	0.032	0.0030	0.0000	0.041	0.011	0.012	1.648	0.0000	0.0051	15.864	28-9
9.798	6.027	0.0000	0.004	0.000	0.000	0.015	0.0000	0.0016	0.050	0.003	0.010	1.861	0.0008	0.0018	15.910	28-9
9.747	6.061	0.0009	0.001	0.000	0.000	0.007	0.0000	0.0006	0.020	0.006	0.033	1.792	0.0014	0.0048	15.881	28-9
9.879	5.994	0.0000	0.002	0.000	0.000	0.015	0.0000	0.0000	0.041	0.013	0.028	1.902	0.0029	0.0000	15.974	28-9
9.803	5.972	0.0064	0.019	0.002	0.005	0.003	0.0030	0.0012	0.064	0.009	0.016	1.497	0.0370	0.0211	15.924	4A
9.727	5.965	0.0000	0.000	0.000	0.014	0.021	0.0052	0.0000	0.048	0.006	0.034	1.661	0.0290	0.0643	15.885	4A
9.749	5.987	0.0018	0.014	0.018	0.009	0.000	0.0040	0.0016	0.055	0.010	0.039	1.581	0.0403	0.0194	15.908	4A
9.915	5.954	0.0000	0.000	0.002	0.019	0.005	0.0000	0.0000	0.037	0.010	0.024	1.723	0.0254	0.0228	15.988	4A
9.788	5.999	0.0000	0.010	0.004	0.008	0.007	0.0000	0.0000	0.039	0.016	0.024	1.646	0.0316	0.0218	15.916	4A
9.861	5.942	0.0042	0.013	0.003	0.012	0.008	0.0015	0.0008	0.040	0.012	0.011	1.503	0.0476	0.0444	15.952	4A
9.872	5.961	0.0017	0.006	0.007	0.013	0.003	0.0010	0.0022	0.056	0.009	0.026	1.668	0.0375	0.0127	15.970	4A
9.746	5.965	0.0013	0.007	0.008	0.006	0.042	0.0000	0.0000	0.043	0.001	0.001	1.527	0.0452	0.0683	15.887	4A
9.916	5.959	0.0000	0.003	0.004	0.013	0.006	0.0017	0.0029	0.026	0.011	0.038	1.717	0.0160	0.0176	15.999	29
9.768	6.009	0.0062	0.006	0.000	0.011	0.000	0.0000	0.0000	0.040	0.006	0.016	1.626	0.0267	0.0266	15.888	29
9.895	5.995	0.0014	0.000	0.012	0.011	0.004	0.0000	0.0000	0.013	0.003	0.013	1.901	0.0040	0.0139	15.962	29
9.789	5.994	0.0021	0.005	0.018	0.010	0.000	0.0007	0.0000	0.038	0.002	0.008	1.708	0.0251	0.0307	15.897	29
9.782	5.965	0.0036	0.020	0.013	0.007	0.012	0.0012	0.0000	0.065	0.000	0.023	1.846	0.0249	0.0282	15.919	29
9.898	5.925	0.0043	0.012	0.006	0.009	0.003	0.0072	0.0000	0.064	0.004	0.033	1.428	0.0295	0.0246	15.990	29
9.888	5.944	0.0088	0.007	0.005	0.006	0.000	0.0000	0.0000	0.061	0.005	0.030	1.600	0.0247	0.0197	15.974	29
9.768	5.962	0.0090	0.022	0.000	0.005	0.002	0.0017	0.0020	0.081	0.009	0.039	1.797	0.0232	0.0192	15.921	29

Biotite Weight Percent

SiO2	Al2O3	TiO2	MgO	FeO	MnO	CaO	Na2O	K2O	F	Cl	Total	Sample
37.73	15.95	1.63	13.07	18.45	0.29	0.05	0.02	8.69	0.33	0.12	96.15	4a BIO 1a
36.74	16.05	1.87	12.78	19.44	0.36	0.00	0.00	9.39	0.33	0.13	96.92	4a BIO 1a
37.57	16.34	1.56	13.17	19.07	0.35	0.00	0.02	9.62	0.39	0.13	98.02	4a BIO 1a
37.49	16.32	1.95	12.71	18.97	0.31	0.00	0.01	8.74	0.34	0.16	96.84	4a BIO 2a
37.03	16.00	1.93	12.66	18.81	0.35	0.00	0.00	9.55	0.33	0.13	96.62	4a BIO 2a
36.73	15.99	1.91	12.54	18.76	0.27	0.00	0.02	9.32	0.24	0.16	95.80	4a BIO 2a
37.48	16.13	1.80	13.14	18.79	0.41	0.00	0.04	9.17	0.18	0.14	97.17	4a BIO 3a
37.62	16.03	1.68	12.94	18.58	0.34	0.00	0.00	9.29	0.19	0.17	96.71	4a BIO 3a
36.86	15.91	1.82	12.80	18.76	0.39	0.00	0.03	9.58	0.24	0.16	96.41	4a BIO 3a
37.45	16.39	2.19	12.10	19.48	0.34	0.00	0.00	9.53	0.28	0.14	97.74	4a BIO 4a
37.32	15.93	1.81	12.74	19.59	0.36	0.00	0.02	9.89	0.17	0.12	97.85	4a BIO 4a
38.47	19.00	1.52	10.84	17.78	0.27	0.11	0.01	6.65	0.19	0.10	94.84	4a BIO 4a
36.63	16.12	1.63	12.83	18.72	0.38	0.00	0.01	9.45	0.11	0.05	95.89	16B BIO 1a
35.79	15.89	1.54	12.60	18.66	0.41	0.00	0.04	9.93	0.10	0.09	94.98	16B BIO 1a
37.79	15.96	1.56	12.82	19.01	0.39	0.00	0.04	9.57	0.26	0.06	97.34	16B BIO 1a
38.22	16.12	1.35	13.41	18.44	0.38	0.00	0.01	9.25	0.23	0.02	97.33	16B BIO 2a
38.03	15.65	1.67	13.09	18.27	0.36	0.00	0.03	9.69	0.32	0.00	96.97	16B BIO 2a
37.86	16.23	1.42	13.09	18.27	0.31	0.00	0.01	9.53	0.17	0.03	96.84	16B BIO 2a
37.93	16.15	1.77	12.97	18.63	0.39	0.00	0.03	9.55	0.31	0.03	97.61	16B BIO 3a
37.68	15.92	1.83	12.80	18.67	0.32	0.00	0.03	10.16	0.14	0.02	97.50	16B BIO 3a
38.02	15.79	1.96	12.76	19.28	0.36	0.00	0.03	9.85	0.19	0.04	98.17	16B BIO 3a
37.92	16.06	1.94	12.75	18.97	0.39	0.00	0.08	9.72	0.25	0.05	97.99	16B BIO 4a
38.25	16.06	2.16	12.86	18.86	0.35	0.01	0.07	9.63	0.22	0.07	98.42	16B BIO 4a
37.70	15.37	2.26	12.36	18.94	0.39	0.00	0.01	9.57	0.25	0.06	96.77	16B BIO 4a
36.89	17.00	2.45	9.53	21.32	0.47	0.00	0.00	9.54	0.27	0.07	97.41	30 BIO 1a
36.75	16.71	2.38	9.47	21.76	0.52	0.00	0.00	9.93	0.16	0.11	97.69	30 BIO 1a
37.01	16.86	1.97	9.87	21.76	0.46	0.00	0.00	9.73	0.16	0.08	97.81	30 BIO 1a
36.82	16.64	2.38	9.51	21.11	0.47	0.02	0.04	9.72	0.19	0.06	96.86	30 BIO 2a
36.75	16.26	2.28	9.55	21.38	0.40	0.00	0.05	9.76	0.25	0.09	96.63	30 BIO 2a
37.33	16.62	2.50	9.71	20.85	0.37	0.01	0.06	9.64	0.32	0.09	97.35	30 BIO 2a
37.22	16.67	2.68	9.88	21.40	0.41	0.00	0.03	9.51	0.14	0.08	97.93	30 BIO 3a
37.41	16.74	2.40	9.89	21.43	0.40	0.00	0.02	9.84	0.18	0.05	98.27	30 BIO 3a
37.31	16.80	2.31	10.28	21.26	0.36	0.00	0.03	9.53	0.34	0.10	98.16	30 BIO 3a

37.04	16.49	2.63	9.80	20.97	0.48	0.00	0.00	9.12	0.23	0.11	96.75	30 BIO 4a
37.10	16.49	2.74	9.75	21.66	0.46	0.00	0.02	9.60	0.37	0.09	98.12	30 BIO 4a
36.89	16.43	2.57	10.06	21.39	0.51	0.00	0.03	9.34	0.29	0.11	97.48	30 BIO 4a
36.67	16.08	2.46	8.56	22.35	0.40	0.14	0.11	9.34	0.25	0.08	96.31	41 BIO 1a
36.17	16.09	2.39	8.72	22.68	0.39	0.02	0.09	9.66	0.10	0.08	96.33	41 BIO 1a
36.20	16.07	2.46	8.78	22.77	0.42	0.00	0.08	9.75	0.18	0.06	96.67	41 BIO 1a
36.85	16.71	2.64	9.20	23.41	0.39	0.00	0.03	9.66	0.11	0.05	98.97	41 BIO 2a
36.90	16.80	2.48	9.10	22.71	0.35	0.00	0.06	9.76	0.18	0.01	98.28	41 BIO 2a
36.63	16.59	2.67	9.04	22.92	0.41	0.00	0.03	9.57	0.27	0.04	98.03	41 BIO 2a
34.93	16.91	2.30	9.68	22.80	0.35	0.00	0.01	9.59	0.38	0.01	96.78	41 BIO 3a
35.26	16.93	2.00	9.88	21.87	0.32	0.00	0.03	9.33	0.18	0.02	95.73	41 BIO 3a
36.29	16.84	1.91	9.79	22.34	0.39	0.02	0.01	9.06	0.26	0.03	96.82	41 BIO 3a
35.73	16.88	1.88	9.52	23.64	0.32	0.04	0.00	8.33	0.27	0.06	96.54	41 BIO 4a
36.62	16.68	2.17	9.44	23.23	0.34	0.00	0.00	9.87	0.21	0.05	98.50	41 BIO 4a
36.76	16.90	2.30	9.73	23.03	0.33	0.00	0.00	9.73	0.26	0.03	98.95	41 BIO 4a
37.22	16.10	1.84	10.30	21.89	0.37	0.00	0.01	6.63	0.91	0.07	94.95	28 BIO 1a
37.28	15.84	1.96	9.86	21.77	0.38	0.00	0.00	9.77	0.80	0.11	97.42	28 BIO 1a
37.36	16.14	1.86	10.11	22.14	0.38	0.00	0.01	9.94	0.79	0.11	98.48	28 BIO 1a
37.65	16.08	1.83	10.02	21.94	0.33	0.00	0.02	9.64	1.03	0.07	98.16	28 BIO 2a
37.45	16.20	1.66	10.16	22.05	0.36	0.00	0.02	9.21	0.94	0.09	97.73	28 BIO 2a
37.47	15.95	1.86	10.17	21.39	0.35	0.00	0.04	9.15	1.00	0.09	97.03	28 BIO 2a
37.71	15.65	1.47	10.75	21.80	0.34	0.00	0.02	9.53	0.98	0.09	97.91	28 BIO 3a
37.25	15.83	1.81	10.00	22.25	0.33	0.00	0.03	9.76	0.97	0.10	97.89	28 BIO 3a
37.68	15.88	1.81	10.29	21.96	0.33	0.00	0.01	9.92	0.94	0.10	98.50	28 BIO 3a
37.49	15.96	1.47	10.36	22.30	0.35	0.00	0.00	9.52	0.74	0.06	97.94	28 BIO 4a
37.12	15.87	1.50	10.28	22.26	0.36	0.00	0.00	9.64	0.74	0.07	97.52	28 BIO 4a
37.42	15.88	1.33	10.42	21.67	0.36	0.00	0.00	9.73	0.79	0.05	97.32	28 BIO 4a

Biotite Cation Total

Si	Al	Ti	Mg	Fe	Mn	Ca	Na	K	F	Cl	Total	Sample
2.802	1.396	0.091	1.447	1.146	0.018	0.004	0.003	0.824	0.077	0.015	7.823	4a BIO 1a
2.739	1.410	0.105	1.420	1.212	0.023	0.000	0.000	0.893	0.079	0.016	7.897	4a BIO 1a
2.758	1.414	0.086	1.441	1.171	0.022	0.000	0.002	0.900	0.091	0.016	7.901	4a BIO 1a
2.772	1.422	0.109	1.401	1.173	0.020	0.000	0.002	0.824	0.080	0.020	7.822	4a BIO 2a
2.761	1.407	0.108	1.407	1.173	0.022	0.000	0.000	0.908	0.078	0.017	7.881	4a BIO 2a
2.763	1.418	0.108	1.407	1.181	0.017	0.000	0.002	0.895	0.057	0.020	7.868	4a BIO 2a
2.776	1.408	0.100	1.451	1.164	0.026	0.000	0.005	0.867	0.041	0.018	7.856	4a BIO 3a
2.795	1.404	0.094	1.433	1.155	0.021	0.000	0.000	0.881	0.044	0.022	7.849	4a BIO 3a
2.761	1.405	0.103	1.429	1.175	0.025	0.000	0.005	0.915	0.057	0.020	7.894	4a BIO 3a
2.765	1.426	0.121	1.332	1.203	0.021	0.000	0.000	0.898	0.066	0.018	7.850	4a BIO 4a
2.769	1.393	0.101	1.409	1.216	0.023	0.000	0.002	0.936	0.040	0.015	7.903	4a BIO 4a
2.836	1.651	0.084	1.192	1.096	0.017	0.008	0.002	0.625	0.044	0.012	7.568	4a BIO 4a
2.763	1.434	0.093	1.443	1.181	0.024	0.000	0.001	0.909	0.027	0.007	7.883	16B BIO 1a
2.742	1.435	0.089	1.440	1.196	0.027	0.000	0.006	0.970	0.025	0.011	7.940	16B BIO 1a
2.798	1.393	0.087	1.415	1.177	0.025	0.000	0.005	0.904	0.061	0.007	7.873	16B BIO 1a
2.814	1.399	0.075	1.472	1.136	0.024	0.000	0.002	0.869	0.054	0.003	7.847	16B BIO 2a
2.816	1.366	0.093	1.445	1.131	0.023	0.000	0.004	0.915	0.075	0.000	7.867	16B BIO 2a
2.809	1.419	0.079	1.448	1.134	0.019	0.000	0.002	0.902	0.039	0.004	7.854	16B BIO 2a
2.791	1.401	0.098	1.423	1.147	0.024	0.000	0.004	0.897	0.073	0.003	7.861	16B BIO 3a
2.796	1.393	0.102	1.416	1.159	0.020	0.000	0.005	0.962	0.034	0.003	7.888	16B BIO 3a
2.801	1.371	0.108	1.401	1.188	0.022	0.000	0.004	0.926	0.044	0.005	7.870	16B BIO 3a
2.790	1.393	0.107	1.399	1.167	0.025	0.000	0.011	0.912	0.058	0.006	7.868	16B BIO 4a
2.797	1.384	0.119	1.402	1.154	0.022	0.001	0.009	0.899	0.052	0.008	7.846	16B BIO 4a
2.811	1.351	0.127	1.374	1.181	0.024	0.000	0.001	0.910	0.058	0.007	7.843	16B BIO 4a
2.760	1.499	0.138	1.063	1.334	0.030	0.000	0.000	0.911	0.063	0.009	7.808	30 BIO 1a
2.761	1.480	0.135	1.060	1.368	0.033	0.000	0.000	0.952	0.038	0.014	7.840	30 BIO 1a
2.771	1.487	0.111	1.101	1.362	0.029	0.000	0.000	0.930	0.039	0.010	7.840	30 BIO 1a
2.778	1.480	0.135	1.069	1.332	0.030	0.001	0.005	0.935	0.045	0.008	7.818	30 BIO 2a
2.781	1.450	0.130	1.077	1.354	0.026	0.000	0.007	0.942	0.061	0.011	7.838	30 BIO 2a
2.786	1.462	0.141	1.081	1.301	0.023	0.001	0.008	0.918	0.075	0.012	7.806	30 BIO 2a
2.775	1.464	0.150	1.097	1.334	0.026	0.000	0.004	0.905	0.033	0.010	7.798	30 BIO 3a
2.781	1.467	0.134	1.096	1.333	0.025	0.000	0.003	0.933	0.043	0.006	7.820	30 BIO 3a
2.763	1.466	0.129	1.135	1.316	0.023	0.000	0.005	0.900	0.079	0.012	7.828	30 BIO 3a

2.782	1.460	0.149	1.097	1.317	0.030	0.000	0.000	0.874	0.055	0.014	7.777	30 BIO 4a
2.758	1.444	0.153	1.080	1.347	0.029	0.000	0.003	0.911	0.088	0.011	7.824	30 BIO 4a
2.758	1.448	0.145	1.121	1.338	0.032	0.000	0.005	0.891	0.069	0.014	7.821	30 BIO 4a
2.793	1.444	0.141	0.972	1.424	0.026	0.011	0.017	0.908	0.060	0.011	7.806	41 BIO 1a
2.774	1.455	0.138	0.998	1.455	0.026	0.002	0.013	0.945	0.025	0.011	7.840	41 BIO 1a
2.766	1.447	0.141	1.000	1.455	0.027	0.000	0.012	0.950	0.043	0.008	7.850	41 BIO 1a
2.749	1.469	0.148	1.023	1.460	0.024	0.000	0.005	0.919	0.026	0.006	7.830	41 BIO 2a
2.762	1.483	0.140	1.015	1.422	0.022	0.000	0.008	0.932	0.043	0.001	7.828	41 BIO 2a
2.748	1.467	0.151	1.010	1.438	0.026	0.000	0.004	0.915	0.064	0.005	7.828	41 BIO 2a
2.662	1.519	0.132	1.100	1.454	0.023	0.000	0.001	0.932	0.091	0.001	7.914	41 BIO 3a
2.706	1.532	0.116	1.130	1.404	0.021	0.000	0.004	0.914	0.043	0.002	7.871	41 BIO 3a
2.743	1.500	0.109	1.103	1.412	0.025	0.002	0.001	0.873	0.063	0.004	7.835	41 BIO 3a
2.717	1.513	0.107	1.080	1.503	0.021	0.003	0.000	0.808	0.064	0.008	7.824	41 BIO 4a
2.744	1.473	0.122	1.054	1.456	0.022	0.000	0.000	0.943	0.049	0.007	7.869	41 BIO 4a
2.733	1.481	0.129	1.078	1.431	0.021	0.000	0.000	0.922	0.060	0.004	7.860	41 BIO 4a
2.787	1.421	0.104	1.149	1.371	0.024	0.000	0.002	0.634	0.216	0.009	7.716	28 BIO 1a
2.777	1.391	0.110	1.095	1.356	0.024	0.000	0.000	0.929	0.188	0.014	7.883	28 BIO 1a
2.758	1.405	0.103	1.113	1.367	0.024	0.000	0.001	0.936	0.185	0.014	7.905	28 BIO 1a
2.769	1.394	0.101	1.098	1.349	0.021	0.000	0.003	0.904	0.239	0.009	7.887	28 BIO 2a
2.765	1.410	0.092	1.118	1.362	0.022	0.000	0.003	0.868	0.220	0.011	7.873	28 BIO 2a
2.776	1.393	0.104	1.123	1.326	0.022	0.000	0.006	0.865	0.233	0.012	7.859	28 BIO 2a
2.780	1.360	0.082	1.181	1.344	0.021	0.000	0.002	0.897	0.229	0.011	7.907	28 BIO 3a
2.760	1.382	0.101	1.105	1.379	0.021	0.000	0.004	0.923	0.226	0.012	7.912	28 BIO 3a
2.771	1.376	0.100	1.128	1.351	0.020	0.000	0.001	0.930	0.217	0.012	7.907	28 BIO 3a
2.780	1.395	0.082	1.145	1.383	0.022	0.000	0.000	0.901	0.174	0.008	7.891	28 BIO 4a
2.770	1.396	0.084	1.144	1.389	0.023	0.000	0.000	0.918	0.174	0.009	7.907	28 BIO 4a
2.787	1.394	0.075	1.157	1.350	0.023	0.000	0.000	0.925	0.186	0.007	7.903	28 BIO 4a

Amphibole Weight Percent

SiO2	Al2O3	TiO2	Cr2O3	MgO	FeO	MnO	CaO	Na2O	K2O	F	Cl	Total	Sample #
42.89	9.64	0.80	n/a	11.04	17.96	0.48	12.23	1.14	0.97	0.18	0.13	97.33	4A-hbd1a
41.03	9.69	0.83	n/a	10.94	18.00	0.42	12.58	1.13	1.05	0.18	0.13	95.86	4A-hbd1a
40.93	9.70	0.67	n/a	10.78	18.31	0.44	12.58	1.18	0.95	0.20	0.13	95.75	4A-hbd1a
43.82	8.61	1.37	n/a	11.61	17.01	0.42	11.30	1.03	0.95	0.12	0.10	96.27	4A-hbd2a
43.70	9.35	1.16	n/a	11.15	17.56	0.43	12.15	1.08	0.95	0.18	0.12	97.73	4A-hbd2a
43.97	9.55	0.98	n/a	10.92	18.14	0.44	12.74	1.04	1.05	0.05	0.10	98.93	4A-hbd2a
44.90	8.72	1.40	n/a	11.67	16.90	0.43	12.77	1.06	0.95	0.12	0.12	98.96	4A-hbd3a
45.11	8.62	1.37	n/a	11.81	16.98	0.41	12.90	1.07	0.93	0.12	0.08	99.34	4A-hbd3a
46.32	8.26	1.14	n/a	12.03	16.65	0.39	11.82	1.03	0.81	0.12	0.05	98.57	4A-hbd3a
45.12	9.11	1.13	n/a	11.41	17.47	0.39	12.91	1.07	0.98	0.12	0.13	99.75	4A-hbd4a
45.57	9.11	0.46	n/a	11.32	17.55	0.42	12.23	1.07	0.82	0.02	0.10	98.64	4A-hbd4a
45.03	8.88	1.15	n/a	11.37	17.72	0.40	12.36	1.14	1.03	0.13	0.13	99.24	4A-hbd4a
41.30	8.73	1.25	0.03	11.57	16.27	0.48	12.03	1.20	1.02	0.15	0.09	94.03	4ahbl1
41.07	8.73	1.13	0.02	11.39	17.13	0.45	12.14	1.07	1.01	0.00	0.10	94.20	4ahbl2
40.99	8.91	0.74	0.04	11.31	17.50	0.44	11.82	1.20	0.89	0.12	0.07	93.96	4ahbl3
42.94	8.19	0.79	0.03	12.16	16.32	0.48	12.22	1.00	0.81	0.15	0.07	95.10	4ahbl4
42.17	8.96	0.87	0.04	11.33	17.43	0.47	12.17	1.07	0.94	0.30	0.10	95.68	4ahbl5
41.77	8.81	0.86	0.03	11.40	17.29	0.44	12.06	1.10	0.96	0.20	0.13	94.93	4ahbl6
41.36	8.79	0.79	0.01	11.55	17.31	0.42	12.16	1.06	0.91	0.06	0.09	94.45	4ahbl7
41.12	8.83	0.88	0.03	11.26	17.12	0.43	12.06	1.06	0.98	0.18	0.12	93.96	4ahbl8
41.35	8.69	0.65	0.01	11.52	17.05	0.49	12.20	1.04	0.87	0.20	0.10	94.07	4ahbl9
41.11	8.95	0.89	0.04	11.30	17.05	0.44	12.20	1.17	0.98	0.26	0.09	94.33	4ahbl10
41.25	9.01	0.86	0.05	11.38	17.51	0.40	12.15	1.16	1.00	0.11	0.09	94.90	4ahbl11
41.97	9.01	0.75	0.04	11.37	17.36	0.45	12.05	1.11	0.99	0.00	0.13	95.19	4ahbl12
42.17	8.99	0.89	0.00	11.42	17.26	0.52	12.17	1.06	0.96	0.00	0.11	95.52	4ahbl13
42.42	8.72	0.77	0.04	11.63	17.33	0.43	12.39	1.02	0.87	0.08	0.11	95.76	4ahbl14
41.89	8.73	1.01	0.03	11.43	17.07	0.40	12.11	1.12	0.92	0.17	0.08	94.88	4ahbl15
42.13	8.69	1.14	0.01	11.73	16.54	0.43	12.31	0.97	0.93	0.11	0.08	94.99	4ahbl16
41.86	8.72	1.32	0.04	11.69	16.34	0.41	12.03	1.13	1.00	0.11	0.15	94.71	4ahbl17
43.15	7.76	1.12	0.00	12.47	15.51	0.44	12.10	1.06	0.84	0.09	0.04	94.53	4ahbl18

42.12	8.18	0.74	0.01	12.24	15.48	0.46	12.27	0.96	0.81	0.13	0.08	93.42	4ahbl19
40.82	8.64	0.77	0.07	11.76	16.17	0.43	12.02	1.02	0.90	0.21	0.11	92.81	4ahbl20
40.54	8.78	0.59	0.04	11.54	16.49	0.40	11.92	1.09	0.86	0.07	0.09	92.35	4ahbl21
44.20	6.30	0.63	0.06	13.72	14.23	0.41	12.38	0.80	0.54	0.22	0.03	93.42	4ahbl22
42.36	7.13	0.66	0.06	12.95	14.93	0.44	12.27	0.92	0.63	0.03	0.10	92.43	4ahbl23
40.97	8.44	0.60	0.08	11.82	16.41	0.42	12.04	1.06	0.84	0.01	0.11	92.78	4ahbl24
40.15	7.86	1.35	0.02	11.64	16.48	0.44	11.88	1.15	0.94	0.14	0.11	92.08	4ahbl25
39.28	8.29	1.40	0.07	11.17	16.55	0.45	11.64	1.24	1.01	0.00	0.11	91.18	4ahbl26
38.89	8.78	0.90	0.00	10.85	17.30	0.40	11.78	1.09	0.98	0.21	0.13	91.18	4ahbl27
38.45	8.99	0.94	0.05	10.76	17.10	0.43	11.83	1.10	1.06	0.06	0.15	90.84	4ahbl28
38.24	9.00	0.66	0.07	10.75	17.33	0.45	11.82	1.10	0.93	0.17	0.15	90.57	4ahbl29
38.31	9.06	0.52	0.07	10.69	17.47	0.47	11.73	1.09	0.91	0.04	0.13	90.44	4ahbl30
39.70	8.99	0.98	0.06	10.71	17.69	0.46	11.81	1.12	0.98	0.11	0.15	92.67	4ahbl31
39.92	8.67	1.04	0.04	11.01	17.18	0.46	11.95	1.08	0.95	0.09	0.19	92.49	4ahbl32
39.33	9.04	0.86	0.03	10.77	17.54	0.40	11.94	1.12	0.99	0.26	0.15	92.28	4ahbl33
39.50	9.18	0.86	0.09	10.72	17.68	0.50	11.90	1.10	0.96	0.22	0.19	92.77	4ahbl34
39.71	8.86	0.95	0.10	10.80	17.45	0.47	11.91	1.13	0.97	0.19	0.13	92.55	4ahbl35
39.11	8.91	0.80	0.07	10.63	17.97	0.46	12.07	1.07	0.95	0.22	0.15	92.27	4ahbl36
42.43	8.76	1.05	0.03	11.46	17.65	0.43	12.18	1.07	0.88	0.13	0.14	96.11	4ahbl37
42.40	8.71	1.04	0.04	11.47	17.28	0.48	12.13	1.04	0.94	0.15	0.06	95.64	4ahbl38
41.81	9.33	0.99	0.03	10.99	17.96	0.43	11.96	1.05	1.01	0.23	0.15	95.81	4ahbl39
41.87	8.94	0.82	0.00	11.19	17.89	0.44	11.99	1.11	0.90	0.13	0.14	95.32	4ahbl40
41.35	9.33	0.90	0.07	10.86	18.51	0.51	12.14	1.14	0.97	0.18	0.19	96.04	4ahbl41
40.94	9.72	0.86	0.00	10.62	18.49	0.43	11.80	1.24	1.07	0.24	0.09	95.37	4ahbl42
43.76	9.96	0.85	0.03	10.51	18.91	0.41	12.20	1.22	1.04	0.11	0.08	98.99	20ahbl43
43.46	10.08	0.84	0.07	10.51	18.73	0.44	12.09	1.15	1.14	0.00	0.10	98.59	20ahbl44
43.74	10.03	0.81	0.00	10.49	19.07	0.44	12.23	1.17	1.06	0.16	0.09	99.19	20ahbl45
43.34	10.19	0.98	0.04	10.47	19.00	0.40	12.10	1.28	1.09	0.26	0.05	99.10	20ahbl46
43.54	9.91	1.01	0.04	10.52	18.58	0.40	12.35	1.19	1.15	0.17	0.12	98.87	20ahbl47
44.19	9.91	0.49	0.02	10.78	18.72	0.45	12.25	1.19	0.99	0.00	0.08	99.03	20ahbl48
29.90	1.42	36.95	0.03	0.00	1.05	0.12	29.52	0.00	0.00	0.30	0.05	99.20	20ahbl49
29.86	1.41	36.94	0.03	0.00	1.06	0.02	29.37	0.00	0.01	0.15	0.00	98.79	20ahbl50
29.89	1.57	36.75	0.01	0.00	0.98	0.08	29.64	0.00	0.03	0.57	0.01	99.29	20ahbl51

43.76	9.75	1.00	0.07	10.83	18.55	0.41	12.16	1.19	1.06	0.18	0.08	98.93	20ahbl52
43.71	9.79	1.02	0.07	10.77	18.60	0.42	11.85	1.33	1.11	0.19	0.09	98.84	20ahbl53
43.73	9.76	0.75	0.06	10.72	18.36	0.39	11.97	1.17	1.02	0.20	0.09	98.11	20ahbl54
43.61	9.76	0.88	0.04	10.52	18.75	0.51	12.11	1.28	1.08	0.08	0.07	98.62	20ahbl55
44.02	9.87	0.81	0.04	10.60	18.70	0.42	12.15	1.25	1.06	0.02	0.10	98.98	20ahbl56
45.09	9.18	0.33	0.01	11.11	18.09	0.39	12.28	1.07	0.77	0.13	0.08	98.44	20ahbl57
43.86	9.87	0.93	0.03	10.64	18.46	0.42	12.01	1.29	1.09	0.14	0.10	98.74	20ahbl58
43.55	9.80	0.84	0.03	10.54	18.52	0.43	12.05	1.27	1.08	0.13	0.12	98.26	20ahbl59
43.72	9.96	0.73	0.04	10.54	18.82	0.44	11.93	1.28	1.05	0.22	0.11	98.71	20ahbl60
43.82	9.80	1.08	0.03	10.81	18.51	0.38	12.19	1.20	1.05	0.07	0.09	98.97	20ahbl61
43.74	9.90	0.91	0.03	10.71	18.62	0.42	12.33	1.12	1.08	0.09	0.11	98.98	20ahbl62
43.94	9.79	0.74	0.04	10.76	18.91	0.43	12.06	1.29	1.04	0.07	0.11	99.13	20ahbl63

Amphibole Cation Total												
Si	Al	Ti	Mg	Fe	Mn	Ca	Na	K	F	Cl	Total	Sample #
6.511	1.724	0.091	2.499	2.280	0.061	1.989	0.334	0.188	0.086	0.032	15.796	4A-hbd1a
6.369	1.772	0.097	2.532	2.337	0.056	2.092	0.341	0.207	0.088	0.033	15.922	4A-hbd1a
6.367	1.779	0.078	2.501	2.382	0.058	2.097	0.356	0.188	0.097	0.035	15.938	4A-hbd1a
6.670	1.546	0.157	2.634	2.165	0.054	1.844	0.305	0.185	0.058	0.027	15.645	4A-hbd2a
6.578	1.659	0.132	2.502	2.210	0.055	1.959	0.316	0.183	0.086	0.031	15.711	4A-hbd2a
6.576	1.683	0.111	2.434	2.269	0.055	2.042	0.303	0.200	0.026	0.025	15.723	4A-hbd2a
6.657	1.524	0.156	2.579	2.096	0.054	2.029	0.305	0.180	0.057	0.029	15.667	4A-hbd3a
6.666	1.501	0.153	2.602	2.098	0.052	2.042	0.306	0.175	0.057	0.021	15.671	4A-hbd3a
6.838	1.438	0.126	2.647	2.056	0.049	1.869	0.296	0.153	0.057	0.014	15.541	4A-hbd3a
6.649	1.583	0.125	2.506	2.154	0.049	2.039	0.306	0.185	0.054	0.032	15.680	4A-hbd4a
6.773	1.595	0.051	2.507	2.182	0.053	1.948	0.310	0.155	0.011	0.025	15.610	4A-hbd4a
6.672	1.551	0.128	2.511	2.196	0.050	1.962	0.328	0.194	0.062	0.033	15.686	4A-hbd4a
6.483	1.615	0.147	2.707	2.136	0.064	2.023	0.364	0.204	0.074	0.024	15.844	4ahbl1
6.477	1.622	0.134	2.677	2.260	0.061	2.051	0.327	0.203	0.000	0.027	15.841	4ahbl2
6.474	1.658	0.088	2.661	2.311	0.058	2.000	0.366	0.180	0.060	0.018	15.880	4ahbl3
6.630	1.491	0.092	2.800	2.107	0.063	2.022	0.301	0.160	0.073	0.017	15.760	4ahbl4
6.502	1.628	0.100	2.604	2.248	0.061	2.011	0.321	0.185	0.144	0.025	15.834	4ahbl5

6.503	1.617	0.101	2.645	2.251	0.058	2.011	0.333	0.191	0.100	0.034	15.848	4ahbl6
6.494	1.628	0.093	2.704	2.273	0.055	2.045	0.324	0.182	0.027	0.025	15.851	4ahbl7
6.476	1.640	0.104	2.645	2.254	0.057	2.034	0.324	0.196	0.092	0.032	15.858	4ahbl8
6.499	1.610	0.077	2.698	2.241	0.065	2.054	0.316	0.175	0.101	0.027	15.865	4ahbl9
6.446	1.654	0.104	2.641	2.236	0.059	2.049	0.355	0.196	0.128	0.023	15.896	4ahbl10
6.454	1.661	0.101	2.654	2.291	0.054	2.036	0.352	0.199	0.055	0.024	15.887	4ahbl11
6.535	1.653	0.088	2.639	2.260	0.059	2.010	0.334	0.196	0.000	0.033	15.813	4ahbl12
6.539	1.643	0.104	2.640	2.238	0.068	2.022	0.319	0.190	0.000	0.028	15.790	4ahbl13
6.551	1.588	0.090	2.677	2.238	0.056	2.051	0.306	0.172	0.041	0.027	15.802	4ahbl14
6.521	1.602	0.118	2.653	2.223	0.052	2.020	0.339	0.183	0.082	0.022	15.819	4ahbl15
6.537	1.589	0.133	2.712	2.147	0.056	2.046	0.290	0.183	0.055	0.020	15.771	4ahbl16
6.513	1.599	0.154	2.711	2.126	0.054	2.005	0.340	0.198	0.055	0.038	15.800	4ahbl17
6.682	1.415	0.131	2.879	2.009	0.058	2.008	0.318	0.165	0.046	0.010	15.721	4ahbl18
6.610	1.513	0.088	2.864	2.032	0.061	2.062	0.293	0.162	0.065	0.020	15.773	4ahbl19
6.480	1.617	0.091	2.783	2.147	0.057	2.045	0.315	0.183	0.107	0.031	15.865	4ahbl20
6.494	1.658	0.071	2.754	2.209	0.054	2.046	0.338	0.176	0.033	0.024	15.861	4ahbl21
6.851	1.152	0.074	3.170	1.845	0.054	2.056	0.241	0.106	0.106	0.008	15.669	4ahbl22
6.708	1.330	0.079	3.058	1.978	0.058	2.081	0.283	0.127	0.014	0.025	15.749	4ahbl23
6.533	1.587	0.072	2.809	2.188	0.057	2.057	0.326	0.171	0.005	0.031	15.845	4ahbl24
6.465	1.492	0.164	2.793	2.220	0.060	2.050	0.359	0.193	0.071	0.030	15.900	4ahbl25
6.418	1.596	0.172	2.720	2.261	0.062	2.038	0.392	0.210	0.000	0.031	15.909	4ahbl26
6.353	1.690	0.110	2.641	2.363	0.055	2.062	0.344	0.203	0.109	0.036	15.966	4ahbl27
6.325	1.743	0.116	2.638	2.353	0.059	2.084	0.349	0.222	0.034	0.041	15.970	4ahbl28
6.304	1.750	0.082	2.643	2.389	0.063	2.088	0.352	0.196	0.091	0.042	16.008	4ahbl29
6.339	1.767	0.065	2.638	2.418	0.066	2.080	0.349	0.192	0.019	0.037	15.979	4ahbl30
6.387	1.706	0.119	2.569	2.380	0.062	2.036	0.349	0.202	0.056	0.042	15.914	4ahbl31
6.421	1.643	0.126	2.639	2.311	0.062	2.059	0.336	0.196	0.047	0.052	15.895	4ahbl32
6.344	1.718	0.104	2.589	2.366	0.054	2.063	0.350	0.204	0.131	0.041	15.968	4ahbl33
6.341	1.738	0.104	2.564	2.374	0.068	2.047	0.342	0.197	0.112	0.051	15.950	4ahbl34
6.386	1.680	0.114	2.590	2.346	0.063	2.052	0.353	0.200	0.098	0.034	15.930	4ahbl35
6.333	1.701	0.097	2.565	2.434	0.063	2.094	0.336	0.196	0.112	0.042	15.981	4ahbl36
6.530	1.588	0.121	2.630	2.272	0.056	2.008	0.319	0.173	0.063	0.035	15.799	4ahbl37
6.548	1.586	0.120	2.640	2.232	0.063	2.007	0.311	0.184	0.072	0.016	15.783	4ahbl38

6.460	1.699	0.115	2.531	2.321	0.056	1.980	0.316	0.199	0.112	0.040	15.831	4ahbl39
6.511	1.638	0.096	2.593	2.326	0.058	1.997	0.335	0.179	0.063	0.036	15.832	4ahbl40
6.411	1.705	0.105	2.510	2.400	0.066	2.016	0.342	0.192	0.090	0.050	15.895	4ahbl41
6.387	1.787	0.101	2.469	2.413	0.057	1.972	0.375	0.213	0.117	0.023	15.913	4ahbl42
6.550	1.758	0.095	2.344	2.367	0.052	1.956	0.354	0.199	0.052	0.020	15.750	20ahbl43
6.544	1.788	0.095	2.358	2.359	0.056	1.951	0.337	0.219	0.000	0.025	15.741	20ahbl44
6.534	1.766	0.091	2.337	2.383	0.055	1.959	0.340	0.202	0.074	0.022	15.763	20ahbl45
6.479	1.794	0.111	2.333	2.375	0.051	1.938	0.370	0.208	0.121	0.014	15.800	20ahbl46
6.521	1.750	0.114	2.348	2.327	0.051	1.982	0.345	0.219	0.079	0.030	15.769	20ahbl47
6.609	1.746	0.055	2.403	2.342	0.057	1.962	0.345	0.189	0.000	0.019	15.729	20ahbl48
4.537	0.253	4.217	0.000	0.133	0.015	4.799	0.000	0.001	0.145	0.013	14.118	20ahbl49
4.559	0.254	4.241	0.000	0.135	0.003	4.804	0.000	0.002	0.070	0.000	14.073	20ahbl50
4.513	0.279	4.174	0.000	0.124	0.010	4.796	0.000	0.005	0.270	0.004	14.176	20ahbl51
6.541	1.718	0.112	2.412	2.318	0.051	1.947	0.346	0.203	0.083	0.020	15.759	20ahbl52
6.538	1.726	0.115	2.401	2.327	0.053	1.900	0.387	0.212	0.091	0.022	15.779	20ahbl53
6.575	1.729	0.085	2.402	2.308	0.050	1.929	0.341	0.196	0.096	0.023	15.741	20ahbl54
6.560	1.730	0.099	2.358	2.358	0.065	1.952	0.374	0.206	0.039	0.018	15.764	20ahbl55
6.589	1.740	0.091	2.365	2.341	0.053	1.948	0.362	0.202	0.009	0.024	15.729	20ahbl56
6.727	1.615	0.037	2.470	2.258	0.049	1.963	0.309	0.146	0.061	0.020	15.655	20ahbl57
6.564	1.742	0.104	2.374	2.311	0.053	1.926	0.374	0.208	0.065	0.025	15.750	20ahbl58
6.558	1.740	0.095	2.365	2.332	0.054	1.944	0.371	0.207	0.061	0.031	15.764	20ahbl59
6.547	1.758	0.082	2.354	2.357	0.056	1.914	0.371	0.200	0.104	0.027	15.776	20ahbl60
6.554	1.728	0.122	2.409	2.315	0.049	1.953	0.348	0.200	0.031	0.022	15.733	20ahbl61
6.545	1.745	0.102	2.389	2.329	0.053	1.976	0.324	0.207	0.044	0.026	15.745	20ahbl62
6.571	1.725	0.083	2.398	2.364	0.054	1.933	0.373	0.199	0.035	0.027	15.767	20ahbl63

Potassium Feldspar Weight Percent

SiO2	Al2O3	Fe2O3	CaO	BaO	Na2O	K2O	Total	Sample #
60.81	18.59	0.00	0.00	2.19	0.53	14.96	97.08	16B KSP 1a
61.96	18.31	0.00	0.00	1.32	0.41	15.48	97.46	16B KSP 1a
61.99	18.36	0.00	0.00	1.25	0.52	14.92	97.04	16B KSP 1a
61.66	18.20	0.00	0.02	1.76	0.48	15.26	97.37	16B KSP 2a
61.77	18.38	0.01	0.00	1.59	0.51	15.28	97.54	16B KSP 2a
63.39	18.35	0.02	0.00	1.42	0.46	15.39	99.02	16B KSP 2a
62.27	18.95	0.00	0.00	1.66	0.42	15.13	98.43	16B KSP 3a
62.08	18.32	0.01	0.00	1.35	0.44	14.90	97.10	16B KSP 3a
62.96	18.45	0.11	0.00	1.16	0.35	15.42	98.45	16B KSP 3a
64.32	18.15	0.01	0.00	0.21	0.26	15.51	98.46	28 KSP 1a
62.93	18.16	0.05	0.00	0.31	0.26	15.77	97.48	28 KSP 1a
62.97	18.24	0.00	0.00	0.20	0.35	15.87	97.62	28 KSP 1a
63.47	17.97	0.01	0.00	0.34	0.29	15.71	97.79	28 KSP 2a
63.34	17.99	0.04	0.00	0.25	0.35	15.70	97.67	28 KSP 2a
63.44	18.20	0.00	0.00	0.33	0.34	15.48	97.79	28 KSP 2a
62.78	18.07	0.02	0.07	0.32	0.24	15.90	97.40	28 KSP 3a
62.68	17.86	0.11	0.00	0.26	0.31	16.09	97.31	28 KSP 3a
64.32	18.22	0.13	0.00	0.30	0.35	15.94	99.26	28 KSP 3a
63.51	17.77	0.00	0.00	0.27	0.31	15.88	97.73	41 KSP 1a
63.88	18.14	0.01	0.00	0.34	0.26	15.72	98.35	41 KSP 1a
63.73	18.28	0.00	0.00	0.36	0.30	15.65	98.33	41 KSP 1a
61.88	17.79	0.00	0.01	0.15	0.36	16.05	96.22	41 KSP 2a
63.84	17.88	0.00	0.02	0.38	0.23	15.67	98.02	41 KSP 2a
63.15	17.89	0.00	0.01	0.32	0.38	15.74	97.48	41 KSP 2a
63.44	18.05	0.00	0.00	0.38	0.24	15.90	98.01	41 KSP 3a
64.02	18.18	0.00	0.00	0.36	0.28	15.68	98.53	41 KSP 3a
63.68	18.13	0.02	0.00	0.28	0.28	15.91	98.29	41 KSP 3a
63.54	17.62	0.01	0.00	0.17	0.39	15.35	97.07	30 KSP 1a
63.85	18.10	0.00	0.00	0.22	0.34	15.50	98.01	30 KSP 1a
64.09	17.97	0.09	0.00	0.23	0.40	16.11	98.88	30 KSP 1a
63.90	18.00	0.00	0.00	0.13	0.32	15.83	98.17	30 KSP 2a
64.13	17.82	0.00	0.01	0.15	0.30	15.97	98.37	30 KSP 2a
63.44	17.97	0.00	0.01	0.15	0.33	15.63	97.52	30 KSP 2a
64.90	17.93	0.04	0.00	0.28	0.29	15.59	99.03	30 KSP 3a

64.40	18.16	0.01	0.02	0.18	0.29	15.95	99.01	30 KSP 3a
63.74	18.19	0.00	0.00	0.44	0.35	15.68	98.39	30 KSP 3a
62.29	18.34	0.06	0.00	1.61	0.40	14.98	97.68	4a KSP 1a
61.56	18.18	0.06	0.02	1.29	0.30	15.91	97.32	4a KSP 1a
62.67	18.65	0.08	0.00	1.60	0.55	14.43	97.97	4a KSP 1a
63.31	18.72	0.02	0.00	1.25	0.40	15.44	99.15	4a KSP 2a
62.81	18.80	0.01	0.00	1.97	0.38	14.37	98.34	4a KSP 2a
62.50	18.67	0.02	0.00	1.70	0.39	15.30	98.57	4a KSP 2a
62.08	18.62	0.02	0.00	1.41	0.52	14.85	97.50	4a KSP 3a
61.72	18.24	0.01	0.00	1.38	0.51	14.79	96.65	4a KSP 3a
61.04	18.49	0.07	0.00	1.89	0.52	15.16	97.18	4a KSP 3a

Potassium Feldspar Cation Total

Si	Al	Fe	Ca	Ba	Na	K	Total	Sample #
2.941	1.060	0.000	0.000	0.041	0.050	0.923	5.015	16B KSP 1a
2.967	1.033	0.000	0.000	0.025	0.038	0.946	5.008	16B KSP 1a
2.971	1.037	0.000	0.000	0.023	0.049	0.912	4.992	16B KSP 1a
2.964	1.031	0.000	0.001	0.033	0.044	0.936	5.010	16B KSP 2a
2.961	1.038	0.001	0.000	0.030	0.047	0.935	5.011	16B KSP 2a
2.982	1.017	0.001	0.000	0.026	0.042	0.923	4.992	16B KSP 2a
2.952	1.059	0.000	0.000	0.031	0.038	0.915	4.995	16B KSP 3a
2.974	1.034	0.000	0.000	0.025	0.041	0.911	4.985	16B KSP 3a
2.975	1.028	0.004	0.000	0.021	0.032	0.930	4.990	16B KSP 3a
3.010	1.001	0.001	0.000	0.004	0.024	0.926	4.964	28 KSP 1a
2.988	1.017	0.002	0.000	0.006	0.024	0.955	4.992	28 KSP 1a
2.986	1.020	0.000	0.000	0.004	0.032	0.960	5.001	28 KSP 1a
3.002	1.002	0.001	0.000	0.006	0.027	0.948	4.985	28 KSP 2a
2.999	1.004	0.002	0.000	0.005	0.032	0.948	4.989	28 KSP 2a
2.996	1.013	0.000	0.000	0.006	0.031	0.933	4.979	28 KSP 2a
2.987	1.014	0.001	0.004	0.006	0.023	0.965	5.000	28 KSP 3a
2.990	1.004	0.004	0.000	0.005	0.029	0.979	5.011	28 KSP 3a
2.998	1.001	0.005	0.000	0.006	0.031	0.948	4.989	28 KSP 3a
3.007	0.992	0.000	0.000	0.005	0.028	0.959	4.991	41 KSP 1a
3.002	1.005	0.000	0.000	0.006	0.023	0.943	4.979	41 KSP 1a

2.996	1.013	0.000	0.000	0.007	0.028	0.938	4.981	41 KSP 1a
2.985	1.011	0.000	0.000	0.003	0.034	0.988	5.021	41 KSP 2a
3.010	0.994	0.000	0.001	0.007	0.021	0.942	4.975	41 KSP 2a
2.999	1.002	0.000	0.001	0.006	0.035	0.953	4.995	41 KSP 2a
2.997	1.005	0.000	0.000	0.007	0.022	0.959	4.991	41 KSP 3a
3.002	1.005	0.000	0.000	0.007	0.026	0.938	4.978	41 KSP 3a
2.997	1.006	0.001	0.000	0.005	0.025	0.956	4.990	41 KSP 3a
3.017	0.986	0.000	0.000	0.003	0.036	0.930	4.972	30 KSP 1a
3.005	1.004	0.000	0.000	0.004	0.031	0.930	4.974	30 KSP 1a
3.002	0.992	0.003	0.000	0.004	0.036	0.963	5.000	30 KSP 1a
3.006	0.998	0.000	0.000	0.002	0.029	0.950	4.985	30 KSP 2a
3.012	0.987	0.000	0.001	0.003	0.027	0.957	4.987	30 KSP 2a
3.003	1.003	0.000	0.001	0.003	0.030	0.944	4.983	30 KSP 2a
3.021	0.984	0.001	0.000	0.005	0.027	0.926	4.963	30 KSP 3a
3.005	0.999	0.001	0.001	0.003	0.026	0.949	4.983	30 KSP 3a
2.997	1.008	0.000	0.000	0.008	0.032	0.941	4.985	30 KSP 3a
2.972	1.032	0.002	0.000	0.030	0.037	0.912	4.985	4a KSP 1a
2.962	1.031	0.002	0.001	0.024	0.028	0.976	5.024	4a KSP 1a
2.971	1.042	0.003	0.000	0.030	0.050	0.873	4.968	4a KSP 1a
2.971	1.036	0.001	0.000	0.023	0.037	0.924	4.991	4a KSP 2a
2.970	1.048	0.000	0.000	0.037	0.035	0.867	4.957	4a KSP 2a
2.962	1.043	0.001	0.000	0.032	0.035	0.925	4.997	4a KSP 2a
2.963	1.048	0.001	0.000	0.026	0.048	0.904	4.990	4a KSP 3a
2.972	1.035	0.001	0.000	0.026	0.047	0.908	4.989	4a KSP 3a
2.946	1.052	0.003	0.000	0.036	0.049	0.934	5.019	4a KSP 3a

Plagioclase Weight Percent							
SiO2	Al2O3	Fe2O3	CaO	Na2O	K2O	Total	Sample #
65.072	21.689	0.033	2.055	9.905	0.144	98.898	30-1a
64.615	21.325	0.011	2.156	9.413	0.137	97.657	30-1a
64.776	21.798	0.022	2.283	10.147	0.093	99.119	30-1a
61.09	23.048	0	4.247	8.951	0.062	97.398	28 PLAG 1a
61.567	23.03	0.03	4.295	8.919	0.172	98.013	28 PLAG 1a
61.641	22.702	0	4.079	8.987	0.092	97.501	28 PLAG 1a
61.348	23.205	0.152	4.277	8.665	0.175	97.822	28 PLAG 2a
61.118	23.097	0.044	4.16	8.87	0.065	97.354	28 PLAG 2a
60.997	22.831	0.045	3.913	8.636	0.105	96.527	28 PLAG 2a
61.295	23.379	0	4.151	8.708	0.113	97.646	28 PLAG 3a
60.494	22.827	0.052	4.198	8.866	0.126	96.563	28 PLAG 3a
60.392	23.073	0	4.414	8.908	0.116	96.903	28 PLAG 3a
62.098	21.559	0.03	2.334	9.645	0.057	95.723	28 PLAG 4a
60.643	22.706	0.056	3.946	8.677	0.036	96.064	28 PLAG 4a
61.329	22.746	0.011	3.821	8.95	0.07	96.927	28 PLAG 4a
58.932	23.875	0.167	5.438	7.894	0.131	96.437	4a PLAG 1a
59.709	24.434	0.23	5.569	7.704	0.108	97.754	4a PLAG 1a
59.148	24.609	0.371	5.765	8.03	0.132	98.055	4a PLAG 1a
59.663	24.373	0.163	5.351	8.124	0.06	97.734	4a PLAG 2a
59.473	24.77	0.089	5.728	8.088	0.099	98.247	4a PLAG 2a
57.85	24.746	0.056	6.437	7.267	0.104	96.46	4a PLAG 2a
59.127	24.854	0.093	5.775	8.112	0.103	98.064	4a PLAG 3a
59.941	24.957	0.011	5.752	7.931	0.125	98.717	4a PLAG 3a
56.058	26.089	0.126	7.331	6.806	0.148	96.558	4a PLAG 3a
59.145	23.594	0	5.221	7.93	0.151	96.041	16B PLAG 1a
57.794	24.868	0.059	6.162	7.503	0.135	96.521	16B PLAG 1a
59.295	24.17	0	5.409	8.117	0.081	97.072	16B PLAG 1a
58.611	24.215	0.026	5.716	7.687	0.18	96.435	16B PLAG 2a
59.488	23.924	0.056	5.246	8.154	0.092	96.96	16B PLAG 2a
58.27	24.78	0.037	6.193	7.627	0.168	97.075	16B PLAG 2a
60.5	24.036	0.056	4.901	8.489	0.05	98.032	16B PLAG 3a
60.486	23.313	0.044	4.007	8.431	0.078	96.359	16B PLAG 3a
60.116	24.382	0	5.218	7.982	0.102	97.8	16B PLAG 3a
62.767	22.748	0.044	3.367	9.328	0.186	98.44	30 PLAG 1a

63.032	22.299	0.03	3.108	9.111	0.158	97.738	30 PLAG 1a
63.123	21.925	0	2.859	9.631	0.064	97.602	30 PLAG 1a
63.093	22.243	0.1	2.837	9.597	0.085	97.955	30 PLAG 2a
66.491	19.998	0.037	0.213	11.089	0.041	97.869	30 PLAG 2a
64.022	21.627	0.078	2.214	9.978	0.101	98.02	30 PLAG 2a
63.455	21.152	0.041	2.087	9.494	0.122	96.351	30 PLAG 3a
63.435	21.698	0.06	2.45	9.38	0.083	97.106	30 PLAG 3a
63.004	21.76	0.067	2.71	9.476	0.09	97.107	30 PLAG 3a
61.697	23.096	0	3.95	8.903	0.019	97.665	41 PLAG 1a
60.918	23.572	0	4.603	8.684	0.112	97.889	41 PLAG 1a
63.07	22.502	0	2.95	9.16	0.001	97.683	41 PLAG 1a
61.855	23.417	0.063	4.205	8.914	0.057	98.511	41 PLAG 2a
60.608	23.967	0.056	4.887	8.17	0.119	97.807	41 PLAG 2a
61.129	23.607	0.1	4.544	8.16	0.072	97.612	41 PLAG 2a
59.836	23.953	0.007	4.951	8.103	0.058	96.908	41 PLAG 3a
61.066	22.605	0.011	3.785	8.662	0.032	96.161	41 PLAG 3a
61.037	22.884	0.011	4.168	8.892	0.015	97.007	41 PLAG 3a
61.402	23.111	0.041	4.205	6.6	0.048	95.407	41 PLAG 3a

Plagioclase Cation Total							
Si	Al	Fe	Ca	Na	K	Total	Comment
2.8853	1.1335	0.0011	0.0977	0.8516	0.0081	4.9774	30-1a
2.8964	1.1267	0.0004	0.1035	0.8181	0.0078	4.953	30-1a
2.8716	1.139	0.0007	0.1084	0.8722	0.0053	4.9973	30-1a
2.7737	1.2335	0	0.2066	0.788	0.0036	5.0055	28 PLAG 1a
2.7788	1.2252	0.001	0.2077	0.7806	0.0099	5.0033	28 PLAG 1a
2.7929	1.2124	0	0.1981	0.7895	0.0053	4.9983	28 PLAG 1a
2.7729	1.2363	0.0052	0.2072	0.7594	0.0101	4.9911	28 PLAG 2a
2.7746	1.2359	0.0015	0.2024	0.7808	0.0037	4.999	28 PLAG 2a
2.7877	1.2299	0.0015	0.1916	0.7654	0.0061	4.9823	28 PLAG 2a
2.7722	1.2463	0	0.2012	0.7636	0.0065	4.9899	28 PLAG 3a
2.7721	1.2329	0.0018	0.2061	0.7878	0.0074	5.0082	28 PLAG 3a
2.7605	1.2431	0	0.2162	0.7895	0.0067	5.0161	28 PLAG 3a
2.8512	1.1668	0.001	0.1148	0.8587	0.0034	4.9959	28 PLAG 4a

2.7857	1.2294	0.0019	0.1942	0.7728	0.0021	4.9862	28 PLAG 4a
2.7924	1.2207	0.0004	0.1864	0.7901	0.0041	4.9941	28 PLAG 4a
2.7122	1.2951	0.0058	0.2682	0.7044	0.0077	4.9934	4a PLAG 1a
2.7081	1.3063	0.0078	0.2707	0.6775	0.0063	4.9767	4a PLAG 1a
2.6844	1.3164	0.0127	0.2804	0.7066	0.0076	5.0082	4a PLAG 1a
2.7081	1.304	0.0056	0.2603	0.715	0.0035	4.9966	4a PLAG 2a
2.6898	1.3205	0.003	0.2776	0.7093	0.0057	5.0059	4a PLAG 2a
2.6671	1.3447	0.0019	0.318	0.6496	0.0061	4.9875	4a PLAG 2a
2.6812	1.3285	0.0032	0.2806	0.7133	0.0059	5.0127	4a PLAG 3a
2.6947	1.3225	0.0004	0.2771	0.6913	0.0072	4.9932	4a PLAG 3a
2.5933	1.4226	0.0044	0.3634	0.6105	0.0087	5.0029	4a PLAG 3a
2.7289	1.2832	0	0.2581	0.7095	0.0089	4.9887	16B PLAG 1a
2.6635	1.3509	0.0021	0.3043	0.6705	0.008	4.9993	16B PLAG 1a
2.71	1.302	0	0.2649	0.7193	0.0047	5.001	16B PLAG 1a
2.6985	1.3141	0.0009	0.282	0.6862	0.0106	4.9924	16B PLAG 2a
2.7206	1.2897	0.0019	0.2571	0.7231	0.0054	4.9979	16B PLAG 2a
2.6709	1.3388	0.0013	0.3042	0.6779	0.0098	5.0029	16B PLAG 2a
2.7333	1.28	0.0019	0.2372	0.7437	0.0029	4.9991	16B PLAG 3a
2.7689	1.2579	0.0015	0.1965	0.7484	0.0045	4.9777	16B PLAG 3a
2.7212	1.3009	0	0.2531	0.7006	0.0059	4.9818	16B PLAG 3a
2.8119	1.2012	0.0015	0.1616	0.8103	0.0106	4.9971	30 PLAG 1a
2.8363	1.1827	0.001	0.1499	0.7949	0.009	4.9738	30 PLAG 1a
2.8457	1.1651	0	0.1381	0.8419	0.0037	4.9945	30 PLAG 1a
2.8353	1.1781	0.0034	0.1366	0.8362	0.0049	4.9946	30 PLAG 2a
2.9653	1.0512	0.0012	0.0102	0.9589	0.0023	4.9892	30 PLAG 2a
2.8696	1.1426	0.0026	0.1063	0.8672	0.0058	4.9942	30 PLAG 2a
2.8864	1.1341	0.0014	0.1017	0.8373	0.0071	4.9681	30 PLAG 3a
2.8659	1.1555	0.002	0.1186	0.8217	0.0048	4.9685	30 PLAG 3a
2.8524	1.1612	0.0023	0.1315	0.8319	0.0052	4.9845	30 PLAG 3a
2.7869	1.2297	0	0.1912	0.7798	0.0011	4.9887	41 PLAG 1a
2.7544	1.2562	0	0.223	0.7613	0.0065	5.0015	41 PLAG 1a
2.8351	1.1923	0	0.1421	0.7984	0	4.9679	41 PLAG 1a
2.7743	1.238	0.0021	0.2021	0.7752	0.0033	4.995	41 PLAG 2a
2.7411	1.2776	0.0019	0.2368	0.7165	0.0069	4.9809	41 PLAG 2a
2.7639	1.2581	0.0034	0.2201	0.7154	0.0041	4.9651	41 PLAG 2a
2.7318	1.289	0.0003	0.2422	0.7173	0.0034	4.984	41 PLAG 3a

2.7982	1.2209	0.0004	0.1858	0.7696	0.0018	4.9768	41 PLAG 3a
2.7801	1.2285	0.0004	0.2034	0.7853	0.0009	4.9987	41 PLAG 3a
2.8126	1.2478	0.0014	0.2064	0.5862	0.0028	4.8572	41 PLAG 3a

Titanite Weight Percent

SiO2	TiO2	CaO	Al2O3	FeO	Ce2O3	MgO	MnO	Na2O	SnO2	F	Total	Comment
30.53	38.92	27.89	1.25	1.05	0.56	0.00	0.10	0.00	0.01	0.28	100.46	29 SPHE 1a
30.83	38.59	27.70	1.19	1.00	0.60	0.00	0.09	0.00	0.04	0.40	100.26	29 SPHE 1a
30.50	38.60	27.91	1.22	1.02	0.61	0.00	0.10	0.00	0.01	0.15	100.06	29 SPHE 1a
30.78	38.64	26.45	1.17	0.95	0.46	0.01	0.07	0.00	0.01	0.26	98.69	29 SPHE 2a
30.05	38.61	28.01	1.26	1.08	0.43	0.00	0.09	0.00	0.02	0.25	99.69	29 SPHE 2a
30.16	39.08	27.65	1.21	0.93	0.44	0.02	0.06	0.03	0.00	0.39	99.80	29 SPHE 2a
29.72	38.22	27.04	1.14	1.16	0.89	0.00	0.04	0.00	0.00	0.10	98.28	29 SPHE 3a
30.15	37.97	26.88	1.16	1.22	1.01	0.02	0.11	0.03	0.04	0.26	98.75	29 SPHE 3a
30.20	38.08	26.54	1.13	1.16	0.99	0.03	0.09	0.03	0.00	0.08	98.30	29 SPHE 3a
30.21	38.03	26.64	1.28	1.19	1.22	0.00	0.09	0.01	0.00	0.06	98.71	16B SPHE 1a
30.41	37.11	24.36	1.37	1.44	0.92	0.01	0.14	0.00	0.00	0.27	95.90	16B SPHE 1a
30.46	36.93	26.32	1.53	1.60	0.92	0.00	0.12	0.00	0.00	0.17	97.97	16B SPHE 1a
30.52	37.71	25.32	1.17	1.41	1.04	0.01	0.10	0.00	0.07	0.13	97.42	16B SPHE 2a
30.49	37.59	26.72	1.22	1.28	1.05	0.00	0.10	0.00	0.02	0.30	98.65	16B SPHE 2a
30.56	37.78	26.92	1.43	1.28	0.49	0.02	0.11	0.00	0.04	0.25	98.78	16B SPHE 2a
30.54	37.50	26.32	1.21	1.21	1.20	0.01	0.06	0.01	0.00	0.02	98.08	16B SPHE 3a
30.92	38.93	24.44	0.96	0.80	0.52	0.02	0.00	0.00	0.00	0.00	96.59	16B SPHE 3a
30.56	37.43	27.34	1.36	1.31	0.79	0.00	0.07	0.00	0.00	0.19	98.97	16B SPHE 3a
30.60	37.92	26.46	1.31	1.27	0.78	0.01	0.08	0.00	0.00	0.21	98.55	16B SPHE 4a
30.74	38.06	25.42	1.22	1.31	0.91	0.02	0.12	0.00	0.00	0.13	97.88	16B SPHE 4a
30.38	38.53	26.38	1.13	1.16	1.06	0.02	0.06	0.00	0.00	0.20	98.84	16B SPHE 4a

Titanite Cation Total

Si	Ti	Ca	Al	Fe	Ce	Mg	Mn	Na	Sn	F	Total	Comment
0.992	0.951	0.971	0.048	0.029	0.007	0.000	0.003	0.000	0.000	0.029	3.029	29 SPHE 1a
1.001	0.942	0.964	0.045	0.027	0.007	0.000	0.003	0.000	0.001	0.041	3.030	29 SPHE 1a
0.998	0.949	0.978	0.047	0.028	0.007	0.000	0.003	0.000	0.000	0.016	3.026	29 SPHE 1a
1.012	0.956	0.932	0.046	0.026	0.006	0.001	0.002	0.000	0.000	0.027	3.007	29 SPHE 2a
0.986	0.953	0.984	0.049	0.030	0.005	0.000	0.003	0.000	0.000	0.026	3.035	29 SPHE 2a
0.984	0.959	0.967	0.046	0.025	0.005	0.001	0.002	0.002	0.000	0.040	3.032	29 SPHE 2a
0.992	0.960	0.968	0.045	0.033	0.011	0.000	0.001	0.000	0.000	0.011	3.020	29 SPHE 3a
0.999	0.947	0.955	0.045	0.034	0.012	0.001	0.003	0.002	0.001	0.027	3.026	29 SPHE 3a
1.007	0.954	0.948	0.044	0.032	0.012	0.001	0.003	0.002	0.000	0.009	3.012	29 SPHE 3a
1.005	0.951	0.949	0.050	0.033	0.015	0.000	0.002	0.001	0.000	0.006	3.012	16B SPHE 1a
1.028	0.944	0.883	0.055	0.041	0.011	0.000	0.004	0.000	0.000	0.029	2.995	16B SPHE 1a
1.016	0.927	0.941	0.060	0.045	0.011	0.000	0.003	0.000	0.000	0.018	3.021	16B SPHE 1a
1.022	0.950	0.909	0.046	0.040	0.013	0.001	0.003	0.000	0.001	0.013	2.997	16B SPHE 2a
1.010	0.936	0.948	0.048	0.036	0.013	0.000	0.003	0.000	0.000	0.032	3.024	16B SPHE 2a
1.008	0.937	0.951	0.056	0.035	0.006	0.001	0.003	0.000	0.001	0.026	3.024	16B SPHE 2a
1.020	0.943	0.942	0.048	0.034	0.015	0.001	0.002	0.001	0.000	0.002	3.007	16B SPHE 3a
1.036	0.981	0.877	0.038	0.022	0.006	0.001	0.000	0.000	0.000	0.000	2.961	16B SPHE 3a
1.010	0.930	0.968	0.053	0.036	0.010	0.000	0.002	0.000	0.000	0.020	3.029	16B SPHE 3a
1.012	0.943	0.938	0.051	0.035	0.010	0.001	0.002	0.000	0.000	0.022	3.014	16B SPHE 4a
1.023	0.953	0.907	0.048	0.037	0.011	0.001	0.003	0.000	0.000	0.013	2.995	16B SPHE 4a
1.004	0.958	0.935	0.044	0.032	0.013	0.001	0.002	0.000	0.000	0.021	3.010	16B SPHE 4a

LA-ICP-MS OF FLUID INCLUSIONS

Fluid inclusions were ablated using an Agilent 7500ce ICPMS coupled to a Geolas laser ablation system at Virginia Tech. Before analysis of the inclusions began, inclusion-free quartz was analyzed for impurities that might affect the calculations of fluid composition. For WR-25A, there were no impurities that would affect the calculations. Ablation times range from 65 to 210 seconds. Onset of inclusion ablation is determined from increased Na counts. In some cases, multiple inclusions at different depths in the sample were analyzed. Type I, Type II, and possibly Type III were analyzed. An in-house program, AMS, was used to calculate compositions for each inclusion. Salinites were assumed 31.5 wt % NaCl for Type I inclusions, and 7.9 wt % NaCl for Type II/III. These salinities were used because they approximate the average estimates based on microthermometry results for the sample.

Table A-3: Results of LA-ICP-MS analyses

Sample and chip	Assemblage	Analysis no.	Type	Size (microm)	Ablation time for composition calculation (s)	Comments
WR25A1-b		Quartz	Clean quartz		74-112.2	
	1	1	L-V-D-D-D	20 x 8	81-142	Data reduced also for shorter time (83 - 125 s) - gives greater precision but essentially the same composition.
		2	L-V-D-D-D	20 x 8	70.1-123	Good separation of liquid and solids. Note small copper peak at end, interpreted as a small solid.
		3	L-V-D-D-D	10	76-102	Small copper peak due to solid
		4	L-V-D-D-D	?	74.3-80.5	Small inclusion, probably same assemblage as others, but note high As
				10	99-130	
		5	L-V-D-D-D	10	92-117	
		6	L-V-D-D-D	10	66-81	
	2	7	L(H2O)-V(CO2)	15	65-77	At surface, hence possibility of contamination
				10		
		8	L-V-D-D-D	15 x 8	78-83	One inclusion from 78-129, but as composition dominated by Fe + Mn, there is a large accidental included solid. Analysis from 78-83 attempts (half successfully) to separate the signal from the liquid
					78-129	
		9	L(H2O)-V(CO2)	15 x 8	111-122	
				?	129-148	Small inclusion, probably same assemblage as first
					170-181	Even smaller
		10	L(H2O)-V(CO2)	15	83.5-100	
					101.5-109.5	Smaller inclusion, probably same assemblage as first
		11	L(H2O)-V(CO2)	15	94.5-121	
					138.5-162	

		12	L(H2O)-V(CO2)	10	80-86	
					113-145	Poor signal (too deep?)
		13	L(H2O)-V(CO2)	15	69.2-82	Poor analysis because of accidental solid (K-Fe-Rb = mica)
		14	L(H2O)-V(CO2)	15	69.5-73.1	One inclusion but two calculations to separate Ca-rich solid in second half - probable accidental daughter. Ignore high La - due to tiny solids shown as spikes on the graph
					73.1-79.5	
WR25A2	1	15	L-V-D-D-D	20	103-147	
		16	L(H2O)-V(CO2)	15	108.3-137.5	One inclusion, but two calculations to separate Fe-Mn solid in second half
					137.5-150	
		17	L(H2O)-V(CO2)	15	69.8-74.9	
		18	L-V-D-D-D	15	111-121	Probably all one inclusion. The first analysis is interpreted to be just the liquid, the second includes solid daughters
					111-173	
		19	L(H2O)-V(CO2)	15	87-89	
		20	L(H2O)-V(CO2)	10	95-121	
					170-210	Very poor signal, most elements below detection

Sample:			WR25A1-1.txt		Host Correction Factor:			-		
Date:			08/05/2008 09:02		Wt % NaCl eq:			31.5		
Internal Standard:			Na							
Standard Method:			Microthermometry							
Region:			81.0 : 142.0 seconds							
Element	**Con. (ppm)**	**Con x 2**	**LOD (ppm)**	**LOD x2**	**Weight %**	**Weight x2**	**Sample (cps)**	**Bkg (cps)**	**Std (cps)**	**Bkg (cps)**
Li (7)	-	-	57.414	109.086	-	-	27.	336.	75,316.	341.
Na (23)	87,618.044	166474.2844	72.437	137.631	22.27	42.313	403,419.	11,310.	75,258,887.	10,920.
K (39)	1,631.397	3099.65506	212.807	404.333	0.31	0.589	10,032.	147,215.	472,757.	149,037.
Ca (40)	14,286.17	27143.72205	70.342	133.65	3.96	7.524	105,045.	30,745.	99,295,003.	30,816.
Mn (55)	5,785.499	10992.44715	13.957	26.518	1.33	2.527	59,277.	2,460.	732,758.	2,138.
Fe (56)	14,419.29	27396.65119	7.42	14.098	3.27	6.213	105,573.	382.	552,487.	380.
Cu (63)	86.173	163.72794	23.89	45.391	0.02	0.038	122.	120.	101,255.	122.
Zn (66)	777.246	1476.76816	38.097	72.384	0.16	0.304	960.	216.	93,271.	208.
As (75)	29.046	55.18683	19.505	37.059	0.01	0.019	26.	28.	47,182.	27.
Rb (85)	51.862	98.53723	11.283	21.437	0.01	0.019	620.	1,848.	843,466.	1,682.
Sr (88)	23.432	44.52099	0.283	0.537	0.	0	341.	2.	1,238,381.	5.
Y (89)	0.786	1.49321	0.352	0.669	0.	0	12.	4.	1,182,078.	3.
Mo (98)	-	-	1.788	3.397	-	-	0.	2.	171,720.	2.
Ag (107)	22.177	42.13687	1.127	2.141	0.	0	82.	2.	146,939.	5.
Sn (120)	-	-	3.427	6.511	-	-	16.	66.	487,713.	59.
Sb (121)	3.969	7.54015	1.625	3.087	0.	0	22.	9.	344,063.	6.
Cs (133)	8.764	16.6516	1.376	2.614	0.	0	185.	99.	1,253,957.	53.
Ba (138)	4.961	9.42666	0.25	0.475	0.	0	73.	2.	1,108,568.	2.
La (139)	0.657	1.24868	0.223	0.424	0.	0	9.	1.	1,051,046.	0.
Ce (140)	0.755	1.43526	0.115	0.218	0.	0	12.	0.	1,229,202.	2.
W (182)	-	-	1.211	2.302	-	-	2.	2.	253,236.	6.
Tl (205)	1.061	2.01533	0.584	1.11	0.	0	14.	6.	135,172.	4.
Pb (208)	822.712	1563.15261	1.071	2.035	0.11	0.209	7,583.	11.	649,758.	17.
Bi (209)	9.842	18.69904	0.707	1.344	0.	0	149.	14.	898,148.	13.

Sample:			WR25A1-1.txt		Host Correction Factor:			-		
Date:			08/12/2008 08:15		Wt % NaCl eq:			30.		
Internal Standard:			Na							
Standard Method:			Microthermometry							
Region:			83.0 : 125.0 seconds							
Element	**Con. (ppm)**	**Con x2**	**LOD (ppm)**	**LOD x2**	**Weight %**	**Weight x2**	**Sample (cps)**	**Bkg (cps)**	**Std (cps)**	**Bkg (cps)**
Li (7)	-	-	43.199	86.399	-	-	60.	332.	74,483.	341.
Na (23)	84,239.714	168479.4284	55.467	110.935	21.41	42.82	586,210.	11,269.	74,293,868.	10,920.
K (39)	1,473.221	2946.441	160.44	320.88	0.28	0.56	13,694.	147,465.	467,180.	149,037.
Ca (40)	13,707.523	27415.0456	53.691	107.383	3.8	7.6	152,373.	30,720.	98,129,605.	30,816.
Mn (55)	5,310.699	10621.3972	10.634	21.267	1.22	2.44	82,281.	2,443.	724,904.	2,138.
Fe (56)	13,094.57	26189.1408	5.743	11.486	2.97	5.94	145,002.	384.	546,119.	380.
Cu (63)	85.4	170.7996	17.865	35.729	0.02	0.04	183.	115.	100,011.	122.
Zn (66)	744.41	1488.8208	28.796	57.593	0.16	0.32	1,394.	218.	92,594.	208.
As (75)	27.203	54.406	15.264	30.528	0.01	0.02	37.	28.	46,632.	27.
Rb (85)	47.285	94.5696	8.639	17.277	0.01	0.02	855.	1,845.	832,487.	1,682.
Sr (88)	22.503	45.005	0.182	0.365	0.	0	496.	2.	1,223,798.	5.
Y (89)	0.782	1.5646	0.258	0.516	0.	0	18.	4.	1,166,421.	3.
Mo (98)	-	-	1.479	2.959	-	-	0.	3.	169,675.	2.
Ag (107)	20.506	41.011	0.933	1.866	0.	0	114.	3.	145,518.	5.
Sn (120)	-	-	2.568	5.135	-	-	26.	63.	482,466.	59.
Sb (121)	3.637	7.2736	1.29	2.579	0.	0	31.	10.	340,779.	6.
Cs (133)	8.263	16.526	1.013	2.026	0.	0	265.	99.	1,237,890.	53.
Ba (138)	4.738	9.4764	0.147	0.294	0.	0	106.	1.	1,096,577.	2.
La (139)	0.583	1.165	0.185	0.37	0.	0	13.	2.	1,038,587.	0.
Ce (140)	0.702	1.404	0.095	0.19	0.	0	17.	1.	1,216,187.	2.
W (182)	-	-	1.002	2.004	-	-	2.	3.	251,414.	6.
Tl (205)	1.035	2.0694	0.425	0.851	0.	0	21.	6.	134,150.	4.
Pb (208)	787.304	1574.6082	0.828	1.657	0.11	0.22	11,002.	12.	644,035.	17.
Bi (209)	9.469	18.937	0.546	1.092	0.	0	218.	15.	890,440.	13.

Sample:			WR25A1-2.txt		Host Correction Factor:			-		
Date:			08/05/2008 09:08		Wt % NaCl eq:			31.5		
Internal Standard:			Na							
Standard Method:			Microthermometry							
Region:			70.1 : 123.0 seconds							
Element	**Con. (ppm)**	**Con x1.9**	**LOD (ppm)**	**LOD x2**	**Weight %**	**Weight x2**	**Sample (cps)**	**Bkg (cps)**	**Std (cps)**	**Bkg (cps)**
Li (7)	-	-	265.843	505.102	-	-	17.	320.	75,316.	341.
Na (23)	73,622.777	139883.2765	303.516	576.68	18.72	35.568	77,389.	11,099.	75,258,887.	10,920.
K (39)	19,665.201	37363.88095	942.123	1,790.034	3.75	7.125	27,611.	148,445.	472,757.	149,037.
Ca (40)	7,455.189	14164.85853	349.263	663.599	2.06	3.914	12,512.	30,696.	99,295,003.	30,816.
Mn (55)	6,254.23	11883.03757	68.358	129.88	1.43	2.717	14,624.	2,495.	732,758.	2,138.
Fe (56)	17,044.405	32384.36969	37.621	71.48	3.87	7.353	28,479.	361.	552,487.	380.
Cu (63)	469.287	891.64435	114.849	218.213	0.1	0.19	152.	126.	101,255.	122.
Zn (66)	3,922.146	7452.07664	173.005	328.71	0.82	1.558	1,105.	224.	93,271.	208.
As (75)	-	-	85.306	162.081	-	-	8.	30.	47,182.	27.
Rb (85)	540.448	1026.85044	51.254	97.383	0.08	0.152	1,474.	1,910.	843,466.	1,682.
Sr (88)	160.594	305.12879	1.782	3.385	0.03	0.057	534.	4.	1,238,381.	5.
Y (89)	1.229	2.33548	1.124	2.136	0.	0	4.	2.	1,182,078.	3.
Mo (98)	-	-	7.138	13.563	-	-	0.	2.	171,720.	2.
Ag (107)	-	-	9.033	17.163	-	-	6.	7.	146,939.	5.
Sn (120)	-	-	15.993	30.387	-	-	0.	68.	487,713.	59.
Sb (121)	-	-	7.28	13.831	-	-	5.	9.	344,063.	6.
Cs (133)	87.937	167.07992	5.201	9.882	0.01	0.019	425.	76.	1,253,957.	53.
Ba (138)	50.007	95.01254	1.444	2.743	0.01	0.019	169.	3.	1,108,568.	2.
La (139)	-	-	1.36	2.584	-	-	0.	2.	1,051,046.	0.
Ce (140)	-	-	0.768	1.459	-	-	1.	1.	1,229,202.	2.
W (182)	18.479	35.11029	2.591	4.923	0.	0	14.	0.	253,236.	6.
Tl (205)	18.412	34.98318	1.615	3.068	0.01	0.019	56.	2.	135,172.	4.
Pb (208)	3,965.789	7534.99967	5.033	9.563	0.53	1.007	8,341.	14.	649,758.	17.
Bi (209)	12.705	24.13893	3.267	6.207	0.	0	44.	14.	898,148.	13.

Sample:	WR25A1-3.txt	Host Correction Factor: -
Date:	08/05/2008 09:11	Wt % NaCl eq: 31.5
Internal Standard:	Na	
Standard Method:	Microthermometry	
Region:	76.0 : 102.0 seconds	

Element	Con. (ppm)	Con x2	LOD (ppm)	LOD x2	Weight %	Weight x2	Sample (cps)	Bkg (cps)	Std (cps)	Bkg (cps)
Li (7)	-	-	73.336	139.338	-	-	56.	287.	75,316.	341.
Na (23)	68,433.003	130022.7053	91.253	173.381	17.4	33.06	315,161.	11,049.	75,258,887.	10,920.
K (39)	1,070.352	2033.66956	260.838	495.591	0.2	0.38	6,585.	148,934.	472,757.	149,037.
Ca (40)	14,885.014	28281.52641	99.235	188.547	4.12	7.828	109,421.	31,384.	99,295,003.	30,816.
Mn (55)	10,895.014	20700.52717	20.32	38.607	2.5	4.75	111,567.	2,461.	732,758.	2,138.
Fe (56)	28,531.771	54210.36566	10.678	20.288	6.48	12.312	208,762.	373.	552,487.	380.
Cu (63)	447.531	850.30795	31.411	59.681	0.09	0.171	633.	127.	101,255.	122.
Zn (66)	854.504	1623.5576	45.249	85.973	0.18	0.342	1,054.	189.	93,271.	208.
As (75)	78.529	149.20529	16.849	32.013	0.02	0.038	70.	15.	47,182.	27.
Rb (85)	39.292	74.6548	13.869	26.351	0.01	0.019	468.	1,929.	843,466.	1,682.
Sr (88)	34.387	65.33587	0.738	1.403	0.01	0.019	501.	6.	1,238,381.	5.
Y (89)	0.659	1.25286	0.512	0.973	0.	0	10.	5.	1,182,078.	3.
Mo (98)	-	-	2.975	5.653	-	-	3.	2.	171,720.	2.
Ag (107)	15.497	29.44373	2.399	4.558	0.	0	57.	4.	146,939.	5.
Sn (120)	-	-	4.535	8.616	-	-	5.	67.	487,713.	59.
Sb (121)	5.238	9.9522	2.042	3.879	0.	0	29.	8.	344,063.	6.
Cs (133)	3.64	6.91505	1.864	3.542	0.	0	77.	97.	1,253,957.	53.
Ba (138)	5.604	10.6476	0.246	0.467	0.	0	83.	1.	1,108,568.	2.
La (139)	-	-	0.528	1.004	-	-	5.	4.	1,051,046.	0.
Ce (140)	0.764	1.45179	0.274	0.521	0.	0	12.	1.	1,229,202.	2.
W (182)	26.864	51.04179	1.679	3.189	0.	0	92.	2.	253,236.	6.
Tl (205)	2.392	4.5448	0.632	1.2	0.	0	32.	5.	135,172.	4.
Pb (208)	3,194.19	6068.96176	1.423	2.704	0.43	0.817	29,419.	13.	649,758.	17.
Bi (209)	13.418	25.49325	0.765	1.454	0.	0	204.	9.	898,148.	13.

Sample:			WR25A1-4.txt		Host Correction Factor:			-		
Date:			08/05/2008 09:13		Wt % NaCl eq:			31.5		
Internal Standard:			Na							
Standard Method:			Microthermometry							
Region:			74.3 : 80.5 seconds							
Element	**Con. (ppm)**	**Con x2**	**LOD (ppm)**	**LOD x2**	**Weight %**	**Weight x2**	**Sample (cps)**	**Bkg (cps)**	**Std (cps)**	**Bkg (cps)**
Li (7)	-	-	7,414.59	14,087.72	-	-	50.	300.	75,316.	341.
Na (23)	57,817.739	109853.7035	8,982.013	17,065.825	14.7	27.93	4,810.	11,076.	75,258,887.	10,920.
K (39)	-	-	24,660.9	46,855.71	-	-	977.	149,489.	472,757.	149,037.
Ca (40)	-	-	9,697.409	18,425.076	-	-	1,106.	31,159.	99,295,003.	30,816.
Mn (55)	5,433.692	10324.01442	1,969.983	3,742.968	1.24	2.356	1,005.	2,648.	732,758.	2,138.
Fe (56)	10,448.689	19852.50948	1,084.035	2,059.667	2.37	4.503	1,381.	382.	552,487.	380.
Cu (63)	-	-	2,788.574	5,298.291	-	-	55.	113.	101,255.	122.
Zn (66)	16,891.13	32093.14681	4,650.547	8,836.039	3.52	6.688	376.	211.	93,271.	208.
As (75)	9,413.214	17885.10736	2,001.195	3,802.271	2.28	4.332	152.	23.	47,182.	27.
Rb (85)	-	-	1,454.838	2,764.191	-	-	0.	2,046.	843,466.	1,682.
Sr (88)	348.788	662.69682	46.154	87.692	0.06	0.114	92.	3.	1,238,381.	5.
Y (89)	-	-	28.537	54.221	-	-	0.	1.	1,182,078.	3.
Mo (98)	-	-	228.133	433.452	-	-	7.	3.	171,720.	2.
Ag (107)	-	-	218.183	414.547	-	-	0.	5.	146,939.	5.
Sn (120)	-	-	375.627	713.691	-	-	9.	56.	487,713.	59.
Sb (121)	1,001.047	1901.99006	218.46	415.073	0.19	0.361	102.	8.	344,063.	6.
Cs (133)	-	-	201.371	382.604	-	-	0.	95.	1,253,957.	53.
Ba (138)	388.988	739.07739	24.607	46.753	0.06	0.114	104.	1.	1,108,568.	2.
La (139)	0.	0	0.	0.	0.	0	0.	0.	1,051,046.	0.
Ce (140)	-	-	22.457	42.668	-	-	0.	1.	1,229,202.	2.
W (182)	-	-	183.477	348.606	-	-	0.	3.	253,236.	6.
Tl (205)	-	-	68.958	131.019	-	-	2.	5.	135,172.	4.
Pb (208)	5,684.61	10800.75976	143.82	273.259	0.76	1.444	946.	9.	649,758.	17.
Bi (209)	-	-	84.187	159.955	-	-	12.	13.	898,148.	13.

Sample:		WR25A1-4.txt				Host Correction Factor:		-
Date:		08/05/2008 09:13				Wt % NaCl eq:		31.5
Internal Standard:		Na						
Standard Method:		Microthermometry						
Region:		99.0 : 130.0 seconds						
Element	**Con. (ppm)**	**LOD (ppm)**	**Weight %**	**Sample (cps)**	**Bkg (cps)**	**Std (cps)**	**Bkg (cps)**	**Mix (ppm)**
Li (7)	140.961	122.341	0.09	76.	300.	75,316.	341.	-
Na (23)	70,519.917	148.203	17.93	185,084.	11,076.	75,258,887.	10,920.	-
K (39)	11,299.088	406.904	2.15	39,618.	149,489.	472,757.	149,037.	-
Ca (40)	11,217.984	160.007	3.11	46,987.	31,159.	99,295,003.	30,816.	-
Mn (55)	8,070.799	32.505	1.85	47,086.	2,648.	732,758.	2,138.	-
Fe (56)	21,902.034	17.887	4.97	91,297.	382.	552,487.	380.	-
Cu (63)	439.004	46.011	0.09	354.	113.	101,255.	122.	-
Zn (66)	2,768.609	76.734	0.58	1,944.	211.	93,271.	208.	-
As (75)	97.489	33.02	0.02	50.	23.	47,182.	27.	-
Rb (85)	354.753	24.005	0.05	2,408.	2,046.	843,466.	1,682.	-
Sr (88)	173.065	0.762	0.03	1,436.	3.	1,238,381.	5.	-
Y (89)	0.493	0.471	0.	4.	1.	1,182,078.	3.	-
Mo (98)	-	3.764	-	0.	3.	171,720.	2.	-
Ag (107)	14.285	3.6	0.	30.	5.	146,939.	5.	-
Sn (120)	-	6.198	-	12.	56.	487,713.	59.	-
Sb (121)	6.092	3.605	0.	20.	8.	344,063.	6.	-
Cs (133)	59.264	3.323	0.01	714.	95.	1,253,957.	53.	-
Ba (138)	45.279	0.406	0.01	382.	1.	1,108,568.	2.	-
La (139)	0.586	0.	0.	5.	0.	1,051,046.	0.	-
Ce (140)	0.419	0.371	0.	4.	1.	1,229,202.	2.	-
W (182)	27.67	3.027	0.	54.	3.	253,236.	6.	-
Tl (205)	9.644	1.138	0.	73.	5.	135,172.	4.	-
Pb (208)	4,306.948	2.373	0.58	22,599.	9.	649,758.	17.	-
Bi (209)	14.683	1.389	0.	127.	13.	898,148.	13.	-

Sample:		WR25A1-5.txt		Host Correction Factor:			-		
Date:		08/05/2008 09:17		Wt % NaCl eq:			31.5		
Internal Standard:		Na							
Standard Method:		Microthermometry							
Region:		92.0 : 117.0 seconds							
Element	**Con. (ppm)**	**Con x2**	**LOD (ppm)**	**LOD x2**	**Weight %**	**Weight x2**	**Sample (cps)**	**Bkg (cps)**	**Std (cps)**	**Bkg (cps)**
Li (7)	-	-	233.9	444.409	-	-	50.	303.	75,316.	341.
Na (23)	71,843.839	136503.2932	299.813	569.644	18.26	34.694	97,102.	11,087.	75,258,887.	10,920.
K (39)	16,483.709	31319.04634	963.815	1,831.249	3.14	5.966	29,765.	148,633.	472,757.	149,037.
Ca (40)	8,450.007	16055.01387	334.485	635.521	2.34	4.446	18,224.	31,048.	99,295,003.	30,816.
Mn (55)	2,850.34	5415.64524	68.319	129.805	0.65	1.235	8,562.	2,654.	732,758.	2,138.
Fe (56)	17,823.968	33865.53863	37.26	70.793	4.05	7.695	38,252.	383.	552,487.	380.
Cu (63)	-	-	107.403	204.066	-	-	25.	126.	101,255.	122.
Zn (66)	4,058.889	7711.88948	159.685	303.401	0.85	1.615	1,467.	218.	93,271.	208.
As (75)	140.479	266.91086	76.07	144.532	0.03	0.057	37.	21.	47,182.	27.
Rb (85)	352.43	669.61757	51.273	97.418	0.05	0.095	1,232.	2,036.	843,466.	1,682.
Sr (88)	525.887	999.18492	1.888	3.588	0.1	0.19	2,246.	5.	1,238,381.	5.
Y (89)	-	-	1.68	3.192	-	-	0.	4.	1,182,078.	3.
Mo (98)	-	-	4.584	8.71	-	-	0.	1.	171,720.	2.
Ag (107)	10.887	20.68587	6.761	12.846	0.	0	12.	4.	146,939.	5.
Sn (120)	-	-	13.943	26.492	-	-	0.	60.	487,713.	59.
Sb (121)	-	-	6.673	12.679	-	-	4.	8.	344,063.	6.
Cs (133)	149.573	284.18927	5.796	11.013	0.02	0.038	928.	92.	1,253,957.	53.
Ba (138)	193.876	368.36402	1.194	2.269	0.03	0.057	842.	2.	1,108,568.	2.
La (139)	-	-	0.619	1.176	-	-	2.	0.	1,051,046.	0.
Ce (140)	0.5	0.94962	0.	0.	0.	0	2.	0.	1,229,202.	2.
W (182)	-	-	5.19	9.86	-	-	3.	2.	253,236.	6.
Tl (205)	11.336	21.53897	2.269	4.312	0.	0	44.	5.	135,172.	4.
Pb (208)	13,598.167	25836.51673	3.939	7.484	1.83	3.477	36,733.	8.	649,758.	17.
Bi (209)	4.908	9.32444	2.932	5.571	0.	0	22.	12.	898,148.	13.

Sample:	WR25A1-6.txt	Host Correction Factor:	-
Date:	08/05/2008 09:20	Wt % NaCl eq:	31.5
Internal Standard:	Na		
Standard Method:	Microthermometry		
Region:	66.0 : 81.0 seconds		

Element	Con. (ppm)	Con x1.9	LOD (ppm)	LOD x1.9	Weight %	Weight x1.9	Sample (cps)	Bkg (cps)	Std (cps)	Bkg (cps)
Li (7)	-	-	1,175.027	2,232.552	-	-	17.	296.	75,316.	341.
Na (23)	65,451.539	124357.9239	1,462.312	2,778.394	16.64	31.616	23,361.	11,127.	75,258,887.	10,920.
K (39)	26,824.804	50967.12817	3,997.733	7,595.692	5.11	9.709	12,793.	149,827.	472,757.	149,037.
Ca (40)	7,898.978	15008.05744	1,618.876	3,075.865	2.19	4.161	4,498.	31,611.	99,295,003.	30,816.
Mn (55)	3,520.987	6689.87435	292.486	555.724	0.81	1.539	2,792.	2,712.	732,758.	2,138.
Fe (56)	7,258.923	13791.95351	154.922	294.351	1.65	3.135	4,113.	345.	552,487.	380.
Cu (63)	-	-	472.824	898.366	-	-	46.	116.	101,255.	122.
Zn (66)	8,009.524	15218.09636	732.543	1,391.832	1.67	3.173	764.	207.	93,271.	208.
As (75)	867.816	1648.85021	317.007	602.313	0.21	0.399	60.	21.	47,182.	27.
Rb (85)	954.322	1813.21161	230.847	438.61	0.14	0.266	883.	2,073.	843,466.	1,682.
Sr (88)	667.801	1268.82247	6.854	13.022	0.12	0.228	753.	3.	1,238,381.	5.
Y (89)	-	-	7.864	14.941	-	-	3.	3.	1,182,078.	3.
Mo (98)	-	-	29.949	56.903	-	-	4.	2.	171,720.	2.
Ag (107)	-	-	40.894	77.698	-	-	0.	7.	146,939.	5.
Sn (120)	-	-	72.002	136.803	-	-	0.	59.	487,713.	59.
Sb (121)	74.477	141.5063	26.658	50.649	0.01	0.019	32.	7.	344,063.	6.
Cs (133)	156.207	296.7933	26.58	50.502	0.02	0.038	256.	71.	1,253,957.	53.
Ba (138)	598.335	1136.83707	4.812	9.142	0.09	0.171	686.	1.	1,108,568.	2.
La (139)	-	-	4.054	7.702	-	-	3.	1.	1,051,046.	0.
Ce (140)	5.608	10.65539	3.594	6.828	0.	0	7.	1.	1,229,202.	2.
W (182)	-	-	29.359	55.781	-	-	1.	3.	253,236.	6.
Tl (205)	38.726	73.57845	9.187	17.455	0.01	0.019	40.	4.	135,172.	4.
Pb (208)	19,059.383	36212.82808	28.439	54.034	2.56	4.864	13,592.	17.	649,758.	17.
Bi (209)	64.63	122.79776	13.727	26.081	0.01	0.019	76.	11.	898,148.	13.

Sample:			WR25A1-7.txt						Host Correction Factor:	-
Date:			08/05/2008 07:36						Wt % NaCl eq:	7.9
Internal Standard:			Na							
Standard Method:			Microthermometry							
Region:			65.0 : 77.0 seconds							
Element	**Con. (ppm)**	**Con x 0.82**	**LOD (ppm)**	**LOD x 0.82**	**Weight %**	**Weight x 0.82**	**Sample (cps)**	**Bkg (cps)**	**Std (cps)**	**Bkg (cps)**
Li (7)	141.881	116.343	64.863	53.187	0.09	0.074	188.	288.	75,316.	341.
Na (23)	23,997.797	19,678.193	91.63	75.137	6.1	5.002	155,209.	10,965.	75,258,887.	10,920.
K (39)	5,567.207	4,565.109	253.598	207.95	1.06	0.869	48,101.	151,379.	472,757.	149,037.
Ca (40)	321.236	263.413	95.23	78.089	0.09	0.074	3,313.	31,744.	99,295,003.	30,816.
Mn (55)	-	-	18.162	14.893	-	-	77.	2,298.	732,758.	2,138.
Fe (56)	20.976	17.2	9.249	7.584	0.	0.	215.	337.	552,487.	380.
Cu (63)	-	-	29.615	24.284	-	-	0.	130.	101,255.	122.
Zn (66)	1,190.952	976.581	47.813	39.206	0.25	0.205	2,057.	222.	93,271.	208.
As (75)	-	-	19.976	16.38	-	-	0.	22.	47,182.	27.
Rb (85)	106.919	87.673	13.272	10.883	0.02	0.016	1,793.	1,686.	843,466.	1,682.
Sr (88)	62.206	51.009	0.536	0.44	0.01	0.008	1,271.	5.	1,238,381.	5.
Y (89)	-	-	0.552	0.452	-	-	2.	6.	1,182,078.	3.
Mo (98)	-	-	2.153	1.765	-	-	0.	3.	171,720.	2.
Ag (107)	-	-	1.254	1.028	-	-	0.	2.	146,939.	5.
Sn (120)	-	-	3.668	3.008	-	-	8.	62.	487,713.	59.
Sb (121)	-	-	1.393	1.142	-	-	3.	5.	344,063.	6.
Cs (133)	19.477	15.971	1.689	1.385	0.	0.	579.	76.	1,253,957.	53.
Ba (138)	9.197	7.542	0.31	0.254	0.	0.	191.	2.	1,108,568.	2.
La (139)	303.651	248.994	0.41	0.336	0.05	0.041	6,137.	3.	1,051,046.	0.
Ce (140)	-	-	0.283	0.232	-	-	1.	2.	1,229,202.	2.
W (182)	-	-	1.104	0.905	-	-	4.	1.	253,236.	6.
Tl (205)	4.219	3.46	0.524	0.43	0.	0.	79.	4.	135,172.	4.
Pb (208)	1,390.129	1,139.906	1.478	1.212	0.19	0.156	17,952.	15.	649,758.	17.
Bi (209)	0.936	0.767	0.591	0.484	0.	0.	20.	6.	898,148.	13.

Sample:		WR25A1-7.txt				Host Correction Factor:		-
Date:		08/12/2008 02:29				Wt % NaCl eq:		7.9
Internal Standard:		Na						
Standard Method:		Microthermometry						
Region:		133.0 : 144.0 seconds						
Element	**Con. (ppm)**	**LOD (ppm)**	**Weight %**	**Sample (cps)**	**Bkg (cps)**	**Std (cps)**	**Bkg (cps)**	
Li (7)	-	1,863.485	-	34.	291.	74,483.	341.	
Na (23)	20,479.023	2,612.87	5.21	4,800.	10,960.	74,293,868.	10,920.	
K (39)	-	7,258.114	-	680.	151,420.	467,180.	149,037.	
Ca (40)	2,939.405	2,805.891	0.81	1,099.	31,772.	98,129,605.	30,816.	
Mn (55)	1,126.019	509.613	0.26	587.	2,283.	724,904.	2,138.	
Fe (56)	939.78	266.222	0.21	350.	339.	546,119.	380.	
Cu (63)	-	836.739	-	0.	130.	100,011.	122.	
Zn (66)	-	1,351.921	-	36.	221.	92,594.	208.	
As (75)	-	564.531	-	0.	22.	46,632.	27.	
Rb (85)	-	382.034	-	123.	1,692.	832,487.	1,682.	
Sr (88)	87.577	15.054	0.02	65.	5.	1,223,798.	5.	
Y (89)	-	15.493	-	0.	6.	1,166,421.	3.	
Mo (98)	-	60.276	-	0.	3.	169,675.	2.	
Ag (107)	-	40.474	-	4.	2.	145,518.	5.	
Sn (120)	-	103.206	-	12.	60.	482,466.	59.	
Sb (121)	-	39.006	-	9.	5.	340,779.	6.	
Cs (133)	-	46.434	-	43.	73.	1,237,890.	53.	
Ba (138)	-	8.701	-	1.	2.	1,096,577.	2.	
La (139)	-	11.505	-	0.	3.	1,038,587.	0.	
Ce (140)	-	7.939	-	0.	2.	1,216,187.	2.	
W (182)	-	30.9	-	0.	1.	251,414.	6.	
Tl (205)	15.985	13.626	0.01	11.	3.	134,150.	4.	
Pb (208)	2,524.172	42.589	0.34	1,185.	15.	644,035.	17.	
Bi (209)	-	17.176	-	5.	7.	890,440.	13.	

Sample:	WR25A1-8.txt	-
Date:	08/05/2008 09:24	31.5
Internal Standard:	Na	
Standard Method:	Microthermometry	
Region:	78.0 : 83.0 seconds	

Element	Con. (ppm)	Con x1.9	LOD (ppm)	LOD x1.9	Weight %	Weight % x1.9	Sample (cps)	Bkg (cps)	Std (cps)	Bkg (cps)	Mix (ppm)
Li (7)	-	-	655.313	1,245.095	-	-	127.	289.	75,316.	341.	-
Na (23)	80,987.667	153,876.568	857.087	1,628.465	20.59	39.121	78,687.	10,978.	75,258,887.	10,920.	-
K (39)	28,362.927	53,889.562	2,671.367	5,075.597	5.41	10.279	36,832.	151,486.	472,757.	149,037.	-
Ca (40)	2,490.825	4,732.567	920.23	1,748.437	0.69	1.311	3,858.	32,286.	99,295,003.	30,816.	-
Mn (55)	2,153.108	4,090.905	190.465	361.884	0.49	0.931	4,642.	2,366.	732,758.	2,138.	-
Fe (56)	10,411.345	19,781.556	83.633	158.903	2.36	4.484	16,034.	349.	552,487.	380.	-
Cu (63)	-	-	266.222	505.822	-	-	69.	116.	101,255.	122.	-
Zn (66)	3,214.108	6,106.804	455.898	866.206	0.67	1.273	832.	196.	93,271.	208.	-
As (75)	-	-	215.159	408.802	-	-	10.	21.	47,182.	27.	-
Rb (85)	508.415	965.989	126.557	240.458	0.07	0.133	1,280.	1,739.	843,466.	1,682.	-
Sr (88)	576.847	1,096.009	5.632	10.7	0.1	0.19	1,769.	6.	1,238,381.	5.	-
Y (89)	7.996	15.192	3.101	5.892	0.	0.	26.	2.	1,182,078.	3.	-
Mo (98)	-	-	15.325	29.118	-	-	0.	1.	171,720.	2.	-
Ag (107)	28.095	53.38	17.345	32.955	0.	0.	22.	3.	146,939.	5.	-
Sn (120)	-	-	40.874	77.661	-	-	32.	68.	487,713.	59.	-
Sb (121)	-	-	16.722	31.772	-	-	11.	7.	344,063.	6.	-
Cs (133)	148.934	282.975	14.762	28.049	0.02	0.038	666.	72.	1,253,957.	53.	-
Ba (138)	133.857	254.328	2.836	5.389	0.02	0.038	417.	1.	1,108,568.	2.	-
La (139)	1.905	3.62	1.694	3.218	0.	0.	6.	0.	1,051,046.	0.	-
Ce (140)	-	-	3.663	6.96	-	-	11.	2.	1,229,202.	2.	-
W (182)	-	-	18.802	35.724	-	-	0.	2.	253,236.	6.	-
Tl (205)	24.384	46.329	5.745	10.916	0.01	0.019	68.	3.	135,172.	4.	-
Pb (208)	4,294.132	8,158.85	12.932	24.571	0.58	1.102	8,323.	10.	649,758.	17.	-
Bi (209)	-	-	6.978	13.258	-	-	18.	7.	898,148.	13.	-

Sample:	WR25A1-9.txt	Host Correction Factor:	-
Date:	08/05/2008 07:46	Wt % NaCl eq:	7.9
Internal Standard:	Na		
Standard Method:	Microthermometry		
Region:	111.0 : 122.0 seconds		

Element	Con. (ppm)	Con x 0.82	LOD (ppm)	LOD x 0.82	Weight %	Weight x 0.82	Sample (cps)	Bkg (cps)	Std (cps)	Bkg (cps)
Li (7)	127.624	104.652	37.586	30.821	0.08	0.066	311.	280.	75,316.	341.
Na (23)	18,150.163	14,883.133	47.106	38.627	4.61	3.78	214,816.	10,947.	75,258,887.	10,920.
K (39)	2,662.209	2,183.011	145.548	119.35	0.51	0.418	42,118.	148,108.	472,757.	149,037.
Ca (40)	8,264.996	6,777.296	49.629	40.696	2.29	1.878	155,898.	31,174.	99,295,003.	30,816.
Mn (55)	17.926	14.699	12.211	10.013	0.	0.	471.	3,411.	732,758.	2,138.
Fe (56)	11.535	9.458	6.094	4.997	0.	0.	216.	390.	552,487.	380.
Cu (63)	-	-	15.291	12.539	-	-	36.	128.	101,255.	122.
Zn (66)	599.081	491.246	22.513	18.461	0.12	0.098	1,888.	189.	93,271.	208.
As (75)	-	-	12.401	10.169	-	-	10.	27.	47,182.	27.
Rb (85)	58.144	47.678	8.789	7.207	0.01	0.008	1,783.	2,500.	843,466.	1,682.
Sr (88)	386.097	316.6	0.41	0.336	0.07	0.057	14,423.	8.	1,238,381.	5.
Y (89)	-	-	0.244	0.2	-	-	0.	4.	1,182,078.	3.
Mo (98)	-	-	1.18	0.968	-	-	0.	3.	171,720.	2.
Ag (107)	-	-	1.108	0.908	-	-	4.	4.	146,939.	5.
Sn (120)	-	-	2.391	1.961	-	-	14.	64.	487,713.	59.
Sb (121)	-	-	0.848	0.696	-	-	0.	5.	344,063.	6.
Cs (133)	33.163	27.194	0.815	0.668	0.	0.	1,805.	67.	1,253,957.	53.
Ba (138)	25.203	20.667	0.218	0.179	0.	0.	957.	3.	1,108,568.	2.
La (139)	-	-	0.143	0.118	-	-	2.	1.	1,051,046.	0.
Ce (140)	-	-	0.127	0.104	-	-	0.	1.	1,229,202.	2.
W (182)	-	-	1.325	1.087	-	-	0.	5.	253,236.	6.
Tl (205)	6.161	5.052	0.344	0.282	0.	0.	210.	4.	135,172.	4.
Pb (208)	1,138.813	933.827	0.781	0.64	0.15	0.123	26,875.	14.	649,758.	17.
Bi (209)	-	-	0.464	0.38	-	-	7.	12.	898,148.	13.

Sample:		WR25A1-9.txt				Host Correction Factor:		-
Date:		08/05/2008 07:46				Wt % NaCl eq:		7.9
Internal Standard:		Na						
Standard Method:		Microthermometry						
Region:		129.0 : 148.0 seconds						
Element	**Con. (ppm)**	**LOD (ppm)**	**Weight %**	**Sample (cps)**	**Bkg (cps)**	**Std (cps)**	**Bkg (cps)**	
Li (7)	-	134.092	-	49.	280.	75,316.	341.	
Na (23)	16,474.527	168.056	4.19	44,373.	10,947.	75,258,887.	10,920.	
K (39)	1,118.074	519.258	0.21	4,025.	148,108.	472,757.	149,037.	
Ca (40)	10,989.218	177.057	3.04	47,172.	31,174.	99,295,003.	30,816.	
Mn (55)	-	43.565	-	244.	3,411.	732,758.	2,138.	
Fe (56)	84.998	21.742	0.02	363.	390.	552,487.	380.	
Cu (63)	-	54.553	-	0.	128.	101,255.	122.	
Zn (66)	681.438	80.318	0.14	489.	189.	93,271.	208.	
As (75)	-	44.241	-	0.	27.	47,182.	27.	
Rb (85)	34.733	31.356	0.	242.	2,500.	843,466.	1,682.	
Sr (88)	421.283	1.464	0.08	3,581.	8.	1,238,381.	5.	
Y (89)	-	0.871	-	1.	4.	1,182,078.	3.	
Mo (98)	-	4.21	-	0.	3.	171,720.	2.	
Ag (107)	-	3.953	-	2.	4.	146,939.	5.	
Sn (120)	-	8.53	-	8.	64.	487,713.	59.	
Sb (121)	-	3.026	-	2.	5.	344,063.	6.	
Cs (133)	21.873	2.906	0.	270.	67.	1,253,957.	53.	
Ba (138)	20.097	0.779	0.	174.	3.	1,108,568.	2.	
La (139)	-	0.511	-	0.	1.	1,051,046.	0.	
Ce (140)	-	0.453	-	1.	1.	1,229,202.	2.	
W (182)	-	4.727	-	0.	5.	253,236.	6.	
Tl (205)	5.634	1.228	0.	44.	4.	135,172.	4.	
Pb (208)	783.507	2.786	0.11	4,208.	14.	649,758.	17.	
Bi (209)	-	1.655	-	3.	12.	898,148.	13.	

Sample:	WR25A1-10.txt	Host Correction Factor:	-
Date:	08/05/2008 07:51	Wt % NaCl eq:	7.9
Internal Standard:	Na		
Standard Method:	Microthermometry		
Region:	83.5 : 100.0 seconds		

Element	Con. (ppm)	Con x 0.82	LOD (ppm)	LOD x 0.82	Weight %	Weight x 0.82	Sample (cps)	Bkg (cps)	Std (cps)	Bkg (cps)
Li (7)	419.831	344.261	281.814	231.088	0.26	0.213	117.	258.	75,316.	341.
Na (23)	23,024.621	18,880.189	391.813	321.286	5.85	4.797	31,072.	10,743.	75,258,887.	10,920.
K (39)	4,089.71	3,353.562	1,099.986	901.988	0.78	0.64	7,379.	144,716.	472,757.	149,037.
Ca (40)	1,519.366	1,245.88	381.045	312.457	0.42	0.344	3,267.	30,328.	99,295,003.	30,816.
Mn (55)	312.665	256.385	96.491	79.122	0.07	0.057	935.	3,830.	732,758.	2,138.
Fe (56)	615.076	504.362	44.494	36.485	0.14	0.115	1,314.	386.	552,487.	380.
Cu (63)	-	-	122.994	100.855	-	-	25.	124.	101,255.	122.
Zn (66)	783.206	642.229	172.655	141.577	0.16	0.131	281.	204.	93,271.	208.
As (75)	-	-	73.632	60.378	-	-	6.	18.	47,182.	27.
Rb (85)	83.574	68.531	67.155	55.067	0.01	0.008	292.	2,733.	843,466.	1,682.
Sr (88)	241.774	198.254	3.455	2.833	0.04	0.033	1,029.	9.	1,238,381.	5.
Y (89)	-	-	1.549	1.27	-	-	0.	2.	1,182,078.	3.
Mo (98)	-	-	13.172	10.801	-	-	0.	2.	171,720.	2.
Ag (107)	-	-	5.136	4.212	-	-	4.	1.	146,939.	5.
Sn (120)	-	-	17.445	14.305	-	-	15.	72.	487,713.	59.
Sb (121)	4.711	3.863	4.301	3.526	0.	0.	8.	2.	344,063.	6.
Cs (133)	23.845	19.553	5.966	4.892	0.	0.	148.	64.	1,253,957.	53.
Ba (138)	88.951	72.94	1.464	1.2	0.01	0.008	385.	2.	1,108,568.	2.
La (139)	-	-	1.071	0.878	-	-	1.	1.	1,051,046.	0.
Ce (140)	-	-	0.673	0.552	-	-	1.	0.	1,229,202.	2.
W (182)	-	-	6.361	5.216	-	-	0.	2.	253,236.	6.
Tl (205)	2.851	2.338	2.292	1.879	0.	0.	11.	4.	135,172.	4.
Pb (208)	636.238	521.715	6.665	5.465	0.09	0.074	1,711.	13.	649,758.	17.
Bi (209)	-	-	3.81	3.124	-	-	2.	12.	898,148.	13.

Sample:	WR25A1-11.txt
Date:	08/12/2008 09:06
Internal Standard:	Na
Standard Method:	Microthermometry
Region:	94.5 : 106.8 seconds
Host Correction Factor:	-
Wt % NaCl eq:	7.9

Element	Con. (ppm)	Con x 0.82	LOD (ppm)	LOD x 0.82	Weight %	Weight x 0.82	Sample (cps)	Bkg (cps)	Std (cps)	Bkg (cps)
Li (7)	-	-	163.287	133.896	-	-	83.	277.	74,483.	341.
Na (23)	27,499.979	22,549.982	243.931	200.024	6.99	5.732	71,687.	10,882.	74,293,868.	10,920.
K (39)	2,963.836	2,430.346	630.995	517.416	0.57	0.467	10,329.	148,127.	467,180.	149,037.
Ca (40)	379.163	310.914	256.464	210.301	0.1	0.082	1,575.	31,395.	98,129,605.	30,816.
Mn (55)	-	-	55.576	45.572	-	-	147.	3,092.	724,904.	2,138.
Fe (56)	35.993	29.514	26.893	22.052	0.01	0.008	149.	394.	546,119.	380.
Cu (63)	-	-	71.966	59.012	-	-	0.	127.	100,011.	122.
Zn (66)	197.354	161.83	104.412	85.618	0.04	0.033	137.	188.	92,594.	208.
As (75)	-	-	53.047	43.498	-	-	0.	24.	46,632.	27.
Rb (85)	45.077	36.963	43.278	35.488	0.01	0.008	304.	2,269.	832,487.	1,682.
Sr (88)	79.088	64.852	1.426	1.169	0.01	0.008	651.	6.	1,223,798.	5.
Y (89)	-	-	0.819	0.672	-	-	0.	2.	1,166,421.	3.
Mo (98)	-	-	5.191	4.256	-	-	0.	3.	169,675.	2.
Ag (107)	-	-	5.97	4.895	-	-	0.	5.	145,518.	5.
Sn (120)	-	-	10.768	8.83	-	-	0.	76.	482,466.	59.
Sb (121)	-	-	2.978	2.442	-	-	4.	4.	340,779.	6.
Cs (133)	9.732	7.98	4.037	3.311	0.	0.	117.	71.	1,237,890.	53.
Ba (138)	16.429	13.471	0.962	0.789	0.	0.	137.	3.	1,096,577.	2.
La (139)	-	-	0.771	0.633	-	-	1.	2.	1,038,587.	0.
Ce (140)	-	-	0.787	0.646	-	-	0.	2.	1,216,187.	2.
W (182)	-	-	3.744	3.07	-	-	0.	2.	251,414.	6.
Tl (205)	1.888	1.548	0.963	0.79	0.	0.	14.	2.	134,150.	4.
Pb (208)	206.856	169.622	3.281	2.69	0.03	0.025	1,076.	10.	644,035.	17.
Bi (209)	-	-	2.289	1.877	-	-	3.	12.	890,440.	13.

Sample:	WR25A1-12.txt	Host Correction Factor: -
Date:	08/05/2008 07:57	Wt % NaCl eq: 7.9
Internal Standard:	Na	
Standard Method:	Microthermometry	
Region:	80.0 : 86.0 seconds	

Element	Con. (ppm)	Con x 0.82	LOD (ppm)	LOD x0.82	Weight %	Weight x .82	Sample (cps)	Bkg (cps)	Std (cps)	Bkg (cps)
Li (7)	-	-	1,092.62	895.948	-	-	16.	273.	75,316.	341.
Na (23)	22,860.494	18,745.605	1,593.156	1,306.388	5.81	4.764	11,981.	10,787.	75,258,887.	10,920.
K (39)	7,847.095	6,434.618	4,409.873	3,616.096	1.5	1.23	5,497.	146,430.	472,757.	149,037.
Ca (40)	-	-	1,551.533	1,272.257	-	-	781.	30,986.	99,295,003.	30,816.
Mn (55)	-	-	350.545	287.447	-	-	130.	3,094.	732,758.	2,138.
Fe (56)	313.578	257.134	168.846	138.454	0.07	0.057	260.	377.	552,487.	380.
Cu (63)	-	-	487.956	400.124	-	-	47.	111.	101,255.	122.
Zn (66)	-	-	714.025	585.501	-	-	0.	200.	93,271.	208.
As (75)	-	-	308.359	252.854	-	-	0.	20.	47,182.	27.
Rb (85)	-	-	259.1	212.462	-	-	0.	2,390.	843,466.	1,682.
Sr (88)	-	-	10.014	8.212	-	-	15.	6.	1,238,381.	5.
Y (89)	-	-	6.244	5.12	-	-	0.	3.	1,182,078.	3.
Mo (98)	15.498	12.708	14.672	12.031	0.	0.	5.	0.	171,720.	2.
Ag (107)	-	-	37.41	30.676	-	-	0.	4.	146,939.	5.
Sn (120)	97.538	79.981	68.402	56.09	0.02	0.016	82.	60.	487,713.	59.
Sb (121)	45.062	36.951	21.255	17.429	0.01	0.008	29.	3.	344,063.	6.
Cs (133)	-	-	23.278	19.088	-	-	22.	65.	1,253,957.	53.
Ba (138)	15.666	12.846	0.	0.	0.	0.	26.	0.	1,108,568.	2.
La (139)	-	-	5.554	4.554	-	-	4.	2.	1,051,046.	0.
Ce (140)	-	-	4.924	4.038	-	-	1.	2.	1,229,202.	2.
W (182)	-	-	34.784	28.523	-	-	1.	4.	253,236.	6.
Tl (205)	-	-	12.826	10.517	-	-	4.	7.	135,172.	4.
Pb (208)	92.061	75.49	20.499	16.809	0.01	0.008	96.	9.	649,758.	17.
Bi (209)	-	-	14.015	11.492	-	-	4.	12.	898,148.	13.

Sample:				WR25A1-12.txt					Host Correction Factor:			-
Date:				08/05/2008 07:57					Wt % NaCl eq:			7.9
Internal Standard:				Na								
Standard Method:				Microthermometry								
Region:				113.0 : 145.0 seconds								
Element	**Con. (ppm)**	**Con x 0.82**	**LOD (ppm)**	**LOD x0.82**	**Weight %**	**Weight x 0.82**	**Sample (cps)**	**Bkg (cps)**	**Std (cps)**	**Bkg (cps)**		
Li (7)	-	-	1,106.581	907.397	-	-	43.	273.	75,316.	341.		
Na (23)	22,285.924	18,274.458	1,613.513	1,323.081	5.67	4.649	5,765.	10,787.	75,258,887.	10,920.		
K (39)	-	-	4,466.223	3,662.303	-	-	912.	146,430.	472,757.	149,037.		
Ca (40)	2,602.573	2,134.11	1,571.359	1,288.514	0.72	0.59	1,072.	30,986.	99,295,003.	30,816.		
Mn (55)	356.437	292.278	355.025	291.12	0.08	0.066	204.	3,094.	732,758.	2,138.		
Fe (56)	384.055	314.925	171.004	140.223	0.09	0.074	157.	377.	552,487.	380.		
Cu (63)	-	-	494.191	405.237	-	-	12.	111.	101,255.	122.		
Zn (66)	-	-	723.149	592.982	-	-	43.	200.	93,271.	208.		
As (75)	-	-	312.299	256.085	-	-	4.	20.	47,182.	27.		
Rb (85)	-	-	262.411	215.177	-	-	0.	2,390.	843,466.	1,682.		
Sr (88)	197.355	161.831	10.142	8.316	0.04	0.033	161.	6.	1,238,381.	5.		
Y (89)	-	-	6.324	5.186	-	-	1.	3.	1,182,078.	3.		
Mo (98)	-	-	14.859	12.185	-	-	0.	0.	171,720.	2.		
Ag (107)	-	-	37.888	31.068	-	-	2.	4.	146,939.	5.		
Sn (120)	-	-	69.276	56.806	-	-	19.	60.	487,713.	59.		
Sb (121)	-	-	21.527	17.652	-	-	4.	3.	344,063.	6.		
Cs (133)	-	-	23.576	19.332	-	-	17.	65.	1,253,957.	53.		
Ba (138)	27.034	22.168	0.	0.	0.	0.	22.	0.	1,108,568.	2.		
La (139)	-	-	5.625	4.613	-	-	0.	2.	1,051,046.	0.		
Ce (140)	-	-	4.987	4.089	-	-	0.	2.	1,229,202.	2.		
W (182)	-	-	35.229	28.887	-	-	0.	4.	253,236.	6.		
Tl (205)	-	-	12.99	10.651	-	-	0.	7.	135,172.	4.		
Pb (208)	644.36	528.375	20.761	17.024	0.09	0.074	332.	9.	649,758.	17.		
Bi (209)	-	-	14.194	11.639	-	-	0.	12.	898,148.	13.		

Sample:				WR25A1-13.txt					Host Correction Factor:			-
Date:				08/05/2008 08:04					Wt % NaCl eq:			7.9
Internal Standard:				Na								
Standard Method:				Microthermometry								
Region:				69.2 : 82.0 seconds								
Element	**Con. (ppm)**	**Con x 0.82**	**LOD (ppm)**	**LOD x.82**	**Weight %**	**Weight x 0.82**	**Sample (cps)**	**Bkg (cps)**	**Std (cps)**	**Bkg (cps)**		
Li (7)	105.403	86.43	19.805	16.24	0.06	0.049	445.	280.	75,316.	341.		
Na (23)	2,482.8	2,035.896	28.524	23.39	0.63	0.517	50,935.	11,104.	75,258,887.	10,920.		
K (39)	28,795.743	23,612.509	79.398	65.106	5.49	4.502	789,100.	149,014.	472,757.	149,037.		
Ca (40)	84.196	69.041	32.048	26.279	0.02	0.016	2,746.	31,709.	99,295,003.	30,816.		
Mn (55)	15.843	12.991	7.017	5.754	0.	0.	719.	2,917.	732,758.	2,138.		
Fe (56)	6,858.253	5,623.767	2.979	2.442	1.56	1.279	222,168.	377.	552,487.	380.		
Cu (63)	55.319	45.362	9.047	7.419	0.01	0.008	345.	114.	101,255.	122.		
Zn (66)	61.538	50.461	12.776	10.476	0.01	0.008	335.	198.	93,271.	208.		
As (75)	-	#VALUE!	5.946	4.875	-	#VALUE!	18.	21.	47,182.	27.		
Rb (85)	307.455	252.113	4.531	3.715	0.04	0.033	16,309.	2,128.	843,466.	1,682.		
Sr (88)	6.496	5.327	0.104	0.085	0.	0.	420.	2.	1,238,381.	5.		
Y (89)	-	#VALUE!	0.172	0.141	-	#VALUE!	0.	6.	1,182,078.	3.		
Mo (98)	-	#VALUE!	0.394	0.323	-	#VALUE!	1.	1.	171,720.	2.		
Ag (107)	-	#VALUE!	0.36	0.295	-	#VALUE!	1.	1.	146,939.	5.		
Sn (120)	33.06	27.109	1.242	1.018	0.01	0.008	1,083.	61.	487,713.	59.		
Sb (121)	-	#VALUE!	0.518	0.425	-	#VALUE!	1.	5.	344,063.	6.		
Cs (133)	2.985	2.448	0.433	0.355	0.	0.	281.	62.	1,253,957.	53.		
Ba (138)	37.702	30.915	0.144	0.118	0.01	0.008	2,476.	4.	1,108,568.	2.		
La (139)	13.827	11.338	0.129	0.106	0.	0.	886.	3.	1,051,046.	0.		
Ce (140)	0.218	0.179	0.067	0.055	0.	0.	16.	1.	1,229,202.	2.		
W (182)	9.943	8.153	0.446	0.365	0.	0.	151.	2.	253,236.	6.		
Tl (205)	1.094	0.897	0.197	0.161	0.	0.	65.	4.	135,172.	4.		
Pb (208)	63.826	52.337	0.416	0.341	0.01	0.008	2,602.	9.	649,758.	17.		
Bi (209)	0.564	0.463	0.242	0.198	0.	0.	38.	10.	898,148.	13.		

Sample:		WR25A1-14.txt						Host Correction Factor:		-
Date:		08/05/2008 08:08						Wt % NaCl eq:		7.9
Internal Standard:		Na								
Standard Method:		Microthermometry								
Region:		69.5 : 73.1 seconds								
Element	**Con. (ppm)**	**Con x 0.82**	**LOD (ppm)**	**LOD x0.82**	**Weight %**	**Weight x0.82**	**Sample (cps)**	**Bkg (cps)**	**Std (cps)**	**Bkg (cps)**
Li (7)	465.385	381.616	180.035	147.628	0.28	0.23	378.	294.	75,316.	341.
Na (23)	16,518.679	13,545.317	243.479	199.653	4.2	3.444	65,217.	10,860.	75,258,887.	10,920.
K (39)	12,702.051	10,415.681	792.93	650.202	2.42	1.984	67,023.	150,591.	472,757.	149,037.
Ca (40)	279.077	228.843	268.937	220.529	0.08	0.066	1,752.	32,207.	99,295,003.	30,816.
Mn (55)	-	-	54.796	44.933	-	-	62.	3,006.	732,758.	2,138.
Fe (56)	1,761.728	1,444.617	30.393	24.922	0.4	0.328	10,982.	382.	552,487.	380.
Cu (63)	-	-	86.966	71.312	-	-	44.	128.	101,255.	122.
Zn (66)	409.948	336.157	123.283	101.092	0.09	0.074	429.	194.	93,271.	208.
As (75)	60.036	49.229	50.795	41.651	0.01	0.008	46.	22.	47,182.	27.
Rb (85)	120.494	98.805	43.795	35.912	0.02	0.016	1,230.	2,197.	843,466.	1,682.
Sr (88)	56.286	46.154	1.496	1.227	0.01	0.008	700.	5.	1,238,381.	5.
Y (89)	-	-	0.898	0.736	-	-	0.	2.	1,182,078.	3.
Mo (98)	-	-	4.438	3.639	-	-	0.	1.	171,720.	2.
Ag (107)	-	-	5.023	4.119	-	-	0.	3.	146,939.	5.
Sn (120)	-	-	11.644	9.548	-	-	50.	59.	487,713.	59.
Sb (121)	29.402	24.11	4.927	4.04	0.01	0.008	140.	5.	344,063.	6.
Cs (133)	11.436	9.378	4.165	3.416	0.	0.	207.	70.	1,253,957.	53.
Ba (138)	19.299	15.825	0.821	0.674	0.	0.	244.	1.	1,108,568.	2.
La (139)	1,624.246	1,331.882	0.974	0.799	0.29	0.238	20,043.	2.	1,051,046.	0.
Ce (140)	-	-	0.864	0.708	-	-	0.	2.	1,229,202.	2.
W (182)	5.601	4.593	4.112	3.372	0.	0.	16.	2.	253,236.	6.
Tl (205)	3.31	2.714	1.39	1.14	0.	0.	38.	3.	135,172.	4.
Pb (208)	336.718	276.108	3.793	3.11	0.05	0.041	2,641.	13.	649,758.	17.
Bi (209)	-	-	2.381	1.952	-	-	0.	12.	898,148.	13.

Sample:	WR25A1-14.txt	Host Correction Factor: -
Date:	08/05/2008 08:08	Wt % NaCl eq: 7.9
Internal Standard:	Na	
Standard Method:	Microthermometry	
Region:	73.1 : 79.5 seconds	

Element	Con. (ppm)	Con x 0.82	LOD (ppm)	LOD x0.82	Weight %	Weight x0.82	Sample (cps)	Bkg (cps)	Std (cps)	Bkg (cps)
Li (7)	301.662	247.363	252.809	207.303	0.18	0.148	132.	294.	75,316.	341.
Na (23)	12,345.459	10,123.276	341.899	280.357	3.14	2.575	26,206.	10,860.	75,258,887.	10,920.
K (39)	11,610.012	9,520.21	1,113.451	913.03	2.21	1.812	32,973.	150,591.	472,757.	149,037.
Ca (40)	4,492.899	3,684.177	377.648	309.671	1.24	1.017	15,182.	32,207.	99,295,003.	30,816.
Mn (55)	335.289	274.937	76.946	63.095	0.08	0.066	1,575.	3,006.	732,758.	2,138.
Fe (56)	2,269.543	1,861.025	42.679	34.997	0.52	0.426	7,615.	382.	552,487.	380.
Cu (63)	324.709	266.261	122.12	100.138	0.07	0.057	210.	128.	101,255.	122.
Zn (66)	602.999	494.459	173.117	141.956	0.13	0.107	339.	194.	93,271.	208.
As (75)	-	-	71.327	58.488	-	-	1.	22.	47,182.	27.
Rb (85)	-	-	61.498	50.428	-	-	139.	2,197.	843,466.	1,682.
Sr (88)	38.095	31.238	2.101	1.723	0.01	0.008	255.	5.	1,238,381.	5.
Y (89)	-	-	1.261	1.034	-	-	0.	2.	1,182,078.	3.
Mo (98)	13.977	11.461	6.233	5.111	0.	0.	18.	1.	171,720.	2.
Ag (107)	-	-	7.054	5.784	-	-	2.	3.	146,939.	5.
Sn (120)	-	-	16.35	13.407	-	-	43.	59.	487,713.	59.
Sb (121)	-	-	6.918	5.673	-	-	4.	5.	344,063.	6.
Cs (133)	-	-	5.849	4.796	-	-	56.	70.	1,253,957.	53.
Ba (138)	16.243	13.32	1.153	0.946	0.	0.	111.	1.	1,108,568.	2.
La (139)	1,333.119	1,093.158	1.368	1.122	0.24	0.197	8,843.	2.	1,051,046.	0.
Ce (140)	-	-	1.213	0.994	-	-	8.	2.	1,229,202.	2.
W (182)	7.929	6.501	5.774	4.735	0.	0.	12.	2.	253,236.	6.
Tl (205)	-	-	1.952	1.601	-	-	2.	3.	135,172.	4.
Pb (208)	306.534	251.358	5.327	4.368	0.04	0.033	1,294.	13.	649,758.	17.
Bi (209)	-	-	3.343	2.741	-	-	7.	12.	898,148.	13.

Sample:	WR25A1-15.txt	Host Correction Factor:	-
Date:	08/12/2008 09:36	Wt % NaCl eq:	30.
Internal Standard:	Na		
Standard Method:	Microthermometry		
Region:	106.0 : 132.0 seconds		

Element	Con. (ppm)	Con x1.9	LOD (ppm)	LOD x2	Weight %	Weight % x2	Sample (cps)	Bkg (cps)	Std (cps)	Bkg (cps)
Li (7)	94.226	179.029	28.739	54.603	0.06	0.114	198.	250.	74,483.	341.
Na (23)	70,166.301	133,315.972	42.556	80.855	17.84	33.896	713,241.	11,064.	74,293,868.	10,920.
K (39)	6,512.702	12,374.133	135.601	257.642	1.24	2.356	88,566.	153,174.	467,180.	149,037.
Ca (40)	12,352.375	23,469.512	48.609	92.357	3.42	6.498	199,982.	32,760.	98,129,605.	30,816.
Mn (55)	8,288.18	15,747.542	8.446	16.048	1.9	3.61	186,541.	2,462.	724,904.	2,138.
Fe (56)	19,792.468	37,605.689	4.616	8.77	4.49	8.531	318,071.	379.	546,119.	380.
Cu (63)	57.884	109.98	15.223	28.924	0.01	0.019	179.	126.	100,011.	122.
Zn (66)	2,295.551	4,361.547	21.04	39.976	0.48	0.912	6,198.	208.	92,594.	208.
As (75)	89.331	169.728	8.013	15.225	0.02	0.038	176.	18.	46,632.	27.
Rb (85)	192.309	365.388	6.071	11.535	0.03	0.057	5,060.	1,844.	832,487.	1,682.
Sr (88)	82.522	156.793	0.236	0.448	0.01	0.019	2,646.	4.	1,223,798.	5.
Y (89)	0.319	0.606	0.192	0.365	0.	0.	11.	3.	1,166,421.	3.
Mo (98)	-	-	0.452	0.858	-	-	1.	1.	169,675.	2.
Ag (107)	10.942	20.789	0.889	1.689	0.	0.	88.	3.	145,518.	5.
Sn (120)	-	-	2.099	3.989	-	-	19.	71.	482,466.	59.
Sb (121)	2.39	4.542	0.437	0.83	0.	0.	29.	2.	340,779.	6.
Cs (133)	39.401	74.862	0.738	1.402	0.	0.	1,835.	61.	1,237,890.	53.
Ba (138)	27.526	52.3	0.218	0.415	0.	0.	898.	4.	1,096,577.	2.
La (139)	-	-	0.149	0.282	-	-	3.	2.	1,038,587.	0.
Ce (140)	-	-	0.132	0.25	-	-	4.	2.	1,216,187.	2.
W (182)	2.714	5.157	0.363	0.69	0.	0.	20.	1.	251,414.	6.
Tl (205)	6.659	12.652	0.26	0.493	0.	0.	195.	4.	134,150.	4.
Pb (208)	3,670.193	6,973.367	0.517	0.982	0.49	0.931	74,320.	8.	644,035.	17.
Bi (209)	7.669	14.57	0.422	0.801	0.	0.	255.	13.	890,440.	13.

Sample:			WR25A1-16.txt					Host Correction Factor:		-
Date:			08/12/2008 02:33					Wt % NaCl eq:		7.9
Internal Standard:			Na							
Standard Method:			Microthermometry							
Region:			73.0 : 80.0 seconds							
Element	**Con. (ppm)**	**Con x 0.82**	**LOD (ppm)**	**LOD x 0.82**	**Weight %**	**Weight x 0.82**	**Sample (cps)**	**Bkg (cps)**	**Std (cps)**	**Bkg (cps)**
Li (7)	-	-	451.883	370.544	-	-	24.	276.	74,483.	341.
Na (23)	16,821.396	13,793.545	614.036	503.509	4.28	3.51	18,299.	11,086.	74,293,868.	10,920.
K (39)	8,442.045	6,922.477	1,876.355	1,538.611	1.61	1.32	12,287.	152,696.	467,180.	149,037.
Ca (40)	2,081.894	1,707.153	731.774	600.055	0.58	0.476	3,607.	33,326.	98,129,605.	30,816.
Mn (55)	758.426	621.909	136.243	111.719	0.17	0.139	1,826.	2,489.	724,904.	2,138.
Fe (56)	2,115.1	1,734.382	74.972	61.477	0.48	0.394	3,637.	366.	546,119.	380.
Cu (63)	311.814	255.687	214.727	176.076	0.07	0.057	103.	123.	100,011.	122.
Zn (66)	1,551.355	1,272.111	348.53	285.795	0.32	0.262	448.	215.	92,594.	208.
As (75)	-	-	126.893	104.052	-	-	7.	19.	46,632.	27.
Rb (85)	133.914	109.809	101.066	82.874	0.02	0.016	377.	1,886.	832,487.	1,682.
Sr (88)	11.199	9.183	4.117	3.376	0.	0.	38.	5.	1,223,798.	5.
Y (89)	-	-	2.149	1.762	-	-	0.	2.	1,166,421.	3.
Mo (98)	-	-	14.062	11.531	-	-	2.	2.	169,675.	2.
Ag (107)	-	-	17.145	14.059	-	-	3.	6.	145,518.	5.
Sn (120)	-	-	31.167	25.557	-	-	43.	70.	482,466.	59.
Sb (121)	17.776	14.576	13.414	11.	0.	0.	23.	7.	340,779.	6.
Cs (133)	19.521	16.007	9.484	7.776	0.	0.	97.	53.	1,237,890.	53.
Ba (138)	3.448	2.827	1.853	1.519	0.	0.	12.	1.	1,096,577.	2.
La (139)	352.023	288.659	1.352	1.109	0.06	0.049	1,196.	1.	1,038,587.	0.
Ce (140)	-	-	1.199	0.983	-	-	0.	1.	1,216,187.	2.
W (182)	-	-	8.039	6.592	-	-	3.	1.	251,414.	6.
Tl (205)	4.571	3.748	3.545	2.907	0.	0.	14.	3.	134,150.	4.
Pb (208)	1,396.882	1,145.443	10.902	8.94	0.19	0.156	3,026.	13.	644,035.	17.
Bi (209)	6.64	5.445	5.954	4.882	0.	0.	24.	11.	890,440.	13.

Sample:	WR25A1-16.txt		Host Correction Factor:	-
Date:	08/05/2008 08:15		Wt % NaCl eq:	7.9
Internal Standard:	Na			
Standard Method:	Microthermometry			
Region:	137.5 : 150.0 seconds			

Element	Con. (ppm)	Con x 0.82	LOD (ppm)	LOD x0.82	Weight %	Weight x 0.82	Sample (cps)	Bkg (cps)	Std (cps)	Bkg (cps)
Li (7)	-	-	170.913	140.148	-	-	39.	280.	75,316.	341.
Na (23)	13,493.224	11,064.443	230.671	189.15	3.43	2.813	30,256.	11,061.	75,258,887.	10,920.
K (39)	4,911.374	4,027.327	712.575	584.312	0.94	0.771	14,732.	152,619.	472,757.	149,037.
Ca (40)	3,569.19	2,926.735	278.173	228.102	0.99	0.812	12,731.	33,291.	99,295,003.	30,816.
Mn (55)	2,512.626	2,060.353	51.717	42.408	0.58	0.476	12,460.	2,504.	732,758.	2,138.
Fe (56)	6,653.645	5,455.989	28.546	23.407	1.51	1.238	23,558.	369.	552,487.	380.
Cu (63)	-	-	82.118	67.337	-	-	50.	128.	101,255.	122.
Zn (66)	1,216.103	997.204	132.157	108.369	0.25	0.205	722.	216.	93,271.	208.
As (75)	-	-	48.73	39.959	-	-	0.	19.	47,182.	27.
Rb (85)	69.198	56.742	38.132	31.268	0.01	0.008	400.	1,873.	843,466.	1,682.
Sr (88)	19.468	15.964	1.584	1.299	0.	0.	137.	5.	1,238,381.	5.
Y (89)	-	-	0.789	0.647	-	-	6.	1.	1,182,078.	3.
Mo (98)	-	-	5.176	4.244	-	-	0.	2.	171,720.	2.
Ag (107)	-	-	6.576	5.393	-	-	0.	6.	146,939.	5.
Sn (120)	-	-	11.87	9.733	-	-	0.	71.	487,713.	59.
Sb (121)	-	-	4.947	4.057	-	-	6.	7.	344,063.	6.
Cs (133)	13.086	10.731	3.776	3.096	0.	0.	134.	57.	1,253,957.	53.
Ba (138)	11.772	9.653	0.958	0.786	0.	0.	85.	2.	1,108,568.	2.
La (139)	-	-	0.701	0.574	-	-	0.	1.	1,051,046.	0.
Ce (140)	-	-	0.44	0.361	-	-	2.	0.	1,229,202.	2.
W (182)	-	-	4.163	3.414	-	-	0.	2.	253,236.	6.
Tl (205)	2.213	1.815	1.306	1.071	0.	0.	14.	3.	135,172.	4.
Pb (208)	633.819	519.732	4.14	3.395	0.09	0.074	2,824.	13.	649,758.	17.
Bi (209)	-	-	2.199	1.803	-	-	13.	10.	898,148.	13.

Sample:			WR25A1-17.txt					Host Correction Factor:		-
Date:			08/05/2008 08:16					Wt % NaCl eq:		7.9
Internal Standard:			Na							
Standard Method:			Microthermometry							
Region:			69.8 : 74.9 seconds							
Element	**Con. (ppm)**	**Con x 0.82**	**LOD (ppm)**	**LOD**	**Weight %**	**Weight x 0.82**	**Sample (cps)**	**Bkg (cps)**	**Std (cps)**	**Bkg (cps)**
Li (7)	884.459	725.256	724.326	593.948	0.54	0.443	170.	283.	75,316.	341.
Na (23)	21,277.967	17,447.933	899.846	737.874	5.41	4.436	19,797.	10,863.	75,258,887.	10,920.
K (39)	6,024.449	4,940.048	2,888.209	2,368.331	1.15	0.943	7,508.	152,163.	472,757.	149,037.
Ca (40)	-	-	964.89	791.21	-	-	1,019.	32,896.	99,295,003.	30,816.
Mn (55)	-	-	183.46	150.437	-	-	84.	2,431.	732,758.	2,138.
Fe (56)	180.874	148.316	95.26	78.113	0.04	0.033	266.	325.	552,487.	380.
Cu (63)	-	-	301.02	246.836	-	-	3.	116.	101,255.	122.
Zn (66)	1,923.884	1,577.585	461.96	378.808	0.4	0.328	474.	214.	93,271.	208.
As (75)	-	-	174.009	142.687	-	-	0.	17.	47,182.	27.
Rb (85)	220.034	180.427	154.112	126.372	0.03	0.025	530.	1,820.	843,466.	1,682.
Sr (88)	36.783	30.162	5.443	4.463	0.01	0.008	108.	5.	1,238,381.	5.
Y (89)	-	-	3.648	2.992	-	-	0.	2.	1,182,078.	3.
Mo (98)	11.295	9.262	0.	0.	0.	0.	6.	0.	171,720.	2.
Ag (107)	-	-	18.475	15.149	-	-	0.	3.	146,939.	5.
Sn (120)	70.661	57.942	46.015	37.732	0.01	0.008	105.	83.	487,713.	59.
Sb (121)	29.088	23.852	15.106	12.387	0.01	0.008	33.	5.	344,063.	6.
Cs (133)	17.063	13.992	13.515	11.082	0.	0.	73.	68.	1,253,957.	53.
Ba (138)	156.239	128.116	4.177	3.425	0.02	0.016	466.	3.	1,108,568.	2.
La (139)	-	-	1.763	1.446	-	-	0.	0.	1,051,046.	0.
Ce (140)	-	-	2.209	1.811	-	-	5.	1.	1,229,202.	2.
W (182)	-	-	7.538	6.181	-	-	0.	0.	253,236.	6.
Tl (205)	-	-	5.01	4.108	-	-	3.	3.	135,172.	4.
Pb (208)	289.414	237.32	15.865	13.009	0.04	0.033	535.	15.	649,758.	17.
Bi (209)	-	-	8.522	6.988	-	-	7.	12.	898,148.	13.

Sample:		WR25A1-18.txt						Host Correction Factor:		-
Date:		08/12/2008 09:46						Wt % NaCl eq:		30.
Internal Standard:		Na								
Standard Method:		Microthermometry								
Region:		112.0 : 118.0 seconds								
Element	**Con. (ppm)**	**Con x1.9**	**LOD (ppm)**	**LOD x1.9**	**Weight %**	**Weight % x1.9**	**Sample (cps)**	**Bkg (cps)**	**Std (cps)**	**Bkg (cps)**
Li (7)	536.232	1,018.841	419.32	796.708	0.33	0.627	163.	274.	74,483.	341.
Na (23)	91,740.853	174,307.62	547.729	1,040.684	23.32	44.308	134,933.	11,031.	74,293,868.	10,920.
K (39)	18,997.881	36,095.973	1,450.295	2,755.561	3.62	6.878	37,395.	151,086.	467,180.	149,037.
Ca (40)	3,351.886	6,368.584	583.019	1,107.736	0.93	1.767	7,846.	32,892.	98,129,605.	30,816.
Mn (55)	1,157.705	2,199.64	124.578	236.698	0.27	0.513	3,765.	2,531.	724,904.	2,138.
Fe (56)	262.427	498.612	59.624	113.285	0.06	0.114	609.	391.	546,119.	380.
Cu (63)	-	-	206.959	393.222	-	-	54.	138.	100,011.	122.
Zn (66)	2,802.231	5,324.239	276.216	524.81	0.58	1.102	1,091.	201.	92,594.	208.
As (75)	-	-	102.847	195.409	-	-	0.	19.	46,632.	27.
Rb (85)	582.752	1,107.23	84.375	160.312	0.08	0.152	2,217.	1,902.	832,487.	1,682.
Sr (88)	792.129	1,505.045	3.331	6.328	0.14	0.266	3,672.	5.	1,223,798.	5.
Y (89)	-	-	4.737	9.	-	-	0.	8.	1,166,421.	3.
Mo (98)	-	-	8.032	15.26	-	-	0.	1.	169,675.	2.
Ag (107)	-	-	8.617	16.373	-	-	3.	2.	145,518.	5.
Sn (120)	-	-	22.939	43.583	-	-	0.	61.	482,466.	59.
Sb (121)	-	-	7.448	14.152	-	-	2.	4.	340,779.	6.
Cs (133)	149.391	283.843	7.484	14.219	0.02	0.038	1,008.	50.	1,237,890.	53.
Ba (138)	160.42	304.797	1.825	3.468	0.02	0.038	756.	2.	1,096,577.	2.
La (139)	-	-	1.527	2.902	-	-	0.	1.	1,038,587.	0.
Ce (140)	-	-	2.325	4.417	-	-	0.	3.	1,216,187.	2.
W (182)	-	-	9.161	17.406	-	-	0.	2.	251,414.	6.
Tl (205)	13.045	24.785	2.609	4.958	0.	0.	55.	3.	134,150.	4.
Pb (208)	4,477.431	8,507.118	7.618	14.474	0.6	1.14	13,094.	11.	644,035.	17.
Bi (209)	7.693	14.616	6.127	11.641	0.	0.	37.	16.	890,440.	13.

Sample:	WR25A1-19.txt	Host Correction Factor:	-
Date:	08/05/2008 08:19	Wt % NaCl eq:	7.9
Internal Standard:	Na		
Standard Method:	Microthermometry		
Region:	87.0 : 89.0 seconds		

Element	Con. (ppm)	Con x 0.82	LOD (ppm)	LOD x0.82	Weight %	Weight x0.82	Sample (cps)	Bkg (cps)	Std (cps)	Bkg (cps)
Li (7)	-	-	377.103	309.224	-	-	34.	275.	75,316.	341.
Na (23)	24,164.372	19,814.785	554.853	454.979	6.14	5.035	54,923.	10,891.	75,258,887.	10,920.
K (39)	4,282.487	3,511.639	1,625.493	1,332.904	0.82	0.672	13,027.	152,170.	472,757.	149,037.
Ca (40)	-	-	622.577	510.513	-	-	1,534.	32,949.	99,295,003.	30,816.
Mn (55)	-	-	115.815	94.968	-	-	450.	2,592.	732,758.	2,138.
Fe (56)	-	-	60.732	49.8	-	-	158.	350.	552,487.	380.
Cu (63)	-	-	185.596	152.189	-	-	110.	115.	101,255.	122.
Zn (66)	1,048.182	859.509	290.151	237.924	0.22	0.18	629.	213.	93,271.	208.
As (75)	-	-	110.096	90.278	-	-	0.	18.	47,182.	27.
Rb (85)	213.114	174.754	86.699	71.093	0.03	0.025	1,252.	1,864.	843,466.	1,682.
Sr (88)	823.265	675.077	4.341	3.559	0.15	0.123	5,887.	7.	1,238,381.	5.
Y (89)	-	-	3.074	2.521	-	-	0.	4.	1,182,078.	3.
Mo (98)	-	-	8.322	6.824	-	-	0.	1.	171,720.	2.
Ag (107)	-	-	15.877	13.019	-	-	12.	5.	146,939.	5.
Sn (120)	-	-	25.831	21.181	-	-	0.	53.	487,713.	59.
Sb (121)	-	-	9.155	7.507	-	-	12.	5.	344,063.	6.
Cs (133)	58.879	48.281	8.863	7.268	0.01	0.008	614.	61.	1,253,957.	53.
Ba (138)	280.533	230.037	1.887	1.548	0.04	0.033	2,041.	1.	1,108,568.	2.
La (139)	-	-	2.497	2.047	-	-	0.	1.	1,051,046.	0.
Ce (140)	-	-	2.404	1.971	-	-	0.	3.	1,229,202.	2.
W (182)	19.045	15.617	8.245	6.761	0.	0.	32.	1.	253,236.	6.
Tl (205)	12.071	9.898	3.585	2.94	0.	0.	79.	4.	135,172.	4.
Pb (208)	1,658.092	1,359.636	10.041	8.234	0.22	0.18	7,473.	16.	649,758.	17.
Bi (209)	-	-	5.706	4.679	-		23.	11.	898,148.	13.

Sample:	WR25A1-20.txt	Host Correction Factor:	-
Date:	08/05/2008 08:22	Wt % NaCl eq:	7.9
Internal Standard:	Na		
Standard Method:	Microthermometry		
Region:	95.0 : 121.0 seconds		

Element	Con. (ppm)	Con x 0.82	LOD (ppm)	LOD x 0.82	Weight %	Weight x 0.82	Sample (cps)	Bkg (cps)	Std (cps)	Bkg (cps)
Li (7)	-	-	656.598	538.41	-	-	30.	255.	75,316.	341.
Na (23)	28,892.594	23,691.927	961.581	788.496	7.34	6.019	12,817.	11,046.	75,258,887.	10,920.
K (39)	-	-	2,931.389	2,403.739	-	-	0.	153,258.	472,757.	149,037.
Ca (40)	-	-	965.075	791.362	-	-	528.	33,175.	99,295,003.	30,816.
Mn (55)	-	-	195.768	160.53	-	-	79.	2,380.	732,758.	2,138.
Fe (56)	182.672	149.791	106.393	87.242	0.04	0.033	128.	361.	552,487.	380.
Cu (63)	-	-	283.898	232.796	-	-	11.	126.	101,255.	122.
Zn (66)	-	-	470.467	385.783	-	-	12.	200.	93,271.	208.
As (75)	-	-	212.688	174.404	-	-	2.	23.	47,182.	27.
Rb (85)	-	-	128.753	105.577	-	-	0.	1,703.	843,466.	1,682.
Sr (88)	6.434	5.275	5.197	4.261	0.	0.	9.	4.	1,238,381.	5.
Y (89)	-	-	4.599	3.771	-	-	3.	3.	1,182,078.	3.
Mo (98)	-	-	16.072	13.179	-	-	3.	1.	171,720.	2.
Ag (107)	-	-	18.541	15.204	-	-	0.	3.	146,939.	5.
Sn (120)	-	-	50.523	41.429	-	-	0.	67.	487,713.	59.
Sb (121)	-	-	17.556	14.396	-	-	0.	6.	344,063.	6.
Cs (133)	-	-	13.542	11.104	-	-	3.	57.	1,253,957.	53.
Ba (138)	-	-	1.73	1.419	-	-	1.	0.	1,108,568.	2.
La (139)	-	-	3.512	2.88	-	-	0.	2.	1,051,046.	0.
Ce (140)	-	-	3.479	2.853	-	-	0.	2.	1,229,202.	2.
W (182)	-	-	19.883	16.304	-	-	0.	2.	253,236.	6.
Tl (205)	-	-	3.826	3.137	-	-	1.	2.	135,172.	4.
Pb (208)	42.544	34.886	14.851	12.178	0.01	0.008	37.	11.	649,758.	17.
Bi (209)	-	-	8.581	7.036	-	-	2.	11.	898,148.	13.

APPENDIX 2: METAL CONCENTRATIONS IN WHOLE ROCK SAMPLES FROM WHOLE ROCK GEOCHEMICAL ANALYSIS

Whole Rock samples were analyzed to determine if the samples contain elevated concentrations of metals. The following table provides the ppm concentrations for analyzed metals. Harker diagrams are presented to show any correlation between metals and SiO_2.

TABLE A-2: Metal concentrations of samples using whole rock geochemistry

SAMPLE	Au	Ag	Co	Cr	Cu	Mo	Ni	Pb	Sn	U	W	Zn	As	Hg
WR-4A	0.005	<1	5.1	30	50	3	13	24	1	2.96	3	57	1.3	<0.005
WR-4A2	0.052	<1	36.6	370	10	<2	113	15	5	1.57	2	268	1.3	<0.005
WR-7C	0.003	<1	4.3	20	6	<2	11	25	1	1.46	2	50	0.5	0.005
WR-16B	0.002	<1	10.5	30	9	<2	17	27	2	2.59	1	100	1.1	<0.005
WR-18A	0.002	<1	17.4	30	11	2	26	22	3	3.76	2	151	0.9	0.005
WR-18D	0.019	<1	11.2	30	9	<2	18	26	2	3.11	1	100	1.2	<0.005
WR-20B	0.002	<1	<0.5	30	<5	<2	8	15	<1	0.1	2	14	0.3	<0.005
WR-20C	0.005	<1	6.6	20	<5	<2	12	27	2	2.32	2	61	0.6	0.006
WR-23A	<0.001	<1	3.4	20	<5	<2	10	41	3	3.01	2	58	0.5	<0.005
WR-24B	<0.001	<1	46.6	260	63	<2	127	11	1	0.26	2	109	0.5	<0.005
WR-25B	0.001	<1	0.7	10	20	<2	7	37	1	10.35	2	14	0.3	0.006
WR-28	0.015	<1	5	20	<5	<2	13	33	3	7.01	1	53	1	<0.005
WR-29	0.003	<1	13	20	<5	<2	17	8	2	3.73	2	63	0.4	<0.005
WR-30	<0.001	<1	1.4	10	8	<2	9	44	1	1.33	3	41	0.6	<0.005
WR-41	0.004	<1	3.6	20	11	<2	13	33	1	2.94	2	53	0.4	<0.005
WR-42B	0.013	<1	10.4	20	<5	2	16	<5	1	2.11	5	66	0.8	<0.005
WR-44	0.005	<1	1	10	5	<2	6	42	3	1.73	2	14	1.1	<0.005
WR-45	<0.001	<1	6.9	20	<5	<2	11	18	1	2.06	15	65	0.3	<0.005

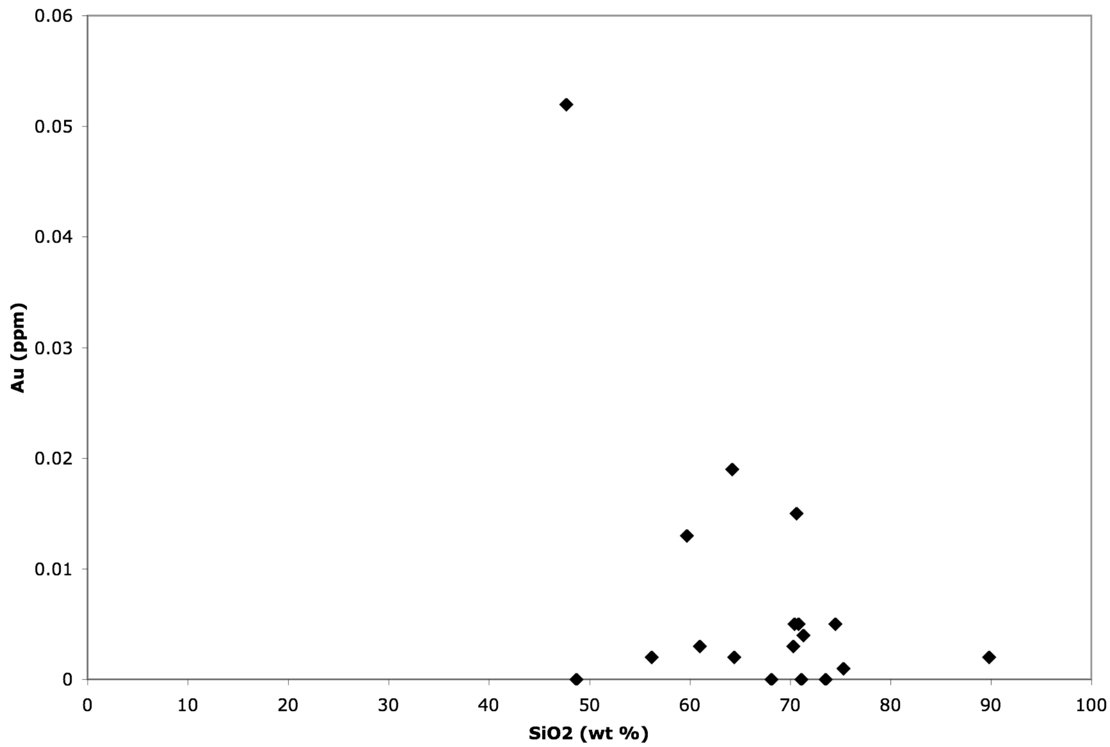
0.06
0.05
0.04
0.03
0.02
0.01
0
Au (ppm)
0
10
20
30
40
50
60
70
80
90
100
SiO2 (wt %)

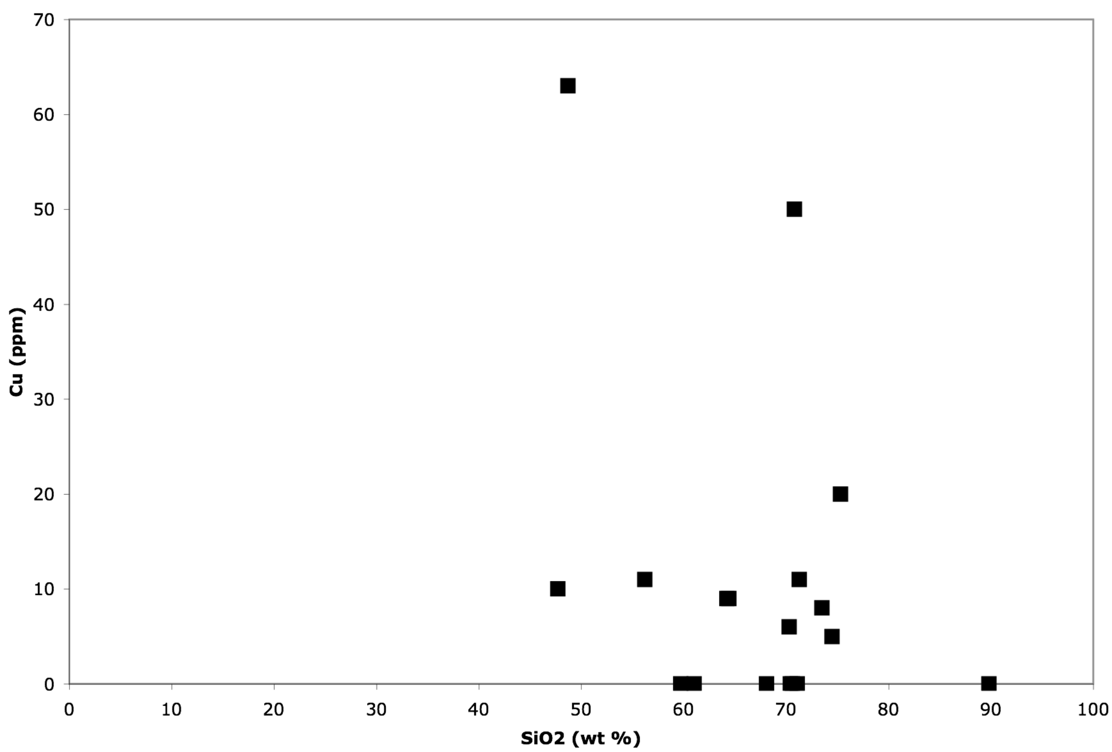
70
60
50
40
30
20
10
0
Cu (ppm)
0
10
20
30
40
50
60
70
80
90
100
SiO2 (wt %)

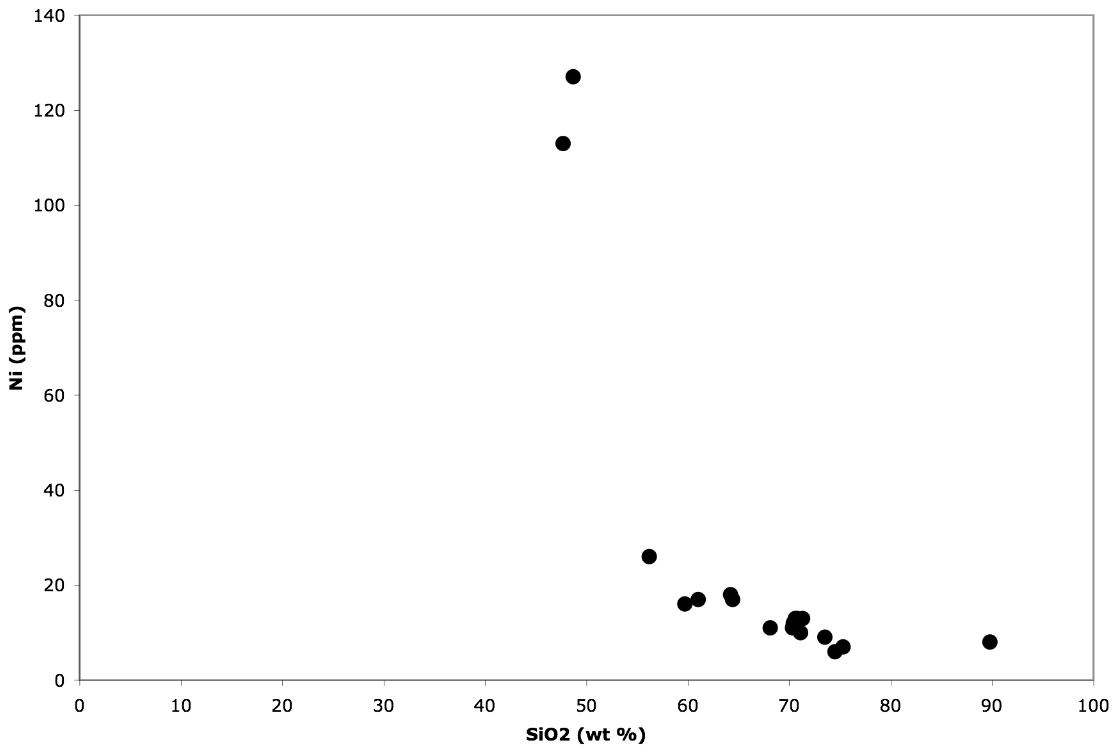

Ni (ppm)
SiO2 (wt %)
0
20
40
60
80
100
120
140
0
10
20
30
40
50
60
70
80
90
100

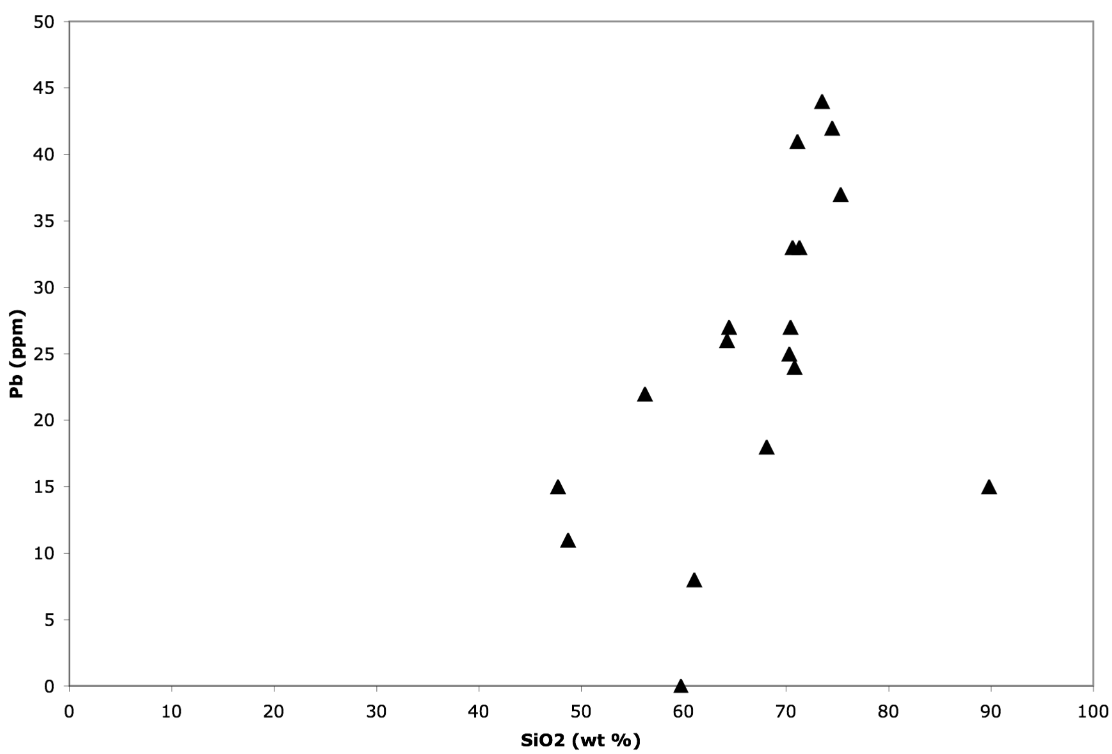

Pb (ppm)
SiO2 (wt %)
0
5
10
15
20
25
30
35
40
45
50
0
10
20
30
40
50
60
70
80
90
100

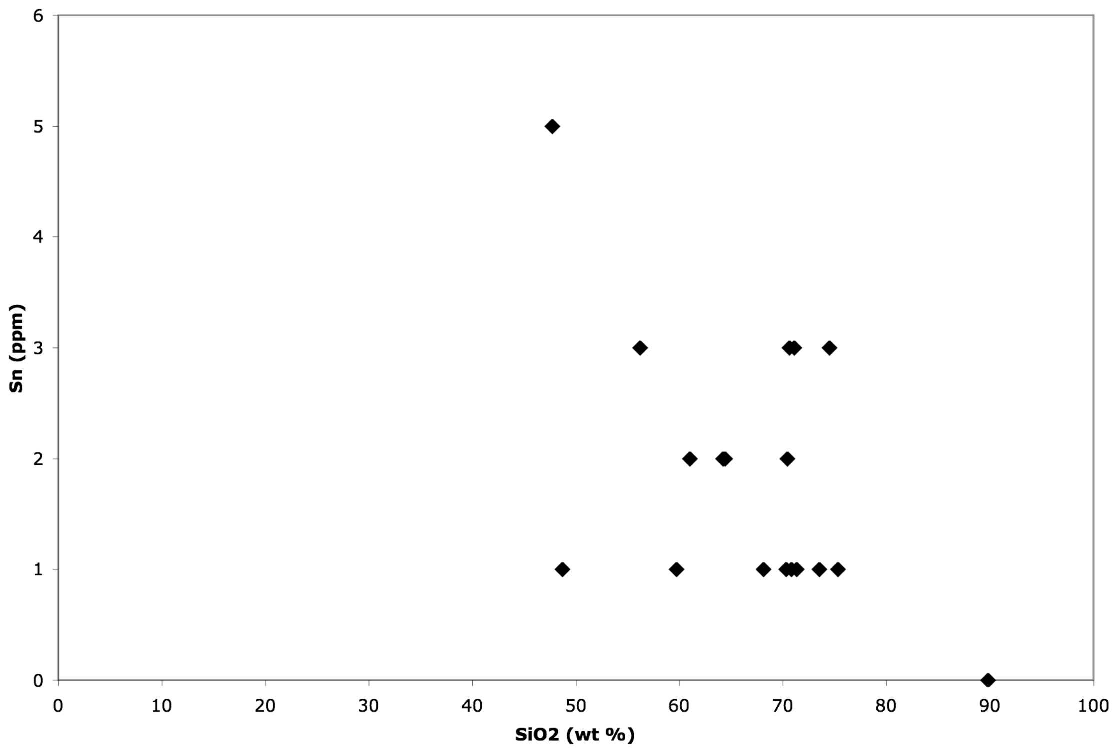

Sn (ppm)
SiO2 (wt %)
0
1
2
3
4
5
6
0
10
20
30
40
50
60
70
80
90
100

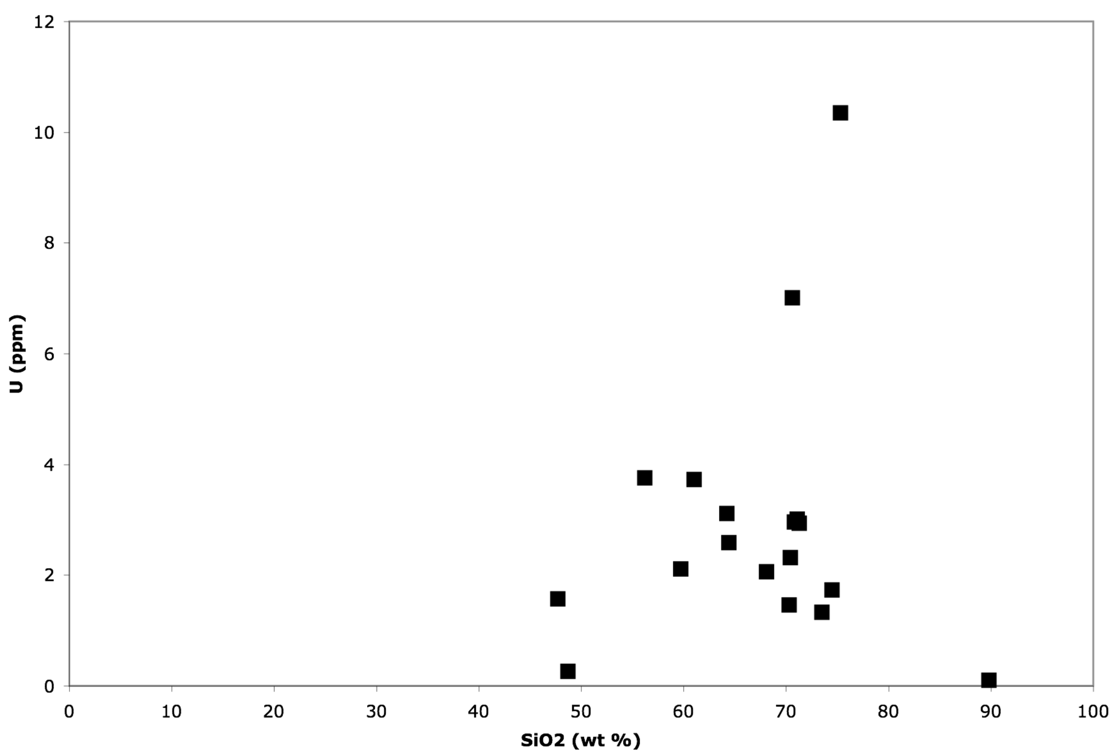

U (ppm)
SiO2 (wt %)
0
2
4
6
8
10
12
0
10
20
30
40
50
60
70
80
90
100

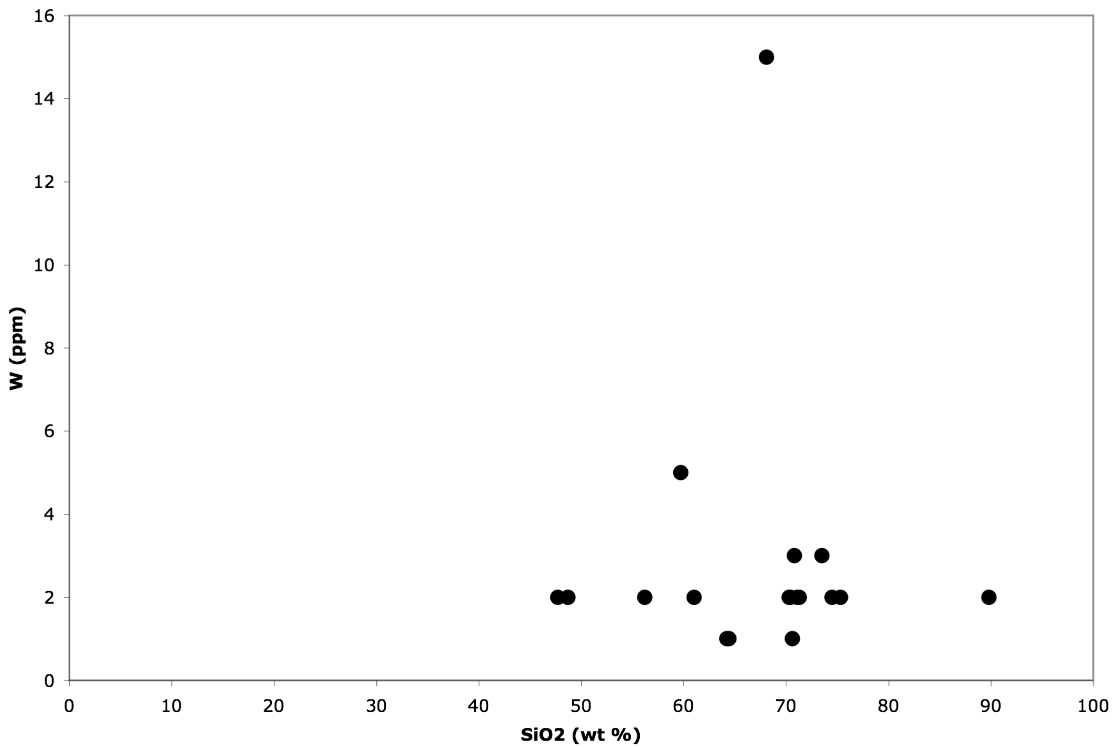
16
14
12
10
8
6
4
2
0
W (ppm)
0
10
20
30
40
50
60
70
80
90
100
SiO2 (wt %)

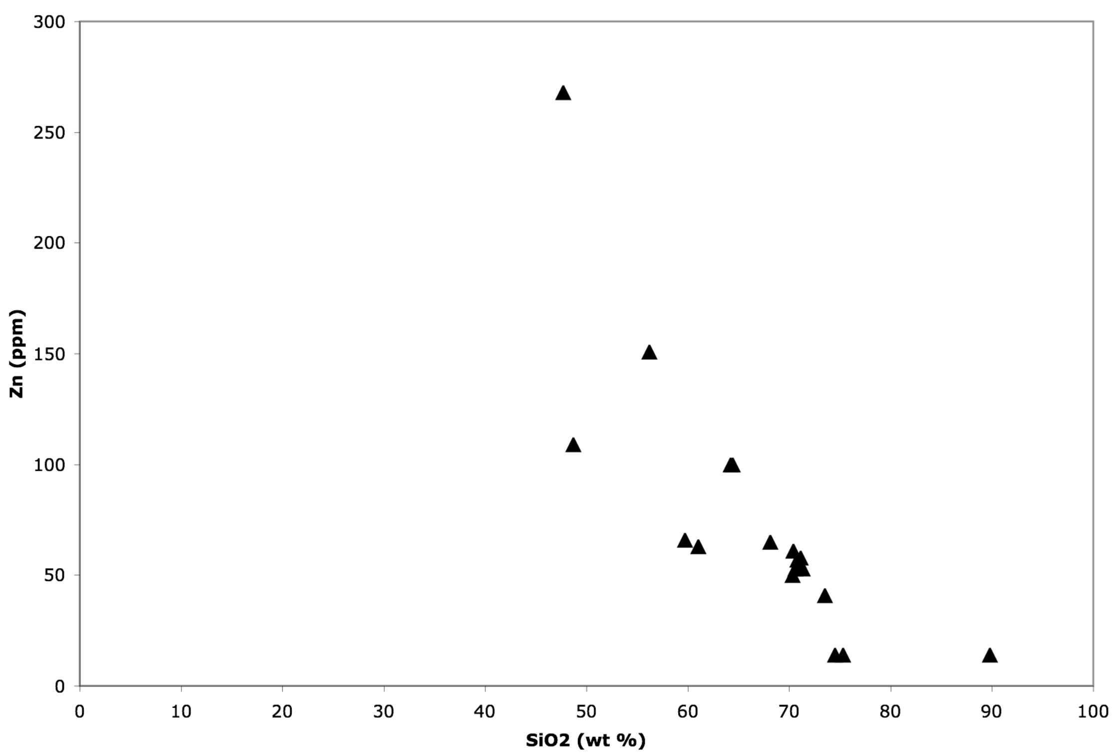
300
250
200
150
100
50
0
Zn (ppm)
0
10
20
30
40
50
60
70
80
90
100
SiO2 (wt %)

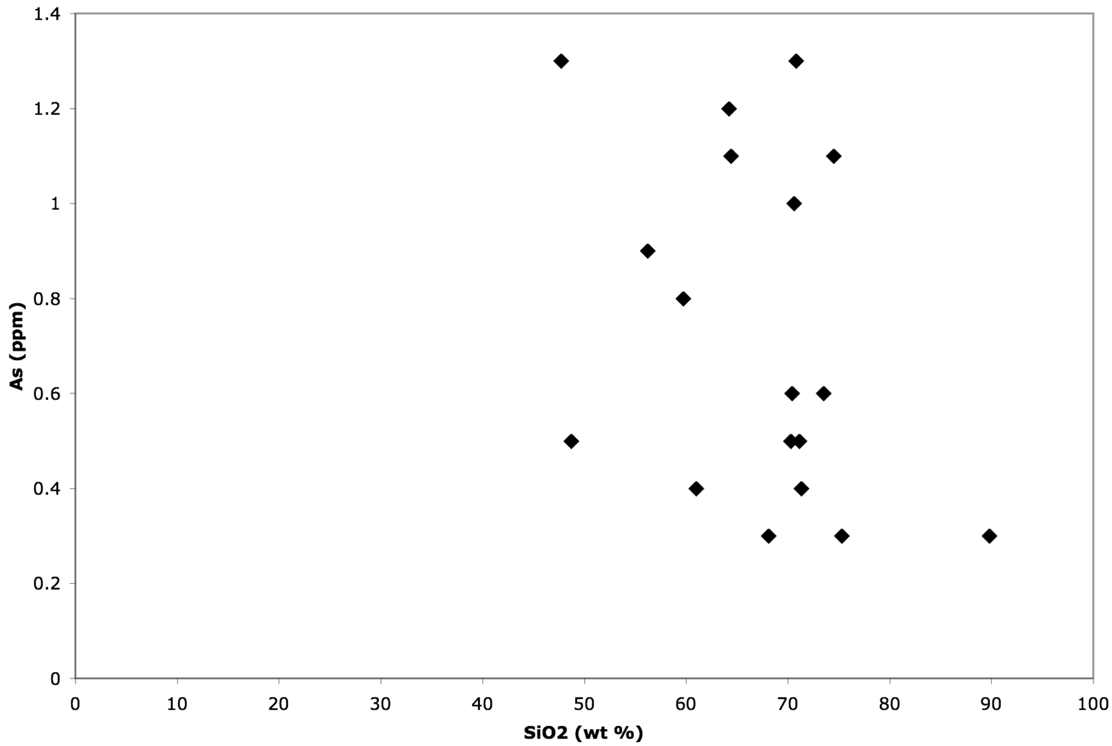
1.4
1.2
1
0.8
0.6
0.4
0.2
0
As (ppm)
0
10
20
30
40
50
60
70
80
90
100
SiO2 (wt %)

APPENDIX 3: THIN SECTION DESCRIPTIONS OF SAMPLES

Sample numbers correspond to locations in Plate A.

WR-1: This sample is a piece of the main Louis Lake phase and contains plagioclase (40%), quartz (35%), K-feldspar (15%), biotite (9%), and magnetite (1%). Plagioclase displays minor sericite alteration, perthite exsolution, and the 400-3200μm grains are mostly anhedral. The quartz is mostly undeformed, anhedral, 240-4000 μm grains with minor undulose extinction. The K-feldspar is present mostly as perthite, and has a similar description to the plagioclase. The olive green biotite is anhedral with some embayed grains, poikiolitic texture, and between 440 and 2900 μm. Magnetite displays significant ilmenite exsolution and the grains are mostly rounded.

WR-3: This sample contains the contact between an aplite and the main granodiorite. The granodiorite is composed of plagioclase (50%), quartz (30%), biotite (10%), K-feldspar (5%), and magnetite (5%). The aplite contains quartz (50%), plagioclase (30%), K-feldspar (18%), biotite (1%) and magnetite (1%). The quartz in the sample is mostly undeformed and anhedral. In the aplite, quartz ranges in size from 200 to 1400μm and is slightly more deformed than that in the granodiorite. In the granodiorite, the quartz is coarser, and ranges between 500 and 2200μm. Plagioclase is subhedral to anhedral and displays minor sericite alteration and perthite exsolution. There is less sericite and perthite in the granodiorite. In the aplite, plagioclase ranges from 318 and 1720μm, and in the granodiorite, it ranges between 420 and 2090μm. K-feldspar is more abundant in the aplite, and has a similar description as the plagioclase. Biotite is coarser and more abundant in the granodiorite. The biotite is mostly anhedral and green-brown with minor alteration. In the aplite, biotite ranges in size from 650 to 1250μm, and in the granodiorite, it is between 300 and 3300μm. Magnetite is coarser in the granite, but is equally as abundant in both rock types. The magnetite shows ilmenite exsolution and the grains are mostly subhedral. Some grains contain small chalcopyrite inclusions about 25μm across. Apatite is present in trace amounts as inclusions in some biotites, and minor hematite is present as an oxidation product on the rims of some magnetite-ilmenites.

WR-4A: Sample is a mafic enclave collected from within the main Louis Lake intrusion. The sample is classified as a gabbro, and the mineral assemblage contains hornblende, biotite, plagioclase, and apatite. Approximate abundances are 50% hornblende, 34% plagioclase, 15% biotite and 1% apatite. Outside the enclave, the mineral assemblage is similar, but with the addition of quartz. The hornblende in the sample is sub- to anhedral and mostly 200-300 μm, but can be as larger as 500 μm. Biotite is interspersed with the hornblende, and shows some slight orientation (smearing?). Biotite is mostly 400-900μm inside the enclave, but around the edge they are up to 1300μm. Biotites and hornblendes are larger and more anhedral away from the enclave. Plagioclase (150-1000μm) is mostl sub-anhedral, show minor sericite alteration, and appear to be interstitial growth between the mafic minerals. Magnetites are mostly subhedral with ilmenite exsolution and appear more concentrated along the periphery of the enclave. Magnetites are also found as inclusions in the hornblende crystals. Significant amounts of apatite are found as inclusions in hornblendes, biotites and feldspars. These apatite inclusions are typically euhedral, acicular crystals and range in size depending on host mineral. Within hornblende, the apatite ranges from 40-60μm and are long, acicular crystals. In biotites, the apatite has more size variability (20-90μm) and the crystals are more "stubby". In plagioclase, they are also more variable, and range from 13-95μm. Apatites become slightly less numerous away from the enclave. K-Feldspar (3400μm) exhibits tartan twinning, and is only found outside the enclave. Quartz, found only outside the enclave, is anhedral with minor grain boundary migration and ranges in size from 1000 to 2000μm.

WR-4B: This sample is the same as sample WR-4A, as it is a sample of the same enclave. Magnetite shows ilmenite exsolution. Some magnetites also contain small intergrowths of chalcopyrite. Chalcopyrite is found within magnetites and as single grains within quartz grains.

WR-5-2: This is a sample of the main Louis Lake phase and contains plagioclase (45%), quartz (35%), biotite (10%), K-feldspar (8%), and magnetite (2%). Plagioclase is moderately sericite alteration, subhedral to anhedral, with perthite exsolution and ranges from 480 to 1980μm. One plagioclase grain contains a biotite inclusion. Quartz grains are anhedral with low to moderate recrystallization and range in size from 350 to 2000μm. Biotite grains are slightly altered, subhedral to anhedral, associated with magnetite, and range in size from 180 to 900μm. K-feldspar is mostly perthite, but there is some true tartan twinning. The K-feldspar is similar in size and shape to the plagioclase. The subhedral magnetites show ilmenite exsolution and range in size from 64 to 270μm.

WR-7C: This sample is typical of the main Louis Lake phase, containing quartz (35%), plagioclase (25%), K-feldspar (24%), biotite (10%), magnetite (5%), and trace apatite and titanite. The quartz is anhedral with undulose extinction and grains between 200 and 5000μm. The mildly sericitic plagioclase is anhedral with perthite exsolution and few biotite inclusions and ranges in size between 860 and 4750μm. K-feldspar is similar in size and description to the plagioclase, and is mostly present as perthite exsolution of plagioclase. Biotite grains are anhedral, somewhat poikiolitic with inclusions of titanite and apatite, slightly altered, and between 440 and 2100μm. Magnetite is subhedral to anhedral, displays ilmenite exsolution, and is associated with biotite. Anhedral titanite grains are found both within biotite grains and as growths around magnetite, and range in size from 600 and 800μm. A single grain of native gold was also found within a quartz crystal measuring about 14μm.

WR-16B: This sample is a typical Louis Lake sample composed of biotite, titanite, magnetite, apatite, quartz, K-feldspar, hornblende, plagioclase, and fluorite. The quartz is moderately recrystallized in this sample with undulose extinction and some grain boundary migration. The quartz has become anhedral due to this recrystallization, and grain size ranges from 180-3500μm. K-feldspar is mostly anhedral with tartan twinning, minor myrmeketic textures, ranges from 1300-8000μm in size, and displays minor sericite alteration. The coarsest K-feldspar grains contain inclusions of quartz and plagioclase. Plagioclase grains are smaller than those of K-feldspar (300-4000μm), and occur as inclusions in the K-feldspar. The plagioclase is subhedral, displays some internal zoning, and has been slightly sericite altered. Biotite in the sample is anhedral, green to olive green, and poikiolitic with inclusions of quartz and apatite. The biotites range in size from 430-4000μm and are associated with hornblende, titanite, and magnetite. Magnetite is subhedral to anhedral, sometimes in aggregates and ranges in size from 50-800μm. Titanites are subhedral to anhedral, 2000-3000μm in size, and are associated with biotite and magnetite. Hornblende is present as 60-500μm anhedral grains and associated with biotite, titanite, and magnetite. Apatite is present as 30μm, euhedral to subhedral inclusions in and near biotite grains. Fluorite is present as purple, isotropic crystals.

WR-18A: This sample is a sample of a granodioritic dike that contains plagioclase (45%), quartz (25%), biotite (15%), titanite (10%), magnetite (3%), apatite (1%), and trace chalcopyrite. Plagioclase is subhedral to anhedral with minor sericite, internal zoning, and perthite. These 210 to 1500μm grains also contain a few opaque inclusions. The anhedral quartz grains display minor undulose extinction and some small (about 180μm) inclusions of biotite and plagioclase. Quartz grains are between 140 and 1300μm in size. Biotites are mostly anhedral, brown and green in color, between 130 and 1460μm, and contain inclusions of titanite, apatite, magnetite and quartz. Titanite is mostly euhedral, slightly altered, and is between 400 and 4000mm. Titanite is found as inclusions in biotite, and can contain round inclusions of plagioclase and magnetite. Magnetite is subhedral with ilmenite exsolution and between 40 and 430μm. Acicular apatite inclusions are found in quartz and biotite and are between 20 and 40μm in length. Small (<10μm), rounded grains of chalcopyrite are found within quartz grains.

WR-18C: This is a sample of granitic dike with quartz (35%), K-feldspar (30%), plagioclase (20%), biotite (9%), magnetite (2%), titanite (1%), and trace allanite and chalcopyrite. Quartz is anhedral with minor undulose extinction and grains between 100 and 2600μm. Plagioclase is subhedral to anhedral with minor sericite alteration, perthite exsolution, zoning of cores and minor myrmeketic intergrowths. Plagioclase grains are between 390 and 3600μm in size. K-feldspar is similar to plagioclase in description, but has a higher percentage of larger crystals. Biotites are anhedral, somewhat altered, brown to green, contain apatite inclusions, and are 260 and 3200μm. Magnetite grains are subhedral to anhedral with ilmenite exsolution and are between 30 and 460μm. Titanite is slightly altered, subhedral to anhedral, between 300 and 1000μm, and associated with magnetite and allanite. Allanite is mostly metamict, associated with titanite and magnetite, subhedral to anhedral and between 450 and 1200μm. Apatites are subhedral to euhedral, with some zoning due to proximity to allanite, and between 70 and 200μm. Isolated grains of chalcopyrite around 22μm are found within quartz crystals.

WR-20A: The sample is a tonalite dike than the main Louis Lake phase and contains plagioclase (40%), quartz (20%), biotite (30%), hornblende (10%) and apatite (<1%). Plagioclase is sub- to anhedral, twinned and displays minor sericite alteration. Plagioclase also has some small apatite inclusions and ranges in size from 100-1300 μm. Biotites are mostly subhedral with apatite inclusions, and range in size from 200-1100μm. Quartz grains are sub- to anhedral with minor undulose extinction and grain boundary migration and ranging from 100-300μm. They contain some apatite inclusions, and are found as small inclusions in the mafic minerals. Hornblendes are sub-to anhedral, 300-600μm, and have inclusions of apatite, biotite, and quartz. Apatites are mostly subhedral inclusions from 40-50μm and have a typical apatite shape.

WR-20C: This sample is a sample of granodiorite that contains quartz (40%), K-feldspar (38%), plagioclase (10%), biotite (8%), magnetite (2%), apatite (1%), and trace allanite and titanite. The quartz is anhedral with undulose extinction, myrmeketic intergrowth with feldspar, and some grains as inclusions in feldspars. The quartz grains range in size from 280 to 3000μm. K-feldspar is poikiolitic with quartz, plagioclase, and biotite inclusions. The K-feldspar is anhedral, displays sericite alteration, and ranges in size from 400-4550μm. Plagioclase is anhedral and poikiolitic with inclusions of quartz and biotite. The anhedral plagioclase shows perthitic and myrmeketic textures and is between 175 and 3850μm. Biotite is green to brown, subhedral to anhedral, has apatite inclusions, ranges from 250 to 1800μm in length, and has some association with apatite and magnetite. Magnetite is subhedral to anhedral with ilmenite exsolution, and grain sizes between 130 and 700μm. Apatite is found as both small inclusions and larger crystals near biotites. The apatites are subhedral to euhedral and are 100 to 160μm in length. Allanite is found as subhedral to anhedral, 700μm crystals. Some of the allanite is found as metamict crystals, while the rest is as green, wavy crystals. A few grains of titanite are found as anhedral, 600 to 700 μm grains that are associated with biotite and magnetite.

WR-23A: This sample is a leucogranite with K-feldspar (40%), quartz (30%), biotite (20%), plagioclase (5%), magnetite (4%), apatite (1%), and trace allanite. K-feldspar is present as perthite with myrmeketic intergrowths with quartz, some sericite alteration and grains are between 230 and 5200μm. Quartz is anhedral with moderate undulose extinction, but relatively undeformed cores. Quartz grains are between 250 and 3900μm. Biotite grains are subhedral to anhedral, mostly brown, slightly altered and contain apatite inclusions. Biotites range in size from 150 to 2040μm in length. Plagioclase is present in minor amounts and has significant perthite and sericite. Plagioclase is also found in the cores of K-feldspar and grain size is between 370 and 600μm. Magnetite is subhedral to anhedral with ilmenite exsolution and grains between 50 to 375μm. Apatite, present as inclusions in biotite and other larger crystals, are subhedral to suhedral and are between 30 and 55μm in length. Allanite is present as metamict, anhedral grains about 400μm.

WR-24B: This sample is a mafic dike that cuts across the Louis Lake Batholith, and it much younger. The dike is composed of hornblende (50%), plagioclase (24%), biotite (24%), apatite (1%), ilmenite (1%), and trace titanite and chalcopyrite. Hornblende is green, subhedral to anhedral, and fine-grained (50 to 570μm). Plagioclase is heavily sericitized, has no perthitic exsolution, and is fine-grained (90 to 410μm). Biotite is mostly green, subhedral to anhedral, and 90-175μm. Apatite is found as subhedral inclusions in biotite and hornblende, and size ranges from 20 to 25μm. Ilmenite is present as subhedral to anhedral grains between 3 and 55μm. Trace amounts of titanite are found around hornblende. Chalcopyrite is found as tiny specks (3-12μm) in hornblende.

WR-24C: This is a sample of the deformed margin of the batholith and is granitic gneiss. It contains quartz (40%), biotite (25%), plagioclase (20%), K-feldspar (13%), epidote (1%), and trace titanite and muscovite. Quartz is heavily recrystallized with grain size reduction, undulose extinction. Bands of quartz have aligned with foliation and quartz grains are larger in the band than in the rest of the sample. Quartz grains are between 80 and 1650μm. Biotite grains are aligned to create dark bands of foliation. They are green-brown, subhedral grains between 76 and 465μm with apatite inclusions. The biotites are reacting to create muscovite along grain boundaries. Plagioclase grains are larger than the quartz grains and larger grains show pressure shadows. The grains are sericitically altered and are between 800 and 5275μm. K-feldspar grains are present as large rolled phenocrysts about 5000μm. These large phenocrysts have recrystallized plagioclase inclusions. Epidote crystals are found near biotite, are subhedral to euhedral, and are about 60μm in length. Trace titanites are found in the mafic bands and are about 200μm. Muscovite is present as the alteration product of biotite and is composed of small grains.

WR-25: This sample is a granodiorite with quartz (35%), K-feldspar (35%), biotite (15%), plagioclase (10%), magnetite (2%), titanite (2%), apatite (1%) and allanite (1%). Quartz grains are anhedral with some undulose extinction, and between 200 and 2600μm. K-feldspar is subhedral to anhedral with tartan twinning and cores of plagioclase. K-feldspar grains are between 620 and 3200μm. Biotite grains are subhedral to anhedral, green to brown color, cores of hornblende, apatite inclusions, and grain sizes between 180 and 3040μm. Plagioclase exhibits moderate sericite alteration, perthite exsolution, anhedral crystal shape and sizes between 530 and 1940μm. Magnetite is subhedral to anhedral with ilmenite exsolution and grains between 75 and 675μm. Subhedral to anhedral titanite grains (440-2650μm) contain inclusions of plagioclase and apatite. Apatite is present as inclusions, and associated with biotite. Apatites are acicular as inclusions, and subhedral as individual crystals. They range in size from 68 to 320μm. Allanite is present as 630 to 960μm, mostly metamict crystals associated with biotite and titanite.

WR-25B: This sample is an aplite, which contains plagioclase (55%), quartz (35%), K-feldspar (9%), and trace amounts of biotite, magnetite, and allanite. Plagioclase has minor sericite alteration, some perthite exsolution, subhedral to anhedral shapes, minor myrmeketic intergrowths with quartz, and is present in the cores of K-feldspar. Plagioclase grain sizes are between 400 and 2370μm. Quartz is anhedral with minor undulose extinction, and grain sizes between 190 and 4000µm. K-feldspar is similar to plagioclase with grain sizes between 620 and 2400µm. Minor amounts of biotite are present as green, anhedral, 190 to 420µm grains that are associated with magnetite. Magnetite is subhedral to anhedral with ilmenite exsolution and grain sizes between 50 and 280µm. Metamict allanite is anhedral and between 97 ad 440µm.

WR-28: This sample is a fine-grained aplitic segregation containing quartz (45%), plagioclase (25%), K-feldspar (20%), biotite (10%), magnetite (3%), apatite (1%), and trace titanite. The subhedral quartz grains are small (140-500µm), appear undeformed, and some are present as inclusions in plagioclase grains. Plagioclase is present as sericitized, subhedral grains with perthite exsolution and a bimodal distribution (about 2000µm and about 400µm). K-feldspar is similar to plagioclase, and may be the result of perthitic exsolution of plagioclase grains. Biotite grains are subhedral to anhedral, brown to green in color, range in size from 170-800µm, and contain inclusions of acicular apatite. Magnetites are associated with biotite, are subhedral to anhedral, and are between 130- 470µm. Apatite inclusions are acicular, present mainly in biotite, and are between 20 and 50µm in length. Titanite is present as trace inclusions associated with magnetite.

WR-29: This sample is a moderately sericitized aplite with chlorite (36%), plagioclase (60%), titanite (2%), magnetite (1%), and trace amounts of biotite. The quartz displays some undulose extinction in anhedral grains that range from 100-2500 µm. The centers of the grains remain mostly undeformed. Plagioclase grains range from 800-3000µm, are anhedral, and the larger grains have less sericitized cores. Titanite occurs as anhedral, brown grains, ranges in size from 200-1800µm, and is associated with magnetite and chlorite. Magnetite in this sample exhibits magnetite-ilmenite exsolution, typically in aggregates associated with titanite rims, and range in size from 300-700µm. Chlorite in this sample is present as yellow-green to green grains with small biotite grains in some cores. The chlorite is anhedral and ranges in size from 200-1500µm.

WR-30: This sample is an aplite composed of quartz (60%), plagioclase (30%), K-feldspar (6%), biotite (2%), and magnetite (1%). The quartz is subhedral to anhedral with some undulose extinction, but larger crystals have undeformed cores. Quartz grains range from 100-900µm with some myrmeketic intergrowth with feldspar. Plagioclase grains are subhedral to anhedral and range in size from 200-1500µm in size, with minor sericite alteration and perthite exsolution. K-feldspar is present mostly as perthite, but some crystals exhibit true tartan twinning, and are similar in size to the plagioclase crystals. Biotite grains are green to brown in color, subhedral to anhedral, approximately 500µm in length, moderately altered, associated with magnetite, and contains inclusions of apatite. Magnetite is subhedral, 65-600µm and somewhat associated with biotite.

WR-40B: This is a sample of altered granite with epidote, titanite, muscovite, quartz, and plagioclase. Epidote is found as anhedral grains between 200 and 1365µm. Titanite is found as euhedral crystals that are virtually unaltered and between 340 and 1300µm. Muscovite is found as radiating masses that are about 500µm wide. Quartz is found as small (100μm) grains between epidote. Only trace amounts of plagioclase are found as anhedral, unaltered crystals between 400 and 650μm.

WR-41: This sample is part of the main phase of the batholith. It is composed of K-feldspar (55%), quartz (35%), biotite (9%), magnetite (1%) and trace amounts of apatite and allanite. K-feldspar exhibits myrmeketic textures, is sub to anhedral, and shows minor sericite alteration. The feldspars (800-2000μm) may be the result of perthite exsolution of plagioclase. Quartz is mostly anhedral, 100-2000μm in size, and shows minor amounts of myrmeketic intergrowths with feldspar, but is otherwise relatively undeformed. Biotite grains are much smaller than the feldspar and quartz (100-600μm), subhedral, and sometimes associated with magnetite. Magnetite grains are subhedral to anhedral, approximately 1000μm, and exhibit magnetite-ilmenite exsolution. Allanite crystals are sub to subhedral, approximately 650 μm, and predominately metamict. Few small apatite grains are present within biotite crystals.

WR-42A: This sample is from a hematite + quartz vein. The vein is composed of approximately 60% quartz and 40% hematite. Hematite within the vein is bladed and ranges from 100-200μm in length. The hematite grows into quartz that makes up the inner part of the vein. It appears that a layer of quartz was laid down first, then by deposition of hematite + quartz. This is witnessed by the fact that the hematite seems to have grown from the outside quartz into open space, created crystals that are flat on one side, and are bladed on the other. Subhedral quartz grains are small in the middle of the vein (100-500μm), and larger in the outer portion (about 3000μm).

WR-42B: This sample is a quartz-hematite shear with 70% quartz, 20% hematite and 10% chlorite. The quartz grains range in size from 600-1400μm and are subhedral to anhedral. The hematite is bladed and ranges from 40-2000μm with some bent blades and fine-grained hematite away from the vein itself. Chlorite is green-brown and ranges in size from 370-1800μm.

APPENDIX 4: TABLE OF FLUID INCLUSION MICROTHERMOMETRIC DATA

The following table represents the results of micro thermometric data that was collected from the LLB samples. Both FLUIDS (Baker 2003) and CLATHRATES (Bakker 1997) were used to calculate the wt % NaCl. The XCH_4 was estimated using the melting and homogenization temperatures of CO_2. Multiple values in the Tmsalt column represent melting temperatures for multiple salts in a single inclusion.

TABLE A-5: Microthermometric data from fluid inclusions

Inclusion	Type	vol % vapor	mole % CO2	wt % NaCl	XCH4 in CO2	Tm CO2	Teutectic	Tice melt	Tmsalt	Tm clathrate
WR-6										
1	III	30	0.105	16.414	0.01	-57	-32.7	-12.3	5	0
2	III	25	0.089	16.602	0	-56.9	-32.7	-12.5	-9	-2
3	III	25	0.129	17.067	0	-56.5	-32.5	-13	-10	
4	IV	65	0.399	22.284	0	-56.5	-33	-		-3.5
5	IV	55	0.316	22.99	0	-56.5	-	-		4
6	IV	75	0.421	10.627	0	-56.5	-	-	-3	4
7	IV	60	0.282	17.106	0	-56.5	-34.1	-11.3	-	0
8	IV	75			0	-56.5	-	-	-	
9	II	25	ng		0	-56.5	-34	-4.8	-	10
10	II	25	0.102	7.689	0	-56.6	-34	-4.8	-	
11	II	25	0.102	7.689	0	-56.6	-34	-4.8	-	
12	II	25	ng		0	-56.5	-34	-3.8	-	10.4
13	II	25	ng		0	-56.5	-34	-3.8	-	10.2
14	IV									
15	II									
WR-8A										
1a	I	5		25.917			-56.3	-33.2		
2a	I	5		26.768				-36		
3a	I	5		23.993				-27.7		
4a	I	5		23.915				-27.5		
5a	I	5		26.043			-60	-33.6		
6a	I	5		27.893			-59	-40		
7a	I	5		24.88			-61	-30.1		
8a	I	5		28.164			-67	-41		
9a	I	5		24.845			-71	-30		
10a	I	5		25.529				-32		
11a	I	5		26.768			-53	-36		
12a	I	5		23.719				-27		
1	I	2	0	25.676	-	-	-32.3	-24	-8.5, 3.5	-
2	I	35	0	25.043	-	-	-31.3	-23	-13, -8.5	-

3	I	2	0	31.304	-	-	-58	-34.8		-
4	I	5	0	28.849	-	-	-50	-29.6	16	-
5	I	5	0	31.304	-	-	-50	-34.8	-32.6, 30	-
6	I	5	0	14.183	-	-	-56	-10	-4	-
7	I	5	0	20.73	-	-	-56	-17		-
8	I	5		22.981	-	-	-57	-25.2		-
9	I	5	0	17.707	-	-	-37.2	-13.5		-
10	I	2	0	6.831	-	-	-31.4	-4.2		-
WR-12										
1	II	30	0.127	4.708	0.03	-56.9	-33	-12.3	19	9
2	IV	70	0.226	16.318	0.02	-56.9		-12.2		9
3	II	30	0.072	4.071	0.02	-56.9	-33.7	-12.4	19.2 and -23	9
4	III	15	0.0482	16.413	0.01	-57	33.1	-12.3	20.8 and -23	9
5	III	40	0.065	16.413	0.02	-57	-34.7	-12.3	5; 13 and 23.1	9
6	II	50	0.164	12.508	0.01	-56.9	-34.3	-12.4		4.5
7	IV	40	0.154	6.965	0.01	-56.9		-12.1		7.4
8	III	50	0.117	16.931	0	-56.9	-33.1	-12.3	15.5	2
9	III	25	0.06	16.318	0	-56.8	-33.2	-12.2	6 and 13 and 17	2
10	IV	75	0.202	21.918	0.01	-56.9	-36.4	-12.3		-1
11	I	15	0	24.317	-	-	-33.8	-25		-
12	I	20	0	26.347	-	-	-37.1	-25.1		-
13	I	20	0	26.347	-	-	-37	-25.1		-
14	II	15		27.535	0.1	-59.4	-36	-13.2		-2.4
15	II	15		27.537	0.1	-59.8	-33	-12.9		-2.4
WR-20B										
1	I	15	0	26.878			-83.4	-26		
2	I	15	0	14.183			-83.1	-10	-26.8	
3	I	15	0	6.536			-83.8	-4	-30	
4	IV	50	0.107	29.039	0.5	-65.5	-30			-2
5	IV	50	0.111	29.039	0.5	-65.2	-29			-2
6	IV	30	0.077	26.835	0.35	-64	-30.6			-4.1

7	IV	30	0.073	14.735	0.4	-64.6	-30.4			-0.4
8	IV	55	0.128	29.039	0.5	-65.4	-29			-0.6
9	IV	40	0.085	29.039	0.5	-65	-29.8			-2.8
10	I	20	0.074	26.077	0.06	-57.9	-33	-13.1		-2
11	I	25	0.01	23.908	0.03	-57	-33	-13		-2
12	I	20	0.078	28.774	0.04	-57.6	-35.6	-14.3		-4
13	I	25	0.073	24.786	0.1	-57	-33.6	-14.6		-5.3
WR-20E										
1a	I	15	0	19.911				-16		
2a	I	15	0	5.017				-3		
3a	I	15		0				0		
4a	I	15		0				0		
5a	I	15		27.8934			-85	-40		
6a	I	15	0	19.911				-16		
7a	I	15	0	11.89				-8		
8a	I	15		27.368			-88	-38.1		
9a	I	15		24.557				-29.2		
10a	I	15		27.619				-39		
11a	I	15		27.729				-39.4		
12a	I	15		27.893				-40		
1	I	20	0	30.921			-80.1	9	-46.5	
2	I	15	0	30.058			-82.6	11.5	-47.3	
3	I	25	0	45.331			-80	10	-46, 19	
4	I	25	0	30.921			-79.3	8	-56, -30.6, 19	
5	I	30	0	28.925			-79	8	19	
6	I	15	0	30.921			-83		-54, 16.5	
7	I	25	0	1.591			-81.4		-50.2,-40	
8	I	25					-82.3		-41, -20	
9	I	15					-81.2		-31	
10	I	15					-79.6		-37.2	
11	I	20					-80.6		-54	
12	I	20					-80		-50	

WR-25A										
1a	II	20				-62		-27		
2a	II	25	0.095	15.72	0.01	-57.7		-11		8
3a	I	40				-58		-27		
4a	IV	60	0.321	3	0.1	-57.9				9
5a	IV	70	0.445	3.2	0.1	-57.8				8.6
6a	I	15	0	42.403	0			15	-54	
7a	IV	75	0.47	6	0.1	-58		-20		6.9
8a	IV	75	0.49	6	0.1	-58		-20		6.9
9a	IV	75	0.415	9.5	0.1	-58		-20		5
10a	IV	75	0.481	10.684	0.1	-58		-20		5
11a	IV	75	0.481	10.684	0.1	-58		-20		5
12a	IV	70	ng	0	0	-56.5				10
13a	IV	65	0.399	12.5	0	-56.5		-5		3
1	IV					-61				8.4
2	IV		0.054	14.273	0.25	-62.1				4.2
3	IV		0.724		0.2	-61.5				16
4	IV	75			0.25	-62.4		-17		21.5
5	IV	75	0.679	10	0.25	-62.6				4.8
6	IV	75	0.335	17.702	0.27	-62.5		-33		1
7	IV	75			0.2	-62.1				25.3
8	IV	75	0.443	16.82	0.25	-62				9.4
9	IV	80			0.25	-61.9				28.8
10	I	20	0	40.612	0		-80.4	8.6	-36.3	
11	I	20	0	40.612	0		-78.6	3.7	-36.4	
12	I	20		**27.472**	0		-79.4	8	-35.8	
13	I	20	0	33.481	0		-79.1	8	-35.1	
14	I	25	0	47.444	0		-84	6.3		
15	I	25		59.768	0.15	-61.8	-28.4			24.3
16	II	20	0.303	3.4	0.2	-61.9				8.4
17	II	20	0.068	12.576	0.2	-62.1				4.2
18	II	20			0.18	-61.5				16

Inclusion	Th CO2	L + V	Tmsolid	Th total	L + V
WR-6					
1	0.3	L			L
2	15.6	L			L
3	-4	L	247	250	V
4	10.3	L		224.6	V
5	4.7	L			V
6	9.8	L			L
7	7.2	L			L
8	5.6	L			L
9	21.7	L	247	253.7	L
10	28.1	L		191	L
11	28.2	L	247	250	L
12	27.4	L	-	254.2	L
13	25.1	L	-	157	L
14				370	V
15				above 389	V
WR-8A					
1a				157.3	L
2a				130.5	L
3a				148.9	L
4a				130	L
5a				133.2	L
6a				127	L
7a				126.1	L
8a				159.3	L
9a				160	L
10a				140	L
11a				140	L
12a				157.7	L
1	-	L	above 500	420	L
2	-	L	above 300	above 300	L
3	-	L	164	176	L
4	-	L	164, 230, 320, above 500	106.4	L
5	-	L	250, 266.5, 288, above 500	159.5	L
6	-	L	-	120	L
7	-	L	-	120.5	L
8	-	L	-	124	L
9	-	L	-	231.3	L
10	-	L	-	206.7	L
WR-12					
1	30	L	above 250	above 250	L
2	11.1	L	above 250	above 250	L
3	21.7	L	above 250	above 250	L
4	31.2	L	208 and above 250	above 250	L
5	24.7	L	197 and above 250	above 250	L
6	16.8	L	above 230	above 230	L
7	26	L		above 250	V
8	15.6	L	above 230	188 and above 230	V

9	30.6	L	above 250	above 250	L
10	16.3	L	above 230	above 230	V
11	-			160	L
12	-			150	L
13	-		above 200	158	L
14	30.5	L	173, above 332	332	L
15	30.9	L	150, above 332	332	L
WR-20B					
1		L		173	L
2		L	160	165.7	L
3		L	above 300	173.2	L
4	-1.6	L		above 200	
5	6.7	L		above 250	
6	13.7	L		above 200	
7	10.9	L		above 250	
8	4.1	L		above 300	
9	12.6	L		above 250	
10	28.7	L	above 290	above 290	
11	28.7	L	above 280	above 280	
12	27.4	L	240	above 300	
13	30.7	L	above 280	above 280	
WR-20E					
1a				132.3	L
2a				132.8	L
3a				102	
4a				135.7	L
5a			173.5	113.5	L
6a				128.9	L
7a				113	L
8a			153.4	113.4	L
9a				113	L
10a				130	L
11a				106.4	L
12a				127.1	L
1			180, >472	164	L
2			101.4,160, >380	129.9	L
3			130, >380	169	L
4			130, 180	171	L
5			126.5, 130	161.6	L
6			180	124.7	L
7				171	L
8				171	L
9				143.1	L
10				159.1	L
11				289	L
12				304	L
WR-25A					

1a			310, above 350	above 350	L
2a	30	L		280	V
3a				180	L
4a	24.6	L		260	L
5a	18	L		290	L
6a			>350	200	L
7a	25.5	L		280	V
8a	22.5	L		285	V
9a	26.4	L		290	V
10a	26.4	L		290	V
11a	26.4	L		290	V
12a	11.5	L			
13a	4.9	L			
1					
2	27.1	L			
3	28.5	L			
4	30.5	L		303.2	L
5	28.4	L		300	L
6	24.4	L		300	L
7	25.3	L			L
8	10.5	L		above 330	L
9	30	L		276.9	L
10			60, above 330	162.5	L
11			above 330	above 330	L
12					L
13			230	above 330	L
14			400, above 450	above 450	L
15	27.1	L	above 500	230.2	L
16				441.6	L
17	27	L		above 500	L
18	28.5	L		275	L

REFERENCES

Bayley, R.W., 1965a, Geologic map of the South Pass City quadrangle, Fremont County, Wyoming: U. S. Geological Survey Geologic Quadrangle Map GQ-458, scale 1:24,000.

Bayley, R.W., 1965b, Geologic map of the Louis Lake quadrangle, Fremont County, Wyoming: U. S. Geological Survey Geologic Quadrangle Map GQ-461, scale 1:24,000.

Bayley, R.W., Proctor, P.D., and Condie, K.C., 1973, Geology of the South Pass area, Fremont County, Wyoming: U. S. Geological Survey Professional Paper 793, 39 p.

Donohue, C., 2002, Late Archean metamorphic history of the Wind River Range Wyoming [Ph.D. dissert.]: Ann Arbor, Michigan, University of Michigan, 228 p.

Hausel, W.D., 1991, Economic geology of the South Pass granite-greenstone belt, southern Wind River Range, western Wyoming: The Geological Survey of Wyoming Report of Investigations No. 44, 129 p.

Hull, J.M., 1988, Structural and tectonic evolution of Archean supracrustals, southern Wind River Mountains, Wyoming [Ph.D. dissert.]: Rochester, New York, University of Rochester, 280 p.

Frost, C.D., Frost, B.R., Chamberlain, K.R., and Hulsebosch, T.P., 1998, The Late Archean history of the Wyoming province as recorded by granitic magmatism in the Wind River Range, Wyoming: Precambrian Research, v. 89, p. 145-173.

Frost, C.D., Chamberlain, K.R., and Frost, B.R., 2001, An example of Precambrian crustal growth by lateral accretion; the South Pass supracrustal belt, Wyoming: Geological Society of America Abstracts with Programs, v. 33, no. 6, p. 401-402.

Frost, C.D., Fruchy, B.L., Chamberlain, K.R., and Frost, B.R., in press, Archean crustal growth by lateral accretion of juvenile supracrustal belts in the southern Wyoming province: Canadian Journal of Earth Sciences.

Naylor, R.S., Steiger, R.H., and Wasserburg, G.J., 1970, U-Th-Pb and Rb-Sr systematics in 2700 x 106-year old plutons from the southern Wind River Range, Wyoming: Geochimica et Cosmochimica Acta, v. 34, p. 1133-1159.

Schmitz, P. J. (2005). Emplacement of the late Archean Louis Lake Batholith and accretion of the Miners Delight Formation allochthon, southern Wind River Range, Wyoming. United States, University of Wyoming.

Stuckless, J.S., Hedge, C.E., Worl, R.G., Simmons, K.R., Nkomo, I.T., and Wenner, D.B., 1985, Isotopic studies of the late Archean plutonic rocks of the Wind River Range, Wyoming: Geological Society of America Bulletin, v. 96, p. 850-860.

Talpey, J.G., 1984, Geochemical and structural evolution of Archean gneisses at South Pass, Wyoming [M.S. thesis]: Rochester, New York, University of Rochester, 102 p.

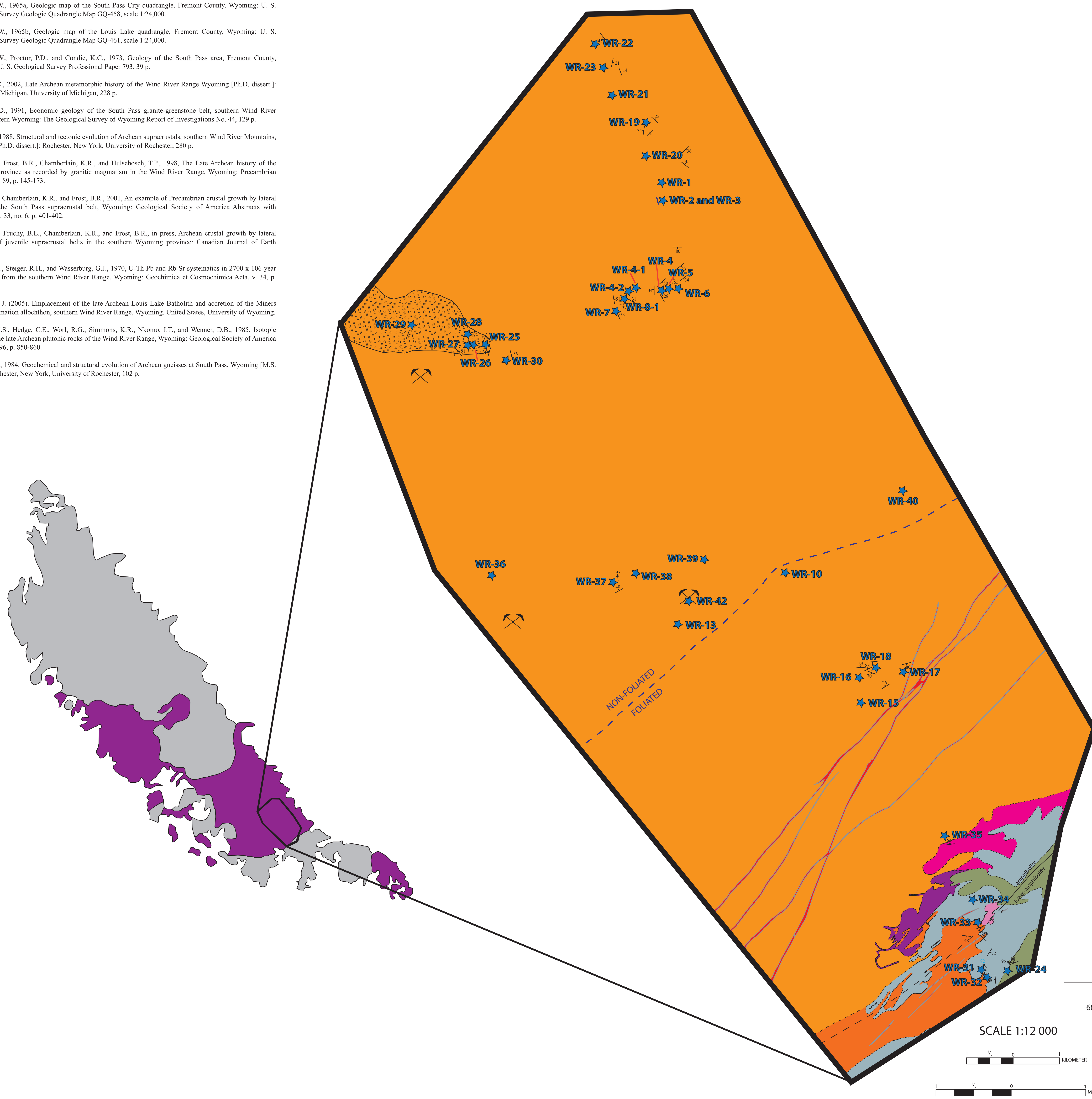

Tectonostratigraphic Map Explanation

Proterozoic Mafic Dikes
Yd *Diabase dikes that have an Ar/ Ar cooling age to 1566±4 to 1465±3 Ma (Donohue, 2002).*

Leucogranite
Wllg *Pematitic and aplitic late differentiate of Wlg identified by Schmidtz (2005). Believed in this study to be similiar to the area around Cony Mountain that consists of a concentration of aplite and pegmatite dikes. The primary phases are alkali feldspar + plagioclase + quartz + biotite with secondary white mica + epidote. A definite lineation is present near the deformed contact, and this fabric decrease further from the contact.*

Louis Lake Granodiorite
Wlg *Foliated to non-foliated, medium- to coarse-grained, I-type granodiorite. Foliation is subvertical near the southern margin of the batholith but the foliation becomes less apparent in the northern part of the map area. Contact with wall rocks is sharp, and small,rounded mafic enclaves are common. This unit is often cross-cut by aplite and pegmatite dikes. Primary igneous minerals are plagioclase + quartz + alkali feldspar + biotite + hornblende + titanite + magnetite + allanite + zircon + apatite. A U-Pb zircon age of ~2.63 Ga has been reported by Naylor et al. (1970), Stuckless et al. (1985), Frost et al. (1998), and Frost et al. (2000). This unit locally contains xenoliths of banded iron formation (Bayley, 1965b), Miners Delight Formation (Hull, 1988), and biotite granite (Schmidtz 2005).*

Quartz Diorite
Wlqd *Medim to coarse-grained quartz diorite. The primary assemblage was noted by Schmidtz (2005) to be hornblende + plagioclase + Fe-Ti oxides ± quartz ± clinopyroxene ± orthopyroxen with secondary tremolite + cummingtonite + white mica + epidote + chlorite + titanite. Believed by Schmidtz (2005) to be an underformed mafic phase of Wlg.*

Deformed Louis Lake Granodiorite
Wldg *Medium- to fine-grained, deformed granodiorite. It contains strong, steeply dipping, foliation and lineation. The mineral assemblage is similar to Wlg and contains plagioclase + alkali feldspar + quartz + biotite + Fe-Ti oxides + titanite + apatite + zircon ± hornblende. Few mafic enclaves occur in this unit. Low-grade metamorphism introduced epidote + white mica.*

Biotite Granite
Wlbg *Medium-grained biotite granite variable foliation. Noted by Schmitz (2005) to contain primary quartz + alkali feldspar + biotite + Fe-Ti oxides + apatite. Secondary epidote and clay minerals are also found.*

Roundtop Mountain Greenstone Formation
Wrmg *Metabasalt, metadiabase, metagabbro, banded iron formation, and quartzofeldspathic schist. Contains Wrmg, Wbif and Wes of Schmidtz (2005). A metamorphic mineral assemblage of in Wrmg is hornblende + plagioclase + quartz + Fe-Ti oxides + epidote ± titanite with retrograde epidote, chlorite, white mica, actinolite, and carbonate has been noted. Wbif contains banded quartz + magnetite. Wes contains quartz + chlorite + plagioclase + apatite ± actinolite ± hornblende ± white mica ± titanite ± zircon ± cordierite.*

Leucogranite Gneiss
Wlgg *Medium-grained leucogranite to mylonitic leucogranite gneiss. Steeply dipping foliation and lineation with a metamorphic mineral assemblage of alkali feldspar + quartz + plagioclase + biotite ± hornblende ± epidote ± garnet and secondary epidote + white mica. Is intruded by mafic dikes of Roundtop Mountain Greenstone and mafic dikes inferred to be related to the Louis Lake batholith.*

Contact
Solid line where confident, dashed line where approximate, and dotted line where inferred.

Orientation Data

Strike and dip of foliation | *Strike and dip of foliation, trend and plunge lineation* | *Strike and dip of contact* | *Trend and plunge of lineation* | *Strike and vertical dip of contacts*

Area with a high concentration of aplite and pegmatite dikes near Cony Mountain in the northern portion of the map area. These represent a fractionated portion of the Wlg.

WR-15 *Star denotes where a sample was collected. The corresponding number is the sample number.*

13°00′
231 MILS
Approximate Declination
1994

Geology mapped in 2007 by E. Vaughn with map additions from Schmitz (2005), Bayley (1965a), and Hausel (1991)

Plate A: Geologic map of the central and southeastern portions of the Louis Lake Batholith, Fremont County, Wyoming
by
Elizabeth Vaughn
2010